Doctoral Dissertation
Doctoral Program in Civil and Environmental Engineering (36th Cycle)

Engineered design frameworks for the seismic retrofitting of existing structures

Antonio P. Sberna
* * * * * *

Supervisors
Prof. G. C. Marano
Prof. F. Di Trapani

Doctoral Examination Committee:
Prof. P. Castaldo, Politecnico di Torino
Prof. L. Cavaleri, Università degli Studi di Palermo
Prof. R. De Risi, University of Bristol
Prof. C. Galasso, University College London
Prof. E. Spacone, Università degli Studi Chieti-Pescara

Politecnico di Torino
2024

I hereby declare that the contents and organization of this dissertation constitute my own original work and do not compromise in any way the rights of third parties, including those relating to the security of personal data.

Antonio P. Sberna
Turin, September 2024

This dissertation is presented in partial fulfillment of the requirements for Ph.D. degree in the Graduate School of Politecnico di Torino (ScuDo).

"There is grandeur in this view of life, with its several powers, having been originally breathed into a few forms or into one; and that, whilst this planet has gone cycling on according to the fixed law of gravity, from so simple a beginning endless forms most beautiful and most wonderful have been, and are being, evolved."

C. Darwin (1859). On the Origin of Species.

"It is a familiar and significant saying that a problem well-put is half-solved."

J. Dewey (1938). Logic: The Theory of Inquiry.

Acknowledgments

"The highest reward for a person's toil is not what they get for it,
but what they become by it"
J. Ruskin

The journey that has led me to the highest level of university education has been marked by encounters with exceptional individuals, some of whom I have had the honor to meet and work with. The insightful discussions and collaborative efforts with these individuals have contributed, at various levels, to the development of the research activities presented in this Ph.D. thesis.

I would like to express my deepest gratitude to Professor F. Di Trapani for introducing me to the world of research and for consistently guiding me through every aspect of it. Your mentorship has been a cornerstone of my academic journey, providing me with the technical knowledge needed to navigate the complexities of this field, as well as the confidence to pursue my ideas and forge my own path. Your support and encouragement have been instrumental in shaping my growth and have profoundly influenced both my academic and professional development.

I would like to sincerely thank Professor G.C. Marano for introducing me to the field of structural optimization and for giving me the opportunity to explore this fascinating area. Your belief in my abilities and your support have

been invaluable, and I am deeply grateful for the confidence you have shown in me throughout this journey.

My sincere thanks go to all the professors, researchers, and colleagues I have encountered throughout this journey. You have been a constant source of inspiration, knowledge, and motivation, each contributing in your own way to my development.

I also extend my heartfelt thanks to my colleagues at the Politecnico di Torino, with whom I have spent a lot of time. Your companionship, collaboration, and the discussions we've shared have been instrumental in making this journey both rewarding and enjoyable. The conversations and challenges we experienced together have not only enriched my academic life but also forged friendships for which I am truly grateful.

I wish to express my deepest gratitude and profound respect to Professor J.P. Conte for his exceptional guidance and support. His introduction to the world of Performance-based Earthquake Engineering has had a significant impact on my academic journey. I am incredibly thankful for the opportunity he provided me to spend my visiting period at UCSD, an experience that has been so much more than just academically enriching, it has been transformative. His insights, wisdom, and the generous time he dedicated to my development have not only expanded my knowledge but also inspired me to pursue my goals with greater confidence and determination.

I would also like to extend my sincere thanks to Dr. A. Deb and all the colleagues at UCSD. Your support, collaboration, and camaraderie made my time in San Diego *so much* more enriching. The discussions, shared experiences, and the welcoming environment contributed to my professional and personal growth. I am deeply grateful for the opportunity to work alongside such talented individuals and for the many ways in which you all have influenced my journey.

Finally, I would like to thank the reviewers of this thesis, whose feedback and constructive criticism have helped in refining this work, and I appreciate the time you dedicated to this process.

Summary

A significant portion of existing structures were designed and constructed before the implementation of seismic codes, necessitating seismic retrofitting interventions to ensure their safety and resilience. This situation is particularly prevalent in regions with a long history of construction, where many buildings were erected using outdated engineering practices that did not account for seismic actions. The lack of seismic detailing has led to these structures being highly vulnerable to earthquake damage and having low ductility capacity.

Currently, there are no formal methods for designing such retrofitting interventions. This lack of standardized procedures presents a critical gap in the structural engineering field, as engineers must rely only on intuition and experience that may not consistently deliver optimal results. The traditional trial-and-error methods are not only time-consuming but also often lead to over-conservative designs, which can result in unnecessary costs. Moreover, these methods do not guarantee that the retrofitting solutions will meet the desired performance levels under seismic conditions, thus potentially compromising the safety and functionality of the retrofitted structures.

To address this gap, this thesis aims to propose an ensemble of four design frameworks for seismic retrofitting. These methods are specifically designed to provide efficient and cost-effective retrofitting solutions for reinforced concrete (RC) frame structures and masonry buildings.

The first three methods are based on the genetic algorithm (GA) approach. The first proposed framework focuses on retrofitting existing RC frame structures, aiming to minimize implementation costs. By leveraging GA's capability to explore a wide and non-homogeneous search space, this method determines the optimal placement and size of seismic retrofitting, ensuring cost-effective retrofitting configurations. New subroutines have been proposed to be able to analyze structures with deficiencies in terms of both ductility and brittle failures.

The second method extends this approach by optimizing both the position and sizing of retrofitting, thereby minimizing both implementation costs and the expected annual loss. This dual-objective optimization considers the long-term financial implications of retrofitting.

The third framework is tailored specifically for masonry structures, the proposed method introduces a topological optimization algorithm on a structural scale. By considering the unique characteristics and vulnerabilities of masonry structures and the effect of reinforced plasters, the proposed algorithm efficiently determines the optimal reinforcement configuration, enhancing the seismic performance of these buildings.

The fourth method is a performance-based earthquake engineering (PBEE) design procedure for the seismic retrofitting of non-ductile RC frame structures. This method provides a valid tool for risk-targeted design of reinforcement interventions, ensuring that retrofitting efforts meet specific performance criteria under seismic loads. By integrating a scientific-based uncertainties quantification approach, the PBEE-based framework provides a comprehensive assessment of the retrofitted structure's performance, guiding engineers in making informed design decisions that balance safety, and cost.

The proposed methods have been validated through a series of case studies involving reference structures. These tests confirmed the generality and robustness of the approaches, demonstrating their effectiveness in providing optimized, cost-efficient, and reliable retrofitting solutions. For the RC frame structures, case studies included various configurations of shear-critical and ductility-deficient structures, highlighting the flexibility and adaptability of the proposed GA-based methods. The masonry structure case studies involved buildings with different mechanical properties, further validating the topological optimization approach.

The results highlight the potential of these optimization frameworks to significantly improve the safety and resilience of existing structures in earthquake-prone areas, offering a systematic and scientifically rigorous approach to seismic retrofitting design. The proposed frameworks not only optimize retrofitting costs but also ensure compliance with safety standards and extend the service life of the structures.

In conclusion, this thesis presents a suite of design frameworks that significantly advance the state-of-the-art seismic retrofitting design frameworks. By providing robust, flexible, and cost-effective solutions, these methods aim to be useful tools for engineers, enhancing the resilience of built heritage and ensuring safety and sustainability in the face of future seismic events, ultimately safeguarding lives and reducing economic losses.

Table of contents

1 Introduction: Design methods for the seismic retrofitting of existing structures and scope of the thesis 11

1.1 State of the art of the design procedures for seismic retrofitting of existing structures 17

1.1.1 Review of the initial considerations 19
1.1.2 Selective rehabilitation objectives 20
1.1.3 Select rehabilitation method 21
1.1.4 Perform retrofitting design 25
1.1.5 Verify retrofitting design 25
1.1.6 Realization of the rehabilitation 27

1.2 Scope of the work and thesis organization 27

2 Literature review: Design methodologies for seismic retrofitting of existing structures 30

2.1 Literature review methodology and overview of scientific production 32

2.2 MCDM seismic retrofitting design approaches 35

2.2.1 Key publications in MCDM for seismic retrofitting design . 37
2.2.2 Results considerations and future direction trends 44

2.3 Optimization frameworks for seismic retrofitting design 50

2.3.1 Brief review of the algorithm commonly used in structural optimization 54

2.3.1.1 Classical Optimization Algorithms 55

2.3.1.2 Metaheuristic optimization algorithms 56

2.3.2 Significant studies in optimization frameworks for seismic retrofitting design 59

2.3.2.1 Topology optimization 68
2.4 Other frameworks and tool for the design 76
2.4.1.1 Numerical and theoretical tools for the retrofitting design of existing structures 78
2.5 Conclusions and future trends 80
3 Innovative genetic algorithm-based framework for cost optimization of ductile-critical and shear-critical reinforced concrete frame structures 81
3.1 Design optimization framework 82
3.1.1 General operating principles and position of the problem 82
3.1.2 Definition of the design vector 85
3.1.3 Objective function and penalty function 87
3.2 Definition of the genetic operators 89
3.2.1 Population generator and elitism 89
3.2.2 Crossover and mutation 91
3.3 Reference structural model 92
3.3.1 Model of reinforced concrete elements without steel-jacketing 92
3.3.2 Modelling of steel-jacketing action in RC fiber-section columns 93
3.3.3 Modelling of masonry infills 97
3.4 Analysis and post-processing of the results 98
3.4.1 Feasibility assessment by pushover analysis 98
3.4.2 Post-processing shear verification of RC elements with and without steel-jacketing 99
3.4.3 Evaluation of the additional shear demand due to frame-infill interaction 101
3.5 Tests of the optimization framework and calibration of the genetic operators 102
3.5.1 Details of the reference test structure 102
3.5.2 Test of the modified genetic operators 103
3.5.3 Calibration of the GA settings 106

3.6 Test of the GA framework with different case study structures 109
3.6.1 Case study structure description 109
3.6.2 Preliminary assessment tests 111
3.6.3 Optimization results for the different case studies 113
3.6.4 Final design configurations 118
3.7 Conclusions 119
4 Novel genetic algorithm for optimizing seismic retrofitting costs and Expected Annual Losses in non-conforming reinforced concrete frame structures 122
4.1 Optimization framework 124
4.1.1 Working principles 124
4.1.2 Evaluation of the Expected Annual Loss 125
4.1.3 Encoding of the design vector 128
4.1.4 Definition of the objective function 130
4.2 Optimization algorithm subroutines 132
4.2.1 Algorithm working principle 132
4.2.2 Parent selection operator 133
4.2.3 Crossover and mutation genetic operators 134
4.2.4 Survival selection operator 135
4.2.5 Heuristic repair 136
4.3 Reference structural model 136
4.3.1 General assumptions 136
4.3.2 Modelling reinforced concrete elements with and without CFRP reinforcement 137
4.4 Structural analysis and results post-processing 140
4.4.1 Feasibility assessment by pushover analysis 140
4.4.2 Shear verification of RC elements with and without CFRP reinforcement 141
4.5 Stress-test of the optimization framework 143
4.5.1 Details of the reference structural model 143
4.5.2 Assessment of the as-built structures 144

4.5.3 Retrofitting design details and assumptions on the design space 146
4.5.4 Optimization results and discussion 147
4.6 Conclusions 152
5 Genetic algorithm framework for cost-effective topology optimization of seismic reinforcement in existing masonry structures 154
5.1 Masonry reinforcement with reinforced plasters 156
5.1.1 General features of reinforced plasters 156
5.1.2 Capacity models and in-plane safety checks 156
5.2 Optimization framework 159
5.2.1 Working principles 159
5.2.2 Design vector encoding 161
5.2.3 Definition of the objective function 161
5.2.4 Genetic operator subroutine 163
5.3 Structural modelling and seismic analysis 165
5.3.1 Reference model for the masonry building structure 165
5.3.2 Seismic analysis 166
5.3.3 Safety checks 167
5.4 Case study tests 170
5.4.1 Details of the case study structure 170
5.4.2 Preliminary assessment of as-built structures and non-optimized retrofitted structures 172
5.4.3 Results of the application of the optimization framework . 174
5.5 Conclusions 180
6 Risk-targeted seismic retrofitting design procedure for non-ductile reinforced concrete frame structures 183
6.1 Summary of state-of-the-art of risk-targeted PBEE assessment framework 184
6.1.1 Seismic hazard, response spectra, and ground motion selections 184
6.1.2 Conditional demand model 186

6.1.3 Probabilistic Seismic Damage Hazard analysis and Uncertainty in capacity model 187
6.2 Contribution of collapse cases in the updated PEER PBEE assessment framework 188
6.2.1 Conditional distribution of collapse 189
6.2.2 Probabilistic Demand and Damage Hazard Analysis in case of collapse occurrences 190
6.3 Risk-targeted performance-based seismic retrofitting design framework 192
6.4 Case Study Structure and Computational Model 195
6.4.1 Details of the case study structure 195
6.4.2 Modeling of steel braces 197
6.4.3 Design variables and general assumptions. 197
6.4.4 Engineering Demand Parameter and associated damage LSs 199
6.4.5 Damage hazard analysis 201
6.4.6 Estimation of retrofitting costs 202
6.5 Results of the application of the PBEE framework for retrofitted existing structures 203
6.5.1 Future extension and scalability of the framework 208
6.6 Conclusions 210
6.6.1 Acknowledgments 211
Conclusions 212
References 216

List of Tables

Table 1.1 – Reconstruction costs (normalized), reconstruction period and casualties for earthquakes occurred in Italy in the period 1968-2012..... 14
Table 1.2 – Effect of local and global retrofit measures on building performances (based on [17], [18], [19] and [20]). The character (+) means increase and (-) means decrease. 24
Table 2.1 – Summary of the studies proposing a MCDM design approach for the design of existing structures retrofitting 46
Table 2.2 – Summary of optimization framework for design of seismic retrofitting studies 71
Table 3.1 – Reinforcement details of beams and columns..... 102
Table 3.2 – Steel-jacketing arrangement details. 103
Table 3.3 – GA parameters for the calibration tests 108
Table 3.4 – Geometric and mechanical details of the equivalent struts. . 110
Table 3.5 - Case studies main characteristic. 111
Table 3.6 – GA framework settings used for the case studies..... 111
Table 3.7 – Results of preliminary tests. 113
Table 3.8 – Overview of the optimization results. 118
Table 3.9 – Result details for the final design solutions. 119
Table 4.1 – Mean annual frequency of exceedance (λ) and repair costs (%RC) associated with each LS for a code-compliant building..... 127
Table 4.2 – Geometrical dimensions and reinforcement details of RC elements..... 143

Table 4.3 – Geometric and mechanical modelling parameters for RC elements and infill equivalent struts. 144
Table 4.4 – Results of the assessment of the as-built structures. 144
Table 4.5 – GA analysis parameters set up for the case studies. 148
Table 4.6 – Overview of the case studies optimization analysis results. . 150
Table 5.1 – Amplification factors (α_r) for different masonry typologies and reinforcement interventions. 157
Table 5.2 – As-built mechanical properties of masonry for the case-study structures. 170
Table 5.3 – Mechanical properties of masonry strengthened by reinforced plaster for the case-study structures. 171
Table 5.4 – Outcomes of safety checks for the as-built squared stone masonry (SSM) and tender stone masonry (TSM) structures. 172
Table 5.5 – Reinforcement details and cost of non-optimized retrofitting interventions. 173
Table 5.6 – GA setup parameters 175
Table 5.7 – Results of the optimization procedure compared with the not-optimized configuration. 179
Table 6.1 – Overview of the various cross-section configurations adopted for the braces 199
Table 6.2 – Summary of optimal retrofitting configurations for the case study structure 206

List of Figures

Figure 1.1 – Distribution of Building Stock in EU27 by Construction Period and Building Use (European Commission - Building Stock Observatory 2024 [1]) 12
Figure 1.2 – Seismic Hazard Map Based on the ESHM13 [3] Mean Hazard Model probability of exceedance 10% in 50 years 13
Figure 1.3 – Global Exposure Model for the Mediterranean Area (Silva et al. 2018 [4]) in terms of economic value (in US Dollars) 14
Figure 1.4 – Schematic workflow of the retrofitting design procedure according to FEMA 356 [12]..... 19
Figure 1.5 – Performance matrix (Vision 2000 [9])..... 20
Figure 1.6 – Target building performance levels and ranges (ASCE/SEI 41-17 [13])..... 21
Figure 1.7 – Effect of different retrofitting techniques on seismic performance of the structure in terms of strength and ductility (loosely inspired by [16])..... 23
Figure 1.8 – Schematic representation of the different levels of EDP..... 26
Figure 2.1 – Annual trend in the number of publications on seismic retrofitting design frameworks. 33
Figure 2.2 – Geographical distribution of author affiliations for publications under analysis..... 34
Figure 2.3 – Distribution of funding sponsors (when indicated) 35
Figure 2.4 – Cost and PGA capacity-demand ratio (α^*) results for one of the case-study structures analysed by Zerbin and Aprile (2015)[33]..... 38

Figure 2.5 – Schematic representation of the 4-steps workflow of the MCDM proposed by Passoni et al. (2019) [38] 40
Figure 2.6 – Spyder charts representing the performance of different retrofitting alternatives with respect to different criteria (Labò et al. (2021) [40]) 41
Figure 2.7 – Flowchart of the MCDM procedure proposed by Gentile et al. (2022) [41] for the chose of optimal retrofitting configuration considering insurance. 42
Figure 2.8 - Retrofitting impact assessment procedure proposed by Clemett et al. (2022) [45] 43
Figure 2.9 – Schematic representation of levels of structural optimization application on bridge design (Ramm et al. 1998 [53], Kato et al. 2010 [54]) ... 51
Figure 2.10 – Taxonomy of the optimization algorithms classes with non-exhaustive list of foremost algorithms (based on [68], [69], [70], [71]) 54
Figure 2.11 – Multi-objective Genetic Algorithm for the optimal research of passive energy dissipation systems(Lavan and Dargush (2009) [98]) (a) Flowchart of the GA procedure for the creation of a new generation, (b) Dominance criterion and angular neighborhood distance approach. 61
Figure 2.12 – Schematic representation of Particle Swarm Optimization approach developed by Mahdavi et al. (2019) [102] for the optimization of FRP jacketing in RC frame structures 63
Figure 2.13 – Schematic representation of the PBSD procedure implemented by Laguardia and Franchin (2022) [104] 64
Figure 2.14 – Representation of the optimal configuration for steel braces and micro-piles found by Falcone et al. (2019) [105] 65
Figure 2.15 – Schematic representation of the ANN model developed by Shin and Park (2022) [109] for the safety assessment of each tentative solution analyzed by the optimization framework. 67
Figure 2.16 – Framework of optimization approach proposed by Gharagoz et al. (2023) [110] for the optimization of spring-rotational friction dampers for RC frame structures. 68
Figure 2.17 – Procedure for the topology optimization of CFRP on slabs (Chaves and Cunha 2014 [113]) 69
Figure 2.18 – Optimal fibers orientations of the reinforcement (for Tsai-Wu criterion and homogenized failure surface): (a) deep beam, (b) windowed panel (Bruggi et al. 2014 [115]) 70

Figure 2.19 – Conceptual flowchart of the procedure proposed by Aljawhari et al. (2022) [134] for the seismic retrofitting design based on fragility curve results. 77
Figure 2.20 – Flowchart of seismic retrofitting optimization procedure with the use of ANN for the substitution of the FEM analysis in the step of the safety assessment as proposed by Falcone et al. (2022) [138] 79
Figure 3.1 – Schematic flowchart of the proposed optimization framework 83
Figure 3.2 – Typical possible retrofitting configuration for a RC building having: (a) flexural ductility-related deficiencies; (b) shear-related deficiencies also caused by the interaction with masonry infills. Retrofitted columns are depicted in red. 84
Figure 3.3 – Possible optimization outcomes in case of: (a) design space with prevalence of feasible solutions; (b) design space with prevalence of unfeasible solutions. 85
Figure 3.4 – Representation of the optimization variables: (a) Generic column retrofitting configuration for an RC structure; (b) Typical retrofitting arrangement for a column with generic batten spacing (s_b) 86
Figure 3.5 – Penalty function 89
Figure 3.6 – Proposed approach for the initial population generator 90
Figure 3.7 – Schematic flowcharts of the: (a) uniform scatter crossover function; (b) proposed mutation function 92
Figure 3.8 – Definition of the frame fiber-section elements with and without steel-jacketing reinforcement. 93
Figure 3.9 - Steel jacketing configurations for columns: a) cage with moment-resisting end connections; b) cage without end connections. 94
Figure 3.10 – Modelling of steel-jacketing in fiber-section elements: a) steel-jacketing confinement action only; b) steel-jacketing confinement and flexural resistance. 94
Figure 3.11 - Configuration of the cross-section of a column retrofitted with steel jacketing: a) area effectively confined by stirrups and steel jacketing; b) geometric arrangement. 95
Figure 3.12 – Sample of stress–strain response of concrete in compression for a column without steel jacketing and with steel jacketing 97
Figure 3.13 – Equivalent strut model for masonry infills. 98

Figure 3.14 – Typical equivalent SDOF capacity curve and bilinear equivalent curve for: (a) shear-resistant (ductile) structures; (b) shear-critical structures. 99
Figure 3.15 – Simplified scheme for the determination of actual shear demand on columns for an infilled frames (from Di Trapani and Malavisi 2019 [159]) 101
Figure 3.16 – Geometrical dimensions of the case study structure: (a) 3D frame view; (b) dimensions in plan. 102
Figure 3.17 – Objective function values for GA with standard population generators. 104
Figure 3.18 – Objective function values for GA with modified population generator 105
Figure 3.19 – Objective function values for GA with modified population generator and mutation ad a function of ξ_μ 105
Figure 3.20 – Comparison of the convergence history of the GA with standard population generator, with modified population generator and with modified population generator and mutation. 105
Figure 3.21 – Tests of the modified GA for the calibration of the dimension of the population 107
Figure 3.22 – Tests of the modified GA for the calibration of the dimension of the pPr space 107
Figure 3.23 – Tests of the modified GA for the calibration of the probability of mutation 108
Figure 3.24 – Stability test with the optimal parameters: (a) Convergence history of 5 runs; (b) Optimal retrofitting solution. 109
Figure 3.25 – Case study structures: (a) IFC 1: symmetric positioning of infills with pilotis storey; (b) IFC2: asymmetric positioning of infills. 110
Figure 3.26 – As built preliminary IFC 1 test: (a) capacity curve (b) deformed shape. 112
Figure 3.27 – As built preliminary IFC 2 test: (a) capacity curve (b) deformed shape. 112
Figure 3.28 – Preliminary tests with all 1st and 2nd storey columns retrofitted: (a) IFC1 deformed shape; (b) IFC2 deformed shape; (c) IFC1 capacity curves; (d) IFC2 capacity curves. 113
Figure 3.29 – Convergence history for: (a) IFC1.SR structure; (b) IFC1.SC structure 114

Figure 3.30 – Convergence history for: (a) IFC2.SR structure; (b) IFC2.SC structure..... 114
Figure 3.31 – Comparison of the minimum OF values per generation: . 115
Figure 3.32 – Optimal solution for IFC1.SR structure: (a) Overall capacity curves; (b) First storey columns capacity curves; (c) Retrofitting configuration at the first two stories. 116
Figure 3.33 – Optimal solution for IFC1.SC structure: (a) Overall capacity curves; (b) First storey columns capacity curves; (c) Retrofitting configuration at the first two stories. 116
Figure 3.34 – Optimal solution for IFC2.SR structure: (a) Overall capacity curves; (b) First storey columns capacity curves; (c) Retrofitting configuration at the first two stories. 117
Figure 3.35 – Optimal solution for IFC2.SC structure: (a) Overall capacity curves; (b) First storey columns capacity curves; (c) Retrofitting configuration at the first two stories. 117
Figure 3.36 – Design solutions capacity curves and retrofitting configurations for: (a) IFC1.SR; (b) IFC1.SC; (c) IFC2.SR; (d) IFC2.SC 118
Figure 4.1 – Effect of cost minimization on EAL. 123
Figure 4.2 – Schematic flowchart of the optimization framework..... 125
Figure 4.3 – Reference EAL curve for a code-compliant building. 126
Figure 4.4 - Relationships between capacity demand assessment for LSLS and DLLS and resulting EAL curve: (a) DLLS not satisfied; (b) LSLS not satisfied; (c) DLLS and LSLS not satisfied; (d) DLLS and LSLS satisfied..... 128
Figure 4.5 – Representation of the design variables: (a) Generic FRP and bracing retrofitting configuration; (b) Typical arrangement of bracings; (c) Typical arrangement of CFRP..... 130
Figure 4.6 – Schematic flowchart of the genetic algorithm routine. 133
Figure 4.7 – Working scheme of the proposed parent selection operator. 133
Figure 4.8 – Working principle of the proposed crossover procedure.... 134
Figure 4.9 – Working principle of the proposed survival selection function. 135
Figure 4.10 – Heuristic repair subroutine working principle. 136
Figure 4.11 – Definition of the fiber-section elements in OpenSees, concrete elements with and without FRP wrapping, masonry infills, and steel bracings. 137

Figure 4.12 – Reference configuration and geometric parameters of a column retrofitted by FRP wrapping: (a) in plan; (b) along the height. 139
Figure 4.13 – Samples of stress-strain response in compression of concrete with and without FRP retrofitting: (a) by varying the number of FRP layers $\left(n_{\mathrm{FRP}}\right)$; (b) by varying the spacing of strips $\left(s_{\mathrm{FRP}}\right)$. 140
Figure 4.14 – Limit state conditions: (a) Damage limitation (DLLS); (b) Life safety (LSLS). 141
Figure 4.15 – Geometrical dimensions of the reference structural model: (a) 3D frame view; (b) Plan view and RC element cross-section dimensions. 144
Figure 4.16 – As-built configuration preliminary analysis: (a) SR capacity / demand assessment; (b) SR EAL curve; (c) SC capacity / demand assessment; (d) SC EAL curve. 145
Figure 4.17 – Restricted design space representation for the case study structure. 147
Figure 4.18 – GA optimization convergence history: (a) shear-resistant configuration; (b) shear-critical configuration. 149
Figure 4.19 – Feasible individuals EAL values trend: (a) shear-resistant configuration; (b) shear-critical configuration. 149
Figure 4.20 – Optimal solutions retrofitting configurations (deformed shape): (a) shear-resistant case; (b) shear-critical case. 150
Figure 4.21 – Convergence history of the design vector parameters: a) SR configuration; b) SC configuration. 151
Figure 4.22 – Performance of the optimal solution for the SR configuration: (a) Capacity / demand assessment in AD format; (b) EAL curve. 151
Figure 4.23 – Performance of the optimal solution for the SC configuration: (a) Capacity / demand assessment in AD format; (b) EAL curve. 152
Figure 5.1 - Application of reinforced plasters to masonry walls: (a) electro-welded steel net; (b) GFRP; (c) scheme of arrangement of the reinforcement. 156
Figure 5.2 - Reference scheme for the evaluation of in-plane ultimate moment and shear of a reinforced masonry wall. 158
Figure 5.3 - Unreinforced and reinforced flexure and shear interaction diagrams for a sample masonry wall: (a) $N_0 - M_u$; (b) $N_0 - V_u$. 159
Figure 5.4 - Schematic flowchart of the optimization framework. 160
Figure 5.5 - Schematic representation of the application of the genetic operators in creating a new individual. 163

Figure 5.6 - Working principle of the genetic operators: (a) single-point crossover; (b) mutation. 164
Figure 5.7 – Schematic flowchart of the genetic algorithm framework .. 165
Figure 5.8 – Reference OpenSees FE model of the masonry structure. . 166
Figure 5.9 – Dimensionless interaction domains and safety checks: (a) flexure (n_0 - m_u); b) shear (n_0 - v_u). 169
Figure 5.10 – Geometrical dimensions of the case study structure: a) Ground floor; b) First floor. 170
Figure 5.11 – Reference elastic and design spectra. 171
Figure 5.12 – Assessment of the structure in the as-built configuration: a) Squared stone masonry (SSM); b) Tender stone masonry (TSM). 172
Figure 5.13 – Flexural safety checks for the as-built and non-optimized reinforced structures: (a) Squared stone masonry (SSM); (b) Tender stone masonry (TSM). 173
Figure 5.14 – Shear safety checks for the as-built and non-optimized reinforced structures: (a) Squared stone masonry (SSM); (b) Tender stone masonry (TSM). 174
Figure 5.15 – Subdivision of the walls within the clusters: (a) ground storey; (b) first story. 174
Figure 5.16 – GA optimization convergence history: (a) Squared stone masonry (SSM); (b) Tender stone masonry (TSM). 175
Figure 5.17 – Number of retrofitted clusters during the optimization history: (a) Squared stone masonry (SSM); (b) Tender stone masonry (TSM). 176
Figure 5.18 – Optimal reinforcement layouts for the case studies: (a) Squared stone masonry (SSM); (b) Tender stone masonry (TSM). 176
Figure 5.19 – Trend of the ratio between the moving average of the overall surface of reinforced walls and maximum average surface of reinforced walls during the retrofitting optimization of the two case studies. 177
Figure 5.20 – Flexural safety checks comparisons of the as-built structure and non-optimized and optimized reinforced structures: (a) Squared stone masonry (SSM); (b) Tender stone masonry (TSM). 178
Figure 5.21 – Shear safety checks comparisons of the as-built structure and non-optimized and optimized reinforced structures: (a) Squared stone masonry (SSM); (b) Tender stone masonry (TSM). 178

Figure 5.22 - Shear safety checks for the as-built and non-optimized reinforced structures: (a) Squared stone masonry (SSM); (b) Tender stone masonry (TSM)..... 179
Figure 6.1 – Probabilistic seismic hazard analysis and GM selection: (a) seismic hazard curve in terms of $S_{a,\text{avg}}$, (b) Uniform Hazard Spectrum, Conditional Mean Spectrum range of natural variability, and alongside spectra from the selected ground motion records ensemble..... 185
Figure 6.2 – Conditional demand model: representative of the interpolation of the model in EDP/IM space..... 187
Figure 6.3 – Collapses cases: (a) conditional distribution of collapses w/r to IM, (b) Conditional distribution of EDP with respect to IM and the conditional distribution of collapses 190
Figure 6.4 – (a) Demand Hazard Curve with collapse case; (b) graphical representation of the collapse contribution to the demand hazard analysis.. 191
Figure 6.5 - Schematic representation of the MRP surface..... 193
Figure 6.6 – Schematic flowchart of the workflow of the proposed design framework..... 194
Figure 6.7 – Case study concrete frame: (a), elevation view and geometrical dimensions (b) in-plane view of the slabs..... 195
Figure 6.8 – Definition of the fiber-section and truss elements in OpenSees 196
Figure 6.9 – Restricted design space representation for the case study structure..... 198
Figure 6.10 – Normalized fragility curve for the Near Collapse chord rotation of reinforced concrete structural elements..... 200
Figure 6.11 - Demand curves (in grey) and denormalized fragility curves (in red) for the case study columns. 201
Figure 6.12 – MRP surface for the case study structure with target levels of 2500, 2000, and 1500 years. 203
Figure 6.13 – Optimal reinforcement configuration for the target MRP level of 2500 years..... 204
Figure 6.14 – Optimal reinforcement configuration for the target MRP level of 2000 years..... 205
Figure 6.15 – Optimal reinforcement configuration for the target MRP level of 1500 years..... 205

Figure 6.16 – Relationship between the design parameters and associated costs for different target MRPs 207

Acronyms

BRB	Buckling Restrained Braces
CDM	Conditional Demand Model
CFRP	Carbon Fibers Reinforced Polymers
CLS	Collapse Limit State
DLLS	Damage Limitation Limit State
DV	Design Variable
EAL	Expected Annual Loss
EDP	Engineering Demand Parameter
FEM	Finite Element Method
FRCM	Fiber Reinforced Cementitious Matrix
FRP	Fiber Reinforced Polymer
GA	Genetic Algorithm
GFRP	Glass Fiber Reinforced Polymer
GM	Ground Motion
GMS	Ground Motion Selection
HL	Hazard Level
IDLS	Initial Damage Limit State
IDR	Inter-Story Drift
IM	Intensity Measure
LCA	Life Cycle Assessment
LSLS	Life Safety Limit State
MAR	Mean Annual Rate
MCDM	Multi-Criteria Decision Making
MRP	Mean Return Period
NLTHA	Non-Linear Time History Analysis
NSGA-II	Non-dominated Sorting Genetic Algorithm
OLS	Operational Limit State
PBD	Performance Based Design
PBEE	Performance Based Earthquake Engineering
PEER	Pacific Earthquake Engineering Research
PSHA	Probabilistic Seismic Hazard Analysis
PSO	Particle Swarm Optimization
RLS	Reconstruction Limit State
SHC	Seismic Hazard Curve

Chapter 1

Introduction: Design methods for the seismic retrofitting of existing structures and scope of the thesis

The structural heritage of Europe predominantly consists of buildings designed and built before the advent of modern seismic design technical codes. A significant proportion of these structures were constructed in periods where considerations for seismic forces were minimal or entirely absent. In professional practice of the time, the design of these buildings primarily focused on vertical loads, with seismic effects often addressed in a rudimentary approach mainly using equivalent horizontal force models. Furthermore, prior to the year 2000, there was negligible emphasis on the construction details necessary to achieve significant ductility in structural elements and, consequently, in the overall structural systems.

As a result, many of these edifices, some of which date back several decades or even centuries, were designed with a primary focus on durability and aesthetic values, often overlooking the need for comprehensive seismic resilience and ductility. This oversight has culminated in a vast inventory of aging structures that are particularly vulnerable to seismic events. The inherent deficiencies in these buildings pose substantial risks to both public safety and economic stability in seismically active regions, underscoring the critical necessity for effective seismic retrofitting strategies.

Figure 1.1, based on data from Eurostat [1], illustrates the distribution of residential and service structures in the European Union (EU27), categorized by their construction period. The data reveals several key trends. The period before 1945 shows a substantial number of buildings, with residential buildings forming the majority. This indicates significant construction activity before the introduction of modern seismic codes. The post-war era (1946-1969)

experienced the highest volume of construction, particularly in residential buildings, driven by reconstruction efforts to meet housing demands. In the subsequent decades (1970-1989), there was a notable decline in construction activity, with reduced numbers of both residential and service structures. From 1990 to 2010, the construction volume remained relatively stable, although at a lower level compared to the mid-20th century peak. Residential buildings continued to dominate the new constructions during this period. A sharp decline in new constructions is evident post-2011, reflecting a significant slowdown in building activities in recent years.

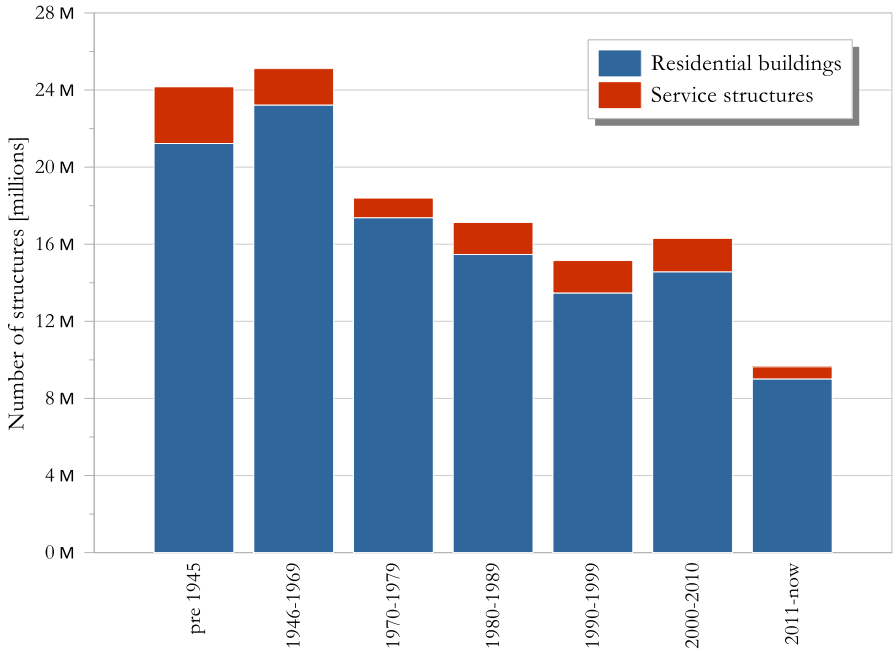

Figure 1.1 – Distribution of Building Stock in EU27 by Construction Period and Building Use (European Commission - Building Stock Observatory 2024 [1])

A worthy observation from Figure 1.1 is that a large percentage of the existing building stock was constructed before the enforcement of modern seismic design codes, which generally came into effect in the late 20th century (JRC Technical Report 2008 [2]). These buildings, particularly those built before 1945 and during the immediate post-war reconstruction era, were often designed without detailed seismic considerations, relying mainly on simplified horizontal force models. This lack of seismic design makes them especially vulnerable to seismic events.

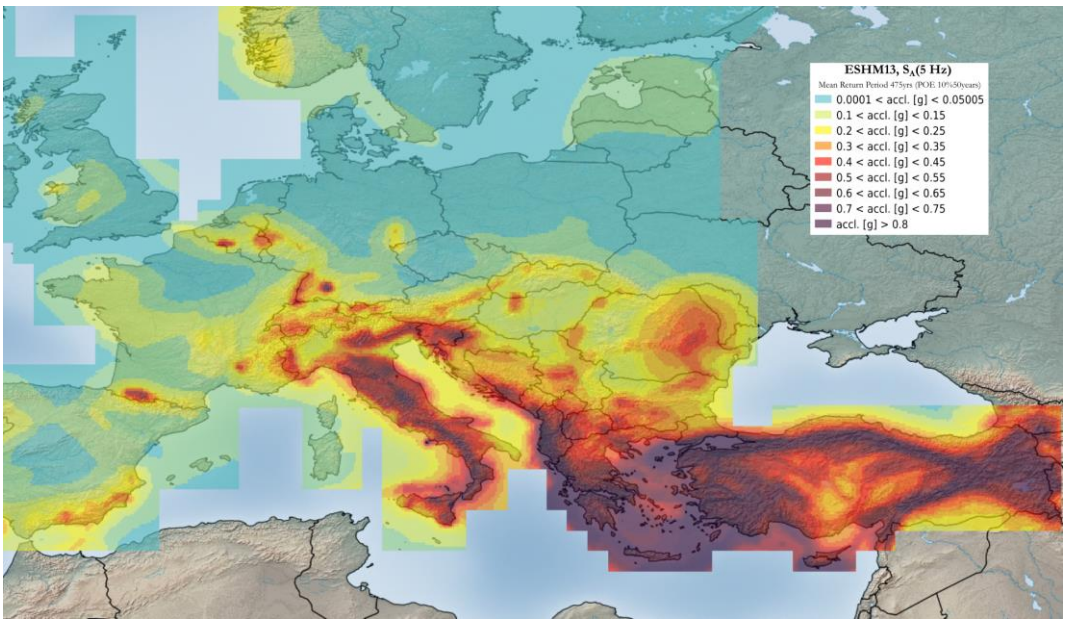

Figure 1.2 – Seismic Hazard Map Based on the ESHM13 [3] Mean Hazard Model probability of exceedance 10% in 50 years

A significant portion of the existing building stock, particularly those constructed before 1945 and during the post-war reconstruction era, lacks adequate seismic design considerations. These buildings, often designed using simplified horizontal force models, are particularly vulnerable to the frequent and severe earthquakes that plague Mediterranean Europe, a region characterized by complex tectonic activity at the intersection of the Eurasian, African, and Anatolian plates.

Figure 1.2 from the European Facilities for Earthquake Hazard and Risk (EFEHR) highlights these high-risk areas, showing the intensity and frequency of seismic activity. The substantial exposure of Mediterranean Europe to seismic hazards poses a grave threat to the safety and integrity of the built environment.

Addressing this pressing issue demands urgent attention to seismic retrofitting and the implementation of robust engineering solutions. These measures are crucial to mitigate the seismic risks and safeguard the lives, livelihoods, and cultural heritage of the region's inhabitants.

The exposure of this region to seismic hazards is substantial, posing a considerable threat to the safety and integrity of the built environment. Most of the buildings in these high-risk areas were constructed before modern seismic codes were implemented, which further worsens the potential for damage during a seismic event.

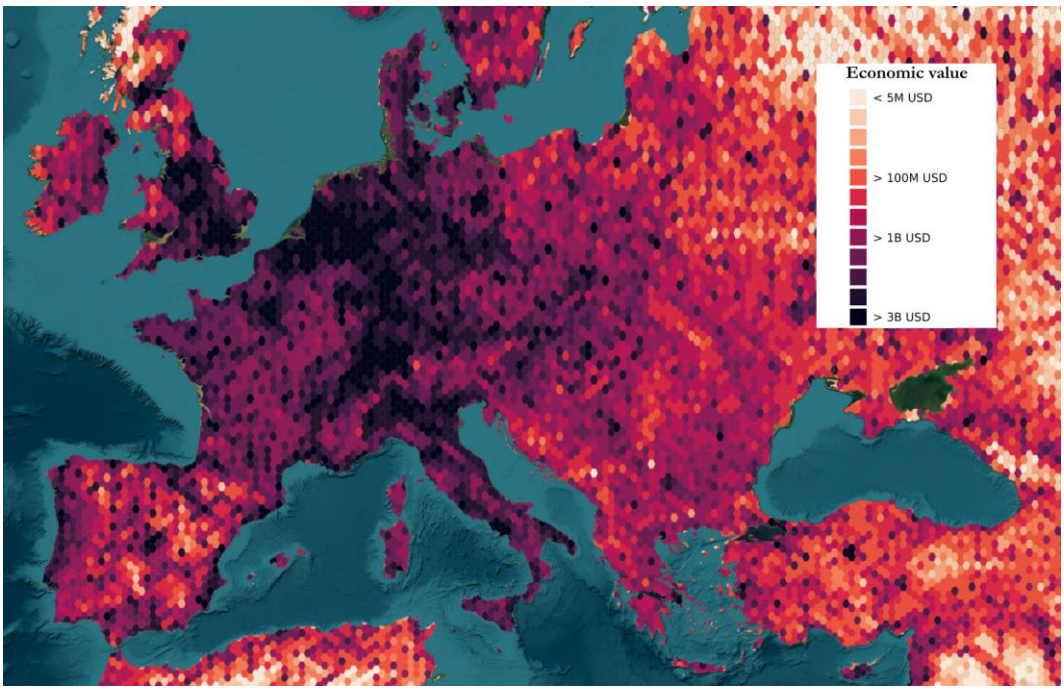

Figure 1.3 – Global Exposure Model for the Mediterranean Area (Silva et al. 2018 [4]) in terms of economic value (in US Dollars)

In addition to the concentration of the region's rich cultural heritage, with numerous historic buildings and monuments, in areas of high seismic risk, a further concern lies in the high economic exposure of these areas. Notably, in Italy, where a significant portion of this heritage resides, the economic value of land exposed to seismic risk is estimated to be around 2-3 billion USD [4] (Figure 1.3).This substantial concentration of economic value, coupled with the seismic vulnerability of historic buildings, renders Italy particularly susceptible to severe economic losses in the event of a major earthquake. Damage to buildings, infrastructure, and businesses could have a devastating impact on the local and national economies.

Table 1.1 – Reconstruction costs (normalized), reconstruction period and casualties for earthquakes occurred in Italy in the period 1968-2012

Seismic event	**Reconstruction period**	**Casualties**	**Reconstruction cost (normalized 2014) [millions €]**
Valle del Belice 1968	1968 - 2028	296	9 179
Friuli Venezia Giulia 1976	1976 – 2006	989	18 540
Irpinia 1980	1980 – 2023	2914	52 026
Umbria – Marche 1997	1997 – 2024	11	13 463
Puglia – Molise 2002	2002 – 2023	30	1 400
Abruzzo 2009	2009 – 2029	309	13 700
Emilia 2012	2012 –	27	13 300
		Total	121 608

This high-risk and high-exposure situation has resulted in excessive costs for post-earthquake repair and reconstruction over the past decades. Table 1.1 presents the estimated reconstruction costs following the major seismic events that have occurred in Italy in the last 40 years [5]. The normalized total cost to 2014 is approximately 120 billion euros, which is equivalent to the annual expenditure of the national healthcare system at that period [6].

As observed from the Table 1.1, the impacts of seismic events on affected territories extend far beyond the direct costs associated with reconstruction. The reconstruction phase often requires prolonged timeframes, leading to significant social and economic repercussions. These prolonged disruptions can result in the disintegration of the social structure of the affected communities, with consequences that may persist for several decades. The delays in rebuilding not only exacerbate the immediate economic burden but also hinder long-term regional development, impeding the recovery of local economies and social structures. This protracted period of instability and uncertainty can lead to population displacement, loss of cultural heritage, and a diminished quality of life for residents, ultimately threatening the continuity and resilience of the communities impacted by these seismic events.

In recent years, recognizing this situation, coupled with the aging of existing structures, has led many governments to promote the seismic retrofitting of existing buildings through tax incentives or funding for private construction. These measures are aimed at encouraging property owners to undertake necessary retrofitting projects, thereby enhancing the overall seismic resilience of communities. By providing financial support and incentives, governments hope to mitigate the risks associated with future seismic events, reduce potential economic losses, and protect the well-being of their citizens. This proactive approach not only addresses the immediate vulnerabilities but also contributes to the long-term sustainability and safety of the built environment in seismically active regions.

This initiative has led to a significant increase in investments in rehabilitation and maintenance activities. In 2019, such investments represented 28% of the total construction investment across the EU, although there are considerable differences between Member States. In the same year, the total investment in construction within the EU27 amounted to 1.324 billion euros [7]. Notably, in Italy, the rehabilitation segment dominated the housebuilding market, accounting for approximately 37% of total investments [7].

Currently, a vast variety of retrofitting systems are available in the market. They have been thoroughly developed, studied in detail, and are now produced

on a large scale. Despite ongoing research by the scientific community and industrial researchers to further understand the behavior and effects of these reinforcements on structures, there are inherent challenges in the design phase of retrofitting interventions.

Formal design criteria aimed at achieving specific performance targets, such as a required safety level or desired structural behavior, are largely absent. The retrofit design process is often based on a trial-and-error method, heavily reliant on the intuition and experience of the engineer. This non-rigorous approach presents several significant issues.

Firstly, identifying an appropriate retrofitting configuration typically necessitates multiple iterations. This challenge is compounded by the type of analyses used to assess the achieved safety levels, which are generally nonlinear. The nonlinear effects of the reinforcement systems contribute to a behavior that is not linear, making it difficult to accurately predict the response of the retrofitted structure with a given reinforcement configuration.

Moreover, certain types of reinforcement, such as braces and concrete jacketing in concrete structures or reinforced plasters in masonry structures, tend to increase the stiffness and/or mass of the structure. This alteration in the structural properties modifies the demand on the elements, potentially attracting more force. As a result, the response becomes even more strongly nonlinear and difficult to predict or analyze. These complexities further complicate the retrofit design process, necessitating sophisticated analytical tools and a deep understanding of structural behavior under seismic loads. This can create significant recursive design challenges. Consequently, engineers must frequently adjust and re-evaluate their designs, leading to a time-consuming and iterative process.

Additionally, it is important to note that overestimations in reinforcement do not proportionally increase safety. Instead, they can lead to unnecessary costs and complications without corresponding benefits in structural performance.

The second major concern, related to the previous points, is the lack of cost control in the retrofitting process. It is often unclear whether a proposed retrofitting solution is the most cost-effective option. This uncertainty frequently leads to overestimation of the necessary reinforcements, resulting in additional expenses due to increased invasiveness and prolonged downtimes. Thus, there is a pressing need for engineered design methodologies that target specific performance goals, ensuring both efficiency and cost-effectiveness in seismic retrofitting efforts.

From a design perspective, employing an empirical approach necessitates multiple trial-and-error attempts, leading to considerable time consumption in seeking an optimal balance between safety and costs. This time requirement is notably increased when safety assessments are conducted using nonlinear analysis methods, such as pushover analyses, which demand significantly greater computational resources for each trial iteration. As engineers work to identify the most suitable retrofitting solution, the extensive computational effort required for nonlinear analyses can substantially prolong the design process, making it even more challenging to efficiently achieve the desired structural performance and cost-effectiveness.

In this context, formalized design methods for seismic retrofitting are far from being mere academic exercises; they are essential tools for protecting communities and their building stocks from the significant effects of seismic events. By developing standardized frameworks, the engineering community can enhance the seismic resilience of building heritage. Such efforts are fundamental for safeguarding lives, preserving cultural heritage, and ensuring the economic stability of regions prone to seismic activity.

Recently, this issue has garnered significant attention, with various authors proposing a range of frameworks and methodologies to address the complex challenges associated with seismic retrofitting of existing structures. These contributions explore diverse approaches, including innovative structural design techniques and optimization algorithms. The proposed methods vary in both application and approach, reflecting the multifaceted nature of the problem. This expanding frame of research underscores the importance of a comprehensive strategy for seismic retrofitting, recognizing that successful implementation requires a careful balance of technical and economic considerations.

1.1 State of the art of the design procedures for seismic retrofitting of existing structures

Seismic retrofitting involves the modification of existing structures to enhance their resistance to seismic activities such as earthquakes. This process aims to improve the building's structural performance, ensuring safety and minimizing damage during seismic events. The main objective is to correct the inherent weaknesses and deficiencies in a building's original design concerning seismic performance. This process can significantly enhance a building's ability to withstand earthquakes, ensuring it meets or even surpasses the limit states set by modern seismic codes.

The global regulatory framework for the assessment and design of seismic retrofitting interventions encompasses a variety of standards and guidelines developed by different regions to address the unique challenges posed by existing structures.

In Europe, the primary reference for the safety analysis and retrofitting design of existing buildings is Eurocode 8, specifically Part 3 (EN 1998-3) [8]. Eurocode 8 provides comprehensive guidelines for evaluating the seismic performance of existing structures, detailing the procedures for assessing structural vulnerabilities and designing appropriate retrofitting solutions. This standard emphasizes the importance of achieving an adequate level of safety and performance, ensuring that retrofitted structures can withstand seismic events in accordance with modern engineering practices.

Eurocode 8 focuses on the strengthening and repair of buildings, outlining methodologies for seismic assessment, performance requirements, verifications procedures and modelling of the effect of retrofitting techniques. It provides detailed criteria for evaluating the capacity of existing structures,

The development of seismic retrofitting guidelines in the United States began with early efforts such as the SEAOC Vision 2000 (Poland et al. 1995 [9]) report and the FEMA 273 [10] and FEMA 274 [11]. These initial guidelines laid the groundwork for systematic approaches to retrofit existing buildings for improved seismic performance. Subsequently, a comprehensive and detailed guide on performance-based design for seismic retrofitting was published: the Pre-standard and Commentary for Seismic Rehabilitation of Buildings, FEMA 356 [12]. This document provided an in-depth framework for implementing performance-based seismic retrofit strategies, further enhancing the ability to design interventions that meet modern seismic resilience standards. An additional standard for seismic evaluation and retrofitting of existing buildings is the ASCE/SEI 41-17 [13]. This standard, developed by the American Society of Civil Engineers (ASCE), provides a comprehensive framework for evaluating and improving the seismic performance of existing structures.

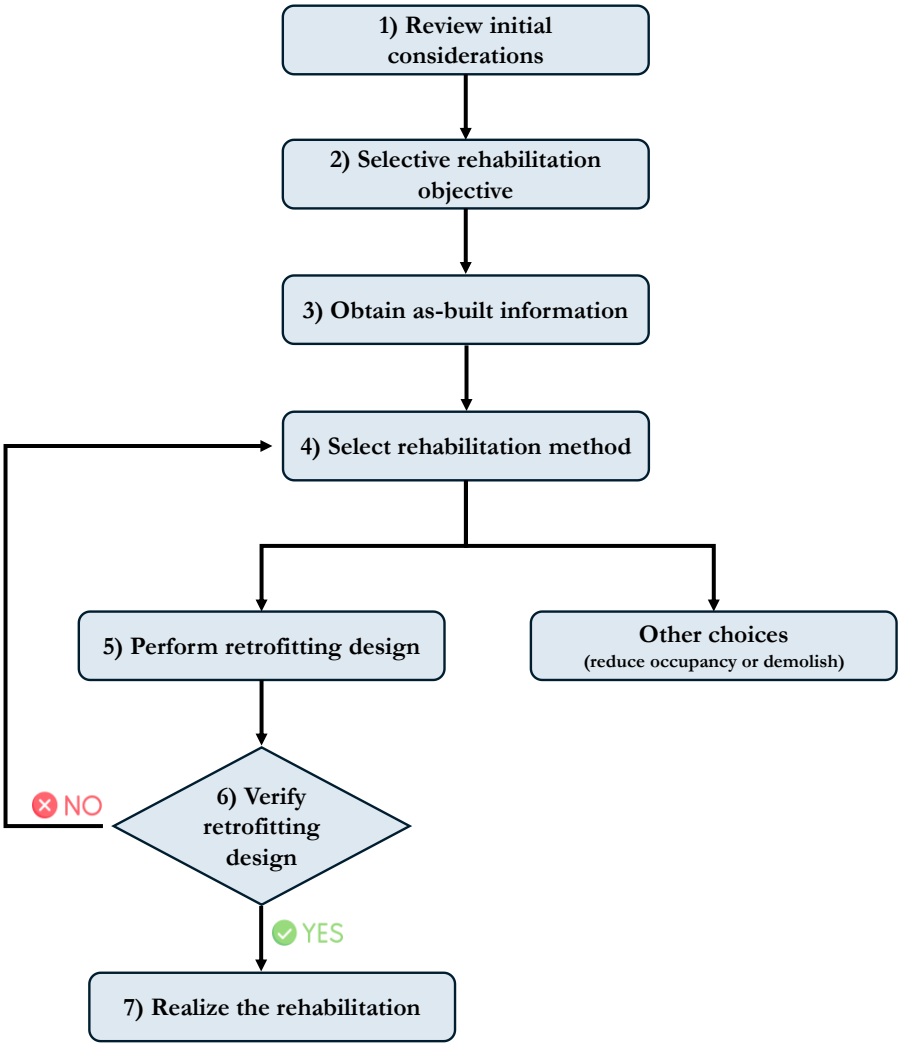

Figure 1.4 – Schematic workflow of the retrofitting design procedure according to FEMA 356 [12]

Figure 1.4 schematically represents the logical workflow proposed by FEMA 356 for the design of seismic retrofitting interventions. Following an initial assessment and the selection of performance objectives, the process includes phases for the selection of appropriate interventions and their subsequent design. The subsequent sections detail the principal aspects of this procedure, emphasizing critical elements and highlighting ongoing challenges that may still need to be addressed.

1.1.1 Review of the initial considerations

The initial review involves assessing several key factors that influence the approach to seismic rehabilitation. These factors include the structural characteristics of the building, such as its design and materials, as part of a phase called *historical-critical analysis*. It is also essential to understand the occupancy, which encompasses the current and future use of the building, the number of

occupants, and the nature of activities conducted within. Economic considerations play a crucial role, involving the evaluation of the financial aspects, including the budget for retrofitting and the cost-benefit analysis of different rehabilitation options. Societal issues must be addressed, considering the potential impact on the users of the structure, such as the displacement of residents or the disruption of local services due to the downtimes required to realize the rehabilitation. Finally, it is imperative to comply with local jurisdictional requirements, ensuring adherence to regional building codes, regulations, and any specific requirements imposed by local authorities.

1.1.2 Selective rehabilitation objectives

The second step involves defining the selective rehabilitation objectives, which include determining the target building performance level and assessing the seismic hazard.

- **Target Building Performance Level**

The performance levels are defined by referencing the damage status described qualitatively. These levels are determined with the goal of minimizing the expected total cost of using an earthquake-resistant facility. Vision 2000 [9] proposed to define structural performances in terms of performance levels (Figure 1.5).

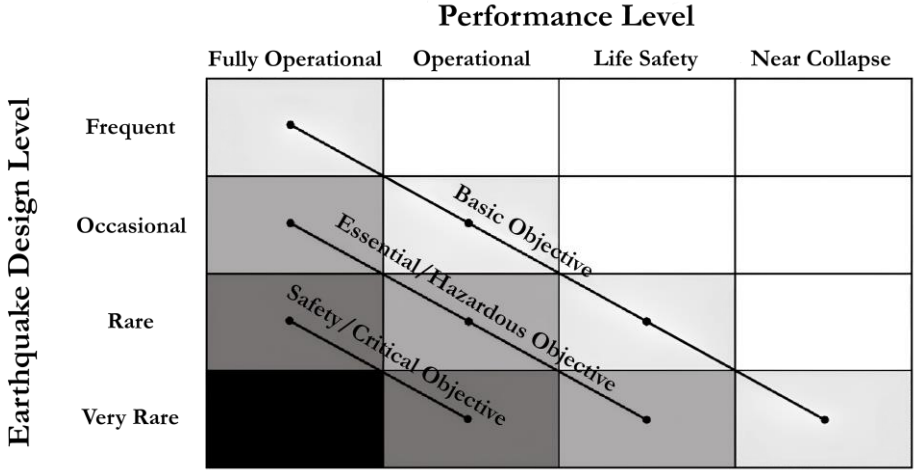

Figure 1.5 – Performance matrix (Vision 2000 [9])

This includes considering the expected costs of any damage consequences, such as repair costs, loss of use, and other potential impacts from future earthquakes. The term "performance level" refers to the structure's ability to protect occupants and contents, representing a discrete physical condition identified from a continuous spectrum of possible damage states under a certain level of earthquake.

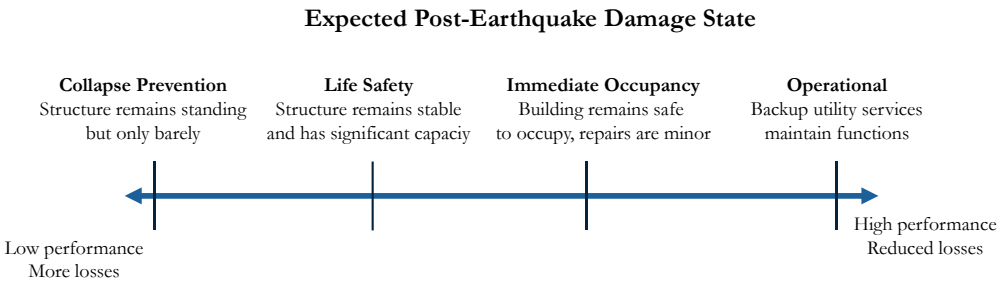

Figure 1.6 – Target building performance levels and ranges (ASCE/SEI 41-17 [13])

For existing buildings, the Performance-Based Design (PBD) approach can balance short-term costs and disruptions against the potential benefits of a retrofitting program. This approach has significantly improved the engineer's decision-making process, leading to more reliable and cost-effective solutions. It provides designers with more choices regarding the building's performance beyond just the objective of human life safety. The limit states commonly used are those proposed by ASCE guidelines.

- **Seismic Hazard**

In this step, seismic hazard is also assessed using either code-prescribed spectra or seismic hazard spectra derived from validated models. These spectra are used to analyze or verify the structure's performance. They can be transformed into equivalent forces or used to check the demand in terms of ductility or displacement, or for the selection of spectrum-compatible accelerograms. This assessment ensures that the rehabilitation design considers the appropriate seismic demands, leading to a robust and effective retrofitting strategy.

1.1.3 Select rehabilitation method

In this step, the appropriate type of retrofitting to be used is selected. A vast range of techniques can be used in seismic retrofitting include strengthening structural elements, adding bracing, and employing advanced materials and technologies to isolate or increase the damping.

Nowadays a vast variety of retrofitting techniques has been developed and are available in the market, which can be broadly categorized into local and global interventions.

Local interventions include techniques that focus on enhancing the strength and ductility of specific structural elements. For concrete structures, this may involve wrapping columns and beams with Fiber Reinforced Polymer

(FRP), steel jacketing, or concrete jacketing. For masonry structures, options include the application of reinforced plasters and the use of Fiber-Reinforced Cementitious Matrix (FRCM) systems. These local methods are effective in targeting and strengthening critical components of the building, thereby improving its overall stability and performance during seismic events.

Global interventions encompass more comprehensive solutions that affect the entire building's behavior. These methods include the addition of concrete shear walls, which provide increased lateral stiffness and strength. Base isolation systems are another global strategy, aiming to decouple the building from ground motion, thereby reducing seismic forces transmitted to the structure. The use of metallic braces can enhance the lateral load-bearing capacity, while the incorporation of viscous dampers, both fluid and solid types, can significantly increase energy dissipation, reducing the building's response to seismic excitations.

Considering

$$F_d = \frac{S_a(T) \cdot m}{q} = \frac{F_E}{q} \tag{1.1}$$

where $S_a(T)$ is the pseudo-acceleration evaluated at the fundamental period of the structure T, m is the mass of the structure, $F_E = S_a(T) \cdot m$ is the elastic design strength, and q is the behavior factor, i.e. the ratio between the inelastic strength and the strength in the hypothesis if the structure remain in the elastic behavior [14] that is a valid index of the capacity of the structure to dissipate energy through inelastic deformations.

Under the simplified hypothesis that the behavior factor is equal to the ductility of the structure, formally valid only for structures with high fundamental period $T \geq T_c$, the previous Equation (1.1) becomes:

$$F_d = \frac{F_E}{q} = \frac{F_E}{\mu} \tag{1.2}$$

thus:

$$q\, F_d = \mu\, F_d = F_E = \text{constant} \tag{1.3}$$

The Equation (1.3) represents an equilateral hyperbola in the ductility-strength space (green curve in Figure 1.7), indicating that if the reduction factor (q) is increased, the design force level is correspondingly decreased in order to keep the elastic response force (F_E) constant. This relationship shows that as

the reduction factor increases, the system's ability to dissipate energy also improves, resulting in a lower design force requirement. Since q can be set directly proportional to the ductility (μ), or is generally related to it (Fajfar et al. 1994 [15]), an increase in q implies that the ductility also increases. This means that the structure's capacity to undergo inelastic deformations without significant loss of strength is enhanced, leading to improved seismic performance.

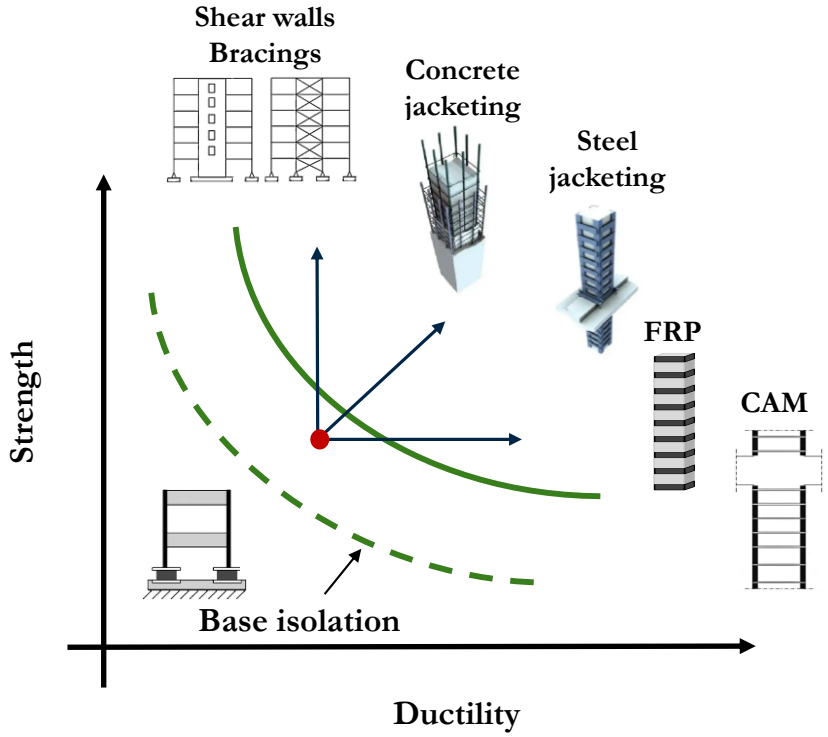

Figure 1.7 – Effect of different retrofitting techniques on seismic performance of the structure in terms of strength and ductility (loosely inspired by [16])

These considerations can be instrumental in defining the type of structural behavior that can be enhanced through a retrofitting intervention. One can choose to proceed by increasing the ductility of the structure, which allows it to undergo greater deformations without significant loss of strength, or by enhancing its capacity, thereby improving its ability to resist higher loads.

Following this, an alternative approach can be considered, which involves reducing the seismic demand on the structure. This can be effectively achieved through base isolation. By decoupling the building from ground motions, base isolation significantly lowers the forces transmitted to the structure, enhancing its overall seismic performance and ensuring greater protection against earthquake-induced damages.

These strategies not only improve the resilience of the building but also provide a flexible framework for engineers to tailor retrofitting measures

according to the specific needs and conditions of the structure. By carefully assessing the building's existing conditions and performance requirements, the most appropriate intervention method can be selected to achieve the desired level of seismic safety.

These interventions are designed to either enhance the ductility and capacity of the structure/element or to reduce the seismic demand on the superstructure (Figure 1.7), thereby improving the overall seismic performance and resilience of the building. The choice methods to implement depends on various factors, including the specific vulnerabilities of the building, architectural constraints, and economic considerations.

Table 1.2 – Effect of local and global retrofit measures on building performances (based on [17], [18], [19] and [20]). The character (+) means increase and (-) means decrease.

	Technique	Strength	Stiffness	Ductility	Irregularity	Force demand	Deformation demand
Local	Concrete jacketing/ reinforced plasters	+	+	+		-	+
	Steel jacketing	+		+			
	FRP jacketing	+		+			
	FRCM (masonry)	+		+		+	
Global	Bracings/ Shear walls	+	+		+	-	+
	Viscous dampers		+				+
	Seismic isolation		-		+	+	+

Different retrofitting systems have distinct mechanisms and can be particularly effective in addressing specific deficiencies in a structure. Table 1.2 presents some of the most commonly used retrofitting systems along with their respective mechanisms. When a structure exhibits multiple deficiencies or when there is a need to achieve various performance criteria (e.g., different limit states), it is common practice to employ multiple retrofitting systems in combination. This integrated approach allows for a more comprehensive enhancement of the structure's seismic performance, ensuring that all critical aspects are adequately addressed.

1.1.4 Perform retrofitting design

The phase of performing retrofitting design involves the detailed planning and specification of the interventions needed to enhance the seismic performance of an existing structure. This critical stage is currently left largely to the discretion of the designer. Based on their experience and intuition, the engineer selects one or more retrofitting systems, determining their size and position in the structure. During this phase, the process is not strictly formalized; the designer estimates and considers various factors such as implementation costs, technical feasibility, and architectural constraints. This approach relies heavily on the individual expertise of the engineer, who must balance these considerations to develop an effective retrofitting solution that enhances the seismic resilience of the structure while adhering to practical limitations.

This phase is associated with significant uncertainties because there are currently no regulatory prescriptions on the approach to be used. In professional practice, decisions are made based on non-formal methods, often relying on the engineer's judgment and experience. This lack of standardized guidelines can lead to variations in the quality and effectiveness of retrofitting designs, making it a challenging aspect of seismic retrofitting projects.

1.1.5 Verify retrofitting design

In the design verification phase, the primary step is on selecting an appropriate model to accurately simulate the effect of the reinforcement on the mechanical behavior of the structural element (local reinforcements) or the entire structure (global reinforcements). This step is crucial as it ensures that the chosen retrofitting strategies will perform as intended under seismic loading conditions. For local reinforcements, the model must capture the enhanced strength and ductility provided by the retrofitting interventions. For global reinforcements, the model should reflect the overall improved performance and stability of the entire structure.

Subsequently, assessment analyses analogous to those conducted during the evaluation of the as-built configuration are performed. These analyses include linear static, nonlinear static, linear dynamic, or nonlinear dynamic assessments. These rigorous analyses and validations are essential to confirm that the retrofitting design meets the required safety and performance standards.

The verification can be carried out in terms of the structure's capacity, such as ensuring it does not exceed target drifts or floor accelerations, or in terms of the structural elements' capacity, by setting target values for shear, bending

moment, chord rotation, etc. Additionally, verifications can be made in terms of structural ductility, or the maximum displacement achieved by the structure. These criteria help ensure that both the overall structure and individual elements can withstand seismic forces without significant damage or failure.

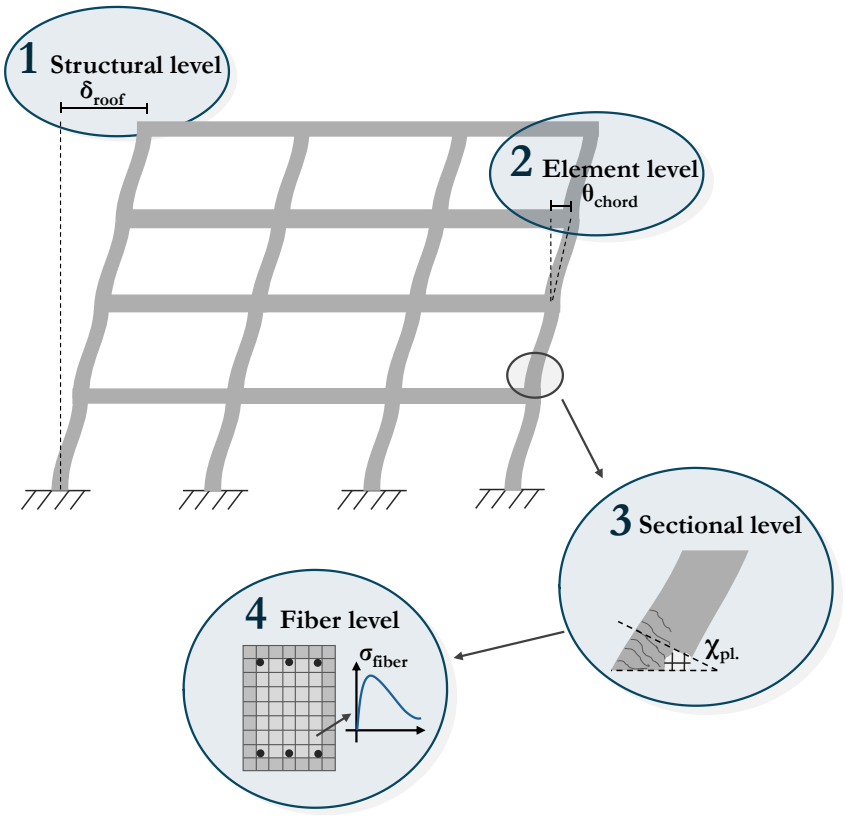

Figure 1.8 – Schematic representation of the different levels of EDP

In this phase, it is fundamental to choose the type of Engineering Demand Parameter (EDP) to be controlled. The selection of the EDP must be made such that it governs the response of the structure and is indicative of the type of deficiencies present in the as-built structure. This careful selection ensures that the chosen EDP accurately reflects the critical aspects of the structure's seismic performance, guiding the retrofitting design to effectively address these weaknesses. EDPs can be selected at various scales within the structure, including:

- **Structural level**: For example, the roof drift ratio, which provides an overall measure of the building's deformation and ductility capacity.
- **Structural element level:** Parameters such as floor drift or chord rotation, which indicate the performance of structural components (beams, columns, masonry piers, etc.) or shear and flexural capacity of them.

- **Plastic hinge region or Cross-section level**: Shear, bending moment, and plastic hinge rotation at the plastic hinge region or curvature at specific cross sections.
- **Fibers level**: If the structure is analyzed using fiber-section models (force-based or displacement-based) the EDP can control stress and strain values within the material fibers, providing detailed insights into the material's response under loading conditions.

Figure 1.8 provides a schematic representation of these different levels, illustrating how EDPs can be used to assess the performance of the structure from the overall building response down to the material level.

This hierarchical approach ensures that the selected EDPs comprehensively cover the critical aspects of the structure's seismic performance, guiding the retrofitting design to effectively address these weaknesses and achieve the desired performance criteria.

1.1.6 Realization of the rehabilitation

In this phase, the designer proceeds to develop comprehensive blueprints detailing the retrofitting system. These blueprints include all necessary specifications and construction details to guide the implementation of the retrofitting measures. Once the design is finalized, the retrofitting system is constructed within the structure. This phase also involves a rigorous quality control process to ensure that the retrofitting work meets the specified standards and requirements. Additionally, a performance monitoring plan is established to continuously assess the effectiveness of the retrofitting interventions over time, checking the aging and degradation of the materials employed, ensuring that the structure maintains its enhanced seismic resilience.

1.2 Scope of the work and thesis organization

As previously highlighted, this formalized approach, as indicated by FEMA 356 [11], has a significant and evident shortcoming: there are no formal, scientific-based methods for the design of retrofitting systems. Currently, this critical phase is accomplished exclusively based on the designer's intuition. This reliance on subjective judgment introduces several critical issues. The primary problem is that the resulting configuration is often not optimal. The lack of standardized methodologies means that designers must rely on personal experience and heuristic approaches, which can vary widely in effectiveness.

To mitigate the inherent uncertainties and ensure safety, designers tend to adopt conservative designs, which frequently involve overestimating the

necessary reinforcements. While this approach errs on the side of caution, it also leads to the inefficient use of financial resources. The excessive allocation of materials and labor not only drives up costs but also diverts funds that could be more strategically invested in other critical retrofitting projects. This misallocation can hinder broader efforts to enhance the seismic resilience of the structural heritage, as financial constraints often limit the scope and scale of retrofitting initiatives.

Furthermore, the absence of formal design methods can result in significant variability in the quality and effectiveness of retrofitting solutions. Different engineers might propose vastly different designs for similar structures, leading to inconsistent levels of safety and performance. This inconsistency further complicates efforts to systematically improve the seismic resilience of existing buildings on a large scale.

Recognizing this significant gap, the scientific community has recently focused on addressing the need for formalized methods in the design phase of seismic retrofitting. In recent years, researchers have analyzed this problem and proposed formal methods to guide the selection and design of retrofit solutions. This emerging body of work aims to standardize the design process, ensuring that retrofitting interventions are both scientifically grounded and practically effective.

The scope of this thesis is to propose some retrofitting design optimization frameworks that are scientifically based and robust enough to serve as valuable tools for practitioners. These frameworks are intended to assist during the design phase of retrofitting projects, specifically addressing phase 4 of the retrofitting design procedure proposed by FEMA 356 (Figure 1.4). The frameworks are designed to aid practitioners in the design phase, offering formal tools to enhance the effectiveness and efficiency of retrofitting interventions.

As suggested by the title of this thesis, albeit lengthy enough, it highlights only the key aspects of the various research activities presented here, all these works share a common goal: addressing the longstanding challenge of designing seismic retrofitting for existing structures, though approached from different perspectives and using diverse methods. The reader should not view this as a mere collection of separate research efforts compiled together, but rather as the development of research activities I have pursued throughout my PhD program on this subject. To paraphrase the introduction to the third edition of Dawkins' *The Selfish Gene:* I fully understand that the title, without the extensive footnote provided by the thesis itself, might give an inadequate impression of its content.

Chapter 2 presents a comprehensive literature review of current scientific research on seismic retrofitting. This chapter analyzes existing optimization frameworks and decision-making approaches used to address this problem. Additionally, it includes a bibliometric analysis of the scientific landscape to provide context and identify trends.

Chapter 3 introduces a novel optimization framework based on a genetic algorithm aimed at minimizing the implementation costs of seismic retrofitting, specifically using steel jackets for existing reinforced concrete frame structures. This chapter details new subroutines tailored to analyze structures with both ductility deficiencies and brittle failure mechanisms.

Chapter 4 proposes a framework for optimizing the life-cycle costs of retrofitting concrete structures. This framework, based on the concept of Expected Annual Loss, allows for the design of retrofitting solutions that balance initial costs with the reduced costs associated with maintaining structures in earthquake-prone areas, thereby accounting for potential restoration and repair expenses.

Chapter 5 presents an innovative optimization framework for retrofitting existing masonry structures. The algorithm focuses on determining the optimal topology of reinforced plasters, a technique that modifies the mass and stiffness of structures, thereby altering seismic demand. This framework is notable for being the first in scientific literature to employ linear static analyses, demonstrating their validity for the safety assessment of retrofitting interventions.

Chapter 6 introduces a design framework based on the seismic reliability of concrete structures, following the PEER Performance-Based Earthquake Engineering (PBEE) approach. This framework evaluates various retrofitting configurations and uses piecewise interpolation of the surface of the mean return period of limit state exceedance to enable risk-informed retrofitting design.

In the Conclusions, the findings are summarized, emphasizing the key innovations introduced through this research. Additionally, a series of proposals for future research activities are outlined, providing directions for further exploration and advancement in this field.

Chapter 2

Literature review: Design methodologies for seismic retrofitting of existing structures

This chapter provides a comprehensive overview of current research and methodologies in seismic retrofitting design frameworks. It examines the development of formalized approaches aimed at addressing deficiencies in the design phase. By analyzing contributions from various researchers, this review includes a detailed analysis of existing frameworks and methodologies, emphasizing their advantages, limitations, and practical applications within the context of seismic retrofitting. This analysis aims to provide a clear understanding of the current state of research and practice, serving as a foundation for further advancements in seismic retrofitting design.

The challenge of whether to retrofit an existing structure, and if so, what type and extent of retrofitting to employ, has been raised in various studies over the past few decades. Notably, in the early 2000s, authors published papers with emblematic titles such as Vanzi "When should seismic retrofitting of existing structures be implemented in order to minimize expected losses" (2001) [21] and Nuti and Vanzi "To retrofit or not to retrofit?" (2003) [22]. They brought significant attention to the issue of the design of retrofitting interventions, emphasizing the need for systematic approaches to determine the most effective retrofitting strategies. Their work laid the groundwork for subsequent research, which sought to formalize the selection and design processes for retrofitting interventions.

In the following years, the development of formal methods for selecting and designing retrofitting interventions continued to evolve. Calvi (2013) [23], for instance, proposed comprehensive guidelines for choosing the optimal reinforcement system. His approach was based on a detailed analysis of implementation costs and the long-term economic benefits of various retrofitting options. These guidelines provided a structured framework for decision-makers, helping them to balance immediate costs with potential future savings and structural performance improvements.

The subsequent body of literature on seismic retrofitting design frameworks is relatively modest, as the problem has only been extensively addressed in recent years. Two primary approaches have been used to tackle this issue. The first approach involves *multi-criteria decision-making* (MCDM) methods, while the second focuses on optimization techniques.

The first approach, multi-criteria decision-making methods, has been utilized in the field of seismic retrofitting. MCDM methods consider a range of factors such as cost, feasibility, and performance to guide the selection of retrofitting strategies, allowing practitioners to evaluate and prioritize different options based on a comprehensive set of criteria. These methods enable practitioners to make informed decisions by considering various factors simultaneously. The use of MCDM in seismic retrofitting has been particularly advantageous due to its structured framework, which allows for the systematic comparison of alternatives and supports the selection of the most appropriate retrofitting strategy for specific contexts.

However, a significant drawback of this approach is that it does not assist in the actual design phase of the retrofit. Instead, it focuses on the selection and comparison of different solutions, leaving the detailed design work to the user of the framework.

In contrast to MCDM methods, *optimization techniques* represent a more recent development in the field of seismic retrofitting. This approach leverages mathematical models and algorithms to identify the most effective and efficient retrofitting configurations. Optimization methods aim to enhance the seismic resilience of existing structures while minimizing costs and impact. The integration of optimization techniques into seismic retrofitting has been facilitated by advancements in computational power, which now allows for the handling of complex calculations and large datasets. This approach benefits from the application of both classical optimization algorithms and metaheuristic methods, providing a robust framework for the design of seismic retrofits. Unlike MCDM, which focuses on evaluating and comparing different retrofitting strategies, optimization techniques are not directly aimed at the

comparison between various methods or the selection of a retrofitting system. Instead, they primarily assist in the detailed design phase, offering precise solutions that can be implemented in practice.

Eventually, it can be stated that MCDM primarily addresses the selection phase of the retrofitting method (phase 3 of the previously presented workflow, as shown in Figure 1.4), this ensures that practitioners can make well-informed choices that align with the specific requirements and constraints of their projects. On the other hand, optimization focuses on the design phase (phase 4), by directly assisting in the design phase, these techniques provide precise, implementable solutions that enhance the overall performance of retrofitted structures. This delineation highlights the complementary nature of these approaches in the overall retrofitting process.

This literature review explores these two major approaches, analyzing their theoretical foundations, practical applications, and potential for improving the seismic resilience of existing structures. The review also assesses the impact of these approaches on enhancing the seismic performance of structures, identifying both the strengths and limitations of each method. Through this comprehensive analysis, the review provides valuable insights into how MCDM and optimization can be effectively integrated into seismic retrofitting practices to achieve optimal results.

2.1 Literature review methodology and overview of scientific production

This literature review presents a comprehensive overview of the research on seismic retrofitting design frameworks. The relevant studies were identified using Scopus as the primary database. The searches were conducted up to June 2024 to include the most recent advancements and findings in the field. To enhance the thoroughness of the review, both backward and forward citation procedures were employed. This involved examining the references of the identified studies (backward citation) and exploring the subsequent works that cited these studies (forward citation), thereby capturing a broader spectrum of relevant literature.

The search strategy was formulated with carefully selected keywords such as "seismic retrofitting design," "structural optimization," and "seismic retrofitting decision making," along with their possible acronyms and proper logical operators to maximize the retrieval of pertinent studies.

To maintain a focused review, the search results were filtered to include only works within the field of engineering. This exclusion criterion was applied to omit theoretical algorithm development studies from other disciplines such as

operations research and computer science, which are outside the scope of this review.

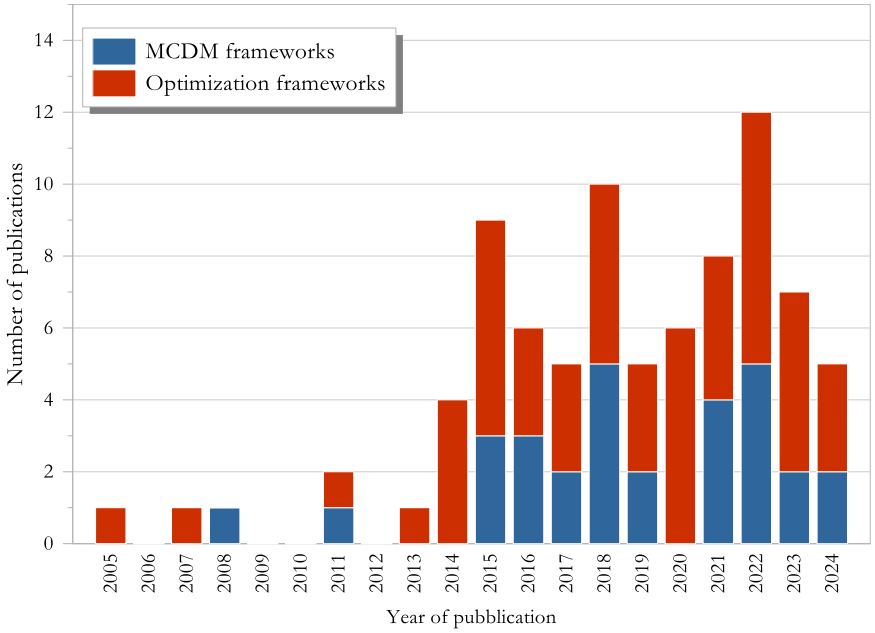

Figure 2.1 – Annual trend in the number of publications on seismic retrofitting design frameworks.

Specific criteria were established to determine which papers should be included or excluded from the study. Duplicates, primarily consisting of conference proceedings and journal papers on the same topic, and non-English records were removed from the collected files. Journal papers were excluded if the research focus was not related to seismic retrofitting design frameworks, if the paper was not peer-reviewed, if the complete paper was not accessible, and if the main findings in the paper were already discussed in prior studies. An additional filter has been applied to the civil structures.

The initial search yielded 146 papers. After removing duplicates, proceedings, and non-relevant records and a further refinement based on the inclusion and exclusion criteria resulted in 89 papers selected for detailed review. Although the body of scientific literature on seismic retrofitting design frameworks appears relatively modest, there is a noticeable and pronounced increase in research activity on this topic. As illustrated in

Figure 2.1, which shows the number of publications per year, there is a clear upward trend starting around 2005 and continuing to the present day. Despite some fluctuations in the volume of publications, the overall trend is increasing. It is important to note that the data for 2024 is excluded from this analysis due to publication lag and the fact that the year is not yet concluded.

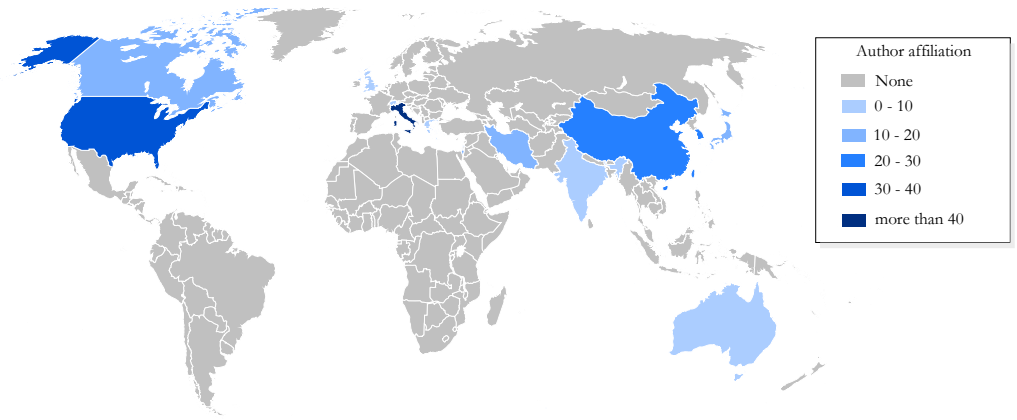

Figure 2.2 – Geographical distribution of author affiliations for publications under analysis

As can be seen from Figure 2.2, the scientific production in this field is notably high in Italy largely due to the pressing need to enhance the seismic resilience of more than 35% of the existing reinforced concrete structures to comply with the current technical codes [24]. Furthermore, recent government initiatives in Italy have introduced tax reductions for property owners who undertake retrofitting projects, significantly boosting research and development activities in this domain [25].

Following Italy, countries such as the United States, China, Canada, Switzerland, and the United Kingdom also exhibit substantial scientific output. This prolific production is driven by their strong emphasis on seismic engineering and the significant role they play in global scientific research. These countries have well-established research institutions and funding mechanisms that support extensive studies in earthquake engineering and structural retrofitting.

Greece, while showing a lower but significant volume of scientific production compared to the aforementioned countries, still maintains a significant presence in this field. This is due to the similarities it shares with Italy concerning the characteristics of existing structures and seismic hazards.

Iran has also made significant contributions to the field, this can be caused by the fact that the country faces high earthquake losses due to factors such as dense population growth [26].

Overall, the distribution of authors in seismic retrofitting research is closely aligned with the seismic risk profiles and the structural characteristics of buildings in these regions, as well as the availability of funding and institutional support for scientific research.

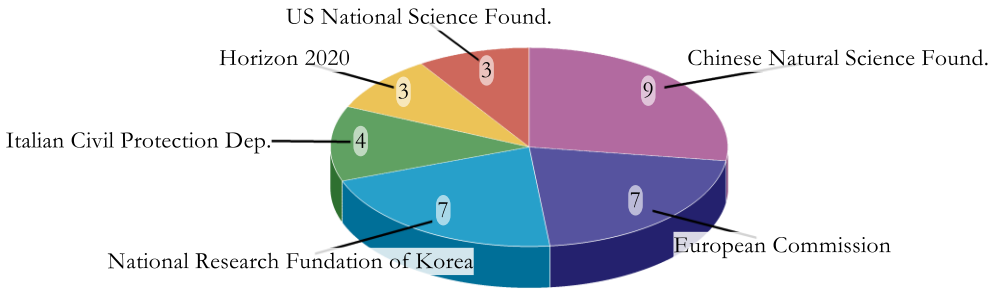

Figure 2.3 – Distribution of funding sponsors (when indicated)

As shown in Figure 2.3, the scientific interest is reflected by a similar funding sponsors plans, with significant contributions from the Chinese National Natural Science Foundation, the European Union (including Horizon 2020 program), the Italian Department of Civil Protection, and the American National Science Foundation (NSF), all contributing in a relatively balanced manner. Given this trend, it is evident that this topic continues to attract increasing financial support for further development and research.

In the following sections, the main works are presented, divided according to the two primary approaches used: multi-criteria decision-making methods and optimization techniques. For each approach, the review aims to present the key characteristics, innovations introduced to the scientific community, and the range of applications. The analysis includes a detailed examination of how these methodologies have been applied in various contexts, their strengths and limitations, and the impact they have had on advancing the field of seismic retrofitting.

2.2 MCDM seismic retrofitting design approaches

Multi-Criteria Decision-Making methods, developed within the field of operations research, are a class of decision-making tools designed to evaluate and prioritize multiple conflicting criteria. These methods support decision-making processes by providing a structured framework that allows for the systematic comparison of different options based on a comprehensive set of criteria. MCDM is particularly valuable in complex scenarios where decisions must balance various factors. Key factors typically assessed include cost, feasibility, structural performance, and implementation time. MCDM methods enable decision-makers to balance these often competing criteria to identify the most suitable retrofitting option.

In the context of selecting a retrofitting system, MCDM is often employed in its specific form commonly known as Multiple-Attribute Decision-Making (MADM). MADM focuses on evaluating a finite set of alternatives based on

multiple attributes. This approach is highly applicable to seismic retrofitting, where various potential solutions must be assessed and compared to determine the optimal strategy for enhancing structural resilience.

To effectively accomplish this kind of analyses in this context, a structured process is followed, which typically includes several key steps (Caterino et al. 2008 [27]):

1. **Definition of the set of alternatives**

This initial step involves identifying all possible retrofitting options available for consideration. These alternatives may include different structural interventions such as base isolation, bracing systems, shear walls, or damping devices. The set of alternatives must be comprehensive to ensure that all viable options are evaluated.

2. **Design of the retrofitting options**

Once the alternatives are defined, each retrofitting option needs to be designed in detail. This includes specifying the materials, methods, and structural changes required for implementation. The design phase ensures that each alternative is feasible and can be realistically implemented within the constraints of the project.

3. **Selection of the evaluation criteria**

The next step is to select the criteria against which the alternatives will be evaluated. These criteria are typically based on factors such as cost, feasibility, structural performance, implementation time, potential impact on the building's usability, and environmental impact. The selection of criteria is critical as it directly influences the decision-making process.

4. **Choose of the relative weighting of the criteria**

After selecting the evaluation criteria, it is necessary to assign relative weights to each criterion based on their importance. This weighting reflects the priorities and preferences of the stakeholders involved in the decision-making process. Various methods, such as pairwise comparison or expert judgment, can be used to determine the weights.

5. **Evaluation of the alternatives**

Each alternative is then evaluated against the selected criteria. This involves a detailed analysis of how well each retrofitting option meets the criteria. Quantitative assessments, such as cost estimation and performance simulation,

along with qualitative assessments, like feasibility and usability, are conducted during this phase.

6. **Application of the chosen MCDM approach**

The chosen MCDM method, such as the Analytical Hierarchy Process (AHP) (Santy 1980 [28]), Technique for Order Preference by Similarity to Ideal Solution (TOPSIS) (Hwang and Yoon 1981 [29]), compromise ranking method (VIKOR) (Yager 1985 [30]) or another suitable method, is applied to rank the alternatives. This step integrates the evaluations and weightings to identify the best retrofit solution based on the comprehensive analysis.

7. **Optional sensitivity analysis**

Finally, a sensitivity analysis can be conducted to investigate the stability of the solution with respect to changes in the weights of the criteria. This analysis tests the robustness of the recommended alternative by varying the importance of different criteria and observing how the rankings of the alternatives change. Sensitivity analysis helps in understanding the influence of criteria weights on the final decision and ensures that the chosen solution remains optimal under different scenarios.

2.2.1 Key publications in MCDM for seismic retrofitting design

In the following sections, a brief overview of the principal works that have proposed Multi-Criteria Decision-Making based frameworks for the design of seismic retrofitting of existing structures is provided.

Caterino et al. (2008) [27] were among the first to apply the TOPSIS technique to evaluate seismic retrofitting strategies for RC structures. This pioneering study compared four retrofit strategies: confinement with Glass Fiber Reinforced Plastics (GFRP), addition of steel bracing, concrete jacketing of columns, and base isolation. The alternatives were assessed based on criteria such as cost, duration, functional compatibility, and risk of significant damage. Using TOPSIS, the authors ranked the retrofit options and performed a sensitivity analysis to ensure robustness. This study's structured framework for integrating multiple criteria into the decision-making process set a precedent for subsequent research in seismic retrofitting design.

Bradshaw, Rajeev, and Tesfamariam (2011) [31] developed a MCDM tool designed to incorporate both engineering and socio-economic factors into the selection process for seismic retrofitting techniques. The study utilized Ordered Weighted Averaging (OWA) proposed by Yager (1985) [30] operators to

evaluate various retrofit options based on multiple criteria, including installation and maintenance costs, aesthetics, duration of work, availability of workmanship and materials, and sustainability. The tool was applied to a three-story RC structure representative of pre-seismic code constructions in southern Europe, evaluating five retrofit alternatives: FRP wrapping, steel braces, concrete jacketing, base isolation, and viscous dampers. The study highlighted the flexibility of OWA operators in accommodating the decision maker's attitude towards risk and provided a comprehensive framework for integrating diverse criteria into the decision-making process.

Zerbin and Aprile (2015) [32] present a sustainable retrofit design framework for RC frames, evaluated under varying levels of seismic demand. The study considers four retrofit solutions for an existing three-story RC school building in Forlì, Italy: light and heavy Carbon Fiber Reinforced Polymer (CFRP) wrapping, and the addition of thin and large RC shear walls. Each retrofit solution is assessed using nonlinear static analysis (pushover) and evaluated with the capacity spectrum method. The sustainability of each solution is determined by balancing structural safety improvements with lifecycle costs, including construction and repair costs. The results indicate that light and heavy CFRP wrapping significantly enhances ductility but do not increase stiffness, making them suitable for low to medium seismic demand. In contrast, the addition of RC shear walls greatly improves both strength and stiffness, suitable for high seismic demand but at a higher cost. This study highlights the importance of considering both safety and economic factors in selecting optimal retrofit strategies for existing RC buildings.

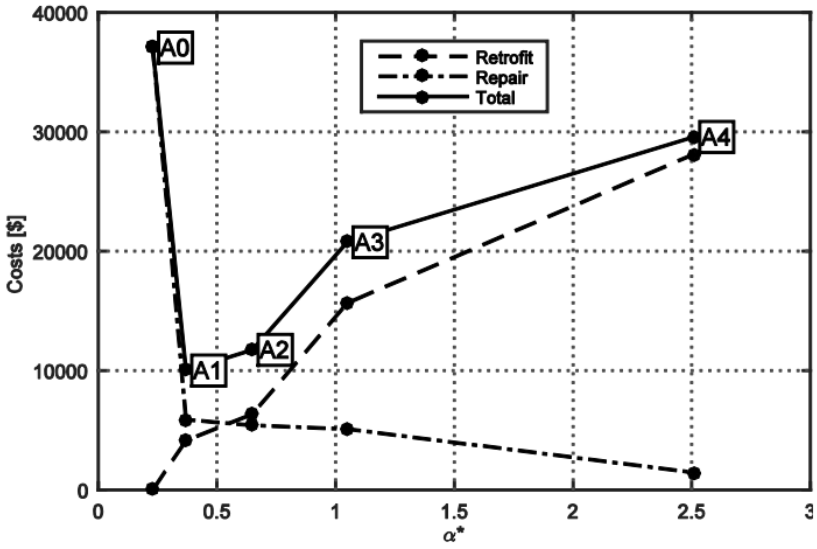

Figure 2.4 – Cost and PGA capacity-demand ratio (α^*) results for one of the case-study structures analysed by Zerbin and Aprile (2015)[33]

Anelli et al. (2016) [34] applied MCDM methods to identify optimal intervention strategies for the seismic retrofitting of school buildings. The study focused on an Italian scientific high school composed of ten independent RC structures. Four retrofit alternatives—base isolation, CFRP wrapping, steel and RC jacketing, and energy dissipation bracing systems—were evaluated using the TOPSIS and VIKOR [35] methods. Evaluation criteria included costs, feasibility, disruption of occupancy, and safety conditions during construction. The study demonstrated that MCDM methods effectively integrate technical, economic, and social criteria, providing a robust framework for selecting the most suitable retrofitting strategy. The results highlighted base isolation as the preferred option, illustrating the practical applicability of MCDM in enhancing urban resilience through strategic building retrofits.

Santa-Cruz et al. (2018) [36] proposed a comprehensive methodology integrating MCDM methods with Building Information Modelling (BIM) tools to enhance the transparency of the selection process for seismic retrofitting techniques. Focusing on public school buildings in Peru, the study employed the TOPSIS method and collaborative workshops to evaluate retrofit alternatives such as base isolation, CFRP wrapping, steel and RC jacketing, and energy dissipation bracing systems. Evaluation criteria included cost, duration, feasibility, and safety during construction, derived from BIM models. This methodology promotes transparency by incorporating stakeholder participation and visualizing decision criteria, ultimately identifying the most industrialized retrofit techniques as optimal for urban areas.

Caterino and Cosenza (2018) [37] improved their first approach (Caterino et al. [27]) proposing a multi-criteria decision-making tool to evaluate alternative seismic retrofit solutions for under-designed RC structures. This study integrates structural performance with socio-economic criteria, incorporating recent Italian tax office that offers significant tax incentives for seismic upgrades of not-conforming existing structures. The framework evaluates four retrofit strategies—confinement with GFRP, steel bracing, concrete jacketing, and base isolation—based on criteria such as installation and maintenance costs, disruption of use, and fiscal benefits. By applying the TOPSIS method, the study highlights how tax incentives can influence the choice of retrofit strategies, making initial costs less critical compared to long-term economic benefits and improved seismic performance.

Passoni et al. (2019) [38] propose a multi-step design framework based on Life Cycle Thinking for the holistic renovation of existing building stock. This study innovatively combines principles of environmental sustainability, structural safety, and economic feasibility. The approach consists of four main

phases: comprehensive assessment of the current state of buildings, identification of the most sustainable solutions, design of interventions according to Performance-Based Design criteria, and quantitative evaluation of alternatives through Life Cycle Assessment and Life Cycle Cost. This framework aims to reduce environmental impact, improve structural safety, and optimize costs throughout the entire life cycle of buildings.

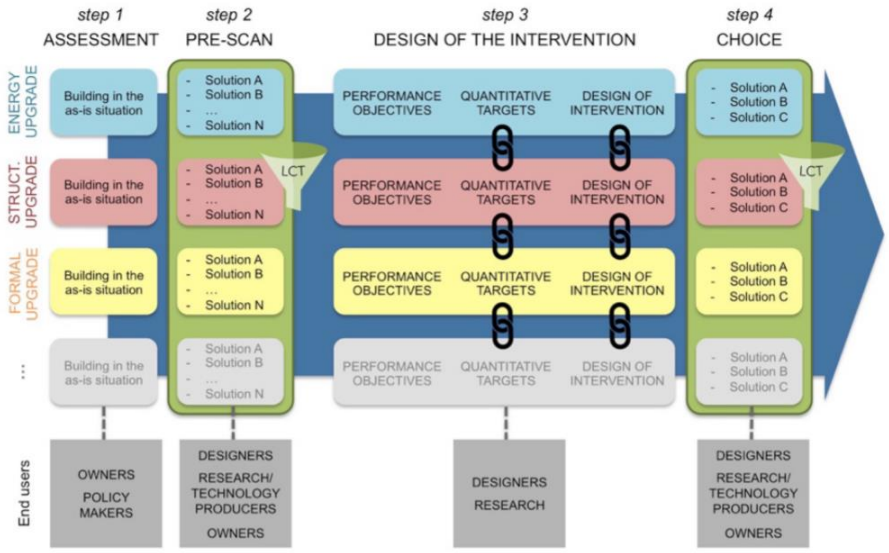

Figure 2.5 – Schematic representation of the 4-steps workflow of the MCDM proposed by Passoni et al. (2019) [38]

Gabbianelli et al. (2020) [39] investigated the effectiveness of various seismic retrofit strategies for RC school buildings using an integrated MCDM approach. The study employed the TOPSIS method combined with pairwise comparison and eigenvalue approaches to evaluate multiple retrofit options. Criteria for evaluation included economic, social, and technical aspects such as cost, execution time, and structural performance. The study focused on an RC school building in central Italy and compared three retrofit strategies: FRP wrapping, external steel braces, and a hybrid approach combining both methods. The results demonstrated that the hybrid strategy provided the most comprehensive improvement in structural performance and economic feasibility, highlighting the utility of integrated MCDM approaches in optimizing retrofit decisions.

Labò et al. (2020) [40] present a comprehensive framework for the sustainable renovation of existing buildings, integrating MCDM methods within a Life Cycle Thinking (LCT) approach. The framework aims to identify the most sustainable retrofit options by evaluating environmental, social, and economic impacts. This study employs the TOPSIS method for the pre-screening of retrofit solutions for a typical post-WWII RC building located in North of Italy.

The framework consists of four steps: evaluation of the existing building's condition, qualitative pre-screening of retrofit solutions using MCDM, design of selected solutions with performance-based methods, and the final choice of the best retrofit option. Criteria inspired by LCT principles are defined to assess potential impacts throughout the building's life cycle. In this application, six retrofit alternatives were considered: frame joint strengthening, strengthening of selected bays, base isolation, RC shear walls, steel shear walls, and a steel diagrid exoskeleton. The criteria included factors such as duration of works, renovation costs, need for additional space, and recyclability.

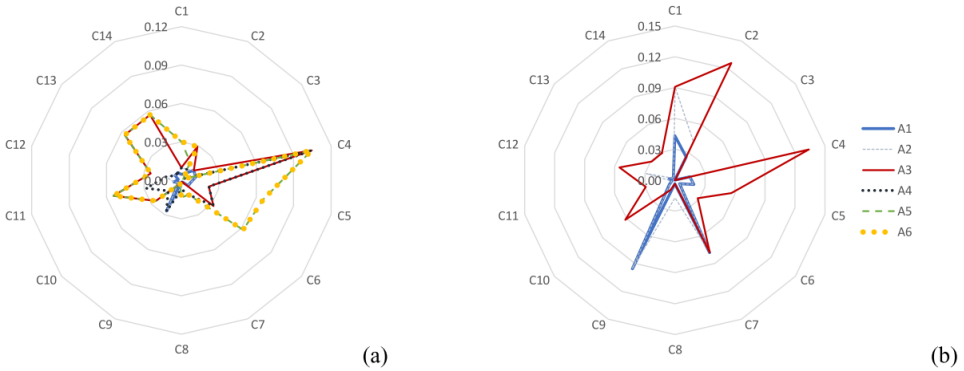

Figure 2.6 – Spyder charts representing the performance of different retrofitting alternatives with respect to different criteria (Labò et al. (2021) [40])

Gentile and Galasso (2022) [41] present a simplified yet effective approach for selecting optimal seismic retrofit solutions for RC buildings. This study applies MCDM explicitly considering earthquake-induced economic loss as a crucial decision criterion. The methodology integrates simplified seismic analysis techniques, including Simple Lateral Mechanism Analysis (SLaMA)[42], pushover analysis, and time-history analysis, to derive fragility and vulnerability relationships.

The study focuses on a seismically deficient RC school building representative of those found in developing countries. Retrofit alternatives analyzed include concrete jacketing, addition of concrete walls, and steel braces, all designed to achieve moderate damage for the design-level seismic demand. The evaluation criteria encompass total retrofit cost, maintenance cost, retrofit duration, functional compatibility, specialized labor requirements, intervention on foundations, and Expected Annual Losses (EAL).

By employing MCDM, the study systematically compares the retrofit options, revealing that the ranking of alternatives is relatively insensitive to the chosen analysis method and loss metrics, even with high weight given to seismic loss. This suggests that simplified analysis methods can be reliably used for the preliminary design of retrofit alternatives, making the decision-making process

more efficient without significantly compromising accuracy. The study's framework provides a practical and robust method for integrating economic loss into the seismic retrofit decision-making process, contributing valuable insights for optimizing retrofit strategies in earthquake-prone regions.

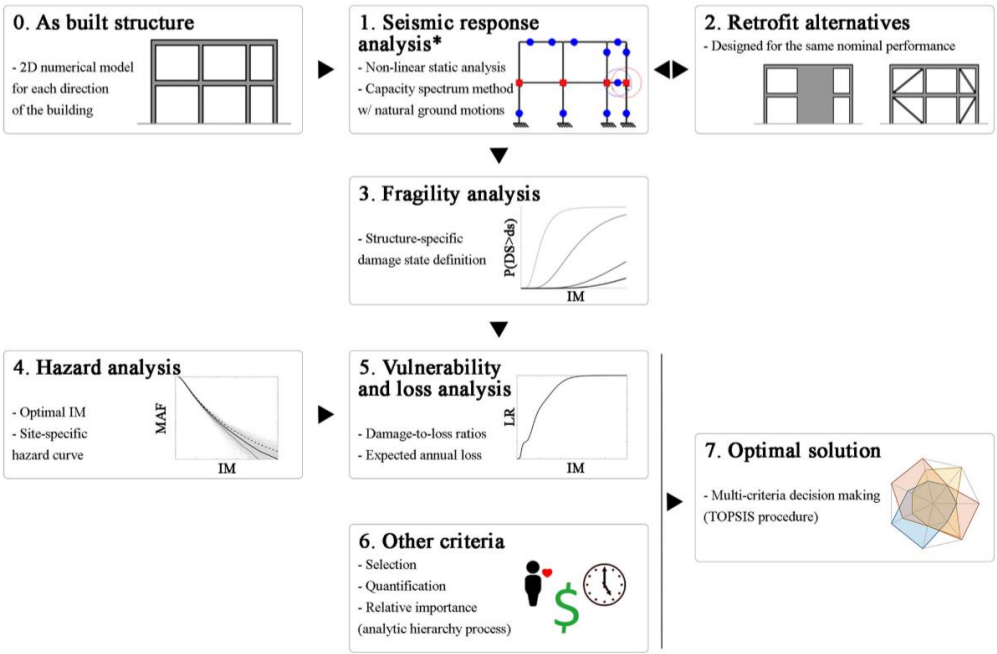

Figure 2.7 – Flowchart of the MCDM procedure proposed by Gentile et al. (2022) [41] for the chose of optimal retrofitting configuration considering insurance.

Gallo et al. (2021) [43] evaluate various MCDM algorithms to determine the optimal seismic retrofitting strategies for existing RC buildings. This study employs different MCDM methods to assess retrofit options based on criteria such as structural performance, economic impact, and operational disruption. Using a detailed numerical model of an RC school building, the study identifies retrofit interventions aimed at mitigating structural deficiencies and improving overall performance. The main novelty of this study lies in its comparative analysis of multiple MCDM methods.

Es-haghi et al. (2022) [44] investigated the seismic retrofitting of high-rise RC wall buildings using energy dissipation devices. The study applied MCDM methods to rank five passive seismic control systems: friction dampers, tuned mass dampers (TMD), viscoelastic dampers, viscous dampers, and lead-core rubber bearings. The criteria for evaluation included structural responses such as drift, acceleration, velocity, displacement, and base shear under various earthquake records. The friction damper emerged as the top-ranked solution due to its independence from velocity and vibration frequency, offering reliable control over structural response. This study emphasizes the effectiveness of

MCDM in handling complex decision-making processes for enhancing the seismic resilience of tall buildings.

Clemett et al. (2022) [45] explore the integration of environmental impact into the MCDM framework for selecting seismic retrofitting strategies. This study evaluates five retrofit alternatives for an existing RC school building in Italy, including FRP wrapping, steel braces, concrete jacketing, base isolation, and energy dissipation devices. The methodology incorporates life cycle assessment (LCA) to estimate the environmental impact of each retrofit option. Criteria such as installation and maintenance costs, structural performance, and EIs are used to rank the alternatives using the TOPSIS method. The study highlights the significance of including environmental considerations in retrofit decisions, demonstrating that environmental impact parameters can influence the choice of optimal retrofitting solutions. This approach promotes sustainable seismic retrofitting by balancing structural, economic, and environmental criteria.

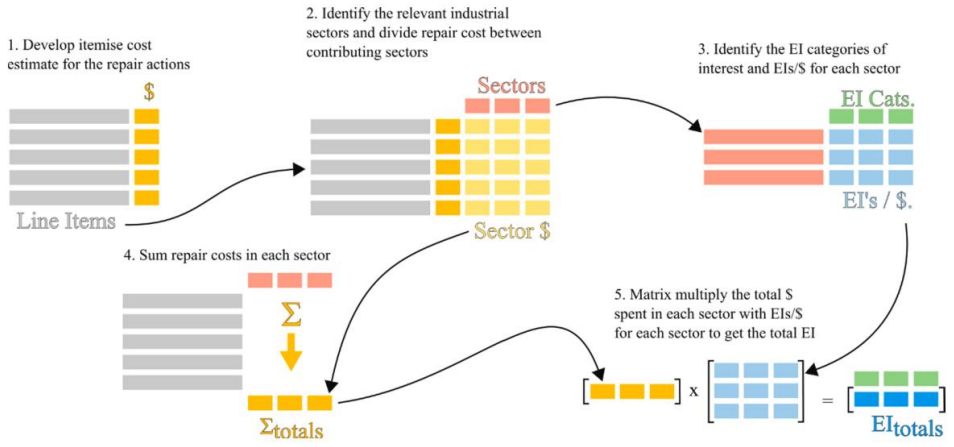

Figure 2.8 - Retrofitting impact assessment procedure proposed by Clemett et al. (2022) [45]

Couto et al. (2024) [46] investigate the combined impact of seismic hazard and climate conditions on the multi-criteria-based retrofitting of existing buildings. The study applies a MCDM framework to an RC school building, considering twelve combinations of seismic and energy retrofitting interventions. The building is analyzed across nine different locations in Italy, each with varying seismic hazards and distinct climate conditions. This dual consideration allows for a comprehensive evaluation of both structural resilience and energy efficiency.

The study highlights the importance of integrating climate-related factors, such as temperature fluctuations and energy demands, into the retrofit decision-making process. By comparing detailed seismic performance assessments with a simplified practice-oriented approach to evaluate annual probability of failure

and expected annual losses, the research underscores the significance of accessible and efficient evaluation methods. The findings stress that simplified approaches can effectively support preliminary retrofit decisions, ensuring that both seismic and climate-related performance criteria are adequately addressed.

Nigro et al. (2024) [47] investigate the use of steel exoskeletons as a seismic upgrading technique for existing reinforced concrete (RC) frame structures. The study evaluates different base shear force intensities to balance seismic performance with economic and ecological impacts. Three design scenarios are assessed using nonlinear static (pushover) analyses and life cycle assessments (LCA) to quantify the environmental impact. The findings suggest that a moderate base shear force intensity, combined with targeted local interventions, provides significant performance improvements while minimizing costs and environmental impacts.

2.2.2 Results considerations and future direction trends

Table 2.1 provide a comprehensive overview of the main characteristics of the principal MCDM framework developed for tackling the seismic retrofitting chose design phase.

In general, it can be observed that the entirety of the studies focusses on reinforced concrete structures, many of which are school buildings, with some more recent research dedicated to high-rise structures. The decision variables in these studies are typically categorized into economic (implementation costs, long-term costs, and, in one case, potential tax deductions), social (downtime periods and invasiveness of the interventions), environmental (primarily equivalent CO_2 emissions during implementation and challenges in recycling materials during decommissioning), technical (operational difficulties, need for specialized or highly specialized workers, safety issues, and additional space requirements), together with the obvious structural performances.

In recent years, the TOPSIS method has seen widespread application in addressing these types of problems. Since the 2010s, TOPSIS has predominantly become the method of choice for tackling such issues, establishing it as the most used tool for multi-criteria decision analysis in this field.

A notable trend in recent literature is the increased emphasis on environmental decision variables. This shift is likely driven by heightened scientific and legislative focus on sustainability and the environmental impact of construction practices. Researchers are increasingly incorporating metrics such as CO_2 emissions and material recyclability into their frameworks, reflecting a

broader commitment to sustainable development and environmental stewardship.

Another emerging direction in the field is the use of more rigorously estimated weights and criteria in MCDM analyses. Historically, the determination of these factors has often been left to the discretion of the final user, introducing a degree of subjectivity and potential inconsistency. Current and future research aims to address this limitation by developing standardized methodologies for estimating weights and criteria more objectively. This advancement is crucial for enhancing the reliability and validity of MCDM frameworks, ensuring that the evaluation and selection of seismic retrofitting strategies are based on robust and reproducible criteria.

Table 2.1 – Summary of the studies proposing a MCDM design approach for the design of existing structures retrofitting

Reference	Structural systems	Retrofitting techniques	MCDM Algorithm(s)	Objective functions
Caterino et al. 2008 [27]	RC frame structures	• GFRP • Steel braces • Concrete jacketing • Base isolation	TOPSIS	• Economical • Social • Technical
Bradshaw et al. 2011 [31]	RC frame structures	• FRP • Steel braces • Concrete jacketing • Base isolation • Viscous dampers	OWA	• Economical • Technical
Zerbin and Aprile 2015 [32]	RC school structures	• Light FRP • Heavy FRP • Thin RC walls • Large RC walls	Multi-step MCDM	• Economical • Technical • Environmental
Formisano and Mazzolani 2015 [48]	RC frame structures	• Base isolation • BRB and shape memory alloy braces • FRP • Metal shear panels	TOPSIS	• Economical • Technical • Reversibility

Anelli et al. 2016 [34]	RC school structures	• Base isolation • CFRP • Steel jacketing • Concrete jacketing • Braces	TOPSIS VIKOR	• Economical • Technical • Safety
Formisano et al. 2017 [24]	RC school structure	• Steel braces • RC walls • Steel plate shear wall • BRB	TOPSIS	• Economical • Technical
Santa Cruz et al. 2018 [36]	RC school structure	• Base isolation • CFRP • Steel jacketing • Concrete jacketing • Braces	TOPSIS	• Economical • Technical • Safety
Caterino and Cosenza 2018 [37]	RC frame structures	• GFRP • Steel braces • Concrete jacketing Base isolation	TOPSIS	• Economical • Fiscal benefits • Long term economic benefits • Technical

Passoni et al. 2019 [38]	RC structure	• Base isolation • RC walls • Steel walls • Base isolation • Steel exoskeleton	TOPSIS	• Economical • Recyclability • Duration of works • Additional space
Gentile and Galasso 2021 [41]	RC school structures	• Concrete jacketing • RC walls • Steel braces	AHP TOPSIS	• Economical • Technical
Gallo et al. 2021 [43]	RC school structures	• FRP • Steel braces • FRP + braces	TOPSIS eigenvalue	• Economical • Technical • Downtimes
Es-Haghi et al. 2022 [44]	High-rise RC buildings	• Friction dampers • TMD • Viscous dampers • Base isolation	TOPSIS	• Performances
Clemett et al. 2022 [45]	RC school structures	• FRP • Steel braces • Concrete jacketing • Base isolation • Dampers	TOPSIS	• Economical • Technical • Environmental

Zuluaga et al. [49]	Masonry structures	• Timber beams • Bio-based infills	Not specified	• Environmental • Energetical • Technical
Carofilis et al. 2022 [50]	RC school structures	• FRP • Steel braces • Viscous dampers	TOPSIS	• Economical • Environmental • Social • Technical
Caruso et al. 2023 [51]	RC structures	• Base isolation • Braces • Energetic insulation • Solar panels	Normalized spyder web plot	• Economical • Environmental
Couto et al. 2024 [46]	RC school structures	• FRP • Steel braces • Viscous dampers • Thermal insulation • Efficient walls	Not specified	• Economical • Technical • Social • Environmental
Nigro et al. 2024 [47]	RC frame structures	• Steel exoskeletons • FRP	Not specified	• Economical • Performance • Environmental

2.3 Optimization frameworks for seismic retrofitting design

In the context of seismic retrofitting, the goal is not merely to select among different retrofitting strategies, but to identify the optimal configuration for a chosen strategy. This shift from a comparative evaluation to an optimization problem necessitates the use of advanced structural optimization algorithms. Unlike Multi-Criteria Decision-Making (MCDM) methods, which focus on comparing various retrofitting systems against multiple criteria, structural optimization aims to fine-tune the design variables of a single system to achieve the best possible performance.

Structural optimization in seismic retrofitting involves the application of mathematical and computational techniques to determine the most effective design parameters that enhance the performance of the structure under seismic loads. These techniques seek to minimize or maximize objective functions—such as cost, material usage, or structural response measures—while adhering to a set of constraints. The overarching aim is to develop retrofit designs that are not only structurally efficient but also economically feasible and practical to implement.

In this view, structural optimization can be a powerful tool for executing phase 4 "Perform retrofitting design" of the retrofitting design workflow presented in Figure 1.4, as opposed to MCDM frameworks which are more useful in the previous phase 3 "Select rehabilitation method". This distinction highlights the role of structural optimization in fine-tuning and implementing the chosen retrofitting strategy, ensuring that it meets the desired performance criteria effectively.

The formalization of the structural optimization problem in seismic retrofitting involves defining the objective function, design variables, and constraints that guide the optimization process. This structured approach ensures that the retrofitting design not only meets performance goals but also adheres to practical and economic considerations.

I. **Objective Function**: The objective function is a function that quantifies the goal of the optimization. In structural optimization, common objective functions include minimizing implementation costs, minimizing labor time, minimizing material usage, or a combination of these factors.

   It is crucial to distinguish the objective function from structural performance criteria, which should be treated as constraints. Structural performance represents the minimum levels that must be complied with. In engineering optimization, despite the name, the primary goal is to

achieve the desired performance levels while minimizing costs or technical complications.

For instance, the objective might be to minimize the total cost, which includes materials, labor, and implementation time, while ensuring that the structure meets predefined performance criteria. This approach ensures that the retrofitting solution is both economically viable and structurally effective. The objective function reflects the priorities of the stakeholders and the specific requirements of the retrofitting project

Recently, there has been increasing interest in incorporating environmental considerations into the optimization process. Objective functions now often include metrics such as the global warming potential, measured in terms of embodied equivalent CO_2 quantities [52]. This shift reflects a growing emphasis on sustainability and the environmental impact of construction practices.

II. **Design Variables**: Design variables are the parameters that can be set during the optimization process. These variables represent the aspects of the retrofit design that can be altered to improve performance. From a mathematical perspective, they are the free parameters of the problem.

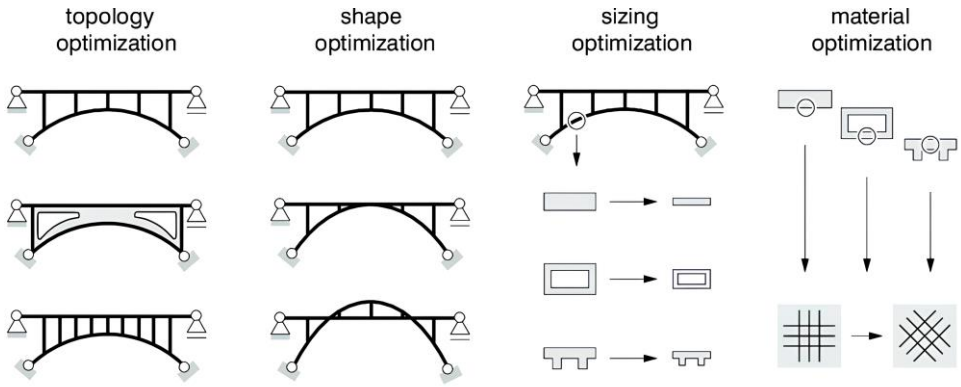

Figure 2.9 – Schematic representation of levels of structural optimization application on bridge design (Ramm et al. 1998 [53], Kato et al. 2010 [54])

In structural optimization, there are four main approaches to structural optimization, each with its specific focus and methodology:

- **Size Optimization**: This approach focuses on determining the optimal dimensions of the structural elements. Size optimization aims to find the best dimensions that balance structural performance and material usage.

- **Shape Optimization**: Shape optimization involves modifying the geometry of the retrofit elements to achieve better performance. Design variables in shape optimization might include the curvature, tapering, and spatial arrangement of these elements.
- **Topology Optimization**: Topology optimization is focusing on the layout of the material within the design space. It aims to find the optimal distribution of material to maximize structural performance while minimizing the objective functions.
- **Material Optimization**: although less explored in structural design, falls within the domain of structural mechanics or material science. It involves optimizing the mechanical properties of materials by modifying certain characteristics. In literature there are some applications related to laminated composites ([55], [56]) or metamaterials ([57], [58]) in developing materials with tailored properties to improve the mechanical performances.

Among the three categories, size optimization is the most straightforward to formalize and address for resolution (Wang et al. 2018 [59]). On the other hand, topology optimization has been extensively studied, and there is a vast body of scientific literature on this subject. This literature covers a wide range of approaches for topology optimization in continuous or approximable as continuous research spaces ([60], [61]).

In the context of retrofitting, optimization efforts primarily focus on size and topology optimization, often in combination. Conversely, applications of shape optimization in retrofitting are not found in the literature, and it is challenging to conceive how shape optimization could be effectively applied to reinforcement systems. A potential application might involve optimizing the shape of metallic braces or the positioning of viscous dampers. However, these problems can typically be addressed directly without the need for complex analytical methods.

III. **Constraints**: Constraints are conditions that must be satisfied for the solution to be feasible. In the context of seismic retrofitting, constraints typically include structural performance requirements (e.g., limitations on inter-story drifts, strength, and ductility), material stress or strains limitations, and compliance with technical codes and regulations.

From the perspective of structural optimization, structural performance criteria are critical constraints. These criteria are evaluated using Finite Element Method (FEM) analyses, which are essential for accurately simulating the behavior of structures under seismic loads. In seismic retrofitting, performance constraints are often assessed through one of the four main types of structural analyses for seismic evaluation (linear static analysis, nonlinear static analysis, linear dynamic analysis, nonlinear dynamic analysis).

Constraints ensure that the optimized design is practical and adheres to safety standards. By integrating these constraints into the optimization problem, engineers can ensure that the resulting design is not only optimal in terms of performance but also viable from practical, economic, and regulatory perspectives.

The formalization of the structural optimization problem in seismic retrofitting involves defining the objective function, design variables, and constraints ([62], [63], [64], [65], [66]). This structured approach ensures that the retrofitting design not only meets performance goals but also adheres to practical and economic considerations. The optimization problem can be mathematically expressed as follows:

$$\begin{aligned} &\text{Find } x \text{ that minimize} \quad f(x) \text{ subject to:} \\ &\qquad g_i(x) \le 0 \quad \text{for} \quad i = 1,2,\ldots,m \\ &\qquad h_j(x) = 0 \quad \text{for} \quad j = 1,2,\ldots,p \\ &\qquad x_k^{\text{lower}} \le x_k \le x_k^{\text{upper}} \quad \text{for} \quad k = 1,2,\ldots,n \end{aligned} \tag{2.1}$$

where x represents the *design variable*, which can also be a set of variables that include parameters that can be adjusted during the optimization process, in that case they are gathered in the so called "*design vector*" (for n variables it can be $\mathbf{x} = [x_1, x_2, \ldots, x_n]$).

The *objective function* $f(x)$ quantifies the goal of the optimization. In some cases, there may be multiple objective functions to minimize, leading to a *multi-objective optimization problem*. In such scenarios, the goal is to find the values of the design variables that simultaneously satisfy all objective functions or achieve a Pareto optimal solution (non-dominant solutions [67]) where no objective can be improved without worsening the others.

The *inequality constraints* $g_i(x) \le 0$, in structural optimization represent the structural performance criteria and other limitations that must be satisfied, limits on some EDPs (inter-story drifts, stresses, and strains in structural elements) or

more global requirements (like maximum displacements or ductility), a brief presentation of the structural performance indexes and EDP has been presented in the Section 1.1.1.5 (page 25).

The *equality constraints*, $h_j(x) = 0$, typically represent physical or design requirements that must be exactly met, even if are generally more easy to handle from mathematical and computational perspective, they are less frequent in structural optimization.

The *bounds on design variables* $x_k^{\text{lower}} \le x_k \le x_k^{\text{upper}}$ define the allowable range for each design variable, ensuring that the solutions are practical and feasible within the given context. These bounds are typically involved in the optimization to exclude solutions of the optimization problem that are not physically possible.

The space where the design variables are defined is called "*research space*", it can be a subset of real numbers for continuous variables restricted between boundaries or discrete for subset of natural numbers or Booleans.

2.3.1 Brief review of the algorithm commonly used in structural optimization

The optimization problems as stated in Equation (2.1) can be tackled with a vast range of optimization algorithms. Mathematically, an optimization problem involves finding the maximum or minimum of a function of one or more variables. The methods for solving this problem vary depending on the type of problem, the characteristics of the search space, and the properties of the objective function.

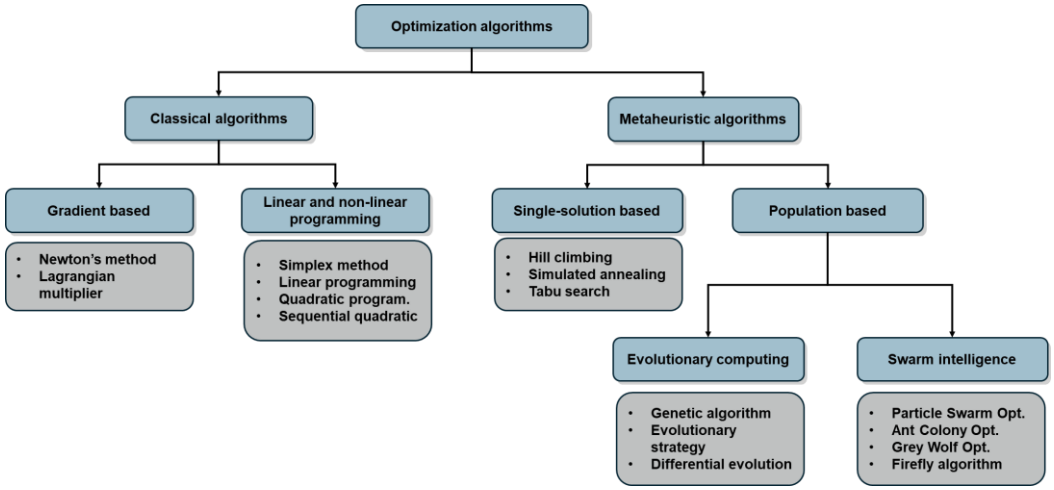

Figure 2.10 – Taxonomy of the optimization algorithms classes with non-exhaustive list of foremost algorithms (based on [68], [69], [70], [71])

Optimization algorithms can be broadly categorized into classical optimization algorithms and metaheuristic algorithms. The former rely on mathematical gradients and deterministic processes to pinpoint the position of the minima. The latter, instead, use probabilistic rules and iterative processes to explore the solution space more broadly, making them suitable for problems where the objective function is difficult to represent analytically. Each category offers distinct advantages and is suitable for different types of optimization problems.

2.3.1.1 Classical Optimization Algorithms

Classical optimization algorithms are well-established methods that typically rely on gradient information to find local or global optima. These algorithms are based on the principles of calculus developed by Newton, Leibniz and Mengoli between the 17th and 18th centuries. They are effective for problems where the objective function and constraints are smooth and differentiable. Classical algorithms are often preferred for their mathematical rigor and efficiency in solving convex problems.

A significant advancement in this field was made by George Dantzig and his research team in the mid-20th century. Between 1946 and 1947, Dantzig proposed a general solution to linear programming problems and developed the Simplex Method. This method revolutionized the field and laid the groundwork for many subsequent developments. Over the following decades, numerous research groups further refined and expanded these techniques, leading to significant improvements in the efficiency and applicability of classical optimization methods.

One of the main advantages of classical optimization methods is that, except for convergence issues, the solution found is the mathematical optimum for the problem, meaning it is the best possible solution within the given constraints and objective function. This guarantees a high level of confidence in the results, making these methods highly reliable for certain types of problems.

Despite their strengths, classical algorithms can struggle with non-convex problems and local minima, and they require gradient information, which may not always be available or easy to compute.

Below are brief descriptions of some commonly used classical optimization algorithms.

- *Gradient Descent* is a simple and widely used optimization algorithm that iteratively adjusts the design variables in the direction of the steepest descent of the objective function. This method is effective for convex problems, where it efficiently converges to a local

minimum. However, it can struggle with non-convex problems and local minima.

- *Newton's Method* extends Gradient Descent by using second-order derivatives (Hessian matrix) to accelerate convergence. This method is faster and more accurate for well-behaved functions, but it is computationally expensive, especially for large-scale problems.

- *Linear Programming* (LP) [72] is an optimization technique used for problems with linear objective functions and linear constraints. It is widely used in resource allocation, scheduling, and logistics. The Simplex Method, developed by George Dantzig, is a popular algorithm for solving LP problems efficiently.

- *Quadratic Programming* (QP) (Frank and Wolfe 1956 [73]) extends linear programming to problems with a quadratic objective function and linear constraints. This method is useful in fields such as portfolio optimization and certain types of structural design problems. QP is efficient for handling quadratic objectives, providing a balance between complexity and performance.

- *Sequential Quadratic Programming* (SQP) (Boggs and Tolle 1995 [74]) is a powerful method for solving non-linear optimization problems by solving a series of quadratic approximations. It is highly effective for constrained non-linear problems, making it suitable for complex engineering designs. Despite its effectiveness, SQP is quite a computationally intensive algorithm and requires accurate gradient and Hessian matrix.

2.3.1.2 Metaheuristic optimization algorithms

Metaheuristic algorithms, in contrast, are a more recent development, emerging in the latter half of the 20th century. These algorithms are designed to find good solutions for complex optimization problems where classical methods may fail. They do not require gradient information and are particularly useful for non-convex, multi-modal, and large-scale problems. Metaheuristics are flexible and robust, capable of exploring large search spaces and escaping local minima. However, they often require careful tuning of parameters and can be computationally intensive.

Significant early developments in metaheuristic algorithms occurred in 1954 when Nils Aall Barricelli proposed to use evolutionary mechanisms to solve

optimization problems [75]. This marked the first practical application of evolutionary concepts in optimization. A decade later, Ingo Rechenberg proposed Evolutionary Strategies (ES) [76] which further advanced the field. In 1975, John Holland introduced Genetic Algorithms (GA) [77], which became one of the most well-known and widely applied metaheuristic techniques. Holland's GA also laid the foundation for a vast array of other metaheuristic optimization algorithms, many of which are essentially variations of the Genetic Algorithm paradigm.

The main drawback of using metaheuristic algorithms is that there is no guarantee that the final solution will be the true optimum of the problem. From a mathematical standpoint, this is a disadvantage because it does not prove that the solution is the best possible one. However, from an engineering perspective, this is often not a significant issue. Engineers are typically more interested in finding a sufficiently good solution that minimizes the problem within acceptable boundaries rather than the absolute mathematical optimum.

Metaheuristics are particularly valued for their ability to handle problems with complex and noisy research spaces, multiple local optima, and high dimensionality. Their flexibility and robustness make them suitable for a wide range of applications where classical methods may struggle or fail to provide satisfactory solutions. Despite the lack of guaranteed optimality, metaheuristic algorithms often yield practical and effective solutions that meet the needs of engineering and applied sciences.

Below are brief descriptions of some commonly used metaheuristic algorithms:

- *Simulated Annealing* (SA) (Van Laarhoven et al 1987 [78]): Simulated Annealing mimics the annealing process in metallurgy, where a solution is gradually improved by exploring the search space and accepting worse solutions with a decreasing probability. This method is effective for escaping local minima but can be slow and requires careful parameter tuning.

- *Genetic Algorithms* (GA) (Holland 1975 [77], Goldberg 1989 [79]): Inspired by the process of natural selection, Genetic Algorithms use a population of candidate solutions that evolve over generations through selection, crossover, and mutation. The class of algorithms based on GA are robust and versatile, suitable for multi-objective optimization. They are particularly useful for problems with complex landscapes but can be slow to converge.

- *Particle Swarm Optimization* (PSO) (Kenney and Eberhart 1995 [80]): Particle Swarm Optimization is inspired by the social behavior of birds flocking or fish schooling. It optimizes a problem by iteratively improving a population of candidate solutions based on their own and their neighbors' best positions. PSO is easy to implement and effective for many problems but can struggle with high-dimensional spaces.

- *Ant Colony Optimization* (ACO) (Gambardella and Dorigo 1996 [81]): Based on the foraging behavior of ants, Ant Colony Optimization uses a population of artificial ants that build solutions by moving on a problem graph and depositing pheromones to guide future ants. ACO is effective for discrete optimization problems like routing and scheduling but can be computationally expensive.

- *Differential Evolution* (DE) (Storn and Price 1995 [82]): Differential Evolution is a population-based optimization algorithm that iteratively improves candidate solutions based on differences between randomly selected pairs of solutions. DE is simple to implement and effective for continuous optimization problems but can be slow to converge and sensitive to parameter settings.

- *Non-dominated Sorting Genetic Algorithm II* (NSGA-II) (Deb et al. 2002 [83]): Based on the Genetic Algorithm is an evolutionary algorithm specifically designed for multi-objective optimization. It involves a non-dominated sorting approach together with a particular elitism function and a crowding distance mechanism to maintain diversity in the population. NSGA-II is particularly effective for solving complex optimization problems with multiple conflicting objectives but requires sensitive tuning of the parameters to achieve good performances.

One of the main characteristics of metaheuristic algorithms is that the search space is examined point by point. Therefore, it is not necessary to know the properties of the entire search space. This makes metaheuristics particularly suitable for structural optimization problems, where each solution corresponds to a different structural configuration that must be analyzed using a specific analysis method, mainly FEM analyses. While this property is advantageous for implementing the optimization process, it also makes metaheuristic algorithms slower and more computationally demanding than classical ones.

In recent years, hybrid approaches that combine different optimization techniques have shown promise in enhancing the efficiency and effectiveness of the optimization process. There is also increasing interest in combining optimization algorithms with neural networks (Falcone et al. 2022 [84]) or statistical predictors (Yi and Taflanidis 2023 [85]) to speed up the optimization process.

Structural retrofit optimization seeks the most effective ways to enhance the performance and resilience of existing structures under seismic loads. This involves balancing objectives like cost, performance, and feasibility while adhering to structural performance requirements and technical codes. Advanced optimization algorithms are essential for handling the complex trade-offs between design variables and constraints, enabling engineers to explore a wide range of retrofit options, identify the best solutions, and ensure that the final design meets all necessary safety and practicality criteria.

2.3.2 Significant studies in optimization frameworks for seismic retrofitting design

The application of this class of algorithms has been extensively utilized in the field of structural optimization, particularly for solving complex and large-scale problems in structural engineering (Quaranta et al. 2020 [86], Falcone et al. 2020 [68], Lagaros et al. 2022 [87]).

Specifically, they have been widely employed in the design of new structures to identify optimal solutions. These solutions often focus on sizing but also extend to the topology and, in some cases, the shaping of new civil structures (Lagaros et al. 2002 [88], Govindaraj and Ramasamy 2005 [89], Govindaraj and Ramasamy 2007 [90], Mitopoulou et al. 2011 [91], Papavasileiou and Charmpis 2016 [92], Babaei and Mollayi 2016 [93], Pham and Hong 2022 [94], Kanyilmaz et al. 2022 [95]).

In recent years, numerous studies have applied these optimization techniques to solve retrofit problems for existing structures. These works demonstrate the practical utility of both classical and metaheuristic algorithms in developing retrofit strategies that meet the complex requirements of structural performance and economic efficiency. Below, it is reported a review of some key contributions to the field, highlighting the approaches and findings of each study. These studies exemplify the diverse strategies employed by researchers to optimize the retrofitting of existing structures, illustrating how optimization algorithms can be harnessed to achieve enhanced structural performance, economic efficiency, and overall feasibility.

Although not directly related to seismic retrofitting of building structures, an early application of optimization for enhancing structural performance in the

seismic field is noteworthy. Wang et al. (2010) [96] introduced a GA algorithm for the design of bridge beam isolation. This pioneering work laid the foundation for subsequent optimization approaches in seismic retrofitting by demonstrating the efficacy of GAs in achieving optimal structural performance.

The first notable application in the area of retrofitting existing structures is a study by Zou et al. (2007) [97], who proposed a closed-form equation for retrofitting concrete columns with FRP. This research addresses the issue of inadequate seismic resistance in concrete structures designed to outdated codes by using FRP jackets to enhance the strength and ductility of columns. The design variables include the thickness of the FRP jackets applied to the columns. The study employs nonlinear pushover analysis to evaluate the seismic performance of the retrofitted structures, with the optimization objective being to minimize the volume of FRP material used while ensuring improved seismic performance.

Lavan and Dargush (2009) [98] proposed one of the first optimization framework for seismic retrofitting strategies for multi-story buildings, focusing on a ten-story industrial frame and a five-story steel frames. Their research explored the use of passive energy dissipation systems, including hysteretic, viscoelastic, and viscous dampers, as well as a combined weakening plus damping approach. The design variables included the type, size, and placement of the dampers within the structures. Time-history analyses were conducted to evaluate the response of these structural models to various seismic events. The optimization objectives were to minimize maximum inter-story drifts and total accelerations, aiming to reduce structural damage and enhance seismic resilience. By leveraging advanced optimization techniques, they systematically explored various retrofit options and identified solutions that met stringent performance criteria while remaining cost-effective.

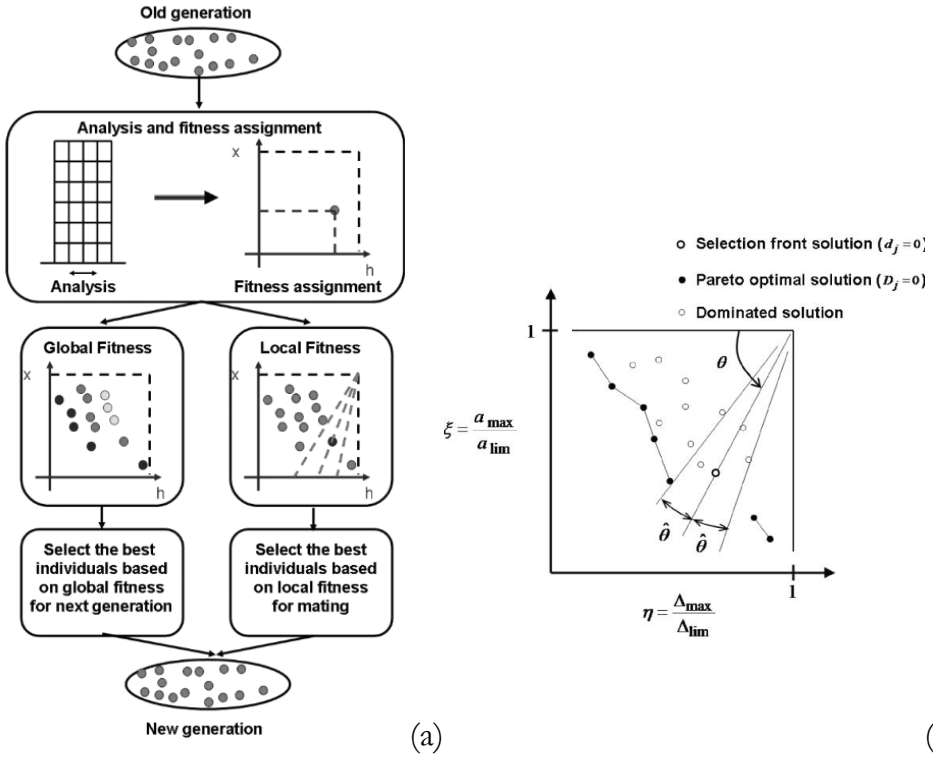

Figure 2.11 – Multi-objective Genetic Algorithm for the optimal research of passive energy dissipation systems(Lavan and Dargush (2009) [98]) (a) Flowchart of the GA procedure for the creation of a new generation, (b) Dominance criterion and angular neighborhood distance approach.

Dargush and Sant (2005) [99] developed a computational framework for the seismic design and retrofit of structures using passive energy dissipation systems, such as metallic plate dampers, viscous fluid dampers, and viscoelastic solid dampers. They utilized ES for the discrete optimization of these systems. The design variables included the sizing and placement of passive dampers. Non-linear time-history analyses were employed to evaluate structural performance under various seismic scenarios. The primary objectives were to minimize inter-story drifts and accelerations, ensuring cost-effective and efficient seismic retrofitting strategies.

Pollini et al (2017) [100] present a study focused on optimizing the use of nonlinear fluid viscous dampers for the seismic retrofitting of multi-story buildings. The research particularly addresses the retrofitting of 3-D irregular frame structures. Their approach aims to minimize retrofitting costs by optimally designing the damping coefficients of the dampers and the stiffness coefficients of the supporting braces. The design variables in this study include the damping coefficients of the dampers and the stiffness coefficients of the supporting braces. The authors employ a mixed integer optimization problem initially, which is then reformulated into a continuous optimization problem to reduce computational effort. The optimization process leverages material

interpolation techniques, allowing for practical final design solutions with reasonable computational resources. Time-history analyses are used to evaluate the structural responses to seismic events, specifically focusing on inter-story drifts at the peripheries of the frames. The optimization objectives include minimizing these drifts and the associated costs. The objective function also considers the costs related to both the topology and sizes of the dampers. One of the key contributions of this study is the formulation of a realistic retrofitting cost function. This function accounts for the costs associated with the manufacturing and placement of the dampers, as well as the stiffness of the supporting braces. The study demonstrates the effectiveness of a gradient-based optimization algorithm in achieving practical and cost-effective retrofit designs.

Seo et al. (2018) [101] presents the first approach that uses a metaheuristic algorithm to optimize the distribution of seismic retrofitting for RC columns in an existing three-story school building. The research utilizes glass fiber-reinforced polymer (GFRP) for retrofitting, aiming to determine the minimum number and optimal locations of retrofitted columns.

The design variables include the selection and placement of retrofitted columns. The study employs the Ant Colony Optimization (ACO) algorithm integrated with non-linear time-history analyses using the LS-DYNA software. These analyses assess the building's response to seismic events, particularly the Kobe and San Fernando earthquakes.

The objective functions are minimizing the number of retrofitted columns and minimizing inter-story displacements, with constraints based on allowable strains and inter-story drifts. By formally identifying the optimal position of retrofitting interventions, the authors effectively enhance the seismic performance of the structure while ensuring economic efficiency.

Mahdavi et al. (2019) [102] propose an optimal plan for seismically retrofitting RC frame structures using fiber-reinforced polymer (FRP) layers. Their study specifically targets the columns of a four-story non-ductile RC frame structure, aiming to enhance its seismic resilience by wrapping the columns along their plastic hinges.

The design variables in this study are the number of FRP layers applied to each column. The researchers utilize two metaheuristic algorithms, genetic algorithms and particle swarm optimization (PSO), to determine the optimal retrofit scheme. The optimization objective is to provide uniform usage of plastic hinge rotation capacity across all columns while minimizing the consumption of FRP materials.

Nonlinear pushover analyses are employed to evaluate the seismic performance of the retrofitted structure. These analyses help in determining the plastic hinge rotation capacity of FRP-confined columns at the life safety

performance level. The study's objective function includes penalty terms to ensure that the optimization considers both the structural performance and material usage. A significant contribution of this work is the application of both GA and PSO to optimize the number and placement of FRP layers.

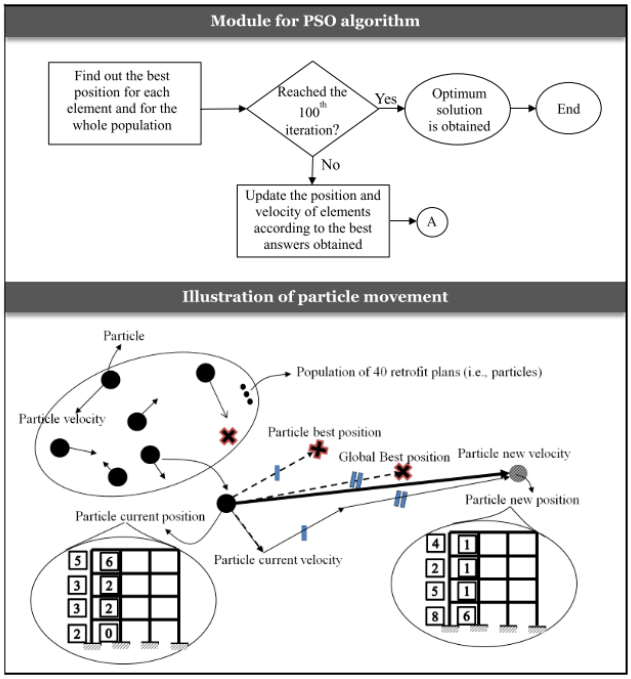

Figure 2.12 – Schematic representation of Particle Swarm Optimization approach developed by Mahdavi et al. (2019) [102] for the optimization of FRP jacketing in RC frame structures

Minafò and Camarda (2022) [103] present an open-source genetic GA framework for optimizing the seismic retrofitting design of RC frames using Buckling-Restrained Braces (BRBs). Their study focuses on enhancing the seismic performance of 2D RC frames by strategically placing BRBs to ensure the required safety level while minimizing costs.

The design variables in this study include the location and orientation of the BRBs within the frame. The GA framework employs selection, crossover, and mutation operators to explore the search space and evolve towards the optimal solution. To evaluate the structural performance static non-linear analyses are conducted. The modal analysis identifies the system's dynamic characteristics, while the pushover analysis assesses the frame's response to seismic loads. The objective function aims to minimize the retrofitting cost, incorporating a penalty function to avoid infeasible solutions that do not meet safety requirements.

A significant contribution of this work is the integration of the GA with OpenSeesPy facilitating a fast and convergent approach to defining the optimal BRB configuration.

Laguardia and Franchin (2022) [104] introduce a pioneering risk-based optimization framework for the seismic retrofitting of reinforced concrete (RC) buildings using bracing systems. This study is notable for being the first known application to incorporate reliability analysis directly into the optimization process. The design variables include the properties and placement of the bracing systems, allowing for a comprehensive approach to retrofit design.

The optimization framework employs nonlinear dynamic analyses to evaluate the structural performance of retrofitted buildings under various seismic scenarios. This approach ensures that the proposed retrofitting strategies not only enhance the seismic resilience of the structures but also maintain a high level of reliability. By integrating reliability analysis, the framework addresses uncertainties in seismic demand and structural response, providing a more robust basis for decision-making.

The primary objective of the study is the dual focus on minimizing retrofit costs while ensuring that the retrofitted buildings meet predefined structural reliability.

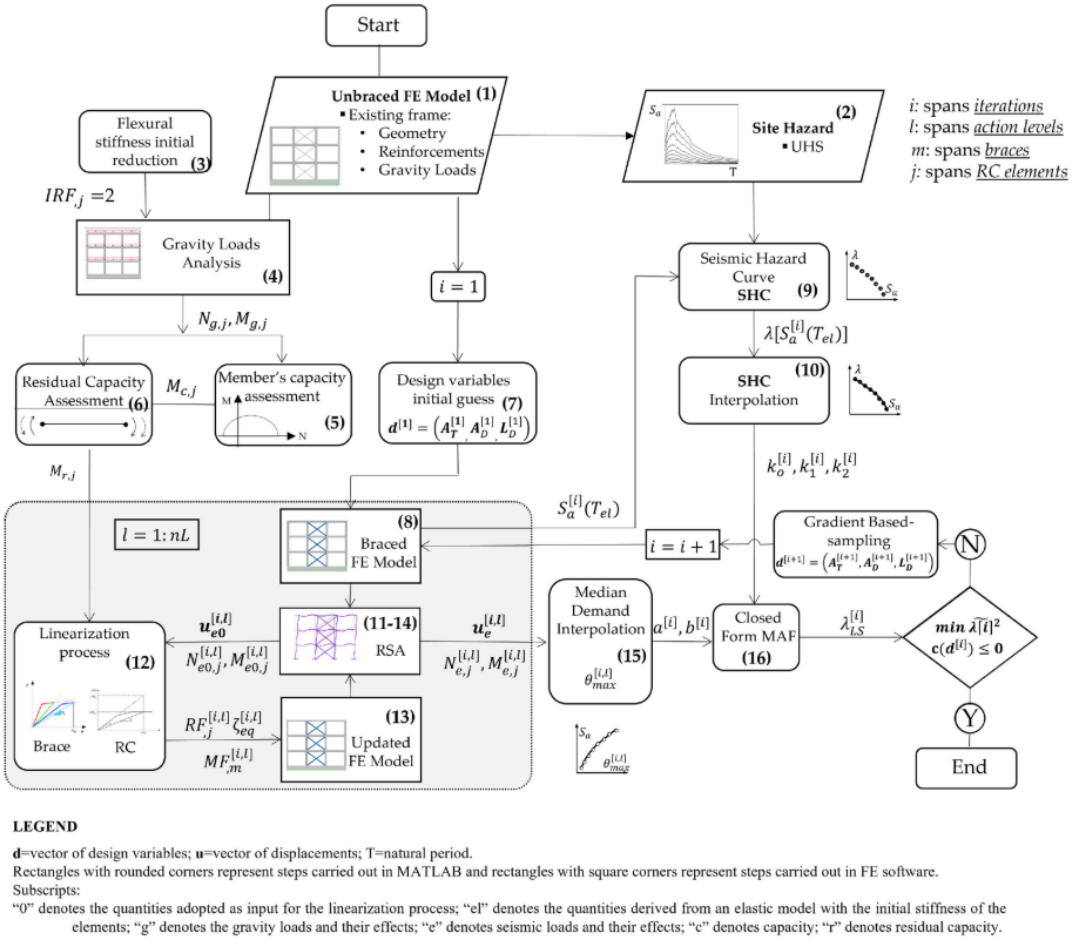

LEGEND

d=vector of design variables; **u**=vector of displacements; T=natural period.
Rectangles with rounded corners represent steps carried out in MATLAB and rectangles with square corners represent steps carried out in FE software.
Subscripts:
"0" denotes the quantities adopted as input for the linearization process; "el" denotes the quantities derived from an elastic model with the initial stiffness of the elements; "g" denotes the gravity loads and their effects; "e" denotes seismic loads and their effects; "c" denotes capacity; "r" denotes residual capacity.

Figure 2.13 – Schematic representation of the PBSD procedure implemented by Laguardia and Franchin (2022) [104]

Falcone et al. (2019) [105] propose a rational selection procedure for the seismic retrofitting of reinforced concrete (RC) buildings using Genetic Algorithms (GAs). The study aims to optimize the selection of the most cost-effective retrofitting solution among various technically feasible options. This procedure is applied to existing RC buildings, focusing on enhancing their seismic performance while minimizing retrofitting costs. The design variables in this study include both member-level interventions (FRP jacketing of columns) and structure-level interventions (concentric X-shaped steel braces). The Genetic Algorithm operates with standard GA operators, including selection, crossover, and mutation, to explore the search space of possible retrofitting solutions.

The primary objective function in this study is to minimize the total cost of retrofitting. This includes the costs associated with local interventions, such as column jacketing, and global interventions, such as the addition of steel bracings, along with potential foundation strengthening. The optimization process ensures that the selected retrofitting solutions meet the required seismic performance criteria while being cost-efficient.

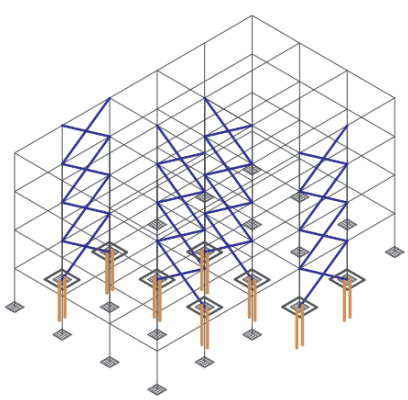

	Floor	Area [cm²]	Section
Beam 4 Beam 17	1st	34.01	HE 120 B
	2nd	26.04	HE 100 B
	3rd	26.04	HE 100 B
	4th	26.04	HE 100 B
Beam 16	1st	42.96	HE 140 B
	2nd	26.04	HE 100 B
	3rd	26.04	HE 100 B
	4th	26.04	HE 100 B
Beam 29	1st	26.04	HE 100 B
	2nd	26.04	HE 100 B
	3rd	26.04	HE 100 B
	4th	26.04	HE 100 B

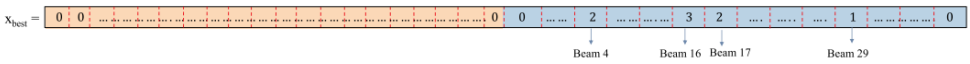

Figure 2.14 – Representation of the optimal configuration for steel braces and micro-piles found by Falcone et al. (2019) [105]

Chisari and Bedon (2016) [106] present a multi-objective optimization procedure for the seismic retrofitting of reinforced concrete (RC) building frames using Fiber-Reinforced Polymer (FRP) jackets. The study aims to improve the seismic response of RC frames by maximizing ductility and minimizing the volume and cost of FRP materials.

The design variables in this study include the thicknesses of FRP jackets applied to the internal and external columns of each floor. The optimization employs a Genetic Algorithm (GA) to explore various configurations of FRP

jackets. The GA operators used include selection, crossover, and mutation to efficiently search the design space.

Nonlinear static pushover analyses are performed to evaluate the seismic performance, focusing on inter-story drifts and overall frame ductility.

The primary objective functions are to maximize the ductility of the RC frame and to minimize the volume of FRP jackets. Additionally, optimization considers the control of the collapse mechanism to ensure a global rather than a local failure mode.

Braga et al. (2019) [107] propose a multiperformance optimization procedure for designing dissipative bracing systems in reinforced concrete (RC) buildings. The study focuses on optimizing both the sizing and topological characteristics of bracing systems to control structural performance while minimizing intervention costs. The procedure is applicable to both new and existing structures, but the objective function is tailored to typical retrofit intervention costs.

The design variables in this study include the area of steel trusses, the yielding force, and the yielding displacement of dissipative devices. The optimization process utilizes a gradient-based algorithm, specifically the a*ctive-set* algorithm available in MATLAB®, to search for the optimal configuration. The algorithm is based on Lagrangian multiplier approach with quasi-Newton iterative method and Karush-Kuhn-Tucker condition [108].

Nonlinear dynamic analyses are performed to evaluate the seismic performance of the retrofitted structures. The structural behavior is controlled through constraint functions on inter-story drift ratios (IDRs), ensuring that the retrofitting design meets predefined performance levels.

The primary objective function aims to minimize the total intervention cost, explicitly considering costs associated with steel elements, dissipative devices, masonry works, and foundation improvements.

Shin and Park (2022) [109] introduce a hybrid optimization framework combining artificial neural networks (ANN) and a GA for the seismic and blast retrofitting of non-ductile reinforced concrete building frames. The study focuses on optimizing FRP jacketing systems to enhance the structural resilience of existing RC buildings under multi-hazard loads.

The design variables include the FRP jacket strength, jacket thickness, inner diameter of the jacketing system, and grout strength. The optimization framework uses the ANN model to rapidly generate structural responses and the GA to identify the optimal retrofit configuration. This hybrid approach allows for efficient exploration of the design space and rapid decision-making.

Nonlinear finite element analyses are performed to simulate the seismic and blast responses of the retrofitted structures. The primary objective functions are

to maximize the confinement ratio and minimize the stiffness ratio, ensuring that the retrofitting meets performance targets while remaining cost-effective. By leveraging the ANN-GA hybrid model, the study efficiently derives optimal retrofit strategies that enhance the performance of RC structures under both seismic and blast loading conditions.

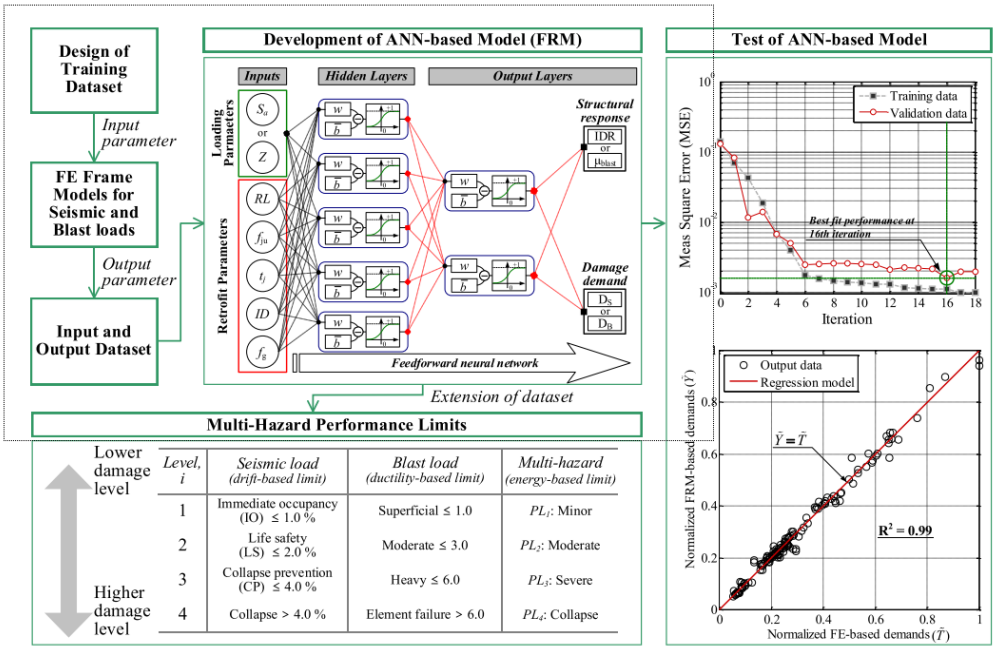

Figure 2.15 – Schematic representation of the ANN model developed by Shin and Park (2022) [109] for the safety assessment of each tentative solution analyzed by the optimization framework.

Similarly to this Gharagoz et al. (2023) [110] introduce a machine learning-based design procedure for seismic retrofitting using a novel spring-rotational friction damper (SRFD) system. The study focuses on the seismic retrofitting of multi-story reinforced concrete buildings, employing a hybrid approach that combines a GA optimization algorithm and ANN.

The design variables include the yield friction force and the stiffness of the springs in the SRFD system. The optimization process aims to minimize life-cycle costs (LCC) and enhance the seismic resilience of the retrofitted structures. Nonlinear time-history analyses are used to evaluate seismic performance, focusing on parameters such as inter-story drifts and residual displacements.

The primary objective functions are minimizing the maximum inter-story drift ratios and reducing the LCC. The optimization also considers the seismic fragility and resilience index of the retrofitted structures. The study demonstrates that the proposed SRFD system effectively decreases story drifts, seismic fragility, and LCC, enhancing the resilience and recovery capabilities of the retrofitted models.

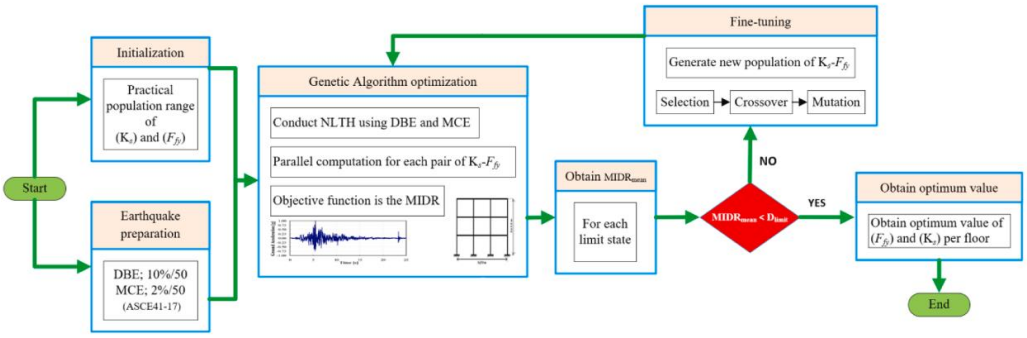

Figure 2.16 – Framework of optimization approach proposed by Gharagoz et al. (2023) [110] for the optimization of spring-rotational friction dampers for RC frame structures.

Papavasileiou et al. (2016) [111] present an optimization approach for seismic retrofitting of non-ductile RC buildings using evolutionary algorithms. The study focuses on a ten-story RC frame, optimizing the placement and sizing of FRP wrapping and steel bracing. Nonlinear static pushover analyses evaluate structural performance. The primary objective is to minimize retrofitting costs while maintaining structural efficiency.

Four years later Papavasileiou et al. (2020) [112] expand their earlier work to steel-concrete composite buildings, optimizing three retrofit methods: RC jacketing, concrete-covered steel caging, and steel bracings. The study uses a gradient-based Evolution Strategies algorithm for optimization. Nonlinear static pushover and eigenvalue analyses assess performance. The main objective is to minimize material costs. Innovations include a detailed cost ratio approach and comprehensive evaluation of retrofit strategies.

2.3.2.1 Topology optimization

Another significant branch of optimization research focuses on the topological optimization of reinforcement systems at the scale of individual structural elements. This approach aims to determine the optimal material layout within a given design space to enhance structural performance while minimizing material usage. The most prominent studies in this area have explored various techniques and applications, demonstrating the potential of topological optimization to revolutionize the field of structural retrofitting. Key contributions in this domain include the following scientific papers.

Chaves and Cunha (2014) [113] explore the use of topology optimization for the reinforcement design of concrete slabs with carbon fiber reinforced

polymers (CFRP). Their study aims to enhance the load-bearing capacity of concrete slabs by optimally distributing CFRP material.

The design variables in this study include the density distribution of CFRP within the slab. The study involves the Density Method for topology optimization, which iteratively redistributes material within the design domain to achieve an optimal layout. The optimization process seeks to minimize material usage while maximizing the stiffness and strength of the slab.

The objective function in this study is to minimize the mean compliance of the structure, equivalent to maximizing its global stiffness. The constraints include volume constraints on the amount of material used.

A significant contribution of this work is the comparison between optimized reinforcement distributions and conventional reinforcement methods.

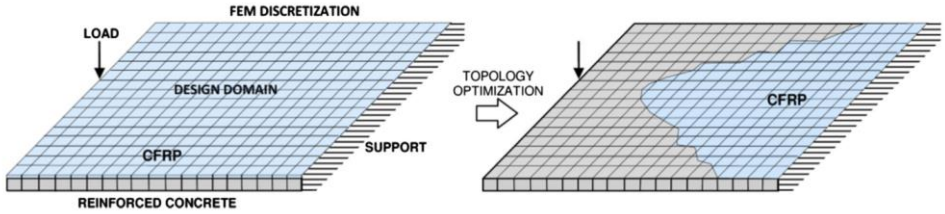

Figure 2.17 – Procedure for the topology optimization of CFRP on slabs (Chaves and Cunha 2014 [113])

In a similar approach, Bruggi et al. (2013) [114] explores the application of topology optimization for the seismic retrofitting of masonry structures using Fiber Reinforced Polymers (FRP). This study focuses on optimizing the placement of FRP strips on masonry walls subjected to in-plane loads. The design variables are the density and orientation of the FRP strips. A homogenization approach is employed to model the masonry and FRP composite structure, aiming to minimize structural compliance. Nonlinear finite element analysis is utilized to evaluate structural performance. The objective function is to maximize the stiffness of the retrofitted walls while minimizing the use of FRP material.

This latter paper has been extended by Bruggi et al. (2014) [115] in the application of topology optimization to the reinforcement of masonry walls subjected to two-way bending. The study targets optimal reinforcement of masonry walls with FRP layers to enhance their flexural rigidity. The design variables include the distribution and orientation of FRP layers on the masonry walls. Numerical homogenization is used to derive the macroscopic flexural rigidity of the composite wall structure. The optimization objective is to

maximize structural stiffness while considering various loading conditions to ensure robustness. The approach's effectiveness is demonstrated through case studies involving masonry walls with different geometrical configurations and loading scenarios.

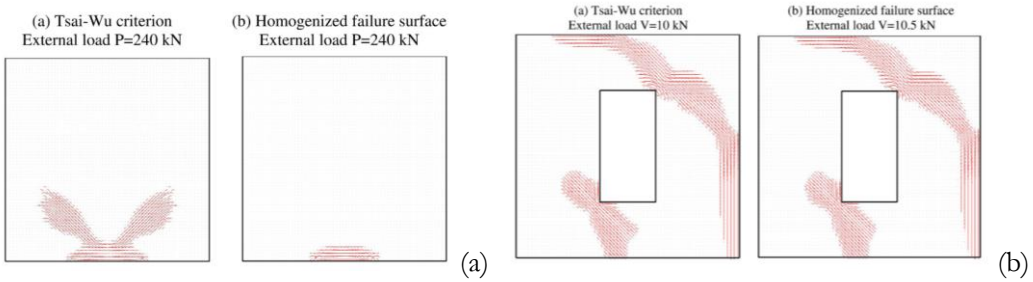

Figure 2.18 – Optimal fibers orientations of the reinforcement (for Tsai-Wu criterion and homogenized failure surface): (a) deep beam, (b) windowed panel (Bruggi et al. 2014 [115])

Bruggi et al. (2015) [116] focuses on the seismic retrofitting of 3D masonry structures using FRP, emphasizing out-of-plane loads. The study examines the optimal distribution of FRP to improve the seismic performance of complex masonry structures. Design variables include the amount and placement of FRP within the structure. Material interpolation techniques and nonlinear static analyses are used to evaluate structural response. The primary objective is to enhance the seismic performance of the masonry structures while ensuring efficient and cost-effective use of FRP.

Together, these last three studies by Bruggi illustrate the versatility and effectiveness of topology optimization in designing optimal reinforcement layouts for various structural elements. The research highlights the potential of advanced computational techniques to achieve material efficiency and enhanced structural performance in seismic retrofitting applications

Table 2.2 – Summary of optimization framework for design of seismic retrofitting studies

Structural system	Reference	Retrofitting technique(s)	Design variable(s)	Algorithm	Objective function(s)	Constraint(s)
Steel structures	Lavan et al. 2009 [98]	• Viscous fluid dampers • Solid viscoelastic dampers • BRB	• Sizing	Multi-objective Genetic Algorithm	• Inter-story drift • Floor acceleration	• Inter-story drift • Maximum floor acceleration • Initial cost
	Beheshti et al.2020 [117]	• Viscous dampers	• Sizing • Mechanical properties	Genetic Algorithm	• Initial cost • Life-cycle costs	• Inter-story drift • Stiffness • Damping
Concrete structures	Zou et al. 2007 [97]	• FRP wrapping	• Sizing	Gradient based	• Material volume	• Flexural capacity • Confinement
	Chiu and Jean 2011 [118]	• RC walls	• Sizing	Brute force sampling (Monte Carlo)	• Initial cost • Life-cycle costs	• Ductility • Inter-story drift • Flexural capacity • Shear capacity
	Daniel et al. 2014 [119]	• Tuned mass dampers	• Sizing	Gradient based	• Material volume	• Inter-story drift • Top acceleration
	Chaves et al. 2014 [113]	FRP wrapping	Position	Topology density method	• Material volume	Flexural capacity

Zerbin et al. 2015 [33]	• FRP wrapping • RC shear walls	• Sizing • Position	Gradient based	• Life-cycle costs	• Ductility
Gidaris et al. 2015 [120]	• Viscous dampers	• Sizing	Gradient based with Kriging metamodel	• Life-cycle costs	• Inter-story drift • Peak floor acceleration • (for different LS)
Charmpis et al. 2015 [121]	• Base isolation	• Sizing • Position	Genetic Algorithm	• Floor acceleration • Initial cost	• Inter-story drift • Base displacements
Chisari et al. 2016 [106]	• FRP wrapping	• Sizing	Genetic Algorithm	• Material volume • Ductility	• Local failures
Pollini et al. 2017 [100]	• Viscous fluid dampers	• Sizing • Position	Gradient-based	• Initial cost	• Inter-story drift
Zou et al. 2018 [122]	• FRP	• Sizing	Gradient based	• Initial cost	• Ductility • Inter-story drift
Seo et al. 2018 [101]	• FRP wrapping	• Position	Ant Colony Optimization	• Material volume • Inter-story drift	• Strains in materials • Inter-story drift
Falcone et al. 2019 [105]	• FRP wrapping • Steel braces	• Sizing • Position	Genetic Algorithm	• Initial cost	• Ductility

Braga et al. 2019 [107]	• Steel braces	• Sizing • Position	Lagrangian multiplier	• Initial cost	• Inter-story drift
Puthanpurayil et al. 2020[123]	• Viscous dampers	• Sizing	Gradient based	• Initial cost • Life-cycle costs	• Inter-story drift • Damping
Reggio et al. 2020 [124]	• Steel exoskeletons	• Sizing	NSGA-II	• Initial cost	• Reliability
De Domenico et al. 2021 [125]	• Viscous dampers	• Sizing	Gradient based	• Initial cost	• Inter-story drift • Plastic rotation • Reliability
Minafò et al. 2022 [103]	• BRB	• Position	Genetic Algorithm	• Initial cost	• Ductility
Velasco et al. 2022[126]	• BRB	• Sizing • Position	Simulated annealing	• Initial cost	• Inter-story drift • Plastic rotation
Omidian et al. 2022 [127]	• Steel jacketing • FRP	• Sizing	NSGA-II	• Initial cost	• Inter-story drift
Shin and Park 2022 [109]	• FRP jacketing	• Sizing • Material properties	Genetic Algorithm + ANN	• Retrofitting material volume	• Stiffness • Confinement
La Guardia et al. 2022 [104]	• BRB	• Sizing • Position	Gradient based	• Seismic risk • Material volume	• Reliability Flexural capacity

Concrete structures	Gharagiz et al. 2023 [110]	• Spring-rotational external steel frames	• Position	Genetic Algorithm + ANN	• Inter-story drift • Life cycle costs	• Ductility
	Dereje et al. 2023 [128]	• Steel dampers	• Sizing • Position	NSGA-II	• Number of devices	• Inter-story drift • Reliability
	Adene et al. 2024 [129]	• Steel frames	• Sizing • Position	Particle Swarm Optimization	• Inter-story drift	• Material stress
Composite structures	Papavasileiou et al. 2020 [112]	• Steel-jacketing • Concrete-jacketing • Steel braces	• Sizing	Evolution strategies	• Initial cost	• Flexural capacity • Shear capacity • Ductility • Fundamental period
	Dargush et al. 2005 [99]	• Viscous dampers • Metallic plate dampers	• Material properties	Evolutionary strategies	• Material volume	Not specified
Timber structures	Yi and Burton 2024 [130]	Not specified (regional analysis)	• Sizing	Bayesian optimization	• Initial cost	• Inter-story drift • Reliability
	Park et al. 2015 [131]	• Steel frames	• Sizing • Position	Genetic algorithm	• Initial cost	• Inter-story drift • Flexural capacity

Masonry structures	Bruggi et al. 2013 [114]	• FRP	• Topology	Gradient based	• Material volume	• Flexural capacity • Materials stress
	Bruggi et al. 2014 [115]	• FRP	• Topology	Gradient based	• Material volume	• Flexural capacity • Materials stress
	Bruggi, Milano 2015 [116]	• FRP	• Topology	Gradient based	• Material volume	• Flexural capacity • Out-of-plane capacity
	Mrozek 2020 [132]	• FRP	• Topology	Gradient Based	• Material volume	• Material stress

2.4 Other frameworks and tool for the design

In addition to the widely utilized Multi-Criteria Decision-Making (MCDM) methods and optimization techniques hereby presented, the literature also includes a smaller but noteworthy body of studies that propose alternative approaches for the design of seismic retrofitting. These approaches do not rely on MCDM or optimization methods, but instead offer unique perspectives and methodologies for addressing the complex challenges associated with seismic retrofit design.

For the sake of completeness and to provide a comprehensive overview of the state of the art, these alternative frameworks and tools are presented in the following sections.

Tonekaboni (2014) [133] introduces a probabilistic approach for assessing the economic feasibility of various seismic retrofit methods. The study employs a Cost-Benefit Analysis (CBA) framework that incorporates seismic hazard and fragility analyses to compute an Economic Feasibility Index (EFI). This index measures the ratio of the present value of benefits from a seismic retrofit to its cost, determining economic feasibility. The study assesses three retrofit methods—RC jacketing, steel jacketing, and CFRP wrapping—for a pre-code RC building in Tehran. The results highlight the importance of site-specific seismic hazards, investment return periods, and interest rates in the economic feasibility of retrofit methods. This framework provides a comprehensive tool for integrating economic considerations into seismic retrofit decision-making, ensuring both structural safety and financial viability.

Aljawhari et al. (2022) [134] propose a fragility-oriented approach for seismic retrofit design, focusing on reinforced concrete (RC) structures. This study presents a practical methodology that correlates the increase in the global displacement-based ratio of capacity to life-safety demand (CDRLS) due to retrofitting with a corresponding reduction in building-level seismic fragility. The approach involves specifying the desired fragility median and finding the corresponding target value of CDRLS to achieve through retrofit design.

The study illustrates this methodology using an archetype RC structure not conforming to modern seismic design requirements, retrofitted with fiber-reinforced polymers (FRP) wrapping, RC jacketing, and steel jacketing. The proposed approach enables the designer to control the desired level of seismic fragility by achieving a specified CDRLS through retrofit interventions. This method effectively connects the desired level of fragility to a measurable performance metric, facilitating a more targeted and efficient retrofit design process.

Gentile et al. (2021) [135] propose a comprehensive computational framework designed to select the optimal combination of seismic retrofit and insurance policy parameters for buildings. This framework addresses both structural and financial risk mitigation by integrating seismic retrofitting strategies with insurance solutions. Initially, a suitable retrofit strategy is selected and incrementally implemented to define interventions with increasing levels of performance. The costs associated with each intervention, including retrofit implementation and property rental during the retrofit period, are calculated.

The framework evaluates alternative insurance options, estimating the insured and uninsured economic losses within a given time horizon for each retrofit-insurance combination. The objective is to minimize the tail value at risk of the life cycle cost, with the selected confidence level reflecting the homeowner's risk aversion. The framework is demonstrated using a case study of an archetype Italian RC frame building retrofitted with concrete jacketing, and it considers the Italian retrofit tax incentives.

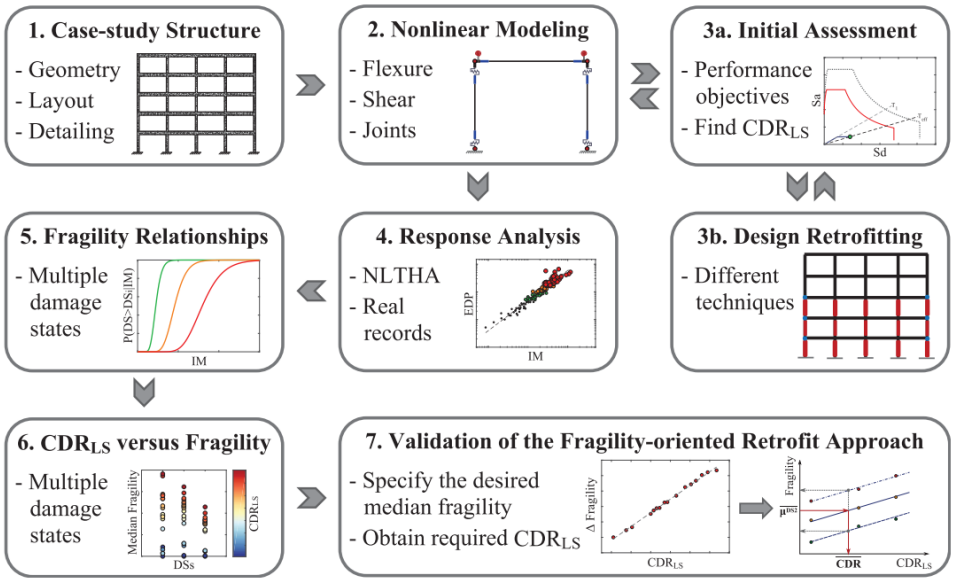

Figure 2.19 – Conceptual flowchart of the procedure proposed by Aljawhari et al. (2022) [134] for the seismic retrofitting design based on fragility curve results.

Lima et al. (2023) [136] propose a conceptual design procedure for the seismic retrofitting of existing RC structures by combining member- and structure-level techniques. The study addresses the challenge of selecting the optimal retrofit solution by formulating the problem as a constrained optimization task. Three retrofit solutions are evaluated: one focusing on structure-level interventions, another on a combination of both member- and structure-level techniques, and the third solely on member-level interventions. The results indicate that a combination of techniques can provide a cost-effective and efficient solution, although it may not always be the optimal choice

from an environmental standpoint. The study highlights the importance of considering both economic and ecological impacts in the design process.

Bruschi et al. (2021) [137] present a simplified design procedure for seismic upgrading of frame structures equipped with hysteretic dampers. The study focuses on optimizing the properties and placement of dampers in multi-story RC frame buildings. The design variables include the stiffness and strength of the dampers. The procedure uses an equivalent Single Degree of Freedom (SDOF) system to represent the combined frame and damper system, simplifying the analysis. Non-linear static and dynamic analyses are involved to evaluate the structural performance. The primary objective is to proportion the damper devices to achieve desired structural performance levels while minimizing costs. This approach streamlines the iterative process typically involved in damper design, making it more accessible for practical applications.

2.4.1.1 Numerical and theoretical tools for the retrofitting design of existing structures

An additional subset of the literature focuses on methods and tools designed to facilitate the design process, which can be utilized in conjunction with both MCDM and optimization techniques. These methods are generally aimed at accelerating the assessment of various retrofit configurations.

Falcone et al. (2022) [138] propose the use of an Artificial Neural Network (ANN) to predict the technical feasibility of seismic retrofitting interventions in existing RC structures. This study aims to replace the computationally intensive Finite Element Method (FEM) with a trained ANN model to accelerate the optimization process. By modeling the seismic response of retrofitted structures, the ANN provides rapid assessments, significantly reducing the design time. The study demonstrates that the ANN can effectively classify retrofit solutions as feasible or unfeasible, making it a valuable tool for speeding up the iterative search for optimal retrofitting strategies.

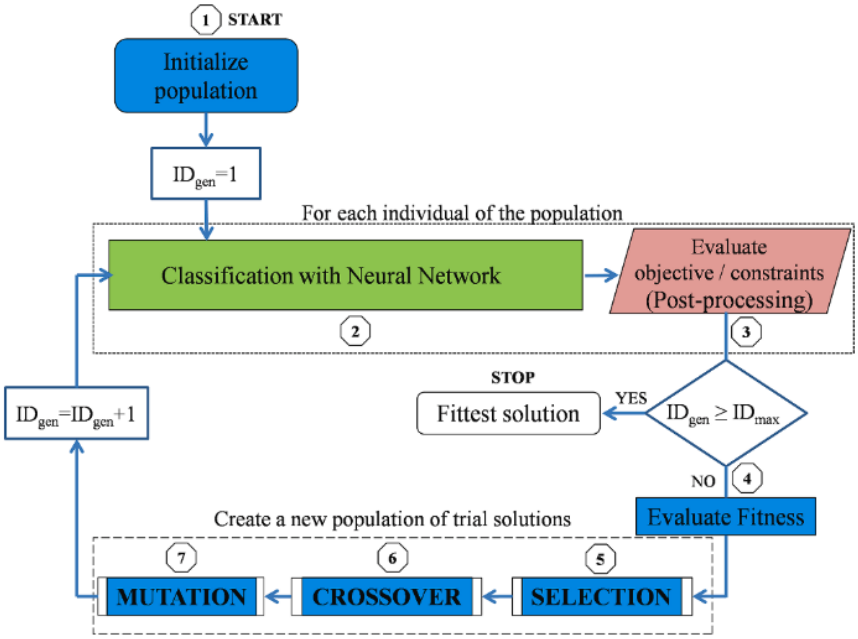

Figure 2.20 – Flowchart of seismic retrofitting optimization procedure with the use of ANN for the substitution of the FEM analysis in the step of the safety assessment as proposed by Falcone et al. (2022) [138]

In this author's opinion, the development of simplified methods for performing Performance-Based Earthquake Engineering (PBEE) analyses is a valuable tool. Such methods can streamline the design process and improve the feasibility of detailed seismic assessments.

However, the actual efficiency gained from using artificial intelligence (AI) algorithms, such as neural networks, for the safety assessment of different retrofit configurations should be carefully evaluated. While these AI-based methods can potentially speed up the assessment process, a critical factor often downplayed by proponents is the time required to train the neural networks effectively, which can offset the time savings achieved when using them for extensive analyses, such as those performed in optimization frameworks.

2.5 Conclusions and future trends

In this review of research works proposing methods for the seismic retrofit design of existing structures, it becomes clear that the literature in this field is relatively recent, indicating a dynamic and rapidly evolving area of study. The imperative to develop formal methods to solve this persistent problem is gaining traction now, enabled by advances in algorithms and, more importantly, the computational capacity that allows us to tackle such complex issues. Frameworks based on Multi-Criteria Decision Making (MCDM) were developed earlier and continue to be explored, with ongoing research extending their application to a broader range of objective functions, including energy isolation and environmental impact.

On the other hand, optimization frameworks have seen more recent developments. Initially, gradient-based methods were utilized, but these were constrained by their requirement for simpler problem formulations. In recent years, there has been a significant shift towards metaheuristic algorithms, which are better suited for addressing more complex and larger problems with heterogeneous search spaces. A notable trend is the increasing use of hybrid methods and the integration of neural networks or statistical metamodels with optimization processes to expedite these computationally intensive analyses. This integration has the potential to address reliability problems, which have only begun to be explored in significant depth over the past couple of years.

However, there is a notable gap in the literature regarding the optimization of masonry structures on a structural scale. In the author's opinion, the near future will likely see an expansion of the range of objective functions considered in optimization studies to include environmental impact, a trend that has already begun to emerge in MCDM research. This development is expected to lead the way in creating more comprehensive and sustainable approaches to seismic retrofitting design. This evolution reflects a broader shift in the field towards incorporating multiple performance metrics, thereby enhancing the resilience and sustainability of retrofitted structures.

Chapter 3

Innovative genetic algorithm-based framework for cost optimization of ductile-critical and shear-critical reinforced concrete frame structures

As highlighted in Chapter 1, a significant portion of global buildings and infrastructure consists of structures designed and constructed before the adoption of modern seismic codes and detailing regulations. A large part of these structures are reinforced concrete (RC) frame structures, which present considerable seismic risks due to their inadequate lateral load-bearing capacity and limited ductility. In particular, RC columns are crucial to seismic performance, often exhibiting structural deficiencies such as poor-quality concrete, insufficient transverse reinforcement, and a lack of seismic detailing. Among the various retrofitting methods available for RC frame members, steel-jacketing (SJ) is widely used. This method typically involves using steel angles and plates (or battens) to create a reinforcing cage that provides additional confinement and transverse reinforcement to the RC elements (Wu et al. 2006 [139]). While effective, steel-jacketing is an invasive procedure that necessitates multiple related operations, including the demolition and reconstruction of adjoining masonry and plaster, significantly impacting the overall cost and downtime of the intervention.

RC frame structures lacking seismic detailing are prone to shear failure in columns; thus, a comprehensive optimization framework must address both shear-critical and ductility-critical frames to inform design decisions effectively. A novel optimization framework has been developed and tested to optimize retrofitting for both ductility-critical and shear-critical RC frames, incorporating shear-induced mechanisms from frame-infill interaction. Genetic algorithms are preferred over classical optimization or other metaheuristic algorithms due to the discrete nature of this optimization problem. The framework includes new genetic operators (population generator, elitism, and mutation) tailored by

modifying the standard MATLAB® GA tool. These genetic operators are calibrated to identify the optimal parameter settings, ensuring computational efficiency and sustainability.

The optimization framework identifies the most cost-effective seismic retrofitting intervention among feasible options, optimizing the configuration of steel jacketing for columns in terms of reinforcement placement (topological optimization) and spacing between steel battens (sizing optimization). Each solution's feasibility is verified through static pushover analyses using the N2 method (Fajfar 2000 [140]), based on results from a 3D fiber-section model developed in the OpenSees software platform (McKenna et al. 2000 [141]). The proposed framework's effectiveness and flexibility are demonstrated through tests on various shear-critical and ductility-critical 3D frame structures.

The application of this proposed method can serve as an efficient tool for designers, helping to identify cost-effective retrofitting configurations. This approach can reduce the waste of private and public funds while enhancing the safety of building heritage.

The outcomes presented in this chapter have been peer-reviewed and published in:

- Di Trapani F., Malavisi M., Marano G.C., *Sberna A.P.*, Greco R., "Optimal seismic retrofitting of reinforced concrete buildings by steel-jacketing using a genetic algorithm-based framework", Engineering Structures, 219:110864, 2020 [142]
- Di Trapani F., *Sberna A.P.*, Marano G.C., "Optimization of steel-jacketing retrofitting of shear-critical and ductility critical RC frame structures by a novel genetic algorithm framework". Engineering Structures, 243:112684, 2021 [143].

3.1 Design optimization framework

3.1.1 General operating principles and position of the problem

The proposed optimization framework utilizes a genetic algorithm (GA) as a soft-computing optimization technique. Genetic algorithms are particularly adept at solving nonlinear or noisy problems. This method is especially beneficial when it is challenging to analytically represent an objective function associated with a discrete design space, necessitating point-by-point evaluation.

The framework connects the MATLAB® genetic algorithm (GA) tool with a finite element (FE) structural model developed using the OpenSees software

platform. The primary goal is to minimize an objective function that calculates the steel-jacketing retrofitting costs based on design variables that define the retrofitting arrangement. These variables include the positioning of the retrofitted columns (topological optimization) and the spacing of the battens (sizing optimization).

Each proposed solution's feasibility is assessed by evaluating the ductility capacity and demand ratio ($\zeta_\mu = \mu_c / \mu_d$) after performing a pushover analysis of the structure within the N2 method framework (Fajfar 2000 [140]). An adaptive penalty function is applied to unfeasible solutions to guide the optimization process towards viable designs.

A flowchart of the framework is illustrated in Figure 3.1, showing the integration of the genetic algorithm in the workflow and the FE model to iteratively optimize the retrofitting intervention.

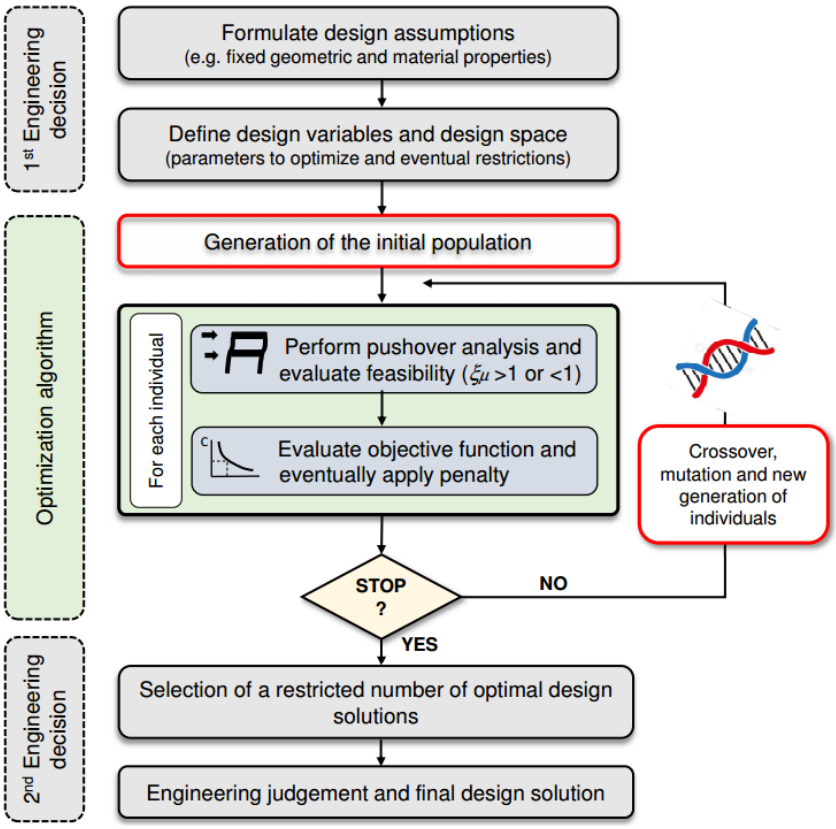

Figure 3.1 – Schematic flowchart of the proposed optimization framework

The engineering decision phases illustrated in Figure 3.1, while not part of the algorithm itself, play a crucial role in enhancing the efficiency of the optimization process. Specifically, defining a restricted design space (e.g., limiting the optimization to a specific portion of the building or to a limited set of variables) based on engineering considerations (1st engineering decision) can significantly reduce the computational costs associated with the optimization.

The optimal solution identified using this framework should not be viewed as an absolute answer. Instead, the framework aims to provide the designer with a limited number of potential retrofitting configurations, aiding in the final design decision (2nd engineering decision).

In particular, substantial revisions have been made to the standard GA scheme to redefine the genetic operators (highlighted in red boxes in Figure 3.1) to generalize the framework for both flexural ductility-critical and shear-critical RC structures. This update is necessary because, unlike RC structures with flexural ductility deficiencies, shear-critical structures may require retrofitting a significant number of columns.

Figure 3.2 illustrates the potential retrofitting configurations (with retrofitted columns shown in red) for an RC building with flexural ductility-related deficiencies (Figure 3.2(a)) and shear-related deficiencies (Figure 3.2(b)). This scenario typically occurs when the base shear demand exceeds the shear capacity of a story. When the number of columns requiring retrofitting constitutes a high percentage of those within the design space, the probability of finding feasible solutions through a standard random selection of individuals defining the population may decrease. This condition can cause the genetic algorithm to stall or find a local minimum solution, even within an unfeasible space (Figure 3.3).

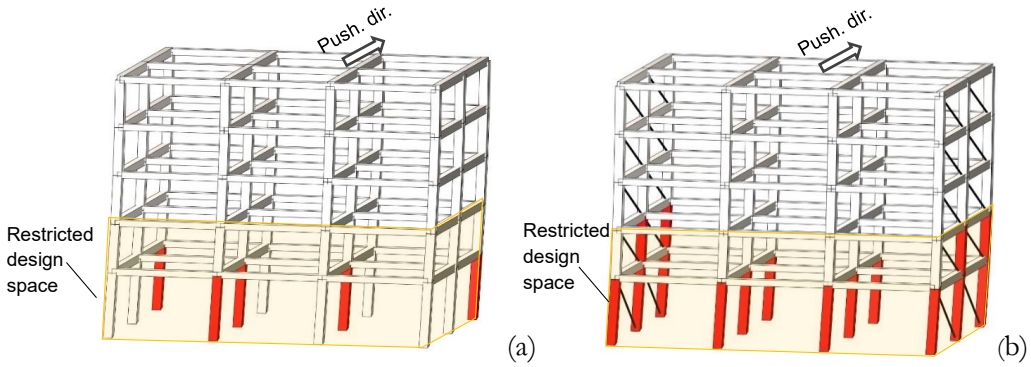

Figure 3.2 – Typical possible retrofitting configuration for a RC building having: (a) flexural ductility-related deficiencies; (b) shear-related deficiencies also caused by the interaction with masonry infills. Retrofitted columns are depicted in red.

One possible remedy to avoid this drawback is to expand the population of individuals within the design space, thereby increasing the chances of including feasible individuals. However, increasing the number of individuals also increases the number of nonlinear static analyses required, which can result in a substantial computational burden. Therefore, maintaining a reduced population and a possibly restricted design space is essential for achieving effective and affordable optimization through a genetic algorithm associated with nonlinear structural analyses.

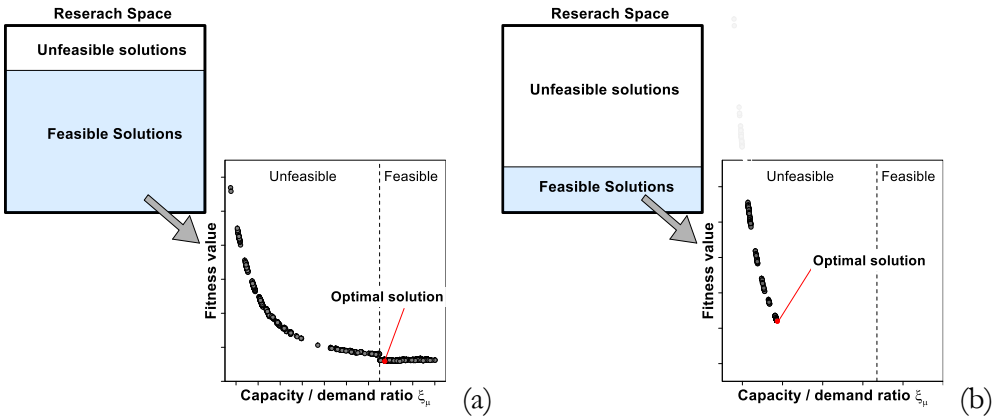

Figure 3.3 – Possible optimization outcomes in case of: (a) design space with prevalence of feasible solutions; (b) design space with prevalence of unfeasible solutions.

To circumvent this drawback and make the framework effective for a general application, a modification to the structure of the standard MATLAB® GA library has been introduced by redefining the following genetic operators and functions:

- Population generator
- Elitism
- Crossover
- Mutation

The introduced modifications are described in depth in the following sections by comparing results of the new approach with those obtained by using the standard tools.

3.1.2 Definition of the design vector

As mentioned in the previous sections, the design optimization variables are the position of the retrofitted columns and the battens spacing (s_b). The following design space restrictions can be assumed for the variables having less relevance in the optimization process, to reduce the computational effort:

i) The angles are constituted by L-shaped steel profiles having fixed lateral length (l_a) and thickness (t_a) for all the retrofitted columns;
ii) The battens are constituted by rectangular plates having fixed thickness (t_b) and width (w_b) for all the retrofitted columns;
iii) Battens spacing is the same for all the retrofitted columns;

iv) The design space can be restricted to a reduced number of columns (e.g. those belonging to the lower storeys).

A schematic representation of the design variables is illustrated in Figure 3.4.

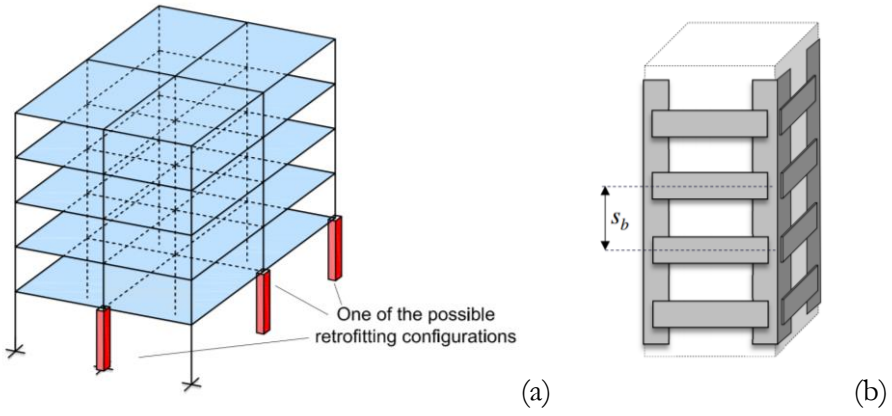

Figure 3.4 – Representation of the optimization variables: (a) Generic column retrofitting configuration for an RC structure; (b) Typical retrofitting arrangement for a column with generic batten spacing (s_b).

The design vector collecting the design variables, therefore, can be formalized as:

$$\mathbf{b} = \begin{pmatrix} s_b \\ \mathbf{p} \end{pmatrix} \tag{3.1}$$

where s_b is a natural number that represent the battens spacing (Figure 3.4(b)), defined inside to the boundaries:

$$s_b \in S = \begin{bmatrix} s_{b,\min} & s_{b,\max} \end{bmatrix} \tag{3.2}$$

where $s_{b,\min}$ and $s_{b,\max}$ are the respectively the minimum and maximum battens spacing allowed.

The second element of the design vector (Equation (3.1) $\mathbf{p}$ is itself a vector defined as:

$$\mathbf{p} = \begin{bmatrix} \dots & \dots & c_{ij} & \dots \end{bmatrix}^{\mathrm{T}} \tag{3.3}$$

in which the generic element c_{ij}, is a Boolean number assuming the value 1 if a column is retrofitted and 0 if not. The subscript i denotes the position of a column in plan and j the story.

In this way, each individual (namely a retrofitting configuration) handled by the GA is univocally defined by the $\boldsymbol{b}$ vector, which define position and battens spacing of the retrofitted columns. The assumption to use the same battens spacing for all the retrofitted columns could be overcome by introducing new variables (e.g. the battens spacing for each column) in vector $\boldsymbol{b}$. However, keeping a reduced dimension of the design vector (*dim(**b**)*) is fundamental since this is directly related to the dimension of the population (P) to be used and therefore to the computational effort.

3.1.3 Objective function and penalty function

The objective function evaluates retrofitting cost intended as the material cost and the manpower cost to realize columns steel jacketing (C_{SJ}) and necessary works for demolition and reconstruction of plasters and masonry (C_M). The general expression of the objective function is therefore:

$$C = C_M + C_{SJ} \tag{3.4}$$

The cost C_M is estimated considering a fixed amount (c_m) of 2000€ per column. Assuming n_c as the number of retrofitted columns one obtains:

$$C_M = n_c \cdot c_m \tag{3.5}$$

The cost C_{SJ} is computed as:

$$C_{SJ} = c_s \cdot \sum_{i=1}^{n_c} W_{s,i} \tag{3.6}$$

where $W_{s,i}$ is the total weight of steel used to arrange a steel jacketing cage and c_s is the manpower and material cost per unit weight, which is estimated as $4.5\ €/\text{kg}$.

If all the potentially retrofitted columns have the same dimension Equation (3.6) becomes:

$$C_{SJ} = n_c\, W_s\, c_s \tag{3.7}$$

where W_s is the weight of each steel jacketing cage. The latter can be computed as:

$$W_s = (V_A + V_B)\,\gamma_s \tag{3.8}$$

in which γ_s is the specific weight of steel ($78.5\ \mathrm{kN/m^3}$) and V_A is the total volume of the steel angles applied at the corners of a columns, that is:

$$V_A = 8 \cdot l_a \cdot t_a \cdot l_c \tag{3.9}$$

where l_a, t_a are the width and the thickness of an angle and l_c is the length of a column.

Finally, V_B is the total volume of the battens belonging to a cage. The latter depends on the spacing (s_b) as follows:

$$V_B = 2 \cdot \left(V_{bx} + V_{by}\right) \cdot \left(\frac{l_c}{s_b}\right) \tag{3.10}$$

where V_{bx} and V_{by} are the volumes of singles batten along the two orthogonal directions, that is:

$$\begin{aligned} V_{bx} &= t_b \cdot l_b \cdot \left(b - l_a\right) \\ V_{by} &= t_b \cdot l_b \cdot \left(h - l_a\right) \end{aligned} \tag{3.11}$$

For a square column Equation (3.10) becomes:

$$V_B = 4 \cdot V_b \cdot \left(\frac{l_c}{s_b}\right) \tag{3.12}$$

in which $V_{bx} = V_{by} = V_b$.

The optimization strategy adopted by the GA does not consider constraints representing the feasibility of the tentative solution. For the current case, the feasibility of a solution is known by the evaluation of the capacity/demand ratio (ζ_μ). A penalty function is therefore introduced to fictitiously consider the effect of a constraint violation. This can be done by summing the objective function (C) the penalty function (P) into the new objective function (F) so defined:

$$F = C + \Pi \tag{3.13}$$

where Π is defined as:

$$\Pi = \begin{cases} 0 & \text{if } \xi_\mu \geq 1 \\ C_{\max} \cdot \left(\dfrac{1}{\xi_\mu} \right)^3 & \text{if } \xi_\mu < 1 \end{cases} \tag{3.14}$$

and in which $C_{\max}$ is the maximum possible retrofitting cost evaluated by considering retrofitting all the columns included in the design space with the minimum battens spacing.

Using this approach, if one tentative solution is not feasible, the current cost is fictitiously augmented by $C_{\max}$ that takes into account a factor $(1/\zeta_\mu^3)$ which estimate the distance of the current tentative solution from the feasibility condition ($\zeta_\mu = 1$). The trend of the penalty function is illustrated Figure 3.5. As can be observed, the penalty function increases the cost by an exponent 3, in the case unfeasible solutions. The choice of severe penalization was formulated to improve more rapidly the fitness of subsequent generations (Coello 2002 [144], Lagaros et al. 2023 [145])

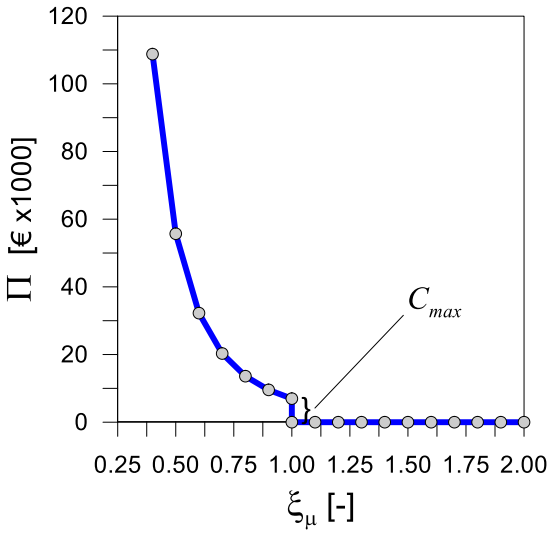

Figure 3.5 – Penalty function

3.2 Definition of the genetic operators

3.2.1 Population generator and elitism

The control of the population in terms of selection of the individuals is essential to the optimization effectiveness, especially in respect of computational effort as it allows maintaining reduced population size. As defined in Equation (3.1), each individual is a vector composed of scalar representing the battens spacing s_b, and a sub-vector ($\mathbf{p}$) collecting a number of

Boolean variables which is the same as the number of the potentially retrofitted columns. The way in which these individuals are selected plays a fundamental role. In the selection phase, the parameter s_b is randomly selected by the S interval which includes all possible spacing values as a multiple of a fixed minimum spacing variation Ds_b. The definition of the sub-vector ($\boldsymbol{p}$) has major relevance.

As mentioned in previous sections, and exemplified in Figure 3.3, in the case of structures having shear-related deficiencies, the number of unfeasible retrofitting solutions belonging to the design space can be relevant, and this can bring the optimization to stall or to find a local minimum solution even in the unfeasible space. In order to avoid this effect, the population generator operator has been modified by introducing two subspaces in the definition of the population (Figure 3.6). The first subspace (p_{rand} space) collects randomly selected individual. The second subspace (p_{Pr} space) is defined by a specified percentage (p_{Pr}) of individuals having an assigned probability of retrofitting (P_r). The percentage of randomly selected individuals (p_{rand}) is the complement to 100%. The probability P_r is typically high (e.g. 90%), this means that an individual included the p_{Pr} space is an individual with a large number of retrofitted columns. Suitable values for p_{Pr} and P_r are determined in the following sections. The introduction of the p_{Pr} space within the population allows a significant improvement of the optimization algorithm, as it increases from the beginning the number of feasible solutions. This allows maintaining a reduced population of individuals and reducing the time of exploration of the design space.

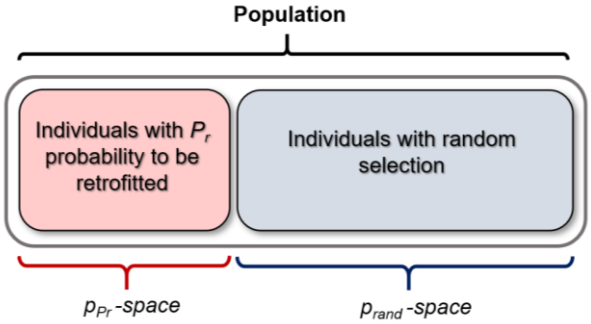

Figure 3.6 – Proposed approach for the initial population generator

To further improve the algorithm performance the elitism function is used. This genetic operator involves copying a small number of the fittest candidates, unchanged, into the next generation. In fact, the fittest individuals of a population can be lost during the crossover operations of consecutive generation analysis. Then, the use of elitism function allows not losing good genetic heritage and consequently speeds up convergence.

3.2.2 Crossover and mutation

The crossover operator is employed to improve the genes in of the individuals at the end of each generation. This is done by mixing chromosomes from parent better individuals. Among many crossover functions proposed in the scientific literature in the past years (Eiben and Smith 2015 [146], Umbarkar and Sheth 2015 [147]), uniform crossover proved to be the best typology of function for dealing with design vectors consisting of elements of different nature (Syswerda 1989 [148]). For this reason, a uniform scatter crossover function is used in the proposed framework. The operating principle provides random selection of pairs of parent individuals from the generation. Their genes mixed with the generation of a random binary string of the same dimension of the parents. Based on the binary value (0 or 1) associated with each position, the gene is transferred to the child from the parent 1 or 2 (Figure 3.7(a)).

The crossover function here used has a standard form, while modifications are made in the *mutation* operator. Mutation is used to bring random changes in the population. The need for mutation is to keep diversity in the population. This is the principal operator that leads the exploitation phase by analyzing unexplored areas and avoiding premature convergence at local optimum solutions. At the same time, the higher frequency of applying this operator may also destroy important information contained in the offspring. Hence, the probability of mutation (P_m) is generally kept low (usually between 0.1% and 0.5%) but can increase when the population size is reduced as shown in the calibration stage discussed in the following.

The standard MATLAB® mutation operator cannot handle heterogeneous vectors (e.g. vectors made of natural numbers and Boolean numbers as $\boldsymbol{b}$ vector, and this made necessary the definition of a new mutation function. The latter works by fixing first a suitable mutation ratio (P_m). Then a real number u ($u \in [0,1] \subseteq \mathbb{R}$) is randomly selected for each gene. If $u \geq P_m$ the gene is maintained unchanged, while if $u < P_m$ the gene is mutated. In this way, the probability of mutation is maintained constant. For the Boolean variables included in the design vector, the mutation of a gene is simply a switch from 0 to 1 or vice versa. For the natural variables (the battens spacing s_b) the same procedure is applied, but in the cases in which a gene has to change ($u < P_m$) a further random number v ($v \in [0,1] \subseteq \mathbb{R}$) is selected in order to decide if the mutation will increase or decrease the battens spacing. The new random temporary parameter v leads the mutation toward an increase or decrease of s_b if $v < 0.5$ or $v \geq 0.5$ respectively. Increases and decreases of s_b have the magnitude of the minimum spacing variation (Δ_{sb}). A flow-chart example of the proposed mutation function is illustrated in Figure 3.7b. The application to the current case, in which a limited dimension of the population is used, requires to increase the mutation to values which are larger than 1%. The relatively high

value of mutation ratio helps in avoiding the stall of the analysis into local optimal solution. Suitable mutation ratio values are evaluated in the subsequent sections.

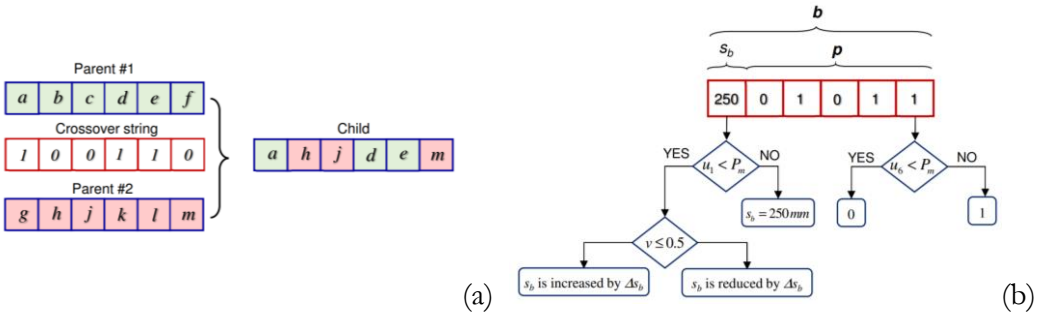

Figure 3.7 – Schematic flowcharts of the: (a) uniform scatter crossover function; (b) proposed mutation function

3.3 Reference structural model

The proposed optimization framework can work with any finite element program handling nonlinear static analysis. Tests and applications presented in the current study are carried out using the *OpenSees* software platform and the structural modelling assumptions below described.

3.3.1 Model of reinforced concrete elements without steel-jacketing

Frame elements are modelled adopting distributed plasticity force-based elements with five Gauss-Lobatto integration points available in *OpenSees* (Figure 3.8). Fiber-section elements are modelled using a *Concrete02* uniaxial material model for the cross-section fibers. It is assumed that the effect of confinement is extended to the whole cross-section (Figure 3.8) both for the cases of columns with and without steel jacketing reinforcement. This simplified assumption allows a formal consistency with the confinement model in the case of concrete confined by stirrups and steel jacketing (Campione et al. 2017 [149]) which provides uniform confinement over the cross-section. In order to simulate the crushing of the cross-section fibers, *Concrete02* material is combined with *MinMax* wrapper material, which removes the contribution of a fiber when a specified strain threshold is achieved. For the current case, it is assumed that crushing of fibers occurs in correspondence of the compressive strain (ε_{cr}) attained at a 30% reduction of the peak strength (Figure 3.8).

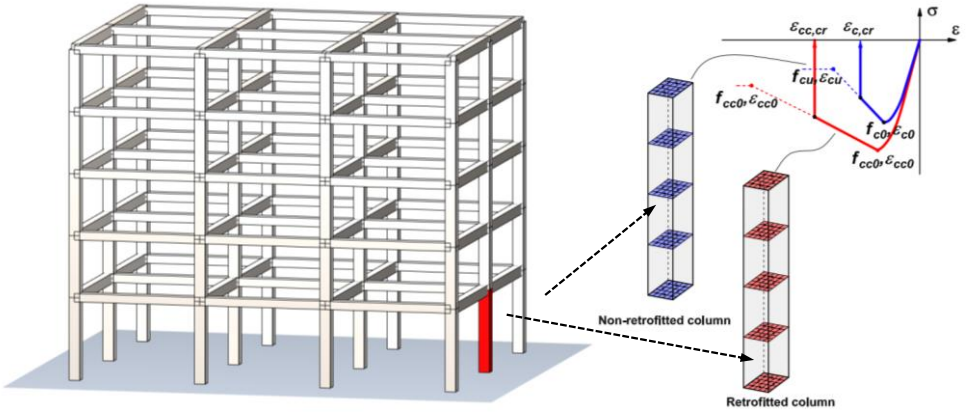

Figure 3.8 – Definition of the frame fiber-section elements with and without steel-jacketing reinforcement.

Confined concrete parameters for the RC elements confined only by stirrups are evaluated using the stress-strain model by Razvi and Saatcioglu 1992 [150].

Steel rebars are modelled using the Steel02 (Giuffrè-Menegotto-Pinto [151]) material model (elastic-plastic with linear strain hardening). Ultimately, rigid diaphragm behavior is imposed at the floor nodes.

3.3.2 Modelling of steel-jacketing action in RC fiber-section columns

The technique of retrofitting reinforced concrete columns using steel jacketing, which involves the installation of steel cages composed of angles and battens, is a common method for enhancing both the strength and deformation capacity of beams and columns in existing structures that face challenges due to seismic and gravity loads. Steel jacketing can be implemented in two primary configurations. The first involves creating a moment-resisting connection between the steel cages and the slabs (Figure 3.9a), which not only provides confinement but also adds flexural strength. However, because establishing moment-resisting connections can be technically challenging, a more frequently employed method involves simply attaching the steel cages to the columns without a rigid connection (Figure 3.9b). Even with this simpler setup, some increase in flexural resistance occurs due to frictional forces between the steel angles and the concrete (Campione et al. 2017 [152]), but the most notable improvement is the significant enhancement of deformation capacity resulting from the effective confinement provided by the steel cage.

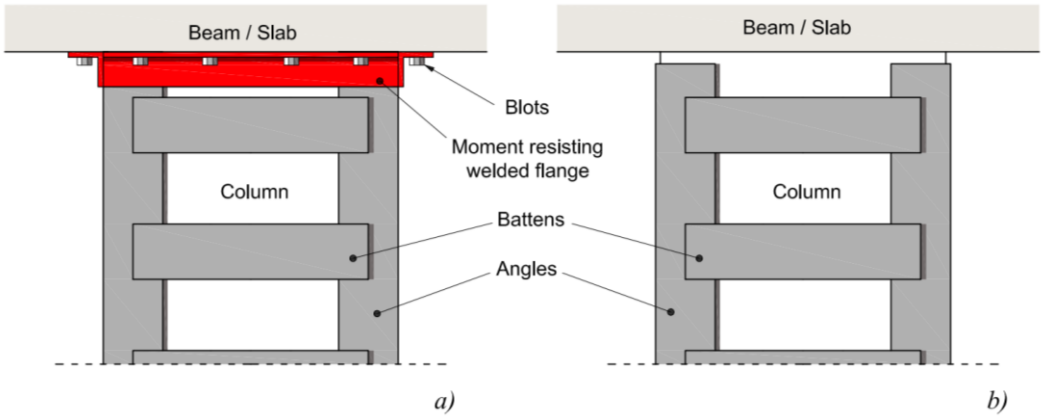

Figure 3.9 - Steel jacketing configurations for columns: a) cage with moment-resisting end connections; b) cage without end connections.

The modeling of steel jacketing in fiber-section elements has been explored by Campione et al. (2017) [152], who demonstrated that when only confinement is accounted for, the steel angles are excluded from the cross-section assembly (Figure 3.10a). Conversely, when a full flexural connection is present, the angles are discretized into fibers with defined uniaxial behavior (Figure 3.10b).

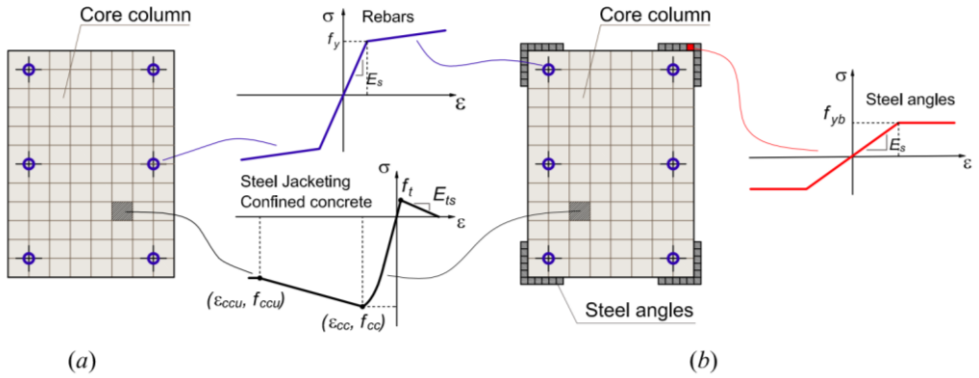

Figure 3.10 – Modelling of steel-jacketing in fiber-section elements: a) steel-jacketing confinement action only; b) steel-jacketing confinement and flexural resistance.

Focusing on the confinement action, regardless of the arrangement method, this is introduced in retrofitted columns by simply adjusting the stress-strain curve of the concrete fibers (Figure 3.10). To determine the confined stress-strain behavior of concrete for the core fibers, the method proposed by Montuori and Piluso (2009) [153]is combined with the expressions by Razvi and Saatcioglu (1992) [150], allowing for an analytical evaluation of peak (f_{cc}, ε_{cc}) and ultimate ($f_{ccu}, \varepsilon_{ccu}$) stress and strain values.

In columns retrofitted with steel angles and battens, the confinement provided by the steel jacketing is additive to that of the stirrups (Figure 3.11a), leading to varying confinement levels across the cross-section. However, since the steel jacketing's confining action predominates, the model employs a single

concrete stress-strain curve for the entire section. This assumption has proven to be sufficiently accurate when compared with experimental results [1-3].

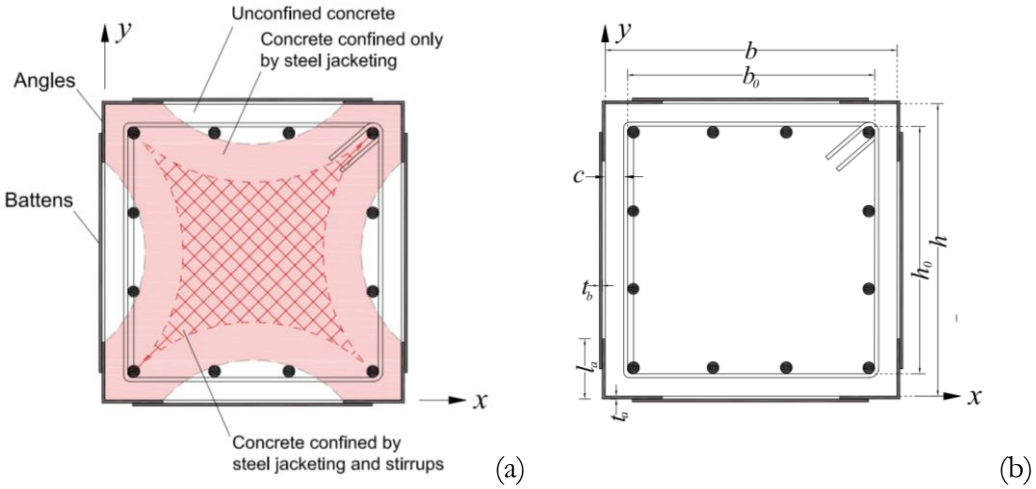

Figure 3.11 - Configuration of the cross-section of a column retrofitted with steel jacketing: a) area effectively confined by stirrups and steel jacketing; b) geometric arrangement.

The lateral confinement pressures $f_{le,x}$ and $f_{le,y}$ along the two directions of the cross-section (Figure 3.11b) are evaluated as:

$$f_{le,x} = k_e \cdot \rho_{st,x} \cdot f_y; \quad f_{le,y} = k_e \cdot \rho_{st,y} \cdot f_y \tag{3.15}$$

in which the calculation of the transverse reinforcement volumetric ratios $\rho_{st,x}$ and $\rho_{st,y}$ consider both the contribution of internal and external transverse reinforcement as:

$$\rho_{st,x} = \frac{n_{bx} A_{st,x} b_0}{s b_0 h_0} + \frac{2 A_{sb,e} b}{s_b b h}; \quad \rho_{st,y} = \frac{n_{by} A_{st,y} h_0}{s b_0 h_0} + \frac{2 A_{sb,e} h}{s_b b h} \tag{3.16}$$

In Equation (3.15) the coefficient k_e expresses the effectively confined area through the expression:

$$k_e = \left(1 - \frac{s_b - \varphi_{st}}{2 b_0}\right)\left(1 - \frac{s_b - \varphi_{st}}{2 h_0}\right) \tag{3.17}$$

In Equation (3.16) and (3.17) b is the cross-section base and h its height, $b_0 = b - 2 \cdot c$ and $h_0 = h - 2 \cdot c$, being c the width of the concrete cover, n_{bx}

and n_{by} are the number of stirrups arms along x and y and $A_{st,x}$ and $A_{st,x}$ the respective areas, $\emptyset_{st}$ is the diameter of stirrups, s and s_b are the spacing of the internal hoops and external battens respectively. The term $A_{sb,e}$ represents the mechanically equivalent transverse area of battens and is calculated as:

$$A_{sb,e} = A_{sb}\frac{f_{yb}}{f_y} \tag{3.18}$$

where A_{sb} is the actual transverse area of a batten. In order to provide an automated determination of confinement parameters, confined peak stress (f_{cc}) and strain (ε_{cc}) and the ultimate stress (f_{ccu}) and strain (ε_{ccu}) are here evaluated by using the expressions provided by Razvi and Saatcioglu (1992) [150] instead of Mander et al. (1989) [154] model. In detail:

$$f_{cc} = f_c + k_1 f_{le} \tag{3.19}$$

where, with reference to Figure 3.11b, f_{le} and k_1 are obtained as:

$$f_{le} = \frac{f_{le,x}b_0 + f_{le,y}h_0}{b_0 + h_0};\ k_1 = 6.7 f_{1e}^{-0.17} \tag{3.20}$$

The confined peak strain ε_{cc} and the confinement factor K are eventually evaluated as:

$$\varepsilon_{cc} = \varepsilon_c(1+5K);\ K = k_1\frac{f_{le}}{f_c} \tag{3.21}$$

The linear softening branch is obtained by joining the peak stress-strain point (f_{cc}, ε_{cc}) with the point at which the compressive strain is reduced by 15% (f_{cc85}, ε_{cc85}). This point is individuated by:

$$f_{cc85} = 0.85 f_{cc};\quad \varepsilon_{cc85} = 0.0036 + 260\rho_{st}\varepsilon_{cc} \tag{3.22}$$

where, in order to include the effect of the steel jacketing, the term ρ_{st} is modified as follows:

$$\rho_{st} = \frac{A_{st,x} + A_{st,y} + 4A_{sb,e}}{\tilde{s}(b_0 + h_0)} \tag{3.23}$$

while $\tilde{s}$ represents the average stirrups / battens spacing that is proposed to calculate as:

$$\tilde{s} = \frac{s + s_b}{2} \tag{3.24}$$

The stress-strain curve becomes constant after the achievement of an 80% reduction of f_{cc}. Considering the linearity of the softening branch, the ultimate stress-strain parameters (f_{ccu}, ε_{ccu}) can be obtained as:

$$\begin{aligned} f_{ccu} &= \alpha f_{cc} \\ \varepsilon_{ccu} &= \varepsilon_{cc} + \frac{(1-\alpha)(\varepsilon_{cc85} - \varepsilon_{cc})}{0.15} \end{aligned} \tag{3.25}$$

where $\alpha = 0.2$. For the current case it assumed that the conventional crushing of concrete fibers occurs when f_{cc} is reduced by 30%. Therefore parameters $f_{cc,cr}$ and $\varepsilon_{cc,cr}$ can be evaluated by Equations (3.25) by setting $\alpha = 0.7$.

The effect of steel jacketing on the resulting stress–strain response in compression of a RC column cross-section fiber is illustrated in Figure 3.12 for different battens spacing. In the same figure, the response of the same column without retrofitting is also provided for comparison.

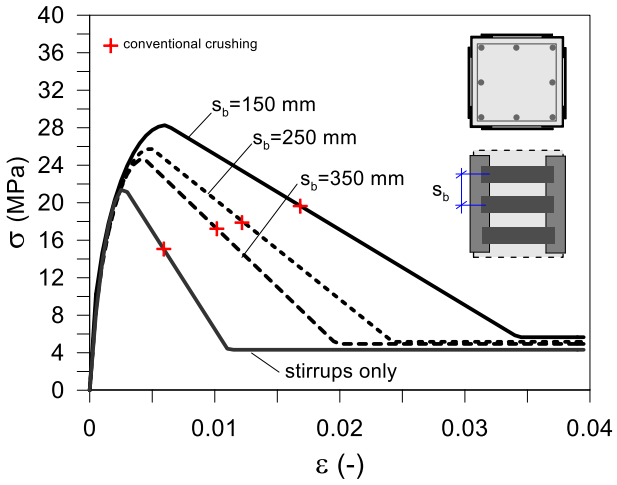

Figure 3.12 – Sample of stress–strain response of concrete in compression for a column without steel jacketing and with steel jacketing

3.3.3 Modelling of masonry infills

Masonry infills (if any) are modelled as equivalent diagonal struts resisting only in compression. The equivalent strut model by Di Trapani et al. 2018 [155] is used for the fiber-section struts (Figure 3.13). The model provides a concrete-type compression-only stress–strain relationship defined by the four

parameters, peak stress (f_{md0}), ultimate stress (f_{mdu}), peak strain (ε_{md0}) and ultimate strain (ε_{mdu}) obtained by empirical equations. The infill is supposed to collapse in correspondence of the axial strain $\varepsilon_{mdc} = 2 \cdot \varepsilon_{mdu}$.

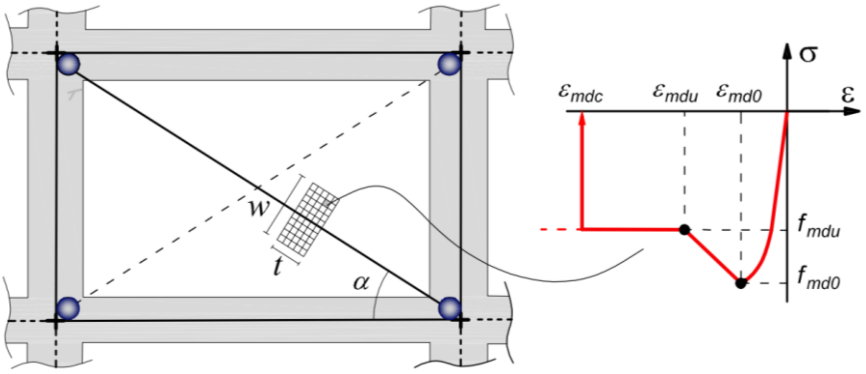

Figure 3.13 – Equivalent strut model for masonry infills.

3.4 Analysis and post-processing of the results

3.4.1 Feasibility assessment by pushover analysis

The feasibility of each solution is assessment by a pushover analysis of the individual. Pushover analysis is carried out in the framework of the N2 method (Fajfar 2000 [140]), also provided by Eurocode 8 [156]. The eventual presence of masonry infills is not considered as a potential source of inaccuracy of N2 method. In fact, in real 3D frame RC structures, collapse is in most cases driven by local failure mechanisms (soft-story, shear failure of columns and joints) even induced by the infills. This is consistent with a quasi-monotonic trend of the pushover curve. The feasibility of each solution is assessed by evaluating the ductility capacity / demand ratios defined by:

$$\zeta_{\mu} = \frac{\mu_c}{\mu_d} \tag{3.26}$$

where the ductility capacity (mc) is obtained as the ratio between the ultimate displacement capacity (d_u^*) and the yielding displacement (d_y^*) of the single degree of freedom bilinear equivalent curve (Figure 3.14), while the ductility demand (μ_d) of an inelastic SDOF system is evaluated as:

$$\begin{cases} \mu_d = \left(q^* - 1\right)\dfrac{T_c}{T^*} + 1 & \text{if } T^* \le T_c \\ \mu_d = q^* & \text{if } T^* > T_c \end{cases} \tag{3.27}$$

where T* is the period of the equivalent SDOF system having mass m*, and stiffness k* and reduction factor q* evaluated as:

$$T^* = 2\pi\sqrt{\frac{m^*}{k^*}}; \quad k^* = \frac{F_y^*}{d_y^*}; \quad q^* = \frac{S_{ae}(T^*)m^*}{F_y^*} \tag{3.28}$$

The coefficient ζ_μ is the final output of the processing of pushover curves and is used as a discriminating factor in the optimization process in order to establish the feasibility of each a single individual ($\zeta_\mu \geq 1$).

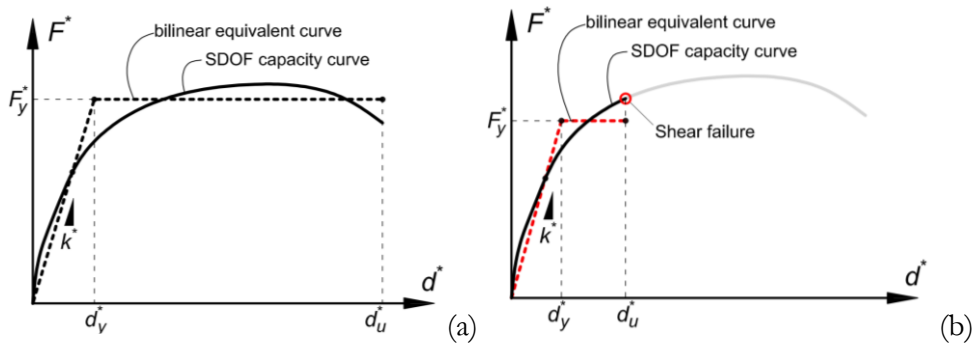

Figure 3.14 – Typical equivalent SDOF capacity curve and bilinear equivalent curve for: (a) shear-resistant (ductile) structures; (b) shear-critical structures.

3.4.2 Post-processing shear verification of RC elements with and without steel-jacketing

The shear verification of columns is carried out in the post-processing phase in terms of strength. The ultimate displacement capacity assumed for the SDOF system is the one associated with the first shear failure of a column. Therefore, if shear failure of a column occurs, the capacity curve is cut in correspondence of that event (Figure 3.14b). Shear verifications are carried out according to the model by Biskinis et al. (2004) [157], also included in Eurocode 8 [8] and in the Italian Technical Code [158] for the evaluation of shear strength of element subjected to seismic loads. This expression evaluates shear resisting capacity as a function of three terms accounting for the strength contribution due the axial load (VN), concrete and longitudinal reinforcement (VC), shear reinforcement (VW) as follows:

$$V_R = V_N + k \cdot [V_C + V_W] \tag{3.29}$$

The coefficient k is reduction factor considering the strength reduction due to cyclic loads as a function of the current ductility demand to the elements. The above described have the following expression:

$$V_N = \frac{h-x}{2L_v} \cdot \min\left(N; 0.55 \cdot A_c \cdot f_c\right)$$

$$V_C = 0.16 \cdot \max\left(0.5; 100 \cdot \rho_{tot}\right) \cdot \left(1 - 0.16 \cdot \min\left(5; \frac{L_v}{h}\right)\right) \cdot \sqrt{f_c} \cdot A_c \quad (3.30)$$

$$V_W = \rho_w \cdot b \cdot z \cdot f_y$$

where h is the height of the cross-section, x is depth of the neutral axis, L_v is the shear span (typically assumed as 0.5 the length of the element), N is the compressive axial force, A_c is the cross-section area, f_c is the concrete compressive strength, $\rho_{tot} = A_{s,long} / (b \cdot h)$ is the total longitudinal reinforcement ratio (b is the base of the cross-section), $\rho_w = A_{sw} / s$ is the transverse reinforcement ratio (with A_{sw} area of the transverse reinforcement and s stirrup spacing), $z = 0.9 \cdot d$ is the length of internal lever arm (d being the effective height of the cross-section) and f_y the yielding stress of the transverse reinforcement. The reduction factor k is evaluated as:

$$k = 1 - 0.05 \cdot \min(5; \mu_{\Delta,pl}) \quad (3.31)$$

where $\mu_{\Delta,pl}$, represents the ratio between the plastic rotation rate of the column and the yielding rotation. The coefficient k ranges between 0.75 and 1. For the sake of simplicity calculations are made simply assuming the average value k=0.875. The shear resistance is updated at each step of the analysis taking into account the variation of the axial load (N) and the related variation of the position of the neutral axis (x). The latter is estimated by means of the following simplified expression, as suggested by the Italian Technical Code [158].

$$x = h\left[0.25 + 0.85 \cdot N / (A_c \cdot f_C)\right] \le h \quad (3.32)$$

Still according to Italian Technical Code [158], the contribution of the steel-jacketing to the shear strength is evaluated with the additional term VJ as follows:

$$V_J = 0.5 \cdot \frac{2 \cdot t_b \cdot w_b}{s} \cdot f_{yb} \cdot 0.9 \cdot d \cdot \cot \vartheta \quad (3.33)$$

where f_{yb} is the yield strength of the steel used for the battens and q is the inclination of shear cracks, while the meaning of other symbols has been explained in previous sections. Given the significant contribution of the steel-jacketing to the shear strength, it is reasonably assumed $\cot \vartheta = 1$, which is also a conservative assumption.

3.4.3 Evaluation of the additional shear demand due to frame-infill interaction

Masonry infills induce a significant increase of shear in adjacent columns. In case of single concentric strut, the additional shear demand due to infills ($V_{C,inf}$) can be estimated as (Di Trapani and Malavisi 2019 [159]):

$$V_{C,inf} = P_{str} \cdot \cos\alpha - \mu \cdot P_{str} \cdot \sin\alpha \tag{3.34}$$

where, referring to Figure 3.12, P_{str} is the current value of the axial force acting on the equivalent strut, α is the angle of inclination of the strut with respect to horizontal direction, and μ the friction coefficient associated with the infill-mortar-frame interface and assumed as 0.7 in absence of more detailed evaluations.

The total shear demand on a column of the frame adjacent to and infill (V_D) will be the evaluated as the sum of shear force currently acting on the column ($V_{C,fr}$) and the additional shear demand ($V_{C,inf}$) so that:

$$V_D = V_{C,fr} + V_{C,inf} \tag{3.35}$$

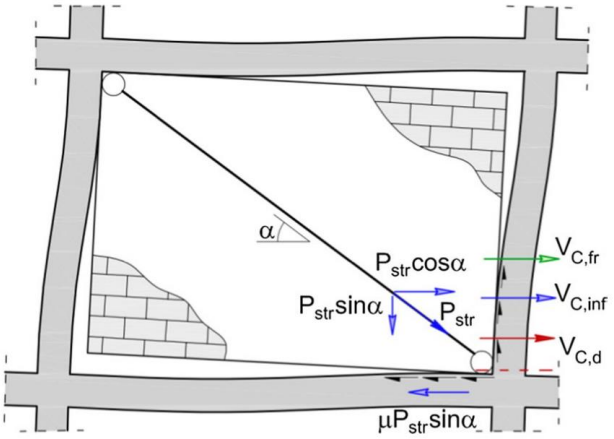

Figure 3.15 – Simplified scheme for the determination of actual shear demand on columns for an infilled frames (from Di Trapani and Malavisi 2019 [159])

3.5 Tests of the optimization framework and calibration of the genetic operators

As illustrated in previous sections, modified genetic operators have been introduced in the optimization framework. Their effectiveness is here tested in comparison with the standard ones, also providing some remarks on the most suitable calibration of parameters. The tests are carried out on a reference reinforced concrete frame case study structure having column with shear deficiencies in a high seismic hazard zone.

3.5.1 Details of the reference test structure

The case study building consists of a five-story reinforced concrete structure designed to resist only gravity loads. The building is supposed being located in Cosenza (Italy), soil type C. The reference nominal life (V_N) is 100 years. The resulting return period is TR=975 years. The structure (Figure 3.16) has double symmetry in plan and is regular in elevation. Modelling assumptions are illustrated in Section 4. Reinforced concrete elements are supposed to be made of concrete having average unconfined strength $f_{c0} = 20$ MPa and steel rebars with nominal average yielding strength $f_y = 455$MPa. Reinforcement details of beams and columns are shown in Figure 3.16b and Table 3.1.

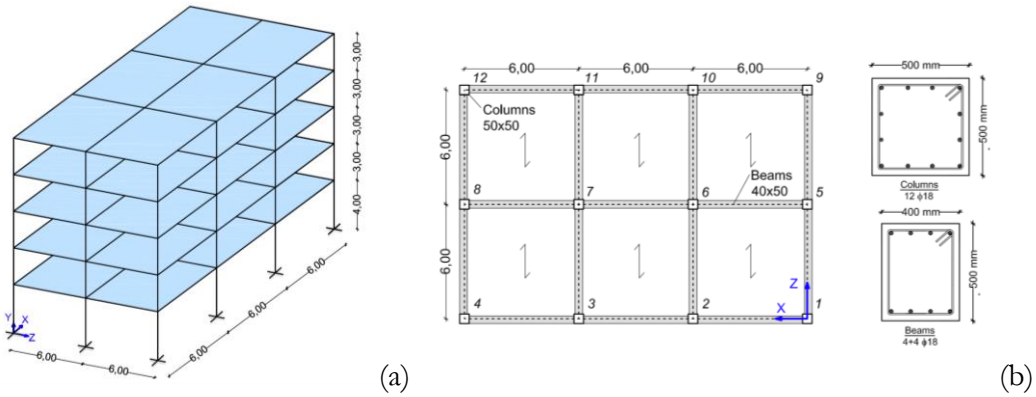

(a) (b)

Figure 3.16 – Geometrical dimensions of the case study structure: (a) 3D frame view; (b) dimensions in plan.

Table 3.1 – Reinforcement details of beams and columns.

RC members	b x h (mm)	Longitudinal reinforcement	Transverse reinforcement
Beams	400 x 500	4+4 Ø18	Ø6 / 200 mm
Columns	500 x 500	12 Ø18	Ø6 / 200 mm

Vertical loads are modelled as point loads applied to the top node of each column as function of the respective tributary areas in plan. This simplified assumption does not significantly modify the response of columns under investigation. The total weight of each floor is $2160\,\text{kN}$. For the sake of simplicity, pushover analyses are carried out by considering only a uniform profile for lateral loads acting along the softer direction of the structure.

Regarding steel-jacketing retrofitting, it is supposed that angles and battens are made of steel having nominal yielding strength $f_{yb} = 275\ \text{MPa}$ and the same dimension for angles and battens (Table 3.2), while the battens spacing (sb) range of optimization is 150-400 mm.

Table 3.2 – Steel-jacketing arrangement details.

Angles		Battens		
Lateral length la (mm)	Thickness wa (mm)	Width wb (mm)	Thickness tb (mm)	Spacing sb (mm)
Columns	5	50	5	150-400

Moreover, to reduce the computational effort the following restriction have been applied to the design space:

i) Retrofitted columns can be only located within the first the second floor.

ii) Battens spacing optimization can vary with a minimum step size Δ_{sb} of 50 mm.

Assumption i is justified by the fact that the maximum deformation demand is expected at the first two (of five) stories. Assumption ii allows reducing the possible combinations of the design vector by limiting sb to assume six possible values as follows:

$$s_b \in [150,\ 200,\ 250,\ 300,\ 350,\ 400] \tag{3.36}$$

The resulting size of the design space is then of 24 Boolean variables and 6 discrete natural values. Consequently, the design space has a dimension of $6 \cdot 2^{24} \cong 10^8$ solutions.

3.5.2 Test of the modified genetic operators

The above-described structure is used as a case-study to test the effectiveness of the introduced modifications in the genetic operators. The effect of the modification of the population generator is first analyzed. A population of 80 individuals per generation is used. As it can be observed in Figure 3.17, a completely random selection of initial population in a shear-

critical structure brings to a probability of obtaining feasible solutions which is so low that the algorithm explores only the field of the unfeasible solutions. Therefore, the standard algorithm is in this case unable to provide an adequate retrofitting solution. On the contrary, the insertion of only 8 individuals having 90% retrofitting probability in the same population ($p_{Pr} = 10\%$, $P_r = 90\%$) definitely improves the result (Figure 3.18), since this allows the replication of similar individuals in the subsequent generations and orient the optimization in the feasible space. To support this process, the elitism function (E) has been also used by bringing the 4 best individuals per generation, unchanged into the next generation ($E = 5\%$). The mutation operator is added in the final test using a mutation probability $P_m = 10\%$. The improvement obtained by adding this operator is not really evident from Figure 3.19, which apparently shows a similar distribution of the solutions found in the previous case (Figure 3.18). The beneficial effect of the mutation is clearer from Figure 3.20, where the convergence performances of the three versions of the algorithm are compared. From Figure 3.20 it can be observed that the application of the mutation operator allows obtaining the optimal solution after processing about 670 individuals instead of 1100 (as performed by the modified GA without mutation). The inclusion of the mutation operator has effectively shown to be fundamental to avoid the stalling of the algorithm in local minimum solutions and save computational time.

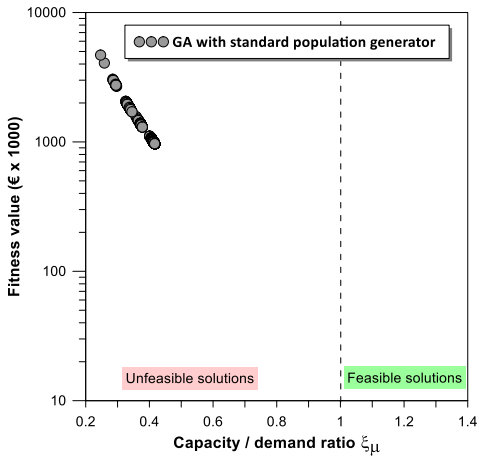

Figure 3.17 – Objective function values for GA with standard population generators.

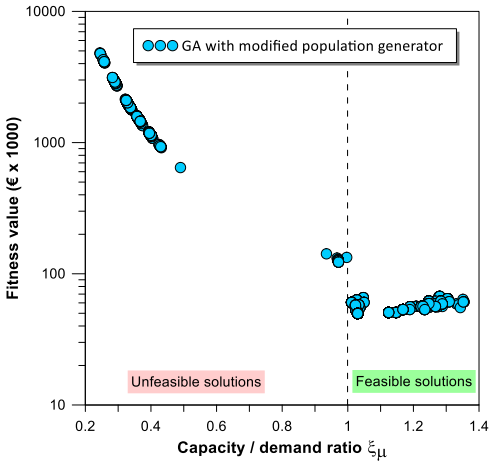

Figure 3.18 – Objective function values for GA with modified population generator

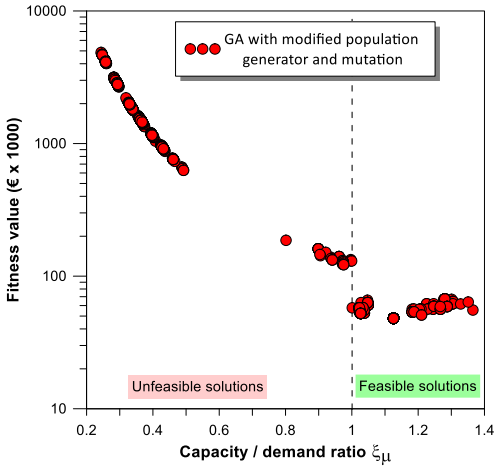

Figure 3.19 – Objective function values for GA with modified population generator and mutation ad a function of ξ_μ

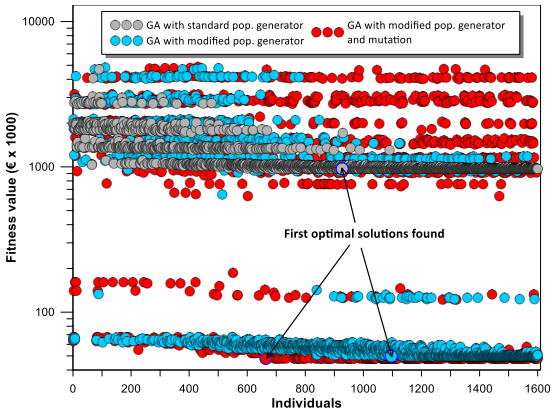

Figure 3.20 – Comparison of the convergence history of the GA with standard population generator, with modified population generator and with modified population generator and mutation.

3.5.3 Calibration of the GA settings

Initial calibration tests have been carried out to provide the most performing parameter settings for the proposed GA framework. Three convergence tests have been performed (Table 3.3) by varying the population size (P) as a function of the dimension of the design vector (dim(b)) (Test #1), the dimension of the p_{Pr} with respect to the population size (Test #2), the probability of mutation (p_m) (Test #3).

Results are shown in the following Figure 3.21 to Figure 3.23 for the different tests. Results of Tests #1 (Figure 3.21) show that the best convergence performance is obtained by setting the population dimension as three times the dimension of the design vector. The use of larger population sizes, besides requiring more computational effort, seems not useful to improve the convergence along with the generation of individuals. In Tests #2 (Figure 3.22) the percentage of population undergoing high retrofitting probability for the columns (p_{Pr}) is varied in the range 20%-80%. The best results in terms of convergence have been found with $p_{Pr} = 50\%$. Reduced dimensions of p_{Pr} still allowed obtaining similar optimal solutions although requiring more generations.

On the contrary, the adoption of a p_{Pr} space larger than 50% brought the algorithm to stall into local minimum solutions associated with larger costs. This is due to the fact that most of the genetic heritage is exchanged between to individuals with very high retrofitting rates. In Test #3, the percentage mutation ration is varied (Figure 3.23). Results have shown that the non-use of mutation or the use low mutation ratios (e.g. 1%) made the algorithm unable to find an optimal solution. Differently, the adoption of mutation ratios of 5% and 10% improved both the solution and the convergence rate. Finally, the use of larger mutation ratios (25% - 35%) provided worse results, as this tends to disperse the genetic heritage of the fittest solutions.

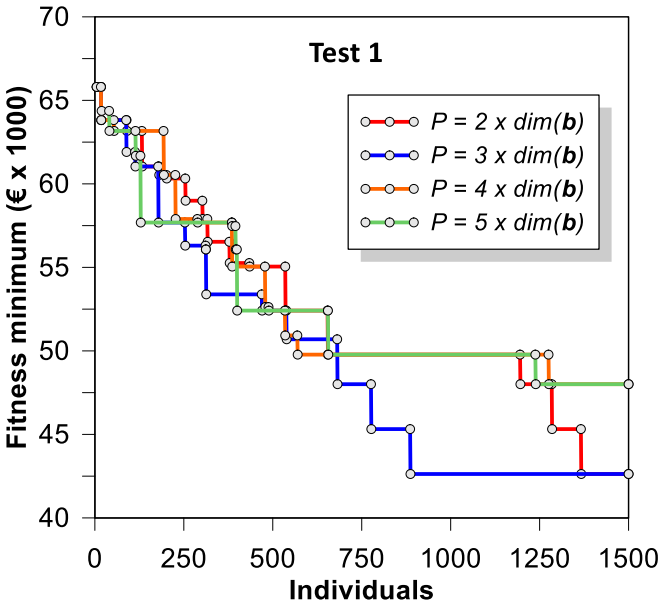

Figure 3.21 – Tests of the modified GA for the calibration of the dimension of the population

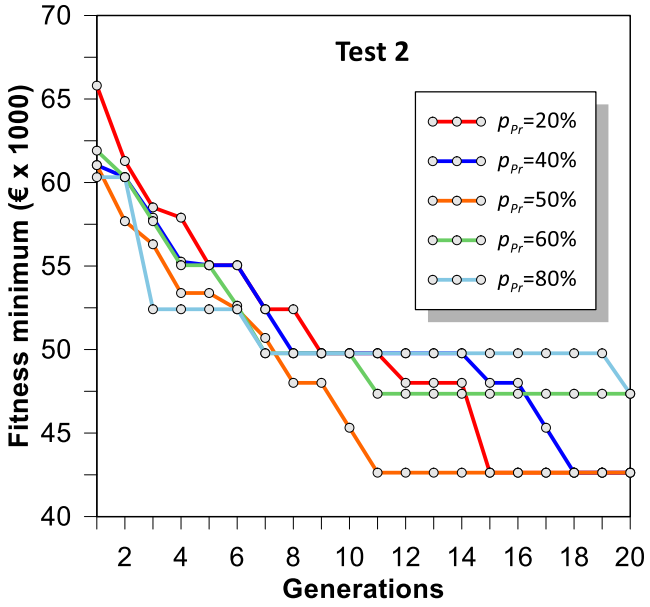

Figure 3.22 – Tests of the modified GA for the calibration of the dimension of the pPr space

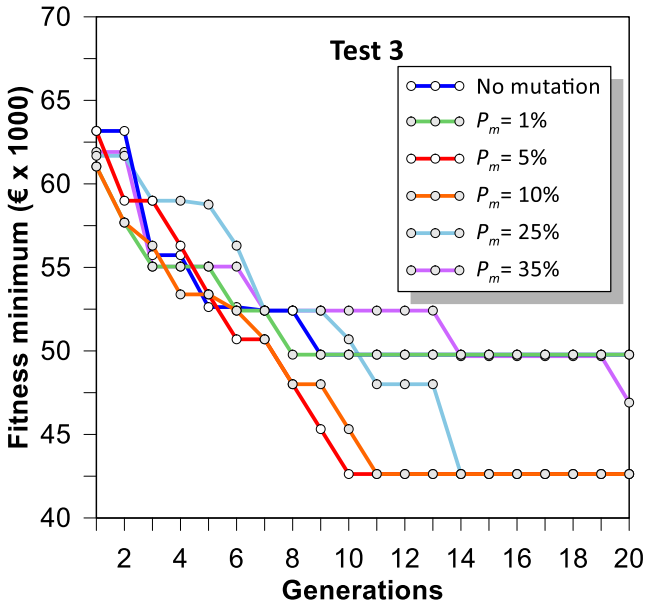

Figure 3.23 – Tests of the modified GA for the calibration of the probability of mutation

In order to check the stability of the algorithm with respect to the optimum result, a further test (Test 4), has been carried out by running 5 times the algorithm with the optimal parameters found ($P = 3 \times \dim(\mathbf{b})$, p_{Pr}=50%, P_m=5%). Results are shown in Figure 3.24a, which also shows the average and dispersion of the different cases run. The optimal solution found is also shown in Figure 3.24(b). The tests showed that all the runs converged to the same optimal solution is achieved each time although with moderate differences in the number of generations, demonstrating sufficient stability of the proposed algorithm.

Table 3.3 – GA parameters for the calibration tests

Test number #	Dimension of the design vector dim (b)	Population size P	Dimension of the p_{Pr} space p_{Pr}	Prob. of retrofitting of an element in the p_{Pr} space P_r	Probability of mutation P_m	No. of indiv. subject to Elitism per gen. E
Test 1		variable	50%		10	
Test 2	25	80	variable	90%	10	5%
Test 3		80	50%		variable	

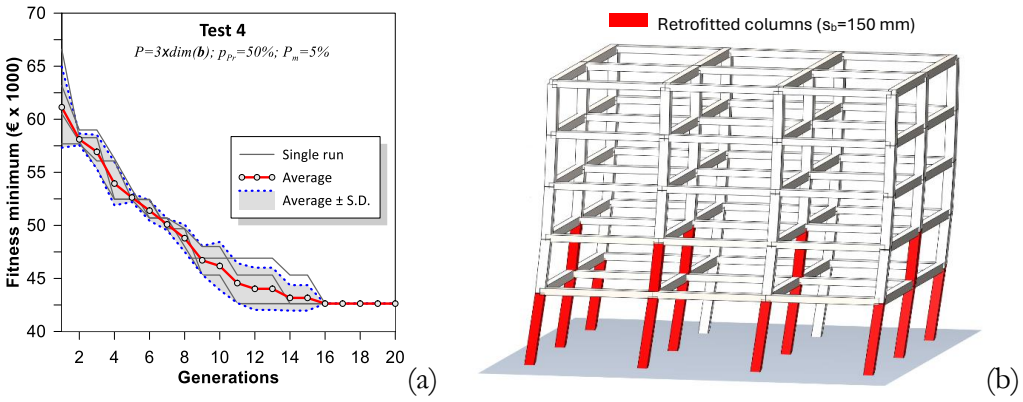

Figure 3.24 – Stability test with the optimal parameters: (a) Convergence history of 5 runs; (b) Optimal retrofitting solution.

Results obtained from the above-described calibration tests can be summarized by the following points:

- The population size (P) can be reasonably set as three times the dimension of the design vector.
- The dimension of the p_{Pr} space should not exceed 50%, which is also a suggested value to set if the percentage of retrofitting is high ($P_r = 90\%$).
- Elitism function should be used. This can be reasonably fixed to 5% of the individuals to pass to each next generation unchanged.
- The probability of mutation can be set as $P_m = 5\% \div 10\%$ if the population size respects the rule of three times dim(b).

3.6 Test of the GA framework with different case study structures

3.6.1 Case study structure description

An application of the proposed framework is carried out for a case study structure supposing two different configurations of the infills. The reference reinforced concrete frame structure is the same as the one described in the previous section. Infills are supposed made clay hollow masonry having thickness $t = 250$ mm, elastic modulus $E_m = 6400$ MPa compressive strength $f_m = 8.6$ MPa and shear strength $f_{vm} = 1.07$ MPa. Equivalent strut properties

defined according to the model by Di Trapani et al. 2018 [160] are reported in Table 3.4.

Table 3.4 – Geometric and mechanical details of the equivalent struts.

t (mm)	w (mm)	f_{md0} (MPa)	f_{md0} (MPa)	ε_{md0} (-)	ε_{mdu} (-)
250	1053	1.88	0.86	0.010	0.073

In the first infilled frame configuration (IFC-1) infills are located in correspondence of the side frames with symmetric arrangement (Figure 3.25(a)). In this configuration infills are not provided on the ground floor. In the second configuration (IFC-2), infills are provided only in one of the side frames and extended to the ground floor (Figure 3.25b). The reason for the choice of these two configurations for the infills is related to the fact that they tend to induce a significantly different seismic demand to the structures in terms of shear and ductility. In this way the responsiveness of the framework to find specific optimal solution is also tested. Moreover, the optimization of the two structures is carried out supposing the RC frame columns being shear-critical (SC) or shear-resistant (SR). In the first case, shear reinforcement of columns is supposed being the one described in Table 3.1.

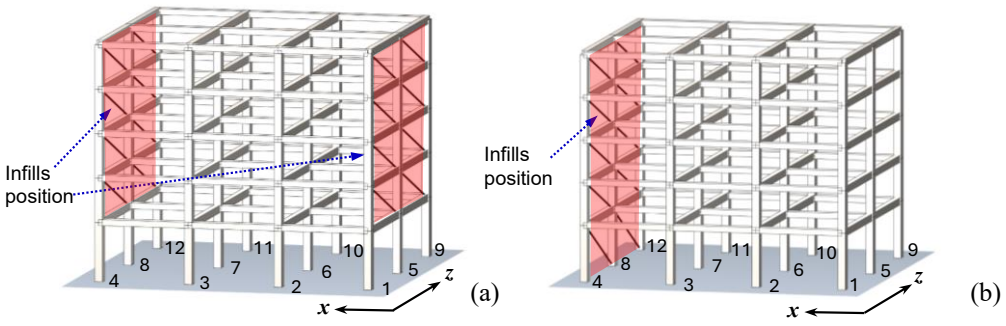

Figure 3.25 – Case study structures: (a) IFC 1: symmetric positioning of infills with pilotis storey; (b) IFC2: asymmetric positioning of infills.

In the second case, columns are supposed to have adequate shear resistance to support seismic loads. This further test allows investigating the general validity of the algorithm to work with both the typologies of structures. A summary of the optimization tests program is provided in Table 3.5.

Table 3.5 - Case studies main characteristic.

Case	Infills configuration	Shear behavior of columns	Optimization space
IFC1.SC	Symmetric with pilotis story	critical	1st and 2nd story columns
IFC1.SR		resistant	
IFC2.SC	Asymmetric	critical	
IFC2.SR		resistant	

Steel-jacketing design assumptions are the same as those illustrated in Table 3.2. Moreover, in order to reduce the computational effort, the optimization space of retrofitted columns is limited to the first two floors (24 columns), where the maximum seismic demand is expected in terms of shear and ductility. Optimization tests are carried out considering a pushover analysis with a uniform distribution of lateral forces along z direction. The adopted settings for the GA optimization framework are consistent with the values obtained in the calibration stage and are summarized in

Table 3.6 – GA framework settings used for the case studies.

Dimension of the design vector dim (b)	Population size P	Dimension of the p_{Pr} space p_{Pr}	Prob. of retrofitting of an element in the p_{Pr} space P_r	Probability of mutation P_m	No. of indiv. subject to Elitism per gen. E
25	80	50%	90%	10	5%

3.6.2 Preliminary assessment tests

Before starting with the optimization process, two reference preliminary tests have been carried out to assess the case study structures in the "as-built" and "full retrofitting" configurations. In the first test, the as-built performance of the IFC-1 and IFC-2 structures is tested. For both the configurations the cases of shear-critical and shear-resistant columns are considered. In the second test, the performance of the structures is assessed considering the full retrofitting of the columns in the optimization space with the minimum battens interaxis (s_b=150 mm). For what concerns the as-built tests, it can be observed that both the structures have insufficient capacity to sustain seismic demand. The capacity is dramatically reduced in the case of shear critical columns. For the IFC-1 structure (Figure 3.26) the major vulnerability source is the activation of a soft-storey mechanism requiring additional ductility ($\zeta_\mu = 0.469$).

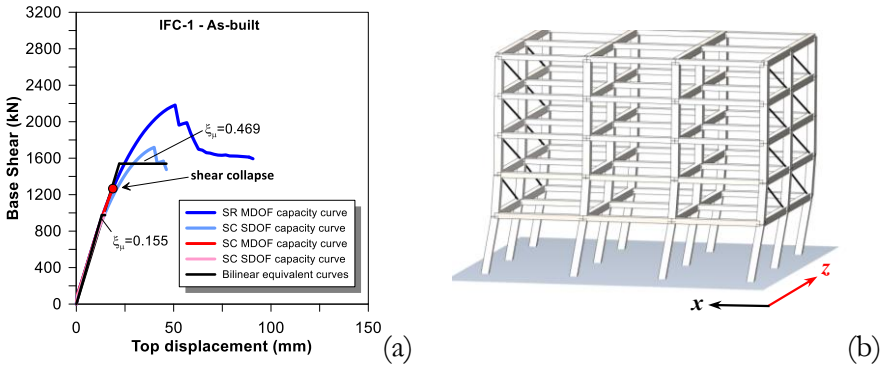

Figure 3.26 – As built preliminary IFC 1 test: (a) capacity curve (b) deformed shape.

The lack of ductility also affects the IFC-2 structure (Figure 3.27) also because of the torsional demand ($\zeta_\mu = 0.659$). In the case of shear-critical columns, the capacity / demand ratios reduction depends on the additional shear demand due to the infills, bringing the ζ_μ ratios to 0.155 and 0.079 for the IFC-1 and IFC-2 structures respectively.

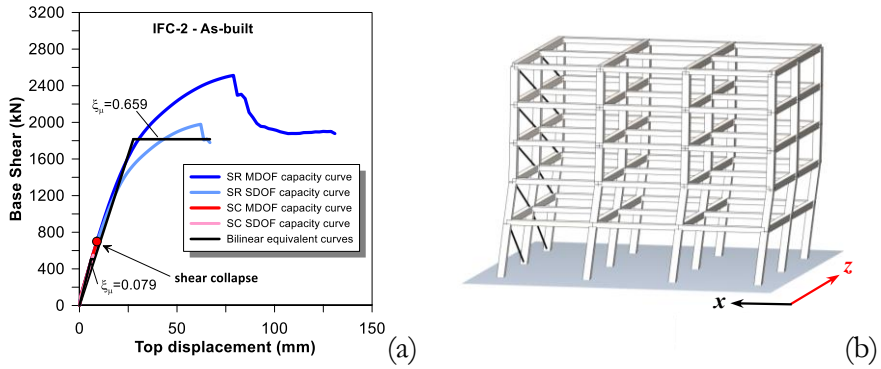

Figure 3.27 – As built preliminary IFC 2 test: (a) capacity curve (b) deformed shape.

In these cases, shear collapse is attained in the quasi-elastic stage. In the full retrofitting cases, the shear and ductility lacks are solved by the steel-jacketing retrofitting both for the IFC-1 and IFC-2 configurations (Figure 3.28), which present similar high ζ_μ ratios ($\zeta_\mu = 1.539$ and $\zeta_\mu = 1.547$ respectively).

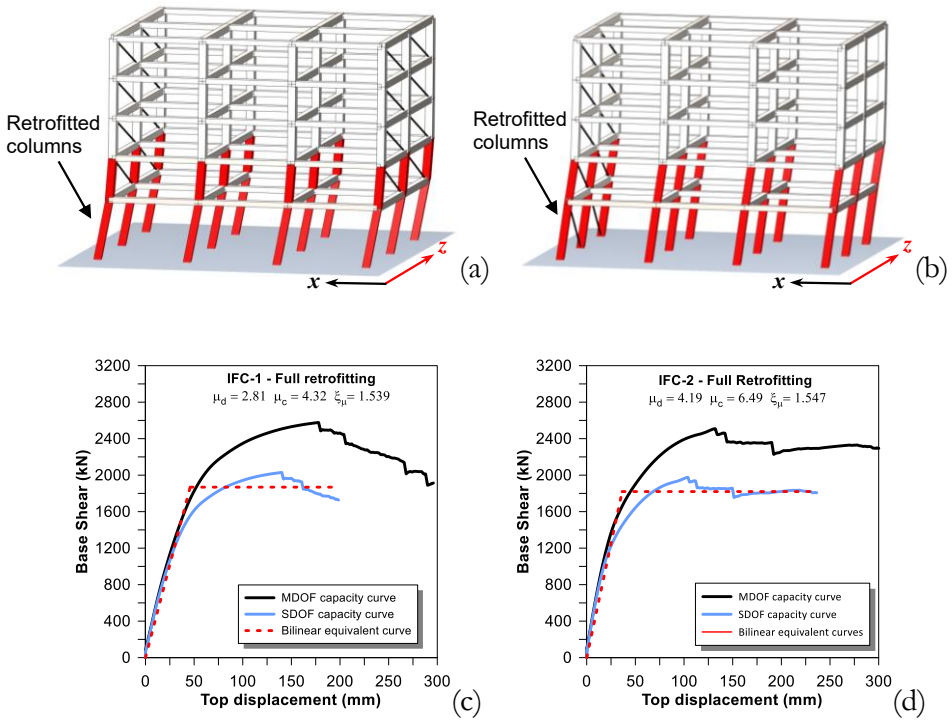

Figure 3.28 – Preliminary tests with all 1st and 2nd storey columns retrofitted: (a) IFC1 deformed shape; (b) IFC2 deformed shape; (c) IFC1 capacity curves; (d) IFC2 capacity curves.

This confirms that the full retrofitting of the columns is surely a feasible solution, although it is not optimized in terms of exploitation of the retrofitting system. Result details of the tests are summarized in Table 3.7.

Table 3.7 – Results of preliminary tests.

Structural configuration	Test	Shear behavior of columns	s_b (mm)	n_c (-)	C (€)	μ_d (-)	μ_c (-)	ζ_μ (-)	Verif. check
IFC-1	As-built	SR	-	-	-	4.46	2.09	0.469	No
		SC	-	-	-	7.27	1.12	0.155	No
	Full retrofitting	-	150	24	69 618€	2.81	4.32	1.539	Yes
IFC-2	As-built	SR	-	-	-	3.67	2.42	0.659	No
		SC	-	-	-	15.05	1.18	0.079	No
	Full retrofitting	-	150	24	69 618€	4.19	6.49	1.547	Yes

3.6.3 Optimization results for the different case studies

As previously mentioned, four optimization tests have been carried out with the aim of assessing first the responsiveness of the proposed framework in finding optimal retrofitting solution under different potential damage scenarios (IFC-1 and IFC-2 configurations). Secondly, the general validity of the

framework, and in particular of the modified genetic operators, has been tested by considering both shear-critical (SC) and shear resistant (SR) configurations for the columns. This allows understanding the algorithm performance as a function of the variety of the population.

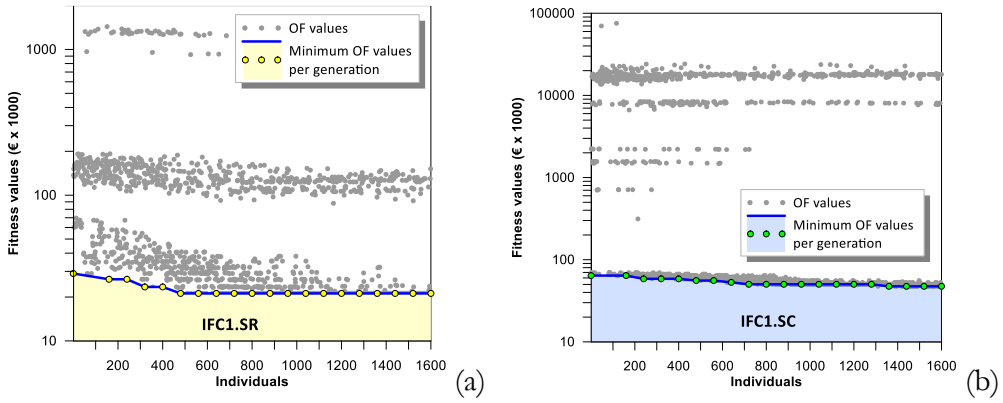

Figure 3.29 – Convergence history for: (a) IFC1.SR structure; (b) IFC1.SC structure

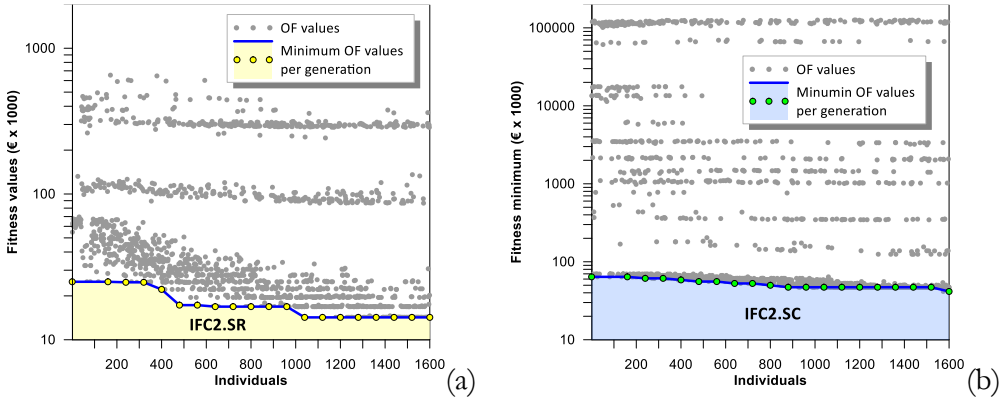

Figure 3.30 – Convergence history for: (a) IFC2.SR structure; (b) IFC2.SC structure

The convergence histories of the tests are illustrated in Figure 3.29 (IFC-1) and Figure 3.30 (IFC-2). As can be observed, the proposed framework allowed the individuation of a specific optimal solution for each of the considered cases. It is noteworthy observing that shear-critical and shear-resistant configuration had very different convergence histories. In fact, shear-critical configurations were associated with a noticeable number of unfeasible solutions with very high fitness values (Figure 3.29b and Figure 3.30b) because of the application of the penalty term. On the contrary, the number of unfeasible individuals was significantly reduced for the SR cases (Figure 3.29a and Figure 3.30a). The framework has been demonstrated to be sufficiently robust against the heterogeneity of the population. Of course, shear-critical configurations were associated with a larger number of generations to get the optimal solutions as it can be clearly observed from Figure 3.31.

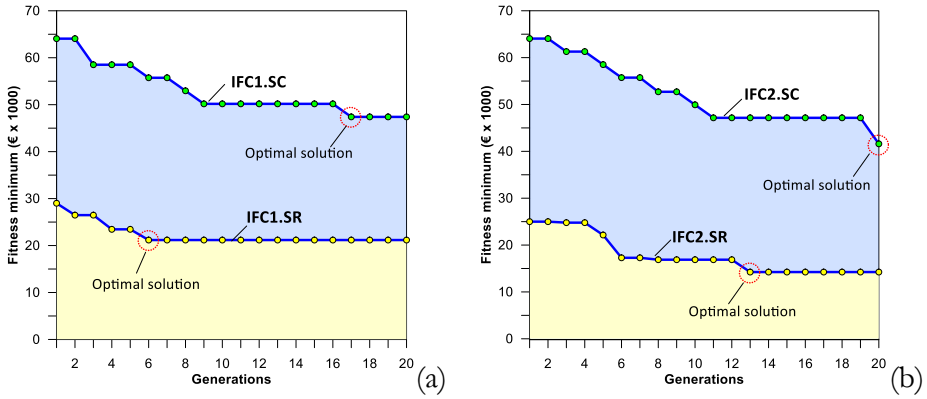

Figure 3.31 – Comparison of the minimum OF values per generation:
(a) IFC1.SR and IFC1.SC structures; (b) IFC2.SR and IFC2.SC structures.

The performances of the optimal retrofitting configurations in terms of capacity curves as well as the respective retrofitting arrangements are shown in Figure 3.32 - Figure 3.35. The consistency of the optimal retrofitting layouts with the expected structural deficiencies if very clear form Figure 3.32c, Figure 3.33c, Figure 3.34(c), Figure 3.35(c), showing the structural deformed shapes under z+ pushover loads and highlighting in red the retrofitted columns. In fact, for both IFC-1 and IFC-2 shear resistant structures, retrofitting was provided for central columns, which have reduced ductility because of the larger axial force, and leeward columns which are subjected to axial force increases because of the base moment. On the contrary, no windward columns were retrofitted for these two configurations as these undergo axial force reduction and ductility increase. The number of retrofitted columns was 7 and 5 respectively for IFC-1.SR and IFC-2.SR configurations. The major number retrofitted of columns for the IFC-1.SR configuration is related to the more severe damage mechanism (soft story) induced by lateral loads with respect to the IFC-2.SR configuration, where this is partially reduced by the bracing action due to the infills at the ground level. For what concerns shear critical configurations IFC-1.SC and IFC-2.SC, more retrofitted columns were found. The shear deficiency of columns, and the associated retrofiring demand is clearer observing Figure 3.33c and Figure 3.35c, which firstly highlight that the additional shear demand due to the pushing action of infills (Equation (3.35)) plays a relevant role. In fact, retrofitting was requested to every leeward column adjected to the equivalent struts. Shear retrofitting was also requested to windward columns because of their axial load reduction under lateral loads and the consequent shear strength reductions according to Equation (3.29). For all the retrofitting configurations low battens spacing was found (s_b=150÷200 mm). This can be justified considering that, at least for the current case, fixed costs influenced more than steel cage-related costs.

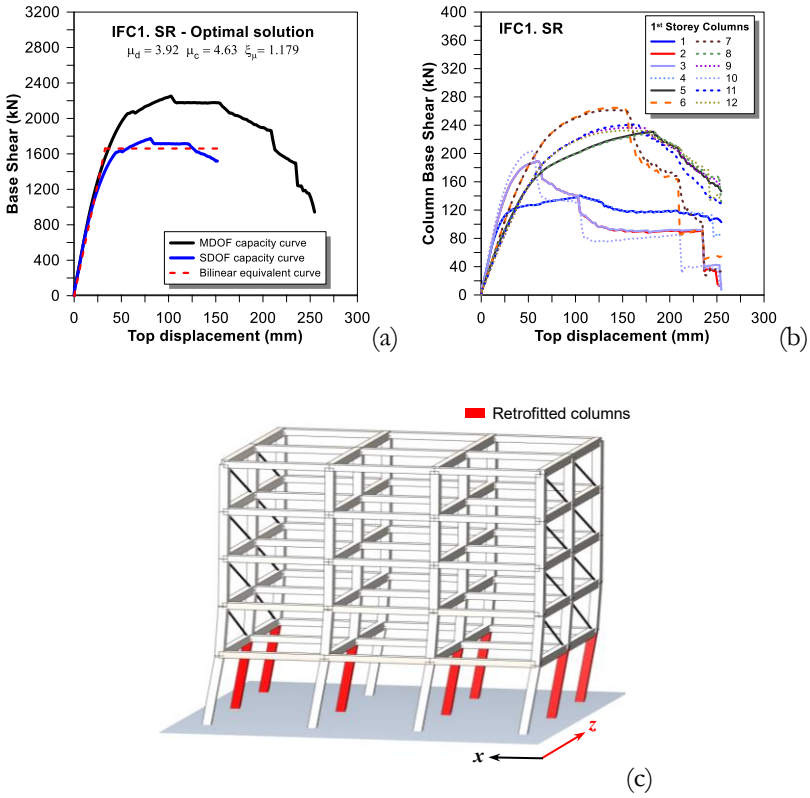

Figure 3.32 – Optimal solution for IFC1.SR structure: (a) Overall capacity curves; (b) First storey columns capacity curves; (c) Retrofitting configuration at the first two stories.

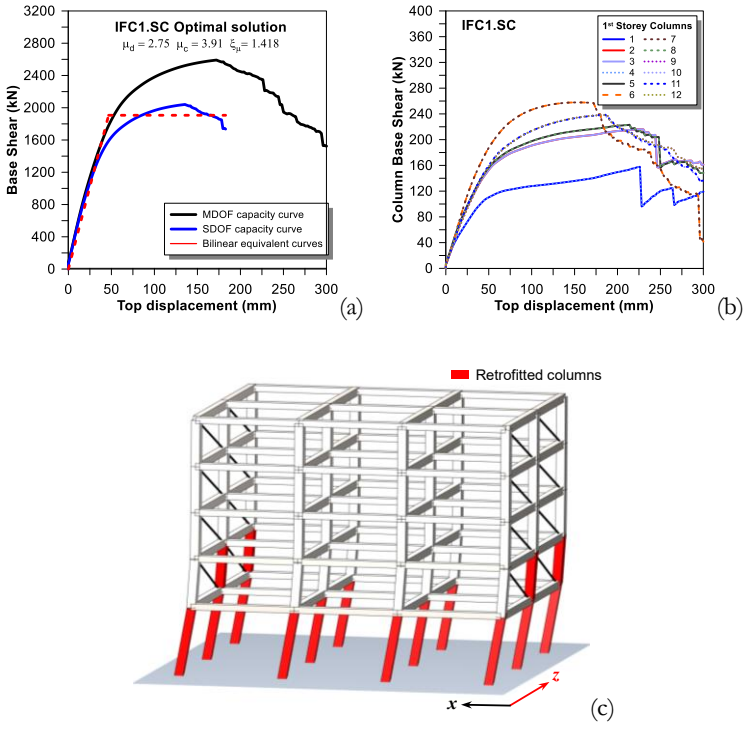

Figure 3.33 – Optimal solution for IFC1.SC structure: (a) Overall capacity curves; (b) First storey columns capacity curves; (c) Retrofitting configuration at the first two stories.

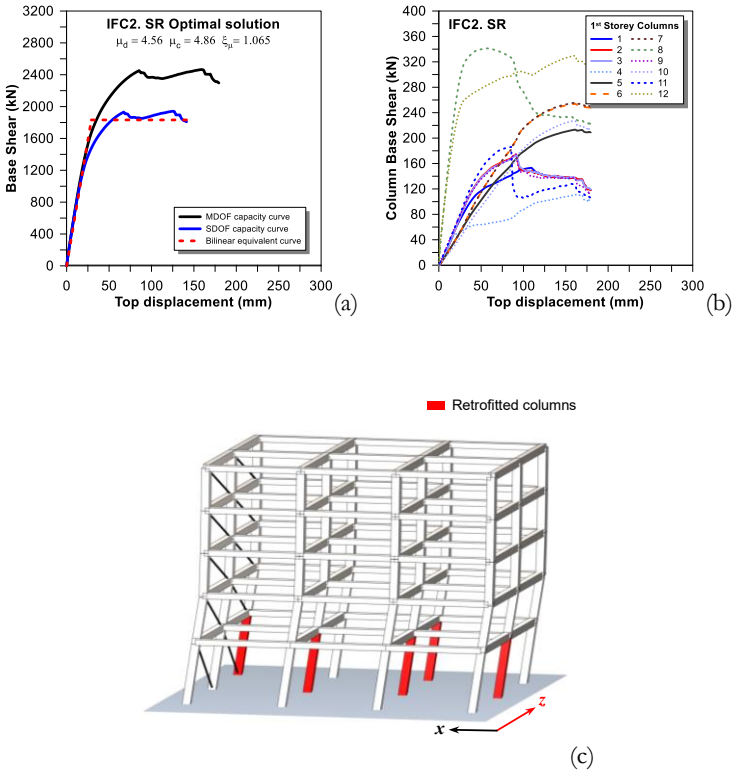

Figure 3.34 – Optimal solution for IFC2.SR structure: (a) Overall capacity curves; (b) First storey columns capacity curves; (c) Retrofitting configuration at the first two stories.

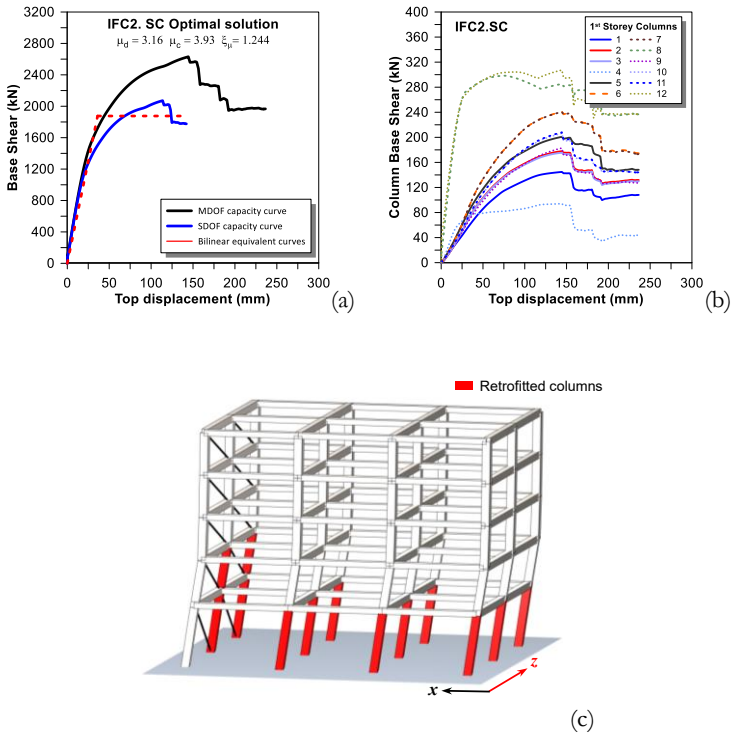

Figure 3.35 – Optimal solution for IFC2.SC structure: (a) Overall capacity curves; (b) First storey columns capacity curves; (c) Retrofitting configuration at the first two stories.

Therefore, the framework tends to prefer solutions providing the minimum possible number of columns even with a reduction of the battens spacing. Results of the optimization test in terms of cost, performance and arrangement are summarized in Table 3.8.

Based on the previously discussed results the proposed optimization tests have demonstrated the expected traits of generality, robustness, and adaptability to the specific damage conditions. The advantages in terms of economical cost savings can certainly justify the application of a retrofitting optimization framework in the current practice. Of course, this is even more true for larger reinforced concrete frames structures, where retrofitting and downtime costs become a crucial issue.

Table 3.8 – Overview of the optimization results.

Structural configuration	s_b (mm)	n_c (-)	C (€)	μ_d (-)	μ_c (-)	ζ_μ (-)
IFC1.SR	150	7	21 171	3.92	4.63	1.179
IFC1.SC	150	16	47 402	2.75	3.90	1.419
IFC2.SR	200	5	14 239	4.56	4.86	1.065
IFC2.SC	150	13	38 823	3.15	3.93	1.244

3.6.4 Final design configurations

Results of the optimization previously shown refer to only one direction of lateral loads (Z+). As mentioned in Di Trapani et al 2020 [142], results obtained for one direction can be easily extended to the other directions in case of structural symmetry as for the current cases. A symmetry criterion was adopted to select the columns to retrofit to resist Z- direction loads. Results in Figure 3.36 show the capacity curves resulting for the final design solution adopted for Z+/- directions. Performance and cost details can be found in Table 3.9.

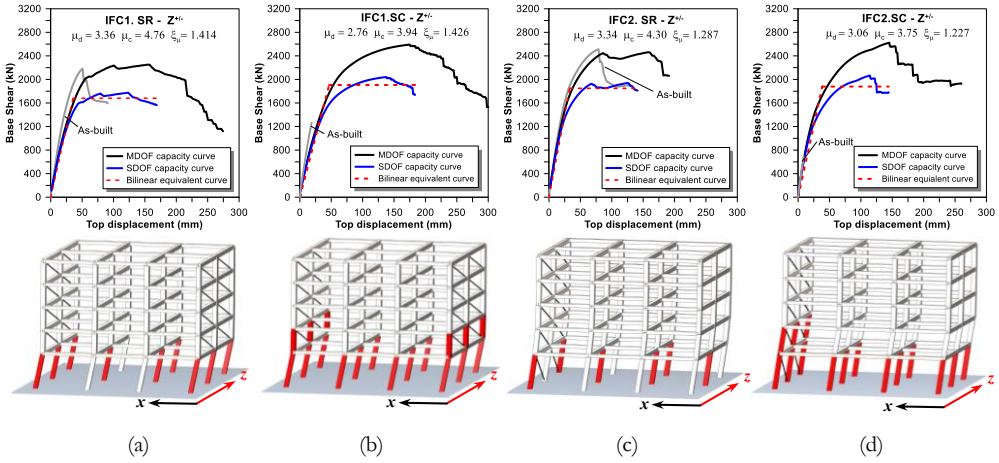

Figure 3.36 – Design solutions capacity curves and retrofitting configurations for: (a) IFC1.SR; (b) IFC1.SC; (c) IFC2.SR; (d) IFC2.SC

In the same diagrams, the as-built capacity curves are also represented for sake of comparison. Results confirm that optimal retrofitting configurations obtained for one-direction optimization can be used as design suggestions that can be extended with simple considerations. Of course, this is especially true for regular structural configuration. In the case of significant structural irregularities "full" optimization can be still performed (Di Trapani et al. 2020 [142]).

Table 3.9 – Result details for the final design solutions.

Structural configuration	Direction	s_b (mm)	n_c (-)	C (€)	μ_d (-)	μ_c (-)	ζ_μ (-)
IFC1.SR	Z+/-	150	9	27 220	3.36	4.76	1.414
IFC1.SC	Z+/-	150	8	52 956	2.76	3.94	1.426
IFC2.SR	Z+/-	200	6	18 146	3.34	4.30	1.287
IFC2.SC	Z+/-	150	15	44 624	3.06	3.75	1.227

3.7 Conclusions

This chapter presented a novel genetic algorithm-based framework designed to optimize steel-jacketing retrofitting interventions for columns in reinforced concrete frame structures subjected to seismic loads. The framework addresses both shear resistance and flexural ductility deficiencies, providing optimized solutions for the position of retrofitted columns (topological optimization) and the amount of reinforcement (battens spacing) to achieve minimum cost. The optimization framework was developed using the MATLAB® GA tool, with significant modifications to the standard genetic operators (population generator, elitism, and mutation) to enhance performance and allow to tackle both ductility-critical and shear-critical cases.

The effectiveness of the new genetic operators was compared with the standard ones, leading to the following observations:

1. The population size (P) impacts the computational cost of optimization and can be effectively set to three times the dimension of the design vector.

2. Standard random selection of the population is unsuitable for shear-critical frame structures. A portion of the population should be defined with a high probability of retrofitting the columns.

3. The elitism function, fixed at 5% of the individuals, prevents the loss of the fittest individuals during crossover.

4. The mutation operator, with a mutation ratio in the appropriate range, prevents the algorithm from stalling in local minima.

The proposed optimization framework was tested on a reference structure with various infill configurations and assumptions regarding the columns' shear-critical or shear-resistant nature. The results demonstrated that the optimization algorithm is sufficiently general and robust for both shear-deficient and ductility-deficient structures. It is flexible in finding specific optimal solutions for structures potentially subject to different damage mechanisms.

In conclusion, the use of artificial intelligence algorithms, such as genetic algorithms, can significantly improve the sustainability of retrofitting interventions and can be extended to various retrofitting systems (e.g., fiber-reinforced polymers (FRP), concrete jacketing, bracings). The solutions provided by GA frameworks should be seen as a support tool for designers, who must ultimately make the final decisions based on their experience and judgment. This framework represents a significant advancement in the systematic and efficient design of seismic retrofitting solutions for reinforced concrete structures.

Chapter 4

Novel genetic algorithm for optimizing seismic retrofitting costs and Expected Annual Losses in non-conforming reinforced concrete frame structures

As already discussed in this thesis, seismic events have a profound impact on communities in earthquake-prone areas, resulting in loss of lives, injuries, and social disruption. But one of the aspects that influence for decades the communities stroked by strong earthquakes are the significant economic losses for restoration and reconstruction (De Martino et al. 2017 [161], Del Vecchio et al. 2018 [162]), necessitating substantial financial resources. The downtime of buildings and infrastructure further exacerbates the impact on communities. Consequently, seismic retrofitting of existing structures has become a fundamental priority for governments to enhance the resilience of urban communities against natural disasters, particularly seismic risks. Investing in seismic risk prevention is essential to prevent extensive economic losses in the event of strong earthquakes, and to mitigate severe damage to structures and human lives.

The Expected Annual Loss (EAL) has proven to be a valid metric for estimating the life-cycle costs of structures. EAL quantifies the expected monetary losses due to seismic damage over the structure's service life, integrating the probabilities of different damage states and their associated repair costs. This index provides a comprehensive measure of the economic impact of seismic events, facilitating informed decision-making in the design and retrofitting of structures.

Conceiving a retrofitting design framework gathering both costs and life-cycle costs optimization is not simple, as in general, minimizing costs under the constrain of achieving ultimate limit state safety does not ensure a feasible

performance in terms of expected annual loss (Figure 4.1). However, controlling EAL in retrofitting design is crucial to maintain the annual rate of exceedance of service and ultimate limit states within acceptable limits.

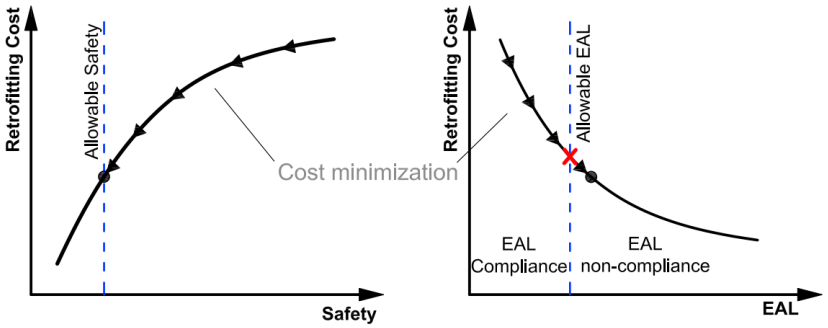

Figure 4.1 – Effect of cost minimization on EAL.

Based on these considerations, this chapter presents a new Genetic Algorithm (GA)-based framework aimed at optimizing retrofitting interventions on RC frame structures to minimize retrofitting costs while simultaneously controlling service-life costs by assessing EAL performance. In line with the performance-based earthquake engineering paradigm, the expected annual loss is evaluated by considering reference design limit states and their probability of occurrence during the nominal service life. The proposed framework determines the optimal retrofitting configuration in terms of reinforcement amount (sizing optimization) and position (topological optimization), while assessing and controlling the resulting EAL through appropriate constraints. The GA-based optimization procedure is specifically tailored to address these issues by introducing a hybrid design vector consisting of Boolean and natural discrete variables. Additionally, a non-penalty approach is implemented to handle constraints effectively using two novel survival selection operators.

Since EAL assessment involves fulfilling different limit states, the proposed framework can accommodate multiple retrofitting interventions to enhance strength, stiffness, or ductility as needed. The framework is tested on a case study of a non-seismically conforming RC frame building, considering two retrofitting techniques: FRP wrapping of columns (to increase ductility and shear resistance) and steel bracings (to enhance global lateral stiffness). The optimization process integrates the GA optimization routine implemented in MATLAB® with a 3D fiber-section model analyzed using the OpenSees software platform (McKenna et al. 2000 [141]). The structural performance of each tentative retrofitting configuration is evaluated based on static pushover analyses within the N2 method framework (Fajfar 2000 [140]). The results demonstrate that seismic retrofitting costs and resulting expected annual loss can be effectively managed using metaheuristic optimization approaches.

The results presented in this chapter have been published in:

- Di Trapani F., *Sberna A.P.*, Marano G.C., "A genetic algorithm-based framework for seismic retrofitting cost and expected annual loss optimization of non-conforming reinforced concrete frame structures", Computers and Structures, 271:106855, 2022 [163]

4.1 Optimization framework

4.1.1 Working principles

The proposed optimization framework is based on a genetic algorithm (GA) optimization routine developed in MATLAB®. This algorithm integrates a structural model implemented in the OpenSees software platform with the GA optimization process. Genetic algorithms, inspired by evolutionary theory, are a class of metaheuristic algorithms that explore the search space by evaluating an objective function at various points. The search for optimal solutions proceeds by combining design parameters (referred to as the genome) that yield the best results in each iteration. This process generates populations of tentative solutions (individuals), each representing different retrofitting arrangements.

Each individual handled by the algorithm is characterized by a design vector that includes all the design variables to be optimized. These design parameters can specify the position of a reinforcement intervention (e.g., which structural element is reinforced) or its amount (e.g., the extent of reinforcement applied to a structural element). The optimization involves defining an objective function that estimates the intervention costs of each tentative solution. The feasibility of each solution is assessed by performing a pushover analysis of the structure and evaluating its performance in terms of safety indices for different limit states ($\zeta_{E,\mathrm{LS}}$).

Simultaneously, the Expected Annual Loss (EAL) is evaluated as a function of the obtained seismic safety indices and compared to the reference EAL for a code-compliant structure (EAL_{α}). In this framework, the optimization process minimizes retrofitting costs during iterations, while EAL is indirectly included as a constraint. The outcome of the optimization provides the minimum-cost retrofitting solution that is feasible in terms of both safety and EAL.

A flowchart of the proposed framework is depicted in Figure 4.2. The optimization algorithm is the core of the framework, with engineering decision phases handled by the designer. The initial engineering decision allows defining a restricted design space, such as limiting the optimization to a portion of the building or to a restricted number of variables, which can significantly reduce

the computational cost. Finally, the optimal solution found by the algorithm is not intended as an absolute solution but as a set of cost- and EAL-effective retrofitting configurations to support the final engineering decision.

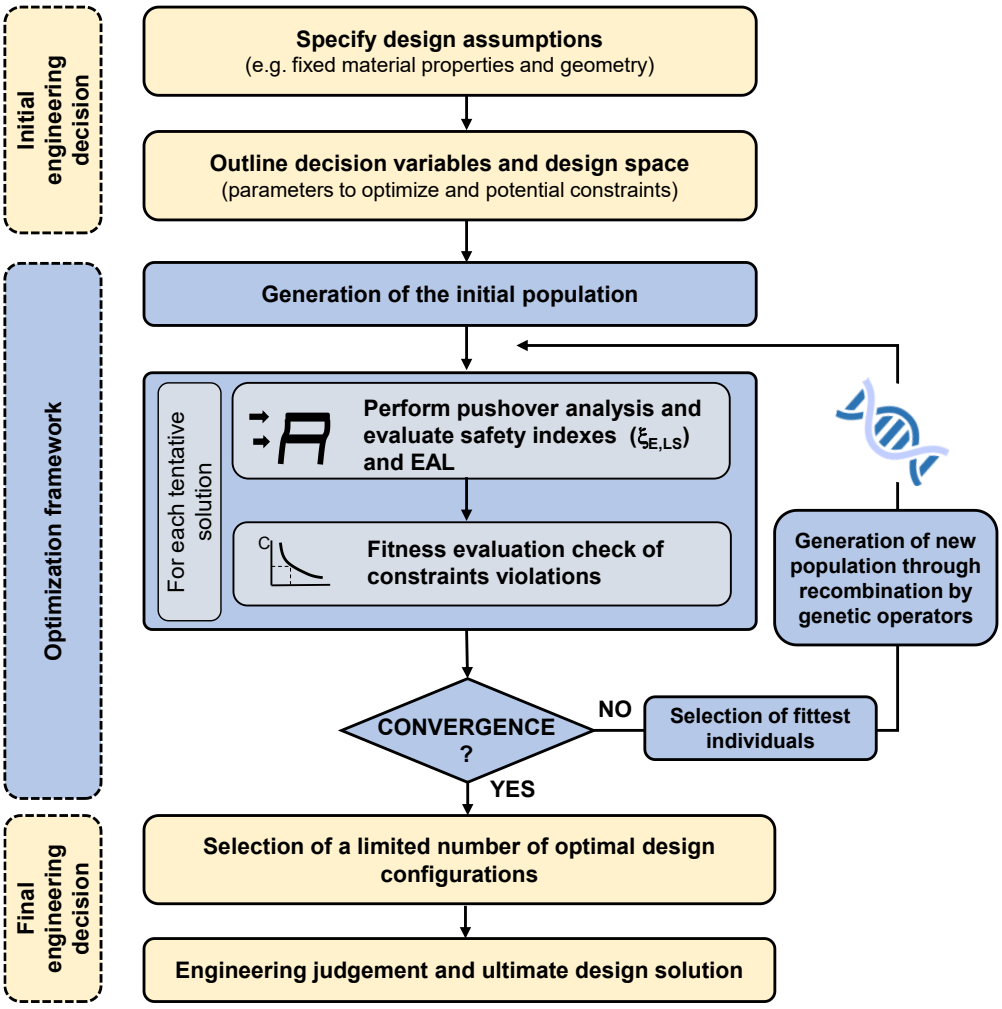

Figure 4.2 – Schematic flowchart of the optimization framework.

4.1.2 Evaluation of the Expected Annual Loss

The expected annual loss represents the annual loss of economic value of a structure in its reference service-life, taking into account the associated seismic risk, which essentially depends on the site hazard and the structural vulnerability. Economic losses are intended as the average annual cost needed to repair the damages and cover losses induced by seismic events. The determination of the EAL requires therefore the assessment of the performance of the structure with respect to different limit states (LS), associated with the respective return periods $T_{R,LS}$ and mean annual rate of exceedance, expressed as the inverse of

the return periods ($\lambda_{LS} = 1 / T_{R,LS}$). The achievement of a limit state is associated with a specific repair cost, which can be computed using different approaches.

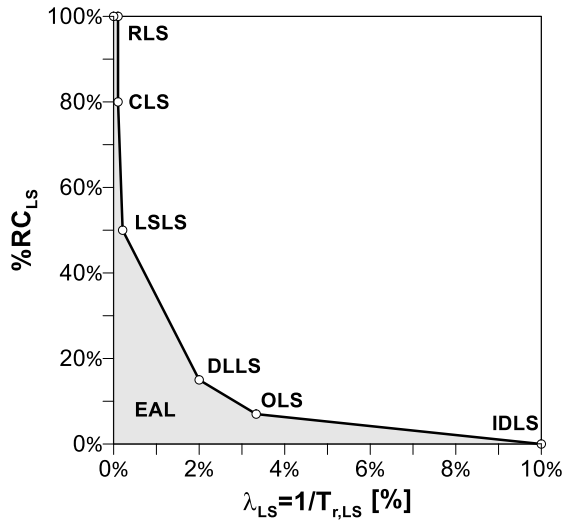

Figure 4.3 – Reference EAL curve for a code-compliant building.

A simplified method to compute EAL has been proposed by Cosenza et al. 2018 [25]. According to this approach, EAL curve connects the annual rate of exceedance for each limit state with the respective repairing cost with straight segments. The major advantage is that repair costs associated with each limit state are defined as fixed percentages of the costs for the complete reconstruction of the structure.

According to Cosenza et al. 2018 [25], eight limit states are considered (Figure 4.3). Ultimate limit states are the reconstruction limit state (RLS), the collapse limit state (CLS) and the life safety limit state (LSLS), that are associated with a repair cost (%RC) equal to 100%, 80% and 50% respectively. Service limit states are the damage limitation limit state (DLLS) and the operational limit state (OLS) with a %RC of 15% and 7% respectively. The initial damage limit state (IDLS) is characterized by a repair cost equal to zero and a mean annual frequency of exceedance that is conventionally assumed as $\lambda_{IDLS} = 10\%$. Table 4.1 summarizes the reference limit states together with the respective return periods ($T_{R,LS}$) and mean annual frequencies (λ_{LS}) for a structure having a nominal life (V_N) of 50 years.

EAL is evaluated as the area under the curve connecting $\lambda_{LS} - \%RC_{LS}$ points for each limit state (Figure 4.3), so that it can be calculated as:

$$EAL = \sum_{1=2}^{5} 0.5 \cdot \left[\lambda_{LS(i-1)} - \lambda_{LS(i)} \right] \cdot \left[\%RC_{LS(i)} - \%RC_{LS(i-1)} \right] + \lambda_{CLS} \cdot \%RC_{RLS} \tag{4.1}$$

For a code-compliant building, namely a building having a capacity exactly coincident with the demand for each limit state ($T_{rC,\mathrm{LS}} = T_{rD,\mathrm{LS}}$), Equation (4.1) results in $\mathrm{EAL}_{\alpha} = 1.13\ \%\mathrm{RC}$.

Table 4.1 – Mean annual frequency of exceedance (λ) and repair costs (%RC) associated with each LS for a code-compliant building.

Limit state	%RC [%]	$T_{rD,\mathrm{LS}}$ [years]	$\lambda_{\mathrm{LS}} = 1 / T_{rC,\mathrm{LS}}$ [%]	EAL_{α}
RLS	100	∞	0.00	1.13%
CLS	80	975	0.10	
LSLS	50	475	0.21	
DLLS	15	50	2.00	
OLS	7	30	3.33	
IDLS	0	10	10.0	

The evaluation of the EAL for a generic structure provides the determination of the capacity return period for each limit state ($T_{rC,\mathrm{LS}}$) based on the determination of the safety index ($\zeta_{E,LS}$), as follows:

$$T_{rC,LS} = T_{rD,LS} \cdot \left(\zeta_{E,\mathrm{LS}} \right)^{\eta} \tag{4.2}$$

where the parameter η is a function of the Peak ground acceleration a_g (Cosenza et al. 2018 [25]), as:

$$\eta = \begin{cases} 1/0.49 & \text{if } a_g \geq 0.25\ g \\ 1/0.43 & \text{if } 0.25\ g \geq a_g \geq 0.15\ g \\ 1/0.35 & \text{if } 0.15\ g \geq a_g \geq 0.05\ g \\ 1/0.34 & \text{if } 0.05\ g \geq a_g \end{cases} \tag{4.3}$$

The corresponding mean annual frequencies of exceedance are then obtained as:

$$\lambda_{\mathrm{LS}} = 1 / \mathrm{T}_{rC,\mathrm{LS}} \tag{4.4}$$

According to Cosenza et al. 2018 [25], the annual rates of exceedance for the operational and collapse limit states can be obtained as a function of those evaluated for DL and LS limit state, so that:

$$\begin{cases} \lambda_{OLS} = 1.67 \cdot \lambda_{DLLS} \\ \lambda_{CLS} = 0.49 \cdot \lambda_{LSLS} \end{cases} \tag{4.5}$$

Therefore, EAL can be simply assessed once λ_{DLLS} and λ_{LSLS} are obtained from structural analysis. These two parameters, according to Equations (4.4) and (4.5) are direct functions of the safety indexes evaluated for LSLS and DLLS (e.g. by performing a pushover analysis).

In this framework, EAL compliance is directly related to the outcomes of seismic structural performance with respect to the reference limit state demands. Figure 4.4 summarizes the relationship between safety assessment in the acceleration-displacement (AD) format and EAL according to the above-described simplified approach for EAL assessment. In the context of the proposed optimization algorithm, examples represented in Figure 4.4, can be interpreted as possible outcomes from potential tentative retrofitting solutions iteratively analyzed within the optimization process. The objective function and the assessment process will be described in detail in the following sections.

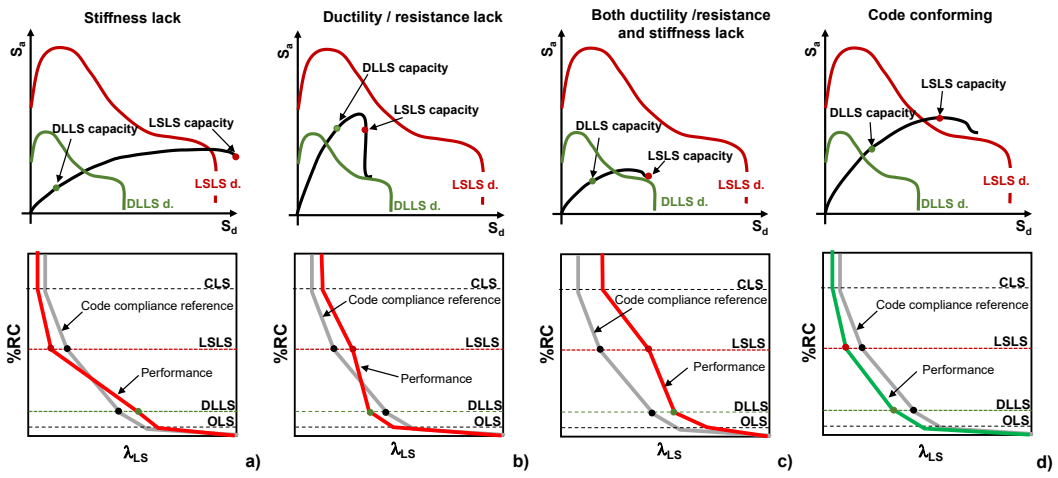

Figure 4.4 - Relationships between capacity demand assessment for LSLS and DLLS and resulting EAL curve: (a) DLLS not satisfied; (b) LSLS not satisfied; (c) DLLS and LSLS not satisfied; (d) DLLS and LSLS satisfied.

4.1.3 Encoding of the design vector

EAL code-compliance requires different limit state verification, hence retrofitting design should simultaneously consider more than one retrofitting system (e.g. to provide additional stiffness, additional ductility or additional

strength). To this goal the proposed framework considers both the potential application of CFRP (or simply called FRP) wrapping of RC columns (providing additional confinement and shear resistance and concentric steel bracing (providing additional stiffness). The decision variables that encode the position and sizing of both retrofits are collected into the so-called design vector. The choice of the parameters to optimize and those to fix as a problem data is made in the first decision phase (Figure 4.2). With reference to the considered retrofitting devices the most meaningful design variables have been individuated as the number of braced frame fields (n_{br}), the cross-section area of braces (A_{br}), the CFRP strips spacing (s_{FRP}), the number of FRP layers (n_{FRP}), and the position of the columns retrofitted by the CFRP (Figure 4.4). All the decision variables are gathered in the design vector b so defined:

$$\mathbf{b} = \begin{pmatrix} n_{br} & A_{br} & s_{FRP} & n_{FRP} & \mathbf{p} \end{pmatrix}^{T} \tag{4.6}$$

in which the term p is an array of binaries representing the position of the FRP retrofitted columns defined as:

$$\mathbf{p} = \begin{bmatrix} \dots & \dots & c_{ij} & \dots \end{bmatrix}^{\mathrm{T}} \tag{4.7}$$

where the generic element c_{ij}, is a Boolean variable assuming the value 1 if the column is retrofitted and 0 if not. The subscript i indicates the position of a column in plan and j the story. The variable n_{FRP}, is a natural value indicating the number of overlapping layers of FRP on each column belonging to the interval:

$$n_{\mathrm{FRP}} \in \left[1, n_{\mathrm{FRP,max}} \right] \tag{4.8}$$

where $n_{\mathrm{FRP,max}}$ is the maximum allowed number of FRP layers. The variable s_{FRP} is a natural discrete values representing the FRP strip spacing (intended as the interaxis distance) and belonging to the interval:

$$s_{\mathrm{FRP}} \in \left[b_{FRP},\ s_{\mathrm{FRP},max} \right] \tag{4.9}$$

where $s_{\mathrm{FRP},max}$ is the maximum allowed spacing between two strips, and b_{FRP} is the width of the CFRP fabric. If $s_{\mathrm{FRP}} = b_{\mathrm{FRP}}$ the wrapping is continuous along the column.

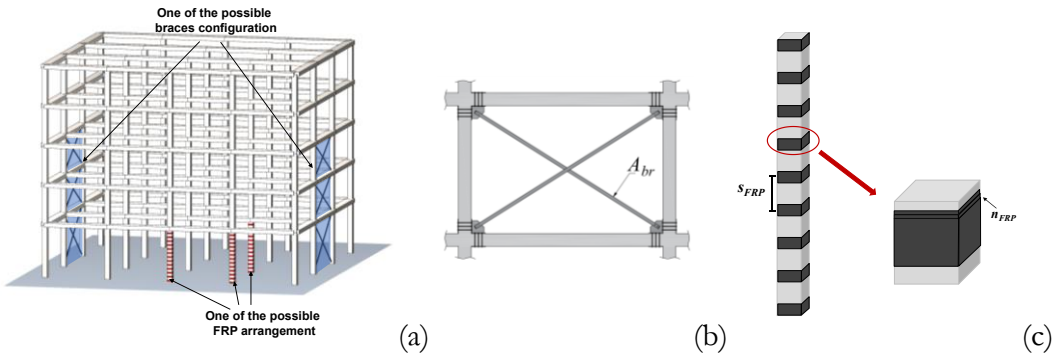

Figure 4.5 – Representation of the design variables: (a) Generic FRP and bracing retrofitting configuration; (b) Typical arrangement of bracings; (c) Typical arrangement of CFRP

Each assignment of the design variables represents a candidate retrofitting solution. Candidate solutions are generated and handled by the GA as described in detail in the following sections. In order to reduce the research space dimensions and so the required computational effort to perform the optimization, the following simplifying hypotheses are introduced:

i) FRP fabrics have fixed width (b_{FRP}) and thickness (t_{FRP}).

ii) The number of FRP layers and the spacing between strips is constant for all the retrofitted columns.

iii) Bracing cross-section dimensions are the same for every frame.

iv) Mechanical properties of the materials used for both the retrofitting systems are constant.

Simplifying hypotheses allow reducing computational time but can be removed if needed. At the same time, more simplifying hypotheses can be added when dealing with large problems.

4.1.4 Definition of the objective function

The objective function evaluates the retrofitting costs of each tentative solution as a function of the design vector. Therefore, in is general form, the functional to minimize is:

$$F(\mathbf{b}) = C_{\text{br}} + C_{\text{FRP}} \tag{4.10}$$

where C_{br} is the cost related to the bracing arrangement and CFRP is the one for the realization of the FRP wrapping of columns. Both the terms consider material and manpower costs and the necessary works for the

demolition and restoration of adjoining plaster and infills. The first term C_{br} can be evaluated as:

$$C_{\mathrm{br}} = \sum_{i=1}^{n_{br}} \left(W_{\mathrm{br},i} \cdot c_{\mathrm{br}} \right) + n_{\mathrm{br}} \cdot c_{\mathrm{br,m}} + n_{\mathrm{br}} \cdot c_{shear} \tag{4.11}$$

where c_{br} is the manpower and material cost per unit weight (estimated in $c_{br} = 6\,€/\mathrm{kg}$), $c_{br,m}$ is the fixed cost related to the demolition and restoring works to include bracings within an infill ($2000\,€$ per braced frame field) and $W_{\mathrm{br,i}}$ is the weight of the bracings in the i$^{\mathrm{th}}$ frame field evaluated as:

$$W_{\mathrm{br}} = 2 \cdot L_{\mathrm{br}} \cdot \left(\frac{\phi_{\mathrm{br}}}{2} \right)^2 \cdot \pi \cdot \gamma_s \tag{4.12}$$

in which L_{br} is the length of one steel brace and γ_s is the unit weight of steel ($78.5\,\mathrm{kN/m^3}$). The term c_{shear} is the fixed cost associated with the shear reinforcement of the ends of the columns adjacent to the bracing systems to support the additional shear demand. As regards CFRP reinforcement, the term C_{FRP} is computed as:

$$C_{\mathrm{FRP}} = \sum_{i=1}^{n_c} \left(A_{\mathrm{FRP,i}} \cdot c_{\mathrm{FRP}} \right) + n_c \cdot c_{\mathrm{FRP,m}} \tag{4.13}$$

where n_c is the number of retrofitted columns, c_{FRP} is the unit cost for the arrangement of the CFRP wrapping (estimated in $c_{\mathrm{FRP}} = 300\,€/\mathrm{m^2}$), $c_{\mathrm{FRP},m}$ is the cost per column for the demolition and reconstruction of adjacent masonries and plasters ($c_{\mathrm{FRP},m} = 1000\,€$ per column) and $A_{\mathrm{FRP},i}$ is the area of the FRP fabric used to retrofit the generic i$^{\mathrm{th}}$ column, evaluated as:

$$A_{FRP,i} = \left\lfloor \frac{l_{c,i} - b_f}{s_{FRP}} + 1 \right\rfloor \cdot n_{FRP} \cdot \left[2 \cdot \left(b_i + h_i \right) - \left(4 - \pi \right) \cdot r_c^2 \right] \cdot b_f \tag{4.14}$$

where $l_{c,i}$ is the length of the i$^{\mathrm{th}}$ column b_i and h_i are the geometric dimensions of each column cross-section, and r_c is the rounding radius of columns edges. It is noteworthy observing that by fixing some parameters on the characteristics of the retrofitting systems (such as the width of the FRP and the unitary costs) the objective function strictly depends on the parameters gathered in the design vector. The optimization problem is then formalized as:

$$\begin{cases} \min F(\mathbf{b}) \\ s.t. \\ \lambda_{DLLS} \le \lambda_{ac_{DLLS}} \\ \lambda_{LSLS} \le \lambda_{ac_{LSLS}} \end{cases} \tag{4.15}$$

meaning that cost minimization is constrained by limiting the annual rated of exceedance of each limit state (λ_{DLLS}, λ_{LSLS}) to that of the code compliant building ($\lambda_{ac\,\mathrm{DLLS}}$, $\lambda_{ac\,\mathrm{LSLS}}$), that implies :

$$EAL \le EAL_{ac} \tag{4.16}$$

The feasibility (or not) of each tentative solution is performed by a non-penalty approach, making use of a specifically defined survival selection operator, as described in the following sections. This approach is more effective in this case, as it allows to handle multiple constraints without performing a specific calibration of the penalty for each of them.

4.2 Optimization algorithm subroutines

4.2.1 Algorithm working principle

The search for the optimal solution follows a GA workflow. Specific modifications are introduced within standard genetic operators in order to improve their effectiveness on the optimization process. A scheme of the GA framework working principle is illustrated in Figure 4.6. A population of random individuals encoded by the design vectors is initially generated. By analyzing each of the population's tentative solutions, the fitness value and the number of violated constraints is estimated. Then, the best individuals are selected by the parent selection operator to generate a new population. Two different genetic operators are employed to improve the genes of the individuals, the crossover, which mixes the genomes of the best individuals, and the mutation that prevents from stuck on local optima by introducing random slight changes in the design vectors. Lastly, the best individuals of the new generation, together with those of the initial population are selected through the survival selection operator. The framework proceeds until one of the stopping criteria (maximum number of generations or stall) is achieved. The genetic operators' subroutines are described in detail in the following sections.

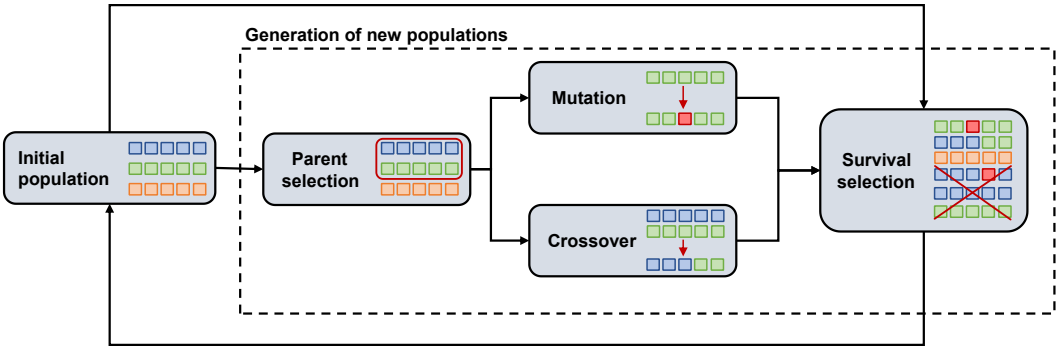

Figure 4.6 – Schematic flowchart of the genetic algorithm routine.

4.2.2 Parent selection operator

Parent selection is the subroutine entrusted with selecting parent individuals to be forwarded to the genetic operators (mutation and crossover) for the generation of a new population. Parent individuals are individuated with a tournament selection, directly comparing the individual's performance. Within the individuals of the initial populations, k individuals are randomly selected (where k is called tournament size), among them the best individual is chosen as the parent for the ensuing mating process (Figure 4.7). To make the algorithm effective in selecting performing parent individuals, the parent selection operator has been implemented to compare both individual fitness Equation (4.10) and constraint violations (Equation (4.15)).

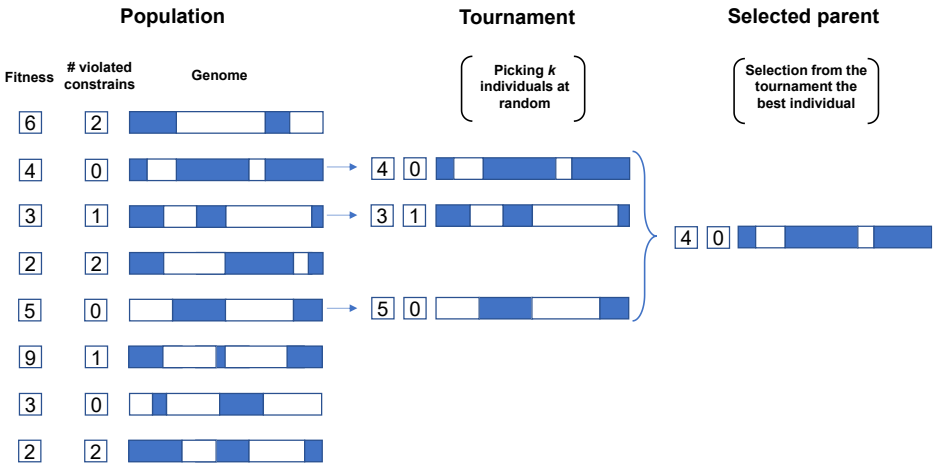

Figure 4.7 – Working scheme of the proposed parent selection operator.

The comparison is carried out firstly by assessing the number of constraints violated (which according to Equation (4.15) can be 0, 1 or 2) and then with respect to the fitness value. In this way, individuals with the lowest number of violated constraints are preferred. Then, for the individuals having the same number of constraints violations the individual with the best fitness is chosen (Figure 4.7). Tournament size is the parameter that rules the selective pressure

provided by parent selection. An increase in size leads to a more thorough selection of the best individuals, a reduction of k allows a greater probability of been selected even for individuals with worse performances.

4.2.3 Crossover and mutation genetic operators

Crossover and mutation operators are employed to generate child individuals with the aim to improve the chromosomes of the genomes of each current generation. Crossover operator works by mixing chromosomes of two selected parent individuals to generate a new offspring. Mutation operator is instead used to introduce a random variation in parent genome.

For the crossover subroutine, a new specific procedure has been defined to correctly handle heterogeneous genomes such as those of the proposed framework, which is composed of natural numbers and Boolean variables. The crossover of natural decision variables is carried out by randomly selecting a value among the chromosomes of the parents. In particular, the proposed crossover function, which can be called random intermediate value crossover, is implemented to smoothly mix the parent's chromosomes. In this way, each new chromosome is obtained as a random value between those belonging to parents including extreme values (Figure 4.8). The choice of implementing this special crossover function is justified by the fact that, for the current problem, the employment of traditional crossovers, such as the widely used one-point, multi-point, or uniform crossover functions, can be disruptive, creating child individuals that have characteristics too different from the parents.

As regards Boolean variables, a single point crossover is employed (Figure 4.8). The operating principle provides the random selection of a position along the string called crossover point. The child individual is constructed by picking, from the beginning of the chromosome to the crossover point the genome of the first parent, while the rest is copied from the second one. In this way, each parent passes down a sequence of genetic information (a substring of binaries) to the offspring ensuring an adequate mixing of the genomes.

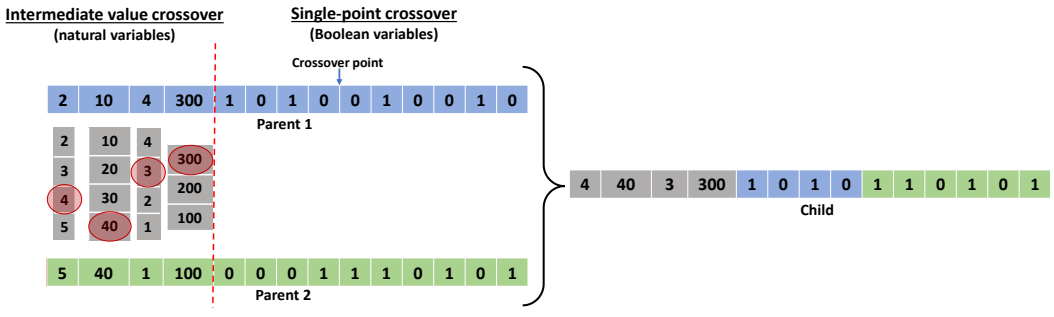

Figure 4.8 – Working principle of the proposed crossover procedure.

As regards mutation, this is applied by selecting one (or more) random positions along the design vector and changing the value of that decision variable. For discrete variables a new random value among the possible ones is drawn. For Boolean variables included in the **p** sub-vector the mutation of a gene is simply a switch from 0 to 1 or vice-versa. It should be finally observed that crossover and mutation are not used sequentially (as it is usually done) but are alternatively used to generate new individuals (Figure 4.6).

4.2.4 Survival selection operator

Survival selection operator is used to allow the best individuals to spread their genome in subsequent generations. The initial population is merged with child individuals, and both undergo the survival selection process. In this way individuals of the initial population having good fitness are forwarded to the next generation, together with most performing children.

A new survival selection function called sorting and truncation selection is implemented to compare individual both from the fitness (Equation (4.10)) and constraints (Equation (4.15)) point of view. Considering Equation violated constraints can be 0, 1 or 2.

The operating principle provides a double sorting process, first ordering individuals based on the number of violated constraints, and then, among the individuals with the same number of constraint violations sorting is based on the fitness value. In this way, the individuals are sorted in ascending order starting from individuals with the minimum (or null) number of violated constraints and the minimum fitness to individuals with maximum numbers of constraints violation and a high fitness value. At the end of the process, only the best individuals are taken for the next generation by eliminating the genomes at the end of the sorted list.

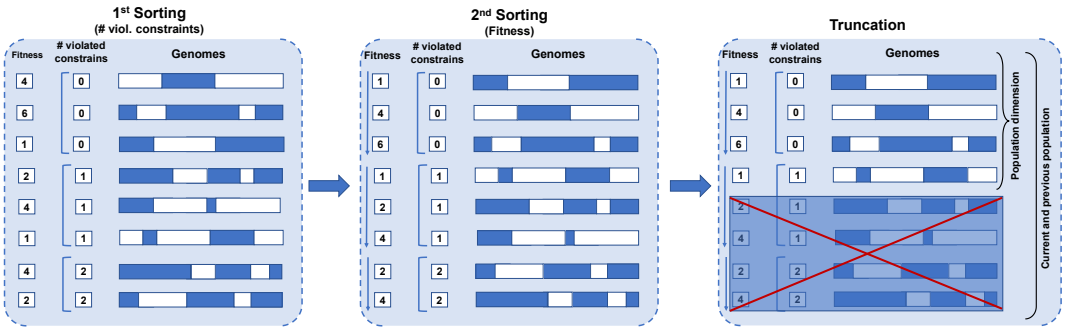

Figure 4.9 – Working principle of the proposed survival selection function.

This proposed sorting and truncation selection function has proved to be a valid operator to manage constrained optimization problems without involving penalty approaches. In fact, the penalty approach requires a burdensome

calibration procedure of the weight of the penalties to be assigned to the boundaries. On the other hand, the proposed approach could result in less performance but certainly more robust, as it allows a proper implementation of the optimization without expensive calibrations and specific GA expertise from users.

4.2.5 Heuristic repair

Heuristic repair of the design vector is used to force some variables to assume a specific value if some conditions occur. In the current application this was necessary to provide shear reinforcement of side columns of braced spans. To introduce CFRP reinforcement into the design vector (if not already present in the retrofitting configuration) the heuristic repair routine controls the position of the bracings and adjusts vector $\mathbf{p}$ so that columns adjacent to the braces are reinforced with the same spacing and number of layers that are encoded into the design vector.

A sample of the working principle of the heuristic repair subroutine is illustrated in Figure 4.10.

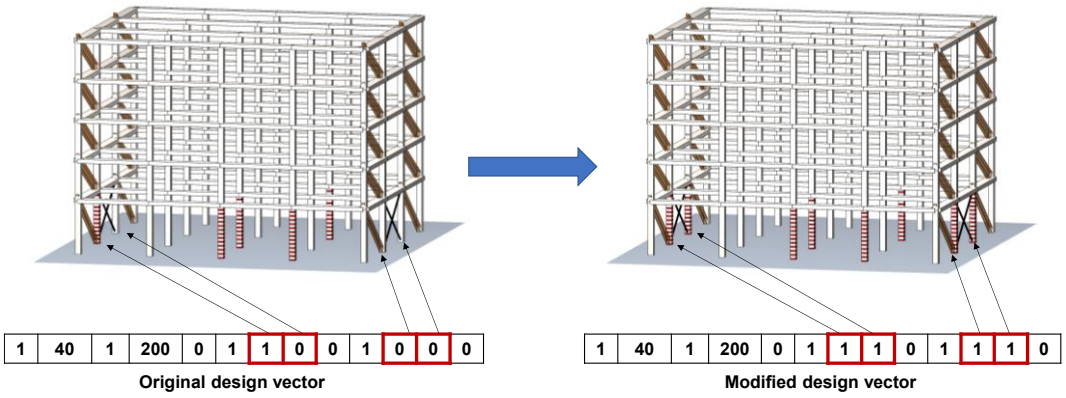

Figure 4.10 – Heuristic repair subroutine working principle.

4.3 Reference structural model

4.3.1 General assumptions

The proposed framework is interfaced with FE software to perform structural analysis and assessment of each tentative solution. Any FE software accomplishing non-linear static analyses can be connected to the optimization framework. For the current application, the OpenSees software platform (McKenna et al. 2000 [141]) has been used.

The frame elements (beams and columns) are modelled using distributed plasticity force-based elements with five Gauss-Lobatto integration points (Figure 4.11). Steel braces and infill equivalent struts are modelled with fiber-section trusses. For concrete elements the Concrete02 uniaxial material model is used. The latter is calibrated according to confinement action of stirrups and FRP wrapping (for reinforced elements) as shown in the following section. Steel rebars and braces are modelled using the Steel02 Giuffrè-Menegotto-Pinto model (elastoplastic with linear strain hardening). Infills are modelled as equivalent struts according to the model by Di Trapani et al. 2018 [155] also using Concrete02 material. Finally, in order to simulate crushing of the cross-section fibers, Concrete02 and Steel02 materials are combined with MinMax material, which removes the contribution of a fiber when a specified strain threshold is achieved (Figure 4.11).

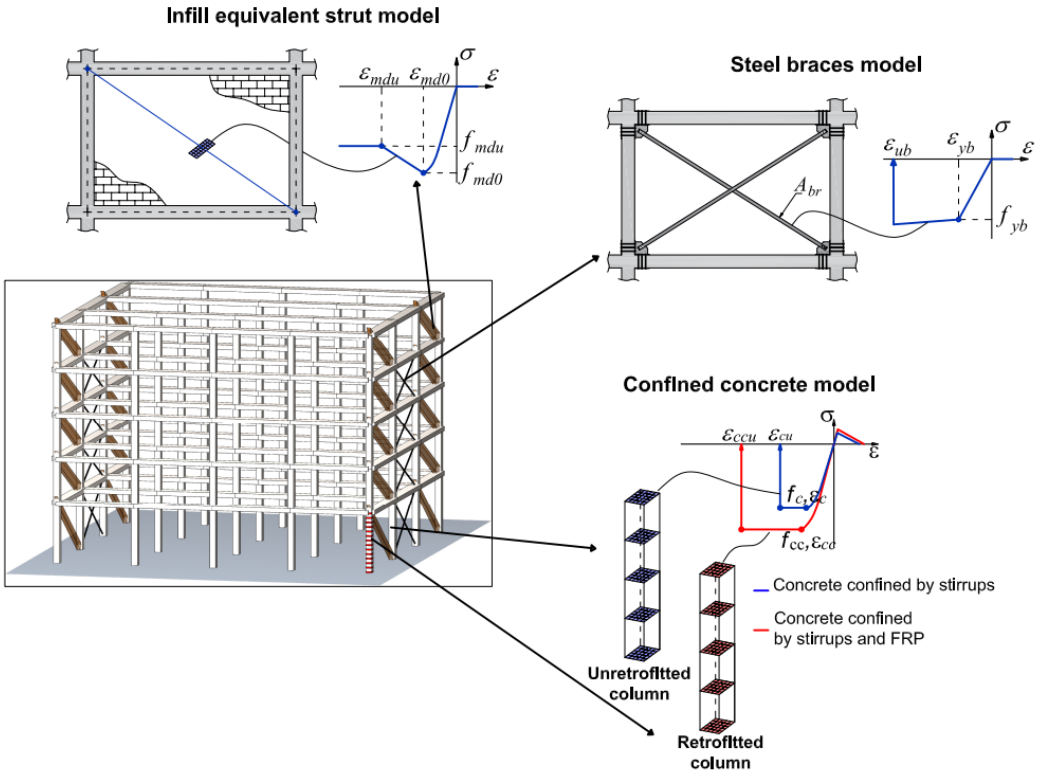

Figure 4.11 – Definition of the fiber-section elements in OpenSees, concrete elements with and without FRP wrapping, masonry infills, and steel bracings.

4.3.2 Modelling reinforced concrete elements with and without CFRP reinforcement

The confined concrete model adopted for RC elements with and without retrofitting is the standard confined parabola rectangle constitutive model (Figure 4.11). According to the CNR-DT200 (2013) [164] and Eurocode 8 [8],

this model can be adapted for concrete elements confined by only stirrups or stirrups and FRP wrapping.

For the sake of brevity, the formulation of the model is here briefly recalled only for the RC elements wrapped by FRP to highlight the dependence with the parameters included in the design vector, namely n_{FRP} and s_{FRP}. In detail, the confined peak stress (f_{cc}) is obtained as:

$$f_{\mathrm{cc}} = f_{\mathrm{c}} \cdot \left(1 + 2.6 \cdot \left(\frac{f_{\mathrm{l,eff}}}{f_{\mathrm{c}}} \right) \right) \tag{4.17}$$

where f_c is the peak stress of the concrete confined by stirrups and $f_{l,\mathrm{eff}}$ is the effective lateral confinement pressure that can be evaluated as:

$$f_{l,\mathrm{eff}} = k_{\mathrm{eff}} \cdot f_l \tag{4.18}$$

where f_l is the confinement pressure exerted by the FRP that can be calculated as:

$$f_l = \frac{1}{2} \cdot \rho_f \cdot E_f \cdot \varepsilon_{fd,\mathrm{red}} \tag{4.19}$$

in which E_f is the elastic modulus of the FRP fabric (along the fiber direction), $\varepsilon_{fd,\mathrm{red}}$ is the reduced FRP peak strain that, in case of ductility evaluations, can be obtained as:

$$\varepsilon_{fd,red} = \eta_a \cdot \frac{\varepsilon_{fk}}{\gamma_{\mathrm{f}}} \le 0.6 \cdot \varepsilon_{fk} \tag{4.20}$$

where ε_{fk} is the design rupture strain of FRP reinforcement, η_a is the environmental reduction factor (set equal to 0.90), and gf is a partial safety factor of the FRP (set as 1.10). In Equation (4.20), rf is the geometric reinforcement percentage that, in the case of a rectangular cross-section is:

$$\rho_f = \frac{2 \cdot t_{FRP} \cdot (b + h) \cdot b_{FRP}}{b \cdot h \cdot p_{FRP}} \tag{4.21}$$

where b and h are the cross-section dimensions (Figure 4.11(a)) and t_{FRP} is the thickness of FRP wrapping that can be evaluated as:

$$t_{FRP} = n_{FRP} \cdot t_{FRP,1} \tag{4.22}$$

where n_{FRP} is the number of FRP layers, also encoded in the design vector (Equation (4.5)), while $t_{\mathrm{FRP},1}$ is the thickness of the fabric.

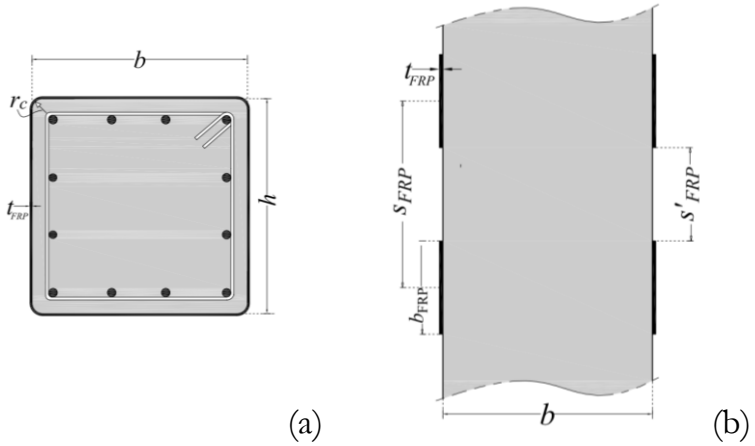

Figure 4.12 – Reference configuration and geometric parameters of a column retrofitted by FRP wrapping: (a) in plan; (b) along the height.

In Equation (4.18) the coefficient k_{eff} represents the confining efficiency exerted by the FRP system that can be calculated as the product of three coefficients:

$$k_{\mathrm{eff}} = k_v \cdot k_\alpha \cdot k_h \tag{4.23}$$

where k_v and k_h are the vertical and horizontal confining effectiveness coefficients and k_α is an effectiveness is related to the fabric tilt. According to Eurocode 8 [8], for a rectangular cross-section, these coefficients can be evaluated as

$$\begin{aligned} k_v &= \left(1 - \frac{p'_f}{2 \cdot min\{b;h\}}\right)^2 \\ k_\alpha &= \frac{1}{1+\left(\tan\alpha_f\right)^2} \\ k_h &= 1 - \frac{\left(b-2r_c\right)^2 + \left(h-2r_c\right)^2}{3 \cdot b \cdot h} \end{aligned} \tag{4.24}$$

In previous equations α_f is the tilt angle with respect to the longitudinal direction of the RC element, r_c is the radius of the column edge rounding and s'_{FRP} is the distance between FRP strips that can be easily calculated as:

$$s'_{FRP} = s_{FRP} - b_{FRP} \tag{4.25}$$

As it can be observed, the design variable s_{FRP} appears in Equation (4.25). Finally, the confined peak strain (ε_{cc}) ultimate strain (ε_{ccu}) are evaluated as:

$$\varepsilon_{cc} = \varepsilon_{c0} \cdot \left(\frac{f_{cc}}{f_c} \right)^2$$
$$\varepsilon_{ccu} = 0.0035 + 0.015 \cdot \sqrt{\frac{f_{l,eff}}{f_c}} \tag{4.26}$$

where ε_{c0} is the peak strain of the concrete confined by stirrups.

The effect of FRP retrofitting is introduced into reinforced concrete elements by simply modifying the constitutive model of concrete fibers. For the sake of simplicity, it is assumed that the confining effect exerted by the FRP wrapping is extended to the entire cross-section fibers. Samples of the resulting stress-strain response in compression for a reference column cross-section are reported in Figure 4.13 by varying the design variables n_{FRP} and s_{FRP}.

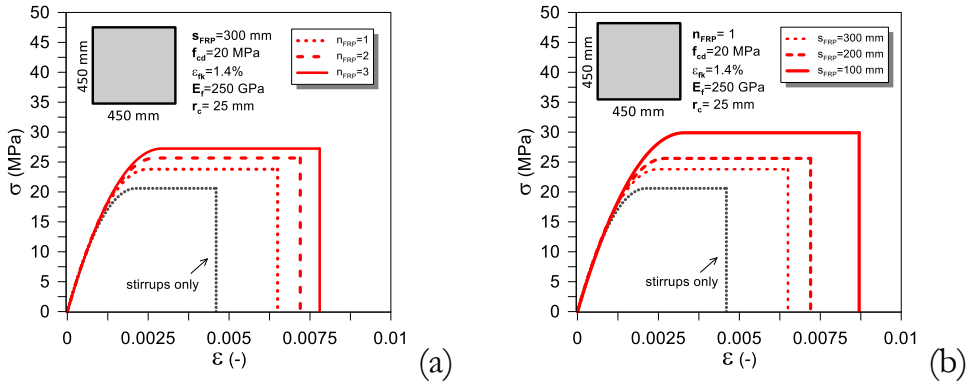

Figure 4.13 – Samples of stress-strain response in compression of concrete with and without FRP retrofitting: (a) by varying the number of FRP layers (n_{FRP}); (b) by varying the spacing of strips (s_{FRP}).

4.4 Structural analysis and results post-processing

4.4.1 Feasibility assessment by pushover analysis

Safety indexes ($\zeta_{E,LS}$) are used to estimate EAL through the evaluation of the mean annual rates of exceedance (λ_{LS}) (Equations (4.2) - (4.4)). Nonlinear static analysis (pushover) combined with N2 method (Fajfar 2000 [140]) is used to assess safety indexes for DL and LS limit states, which are computed by assessing the following capacity / demand ratios:

$$\begin{cases} \zeta_{E,DLLS} = \dfrac{d^*_{DL,c}}{S_{de,\mathrm{DLLS}}\left(T^\star\right)} \\ \zeta_{E,LSLS} = \dfrac{PGA_{c,LSLS}}{PGA_{d,LSLS}} \end{cases} \tag{4.27}$$

where T^* is the period of the bilinear equivalent single degree of freedom system, $S_{de,\mathrm{DLLS}}\left(T^\star\right)$ is the displacement demand from the elastic DLLS spectrum and $d^*_{DL,c}$ is the top displacement associated with the achievement of the damage limitation condition. The latter is conventionally achieved when the stress on the most compressed equivalent struts reaches 50% of the maximum resistance of the strut (f_{md0}) (Figure 4.14). In (Equation (4.27)), $PGA_{d,LSLS}$ is the peak ground acceleration demand associated with the reference seismic hazard (LS limit state), while $PGA_{c,LSLS}$ is the peak ground acceleration associated with the earthquake inducing life safety limit state (shear collapse or maximum base shear reduction larger than 15%) (Figure 4.14(b)).

Once $\zeta_{\mathrm{E,LS}}$ are obtained, mean annual rates of exceedance (λ_{DLLS} and λ_{LSLS}) are evaluated by Equations (4.2) - (4.4). After EAL is computed by Equation (4.1). Constraint violations are finally assessed by Equation (4.15).

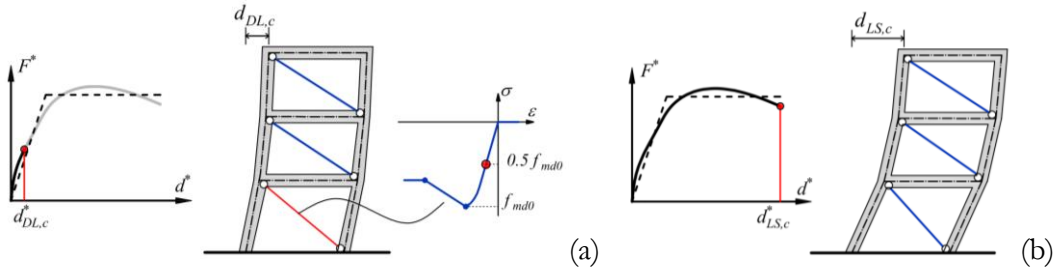

Figure 4.14 – Limit state conditions: (a) Damage limitation (DLLS); (b) Life safety (LSLS).

4.4.2 Shear verification of RC elements with and without CFRP reinforcement

Shear verification of columns is carried out step-by-step during pushover analysis. If shear failure of a column occurs the analysis is stopped, and the capacity curve is considered up to the step where shear failure occurred.

Shear demand on columns is evaluated by taking into account also the additional shear demand due to infills (in the cases of columns adjacent to an infill). The total shear demand on a column (V_D) is obtained as:

$$V_D = V_{D,fr} + V_{D,\inf} \tag{4.28}$$

The where $V_{D,fr}$ is the shear force currently acting on the column from structural analysis, while $V_{D,\inf}$ is the additional shear demand caused by interaction with an adjected infills (if any) that is evaluated according to the model proposed by Di Trapani and Malavisi (2019) [159] as:

$$V_{D,\inf} = P_{str}\cos\alpha + \mu P_{str}\sin\alpha \tag{4.29}$$

where P_{str} is the current value of the axial force acting on the equivalent strut, a is the angle of inclination of the strut with respect to horizontal direction and m the friction coefficient associated with the infill-mortar-frame interface. The latter is assumed as 0.7 in the absence of more detailed evaluations.

Shear verification of columns is carried out step-by-step during pushover analysis. For non-retrofitted columns shear resistance $\left(V_R\right)$ is evaluated according to the model proposed by Biskinis et al. (2004) [157] as:

$$V_R = V_N + k\cdot[V_C + V_W] \tag{4.30}$$

where V_N, V_C and V_W are the contributions of axial force, concrete and transverse reinforcement to shear resistance. The implementation of the model in Equation (4.28) is done in the same way as described in the previous chapter. In the case of columns retrofitted by FRP, shear strength is evaluated according to CNR-DT 200 [164] as:

$$V_R = \min\left\{V_{Rs} + V_{Rf};\ V_{Rc}\right\} \tag{4.31}$$

where V_{Rs} and V_{Rc} are the shear resistances limited by yielding of transverse reinforcement elements and concrete crushing of compressive struts, whereas V_{Rf} is the contribution to shear resistance exerted by the FRPs. When using horizontal FRP strips, the latter can be assessed as:

$$V_{Rf} = \frac{1}{\gamma_{Rd}}\cdot 0.9\cdot d\cdot f_{fed}\cdot 2\cdot t_f\cdot\left(\cot\vartheta\right)\cdot\frac{b_{FRP}}{s_{FRP}} \tag{4.32}$$

where $\gamma_{Rd} = 1.2$ is the partial safety factor, d is the are effective width of the concrete cross section, ϑ is the inclination of the compressed concrete struts, f_{fed} is the effective design strength depending on the debonding strength of the FRP.

4.5 Stress-test of the optimization framework

The effectiveness of the proposed optimization framework is tested by performing the retrofitting optimization for a reinforced concrete 3D building structure having a structural configuration typical of buildings designed before the entry into force of seismic guidelines. In particular, to effectively stress the algorithm and investigate the general validity of the proposed framework in handling different structural arrangements, two different structural configurations are considered. They are defined on the same structural model by supposing the columns being shear-resistant (SR) or shear-critical (SC) in order to enable significantly different retrofitting needs for each configuration. In the following section, the structural model is presented in detail together with the preliminary analysis accomplished to characterize the structural performances of the as-built configuration.

4.5.1 Details of the reference structural model

The case-study building consists of a five-story reinforced concrete structure designed for gravity loads only, with unidirectional frames (Figure 4.15). This kind of configuration was recurring in buildings of the Mediterranean area built up to 1970. Reinforcement details and geometrical dimensions of beams and columns are listed in Table 4.2. In this table, transverse reinforcement arrangement is also reported for the shear-critical structural configuration (SC), whereas for shear-resistant configuration (SR) columns are supposed to have adequate shear reinforcement to resist seismic actions.

Table 4.2 – Geometrical dimensions and reinforcement details of RC elements

Shear critical (SC)/ Shear Resistant (SR)				SC	SR
RC members	b (mm)	h (mm)	Longitudinal reinforcement	Transverse reinforcement	Transverse reinforcement
Beams	800	300	7+7 Ø14	Ø6 / 200 mm	Conforming
Inner columns	450	450	8 Ø12	Ø6 / 200 mm	
External columns	550	550	8 Ø16	Ø6 / 200 mm	

Reinforced concrete elements are assumed to be made of poor resistance concrete having average unconfined cylindrical strength fc=20 MPa and steel rebars with nominal average yielding strength f_y=455 MPa with a strain hardening ratio h=0.01. Infills are made of clay hollow masonry having thickness t=250 mm, elastic Young's modulus E_m=6400 MPa, compressive strength f_m=8.66 MPa, and shear strength f_{vm}=1.07 MPa. Mechanical properties of the infill equivalent struts are evaluated according to the model proposed by Di Trapani et al. (2018) [155].

Table 4.3 – Geometric and mechanical modelling parameters for RC elements and infill equivalent struts.

Concrete	Steel		Infill equivalent struts					
fc (MPa)	fy (MPa)	h (-)	t (mm)	w (mm)	fmd0 (MPa)	fmdu (MPa)	εmd0 (MPa)	εmdu (MPa)
20	455	0.01	250	1053	1.88	0.86	0.0013	0.0073

The position of the equivalent struts is depicted in Figure 4.15. Geometric and mechanical properties of reinforced concrete elements and masonry infills are summarized in Table 4.3. The structure has double symmetry in-plan and is regular in elevation. Vertical loads are modelled as point loads applied to the top node of each column as a function of the respective tributary areas in-plan. Rigid diaphragm behavior is imposed at every floor.

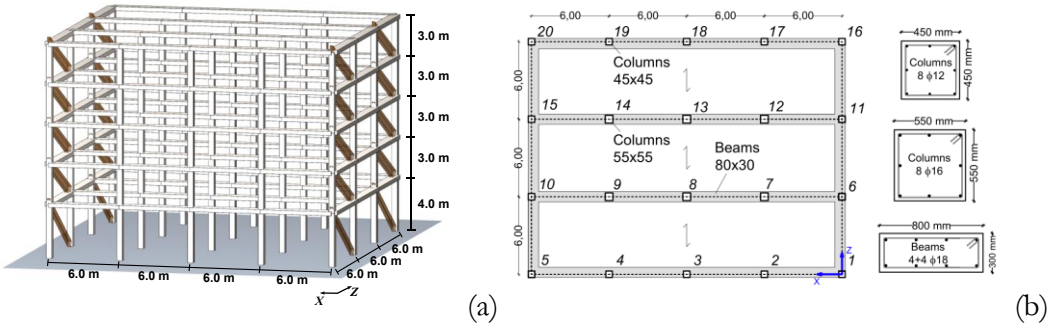

(a) (b)

Figure 4.15 – Geometrical dimensions of the reference structural model: (a) 3D frame view; (b) Plan view and RC element cross-section dimensions.

4.5.2 Assessment of the as-built structures

Preliminary assessment of the as-built SC and SR structures has been carried to evaluate safety indexes ($\zeta_{E,LS}$) and EAL. The building is supposed to be located in Cosenza (Italy) with soil type C according to Eurocode 8 part 1 [156] classification. The nominal life VN is 50 years. The resulting return periods for DLLS and LSLS are $T_{R,DLLS}$ = 50 years and $T_{R,LSLS}$ = 475 years, respectively. Pushover analyses are performed with a uniform profile of horizontal forces acting along Z-axis (Figure 3.1), which is supposed to be the direction where the structure has the major seismic vulnerability because of the absence of resisting frames.

Table 4.4 – Results of the assessment of the as-built structures.

Structural configuration	$\zeta_{E,DLLS}$ (-)	$\zeta_{E,LSLS}$ (-)	$T_{rC,DLLS}$ (years)	$T_{rC,LSLS}$ (years)	λ_{DL} (%)	λ_{LS} (%)	EAL [%RC]
Shear-resistant	0.870	1.482	33.5	1111.1	2.98	0.09	1.40
Shear-critical	0.572	0.151	10.4	10.2	9.61	9.98	8.12

In Figure 4.16(a) and Figure 4.16(c), pushover capacity curves of SC and SR structures are represented together with the demand spectra in the acceleration displacement (AD) plan. The latter shows quite different performances of the two structures. The shear resistant structure showed adequate performance with respect to LS limit state ($\zeta_{E,LSLS} = 1.482$) but is suffering DL limit state ($\zeta_{E,DLLS} = 0.87$) due to the significant lateral deformability along Z direction. This resulted in an EAL of 1.42%. On the other hand, the shear-critical configuration has shown both DL and LS limit states criticalities ($\zeta_{E,DLLS} = 0.572$ and $\zeta_{E,LSLS} = 0.151$) due to the premature shear collapse of columns, mainly associated with the significant interaction between with masonry infills. The resulting EAL was 8.12%. Numerical results of the assessment are reported in Table 4.4. EAL curves, obtained as a function of these results, are depicted in Figure 4.16(b) and Figure 4.16(d). As can be observed, both the structural configurations require retrofitting interventions to achieve conforming safety indexes and EAL although, as expected, the structural deficiencies are different.

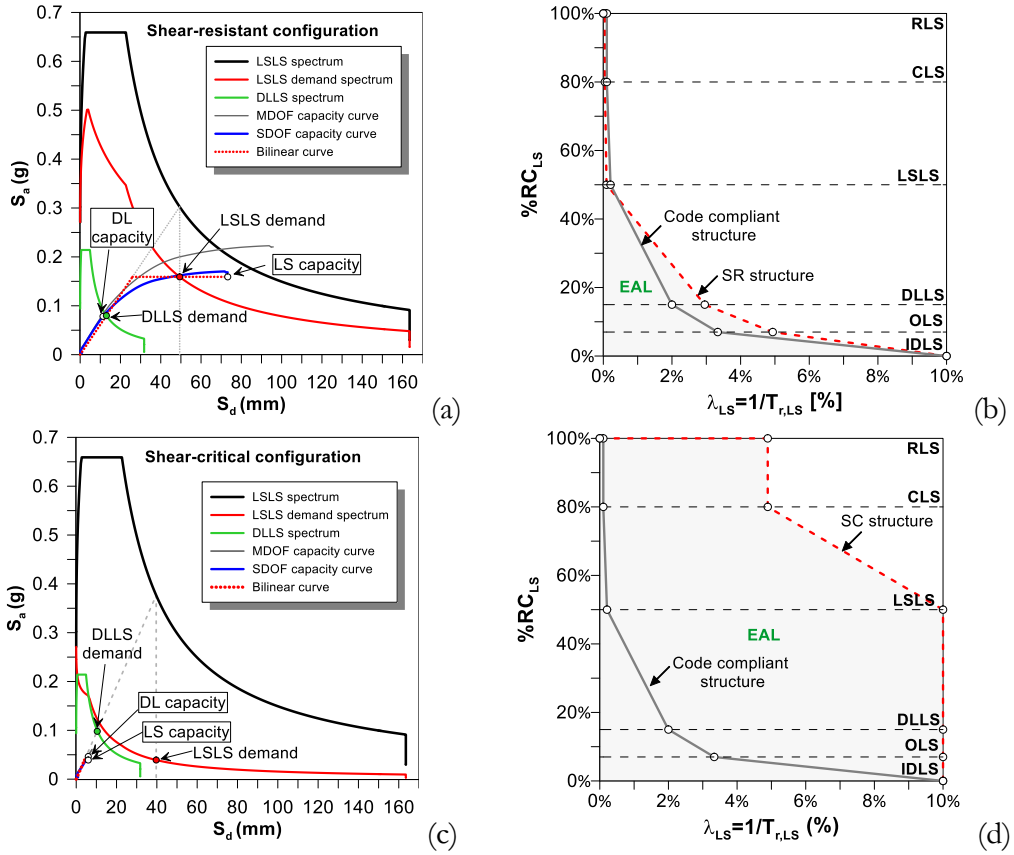

Figure 4.16 – As-built configuration preliminary analysis: (a) SR capacity / demand assessment; (b) SR EAL curve; (c) SC capacity / demand assessment; (d) SC EAL curve.

4.5.3 Retrofitting design details and assumptions on the design space

Fixed design details are initially set for CFRP reinforcement and steel braces. As regards CFRP sheets, fixed parameters are selected from those provided by the producer.

They are the thickness ($t_{FRP,1}$=0.337 mm per layer), the width (b_{FRP} =100 mm), the elastic modulus (EFRP=230 GPa), the ultimate stress (f_{fib}=3250 MPa), and strain ($\varepsilon_{fib} = 1.3\%$). For the implementation of FRP wrapping, it is assumed an horizonal arrangement (α_{FRP} =0°) with a rounding radius of the column corners (r_c) of 22 mm. The braces are supposed to be made of S275 structural steel having nominal strength f_{yb}=275 MPa, elastic modulus E_{sb}= 210 GPa and strain hardening ratio h = 0.01.

In order to limit the design space dimension, and so the computational burden, the following restrictive hypotheses are also made:

i) The frame fields where bracings can be designed are those associated with the inner spans of the two external frames (Figure 4.17)
ii) The optimization space for retrofitted columns by FRP jacketing is limited to the first two floors (Figure 4.17).

Moreover, the following design assumptions are provided:

iii) The maximum number of FRP layers ($n_{FRP,max}$) is 4.
iv) The range for the FPR strip spacing (s_{FRP}) varies between b_{FRP}=100 mm (continuous wrapping) and 300 mm with a step $\Delta_{s_{FRP}} = 100mm$.
v) Bracings are symmetrically designed within the previously identified fields.
vi) The bracing cross-section area is comprised in the range 3.14 cm² - 78.5 cm² with 9 possible steps.

The above defined assumptions result in:

$$\begin{cases} n_{FRP} \in [0,1,2,3,4] \\ s_{FRP} \in [b_{FRP}, 200, 300] \\ n_{\mathrm{br}} \in [0,1,2,3,4,5] \\ A_{\mathrm{br}} \in [3.14, 7.06, 12.6, 19.6, 28.3, 38.4, 50.2, 63.6, 78.5] \end{cases} \tag{4.33}$$

The resulting size of the design space is then of 6 integers that encode the number of floors where the bracings are defined (n_{br}), 9 discrete natural

variables for the bracings cross section area (A_{br}), 4 discrete natural variables encoding the number of FRP layers (n_{FRP}), 3 discrete natural variables for the strip spacing (s_{FRP}), and 40 binary variables as the possible FRP retrofitted columns ($\mathbf{p}$ vector). Therefore, the research space consists of $6\times9\times4\times3\times2^{40} \cong 7\times10^{14}$ different solutions. It should be specified that the restriction of the design space is done to merge specific design choices or design constraints with the need to speed up the optimization process but is not mandatory in general. However, engineering considerations about the design space are recommended to address the design towards consistent and effective solutions.

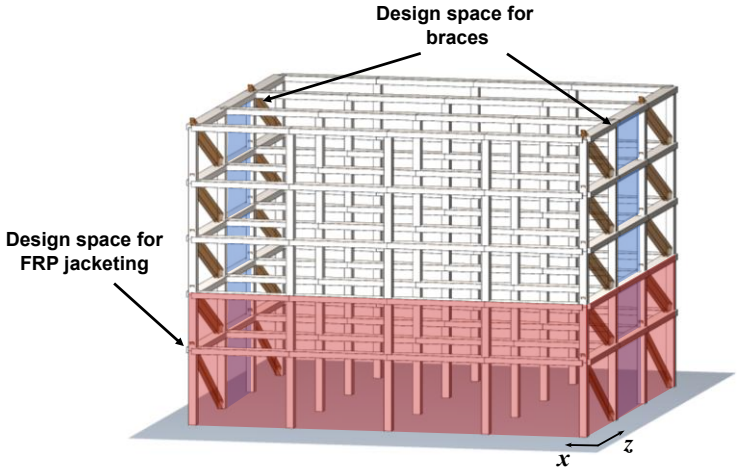

Figure 4.17 – Restricted design space representation for the case study structure.

4.5.4 Optimization results and discussion

The proposed optimization framework has been tested with the two case-study structural configurations above described. The effectiveness of the algorithm in providing suitable retrofitting design solutions in terms of minimum cost with a code-conforming EAL has been assessed. The analyses have been carried out using an initial population ($\mathbf{P}$) of 100 tentative solutions. The generation of the initial population was performed using the approach presented in previous chapter for GA retrofitting optimization of shear-deficient structures. In detail, a subspace (p_{pr}) constituted by 50% the population is reserved to individuals with a high probability (P_r=90%) that each column of the design vector is retrofitted. The algorithm proceeds by generating 100 new children every generation through the previously described routine, involving parent selection, crossover and mutation. A tournament size k=3 is used to for the parent selection operator. Stopping criteria have been set to at a maximum of 25 generations (G_{max}) and a stagnation of 5 generations (Smax), representing the maximum number of generations in which the algorithm does not improve the solution. GA parameters set-up is summarized in Table 4.5.

Table 4.5 – GA analysis parameters set up for the case studies.

Design vector dimension	Population size	Number offspring	Tournament size	Mutation ratio	Max generations	Max stall	Dimension of the ppr space	Element probability retrofitting in the ppr space
dim(**b**)	P	O	k	P_m	G_{max}	S_{max}	p_{pr}	P_r
44	100	100	3	2%	25	5	50	90%

The convergence histories of the optimization analyses for SR and SC structural configurations are illustrated in Figure 4.18. It can be observed that a proper definition of the genetic operators allowed a gradual transition between the exploration and exploitation phases. The convergence trends are quite fast and regular, without significant stalls in local minima due to potential premature convergences. As regards SR configuration, the solution with minimum cost at the first generation was 58 532 €. The optimal one was 28 686 € (-51%) after 20 generations. For SC configuration, as it was expected, the optimization required larger computational effort (25 generations), however the initial minimum-cost solution (155 121 €) was reduced by 60% to 62 620 €, denoting a better performance of algorithm despite the major number of generations required. In Figure 4.18, it also noteworthy observing the trend of the tentative solutions for each generation, which are clearly ordered as a function of their fitness. This is due to the application of the proposed survival selection operator, putting in order the tentative solutions by considering their fitness and the number of violated constraints.

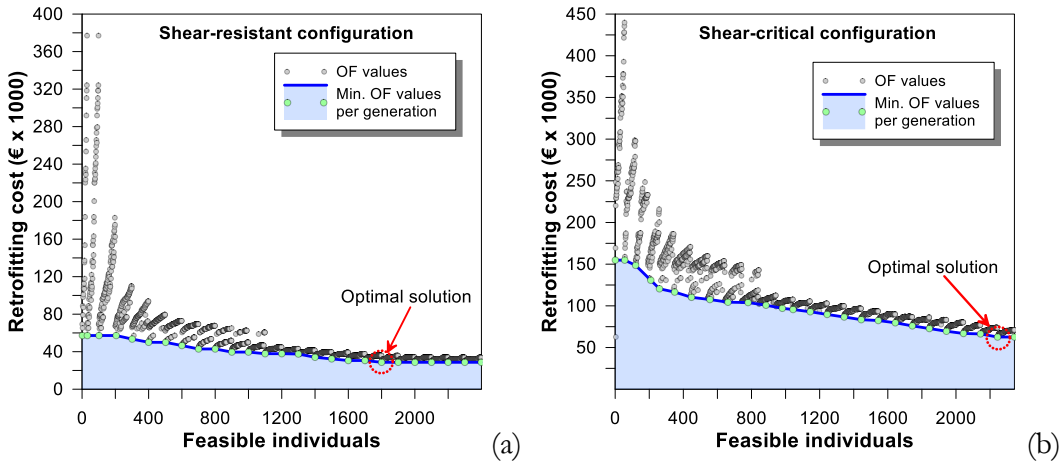

Figure 4.18 – GA optimization convergence history: (a) shear-resistant configuration; (b) shear-critical configuration.

In Figure 4.19 the outcomes of the optimization are analyzed in terms of EAL. For both SR and SC configurations it can be observed that, during the exploration phase, the algorithm evaluated different clusters of solutions characterized by similar EAL values. Then, when the general traits of the optimal solution were localized, the algorithm focused on the exploitation of those genomes. Figure 4.19(a) and Figure 4.19(b) clearly show that, when this occurred, the algorithm focused only on a cluster of solutions. In these figures, it is also interesting to observe the pattern of transition between exploration and exploitation phases. In fact, for the SR configuration the algorithm tended to focalize first on tentative solutions with a higher EAL, while on the contrary, initial solutions for the SC configurations were typically characterized by a lower EAL. This opposite trend is justified by the fact that feasible SC solutions required a larger number of retrofitted columns, hence, initial SC solutions were typically over-retrofitted and so characterized by a lower EAL. In the exploitation phase, the algorithm proceeded by removing the unnecessary reinforcement and so finally obtained EAL values were similar for the SR (EAL=1.016%) and the SC (EAL=1.006%) configurations.

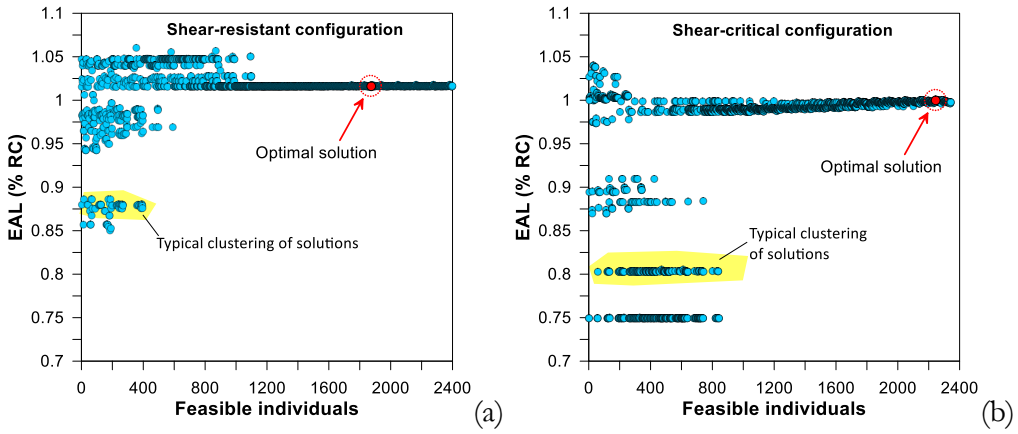

Figure 4.19 – Feasible individuals EAL values trend: (a) shear-resistant configuration; (b) shear-critical configuration.

The finally obtained optimal solutions are illustrated in Figure 4.20 where the structures are depicted in their deformed shape under the lateral loads applied along Z direction. Both SR and SC optimal solutions are characterized by steel bracing of the external frames for the first two stories (n_{br}=2) with a cross-section area of the braces (A_{br}) of 2.83 cm2. This result is the same for both the configurations, because this solution is the minimum cost-one allowing damage limitation limit state compliance. For the SR configuration it is found

that bracing is the only retrofitting intervention needed (FRP reinforcement of columns shown in Figure 4.20b is still associated with bracings). This result is consistent with the fact that SR structure already satisfied LS limit state in the as-built configuration.

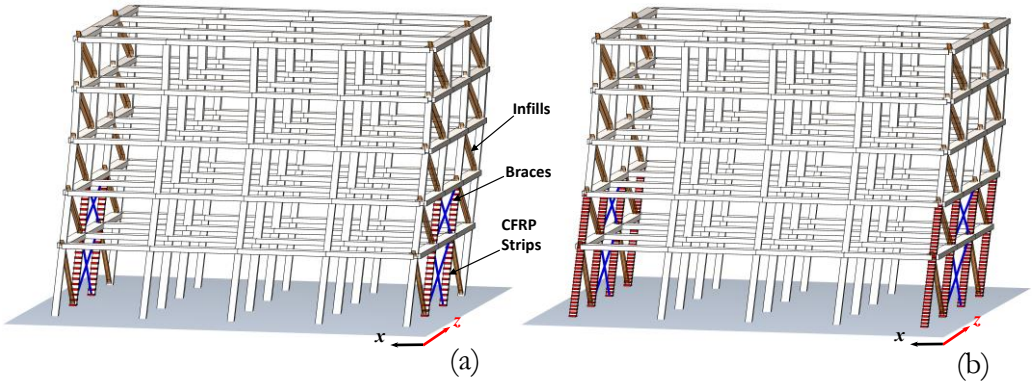

Figure 4.20 – Optimal solutions retrofitting configurations (deformed shape): (a) shear-resistant case; (b) shear-critical case.

The optimal solution found to the SC configuration (Figure 4.20(b)), is characterized by FRP wrapping of 8 columns in the external transverse frames of the first two floors. In this retrofitting configuration, FRPs are implemented with two layers ($n_{FRP} = 2$) and a strip spacing s_{FRP} of 200 mm. It is noteworthy observing that this optimal solution is consistent with the expected structural deficiencies, since retrofitted columns are those adjoining masonry infills. This means that the solution found by the algorithm has effectively pinpointed the need for an increase in increase shear capacity of these columns to face the additional shear demand due to the frame-infill interaction. Parameters obtained at the end of the optimization are reported in Table 4.6.

Table 4.6 – Overview of the case studies optimization analysis results.

Structural configuration	n_{br} (#)	A_{br} (cm2)	n_c (#)	s_{FRP} (mm)	n_{FRP} (#)	$\zeta_{E,DL}$ (-)	$\zeta_{E,LS}$ (-)	EAL (%RC)	Fitness (€)
Shear-resistant	2	2.83	2	300	1	1.024	2.297	1.016	28686
Shear-critical	2	2.83	8	200	2	1.024	2.720	1.006	62620

A representation of the convergence history of the retrofitting design parameters for both the structures is also depicted in Figure 4.21. To provide a concise representation, design vector parameters are here summarized by the total volume of steel bracing (V_{br}), the ratio between the number of FRP layers and their spacing (n_{FRP}/s_{FRP}), the number of retrofitted columns (n_c). It can be observed that parameters related to bracings and FRP arrangement converged

within the first 10 generations, while the topological optimization of the retrofitted columns required more than double the generations.

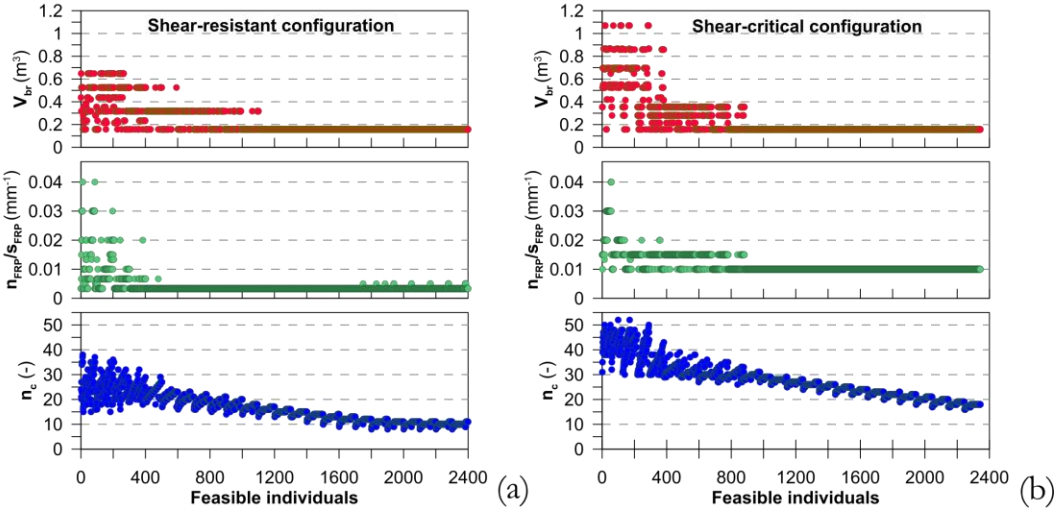

Figure 4.21 – Convergence history of the design vector parameters: a) SR configuration; b) SC configuration.

The capacity curves of the two structural configurations are depicted in Figure 4.22a and Figure 4.23a in the AD space. The latter show both an increase in lateral strength, stiffness and ductility. For what concerns DL limit state, since the bracing system was the same for SR and SC configurations, identical safety indexes (close to unit) were found ($\zeta_{E,DLLS} = 1.024$). On the other hand, LS limit state safety indexes were significantly higher than the unit. In detail they were $\zeta_{E,LSLS} = 2.3$ for the SR structure and $\zeta_{E,LSLS} = 2.7$ for the SC structure. The significant increase of LS safety is a secondary effect of the bracings (used to reduce lateral deformability) and of the FRP wrapping of the columns (used to the increase shear capacity), which influence the overall performance providing additional strength and ductility.

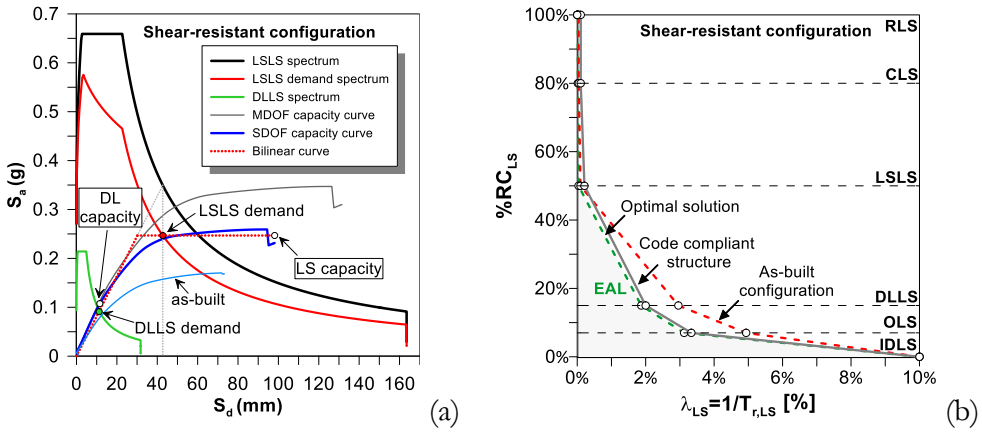

Figure 4.22 – Performance of the optimal solution for the SR configuration: (a) Capacity / demand assessment in AD format; (b) EAL curve.

EAL curves associated with the optimal solutions are finally depicted in Figure 4.22(b) and Figure 4.23(b) and compared with those of the respective as-built configurations. As can be observed code-conforming EAL was obtained for both the cases. It should be also noted that the final EAL of both the structures (1.016% for the SR structure and 1.006 for the SC structure) was quite close to the maximum allowed one (1.13%).

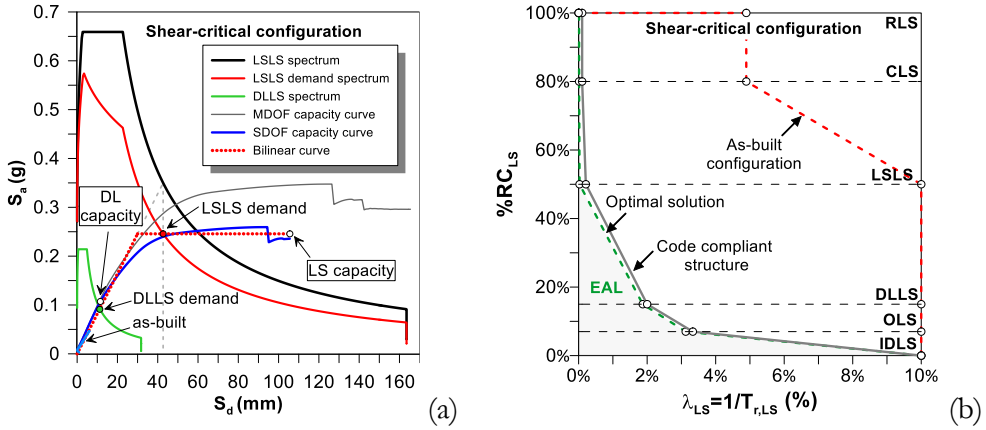

Figure 4.23 – Performance of the optimal solution for the SC configuration: (a) Capacity / demand assessment in AD format; (b) EAL curve.

4.6 Conclusions

In this chapter, a new Genetic Algorithm (GA)-based optimization framework was presented, aimed at minimizing seismic retrofitting costs of RC frame structures while simultaneously controlling service-life costs. The proposed algorithm optimizes the cost of CFRP wrapping for columns, which enhances ductility and shear resistance, and steel bracing, which improves lateral stiffness. The output includes the position and amount of reinforcement, addressing both topological and sizing optimization. The effectiveness of the proposed framework was tested on a non-conforming RC frame structure with two different configurations (shear-resistant and shear-critical) using pushover analysis.

The proposed artificial intelligence-based framework effectively controls seismic retrofitting costs and expected annual loss during the design process. The use of a non-penalty approach is crucial for handling multiple constraints through specifically defined parent selection and survival selection operators. The algorithm has demonstrated robustness and flexibility in finding optimal retrofitting solutions, even for structures with significantly different needs, such as stiffness deficiencies, shear deficiencies, and ductility deficiencies. This flexibility is largely due to the implementation of multiple limit state verifications and retrofitting techniques.

Even though the algorithm does not have prior knowledge of the geometrical and mechanical features of the structure, except for the values that design vector

components can assume, the optimal solutions obtained align with engineering expectations regarding the position of reinforced elements. Cost minimization combined with EAL control successfully integrates multiple reinforcement techniques to address each limit state. This integration has led to a significant increase in safety indexes for some limit states, due to the beneficial interaction of the implemented retrofitting systems.

The presented framework is specialized for RC structures with specific reinforcement techniques. However, the overall concept is generally valid and can be further developed for different structural types and their respective retrofitting techniques. AI-guided design can be a valuable tool to transition from a trial-and-error design approach to a more engineered methodology, providing solutions that are suitable in terms of costs and performance. Nevertheless, the outcomes of this approach should be viewed as supportive aids for the designer, who must retain control over the final engineering decisions.

Chapter 5

Genetic algorithm framework for cost-effective topology optimization of seismic reinforcement in existing masonry structures

In Italy and the Mediterranean area, a significant percentage of the building stock comprises masonry structures. These unreinforced masonry buildings are widespread and often date back several centuries, having been constructed without consideration for seismic loads. Recent seismic events, such as the L'Aquila earthquake in 2009 and the Amatrice earthquake in 2016, have demonstrated the high seismic risk associated with these structures due to their considerable vulnerability. The substantial post-earthquake reconstruction costs have prompted the Italian government, along with other governments in seismic-prone regions, to allocate funds for reducing the seismic vulnerability of existing buildings.

For unreinforced masonry structures, various effective reinforcement and retrofitting techniques are available. These include reinforced plasters, grout injections, prestressed ribbons, and composite materials, which can enhance the flexural and shear resistance of walls. However, formal design criteria for retrofitting interventions to achieve specific performance targets, such as a desired safety level or structural behavior, are largely unavailable. The retrofit design process often relies on a trial-and-error approach, heavily dependent on the engineer's intuition and experience. This non-engineered approach has two main drawbacks.

First, identifying an appropriate retrofitting configuration typically requires multiple iterations, as reinforcing a wall can increase its mass or stiffness, or both, thereby altering the demand on the structural element. This can lead to recursive design challenges. Second, there is no control over retrofitting costs, meaning it is difficult to determine whether a candidate retrofitting configuration is the most cost-effective option. This often results in the

overestimation of reinforcement needs, leading to higher costs, greater invasiveness, and increased downtime.

Given these challenges, there is a clear need for engineered design methodologies that target specific performance outcomes. To address this need, the current chapter proposes a new computational intelligence-based framework to support the seismic reinforcement design of existing masonry structures with adequate structural regularity. The framework aims to minimize retrofitting costs while ensuring compliance with safety checks as per current technical codes.

The proposed optimization algorithm aligns with the capacity models and prescriptions of the Italian National Technical Code (NTC 2018) [158] for masonry wall reinforcement but is robust enough to incorporate different or more general capacity models and safety verification rules. This chapter focuses on the widely used reinforced plaster technique. The objective function within the optimization algorithm evaluates intervention costs based on the surface area of walls where reinforced plasters are applied. The final output is the optimal retrofitting configuration, identifying the topology of walls needing reinforcement at the minimum cost while satisfying safety checks.

The optimization procedure links the GA optimization routine developed in MATLAB® with an equivalent frame 3D finite element model analyzed using the OpenSees software platform (McKenna et al. 2000 [141]). The performance of each tentative solution (i.e., candidate seismic retrofit configuration) is evaluated in terms of in-plane flexural and shear safety under reference seismic design forces. The proposed framework is tested on a two-story masonry building comprising two different types of masonry (squared stone unit masonry and coursed tender stone masonry). The results indicate that the GA-based optimization framework can effectively reduce the extent of seismic upgrading interventions, resulting in cost savings and reduced downtime and invasiveness.

The research results presented in this chapter have been published in:

- *Sberna A.P.*, Demartino C., Vanzi I., Marano G.C., Di Trapani F., "Cost-effective topology optimization of masonry structure reinforcements by a linear static analysis-based GA framework", Bulletin of Earthquake Engineering, in-press, 2024 [165].

5.1 Masonry reinforcement with reinforced plasters

5.1.1 General features of reinforced plasters

The in-plane reinforcement of masonry walls can be performed according to different techniques (Priestley and Seible 1995 [166]). Among these, the use of composite materials (e.g., fiber-reinforced polymers (FRP) or fiber-reinforced cementitious matrices (FRCM)) found significant applications for masonries with regular textures. Similarly, the application of prestressed steel ribbons (CAM) has been used especially for masonry buildings belonging to the historical heritage, or in the case of heterogenous masonries. At the same time, the use of reinforced plasters is very common due to their relatively low cost and ease of implementation in comparison with the other techniques. This retrofitting methodology entails the application of a reinforcement net typically made of steel (Figure 5.1(a)) or Glass Fiber-Reinforced Polymer (GFRP) (e.g. Figure 5.1(b)) on both faces of the masonry wall, embedded in a thick layer (40 – 100 mm) of special cement mortar (Figure 5.1(c)). In the case of GFRP, the net is made up of fiber-glass wires bonded together with an epoxy resin (Gattesco et al. 2015 [167], Gattesco and Boem 2015 [168]). The net shape is created by intertwining the transversal wires with the longitudinal ones. During the implementation, after the demolition of the existing plasters and the outermost layer of mortar joints, the net is placed on the surface of the wall and a layer of shotcrete is implemented. The tiers of reinforced plasters are coupled with underlying the masonry wall by dowels (Figure 5.1(c)) to prevent debonding and provide some additional confining action.

Figure 5.1 - Application of reinforced plasters to masonry walls: (a) electro-welded steel net; (b) GFRP; (c) scheme of arrangement of the reinforcement.

5.1.2 Capacity models and in-plane safety checks

Differently from FRCM, detailed analytical capacity models for masonry walls reinforced by reinforced plasters are substantially not available in the

literature, while Eurocode 8 - Part 3 [8] provides only general recommendations. The Italian Technical Code (NTC 2018) [158] allows the modeling of the effect of reinforced plasters in a simplified way. This provides increasing the original mechanical properties of the masonry (strength and elastic moduli) by an amplification factor (>1), which in the following will be called α_r. The α_r coefficient simultaneously applies to the masonry compressive strength (f_m), shear strength (τ_{0m}), Young modulus (E_m), and shear modulus (G_m), so that:

$$\begin{aligned} \overline{f}_m &= \alpha_r \cdot f_m \\ \overline{\tau}_{0m} &= \alpha_r \cdot \tau_{0m} \\ \overline{E}_m &= \alpha_r \cdot E_m \\ \overline{G}_m &= \alpha_r \cdot G_m \end{aligned} \tag{5.1}$$

where the over-signed terms represent the mechanical properties of reinforced walls. The α_r coefficients are defined as a function of the original typology of masonry where this intervention is realized. For the reinforced plaster intervention α_r coefficients range between 1.2 and 2.5, as shown in Table 5.1. The same approach can be applied in the case of wall reinforcements by grout injection or reinforced stitching of mortar joints (Table 5.1), however, in the case of reinforced plasters, the original thickness of the wall (t) is increased by the thickness of the reinforced plaster, so that the final thickness $\overline{t}$ will be:

$$\overline{t} = t + 2 \cdot t_{rp} \tag{5.2}$$

where t_{rp} is the thickness of the reinforced plaster on each side of the wall.

Table 5.1 – Amplification factors (α_r) for different masonry typologies and reinforcement interventions.

Masonry typology	**Reinforced plasters**	**Grout injection**	**Strengthening of mortar joints**
Non-uniform masonry	2.5	2.0	1.6
Rough-hewn ashlar masonry with non-	2.0	1.7	1.5
Split stone masonry with regular texture	1.5	1.5	1.4
Irregular tender stone masonry	1.7	1.4	1.1
Coursed tender stone masonry	1.5	1.2	1.2
Squared stone block masonry	1.2	1.2	-
Solid brick masonry	1.5	1.2	1.2
Hollow unit masonry	1.3	-	-

In-plane safety checks of reinforced masonry (flexure and shear) are simply carried out by using the upgraded thickness of the wall ($\overline{t}$) and design resistances ($\overline{f}_d$ and $\overline{\tau}_{0d}$), which are defined as:

$$\bar{f}_d = \alpha_r \cdot f_d = \frac{\alpha_r \cdot f_m}{CF \cdot \gamma_M} = \frac{\bar{f}_m}{CF \cdot \gamma_M}$$
$$\bar{\tau}_{0d} = \alpha_r \cdot \tau_{0d} = \frac{\alpha_r \cdot \tau_{0m}}{CF \cdot \gamma_M} = \frac{\bar{\tau}_{0m}}{CF \cdot \gamma_M} \quad (5.3)$$

where γ_M and CF are respectively the partial safety factor and the confidence factor defined according to technical codes ([158]). With reference to Figure 5.2, the ultimate flexural resistance (M_u) is evaluated as:

$$M_u = \frac{\sigma_0 \cdot \ell^2 \cdot \bar{t}}{2} \cdot \left(1 - \frac{\sigma_0}{0.85 \cdot \bar{f}_d}\right) \quad (5.4)$$

where ℓ is the length of the wall, and $\sigma_0 = N_0 / (\ell \cdot t)$ is the average compressive stress, N_0 being the current axial force acting on the wall (Figure 5.2). For an unreinforced wall, the original design strength (f_d) and thickness (t) are used in Equation (5.4).

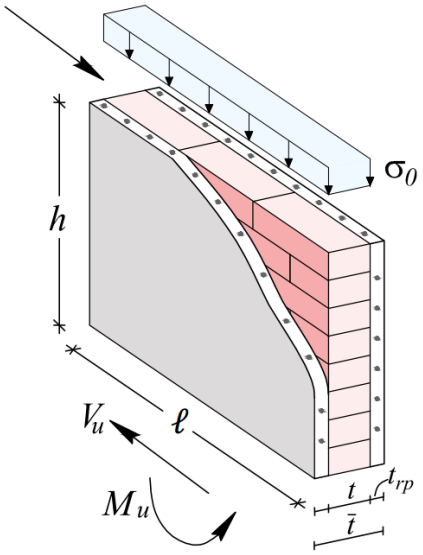

Figure 5.2 - Reference scheme for the evaluation of in-plane ultimate moment and shear of a reinforced masonry wall.

The ultimate shear resistance is evaluated according to the model by Turnšek and Čačovič 1971 [169] as follows:

$$V_u = \frac{\ell \cdot \bar{t} \cdot 1.5 \cdot \tau_{0d}}{b} \cdot \sqrt{1 + \frac{\sigma_0}{1.5 \cdot \bar{\tau}_{0d}}} \tag{5.5}$$

where $b = h / \ell$ is the aspect ratio of the wall ($1 \leq b \leq 1.5$). Again, if the wall is not reinforced, the original shear design strength (τ_{0d}) and thickness (t) are used in Equation (5.4). Equations (5.4) - (5.5) are generally conservative, but they can be eventually updated to consider the effect of T-junctions in correspondence of orthogonal walls.

A comparison of the unreinforced and reinforced flexural and shear interaction domains ($N_0 - M_u$) and ($N_0 - V_u$) by Equation (5.4) and Equation (5.5) is represented in Figure 5.3 for a sample masonry wall. It is noteworthy observing that capacity models in Equation (5.4) and Equation (5.5), can be replaced anytime by different, or more refined models without any drawback for the below-discussed optimization framework.

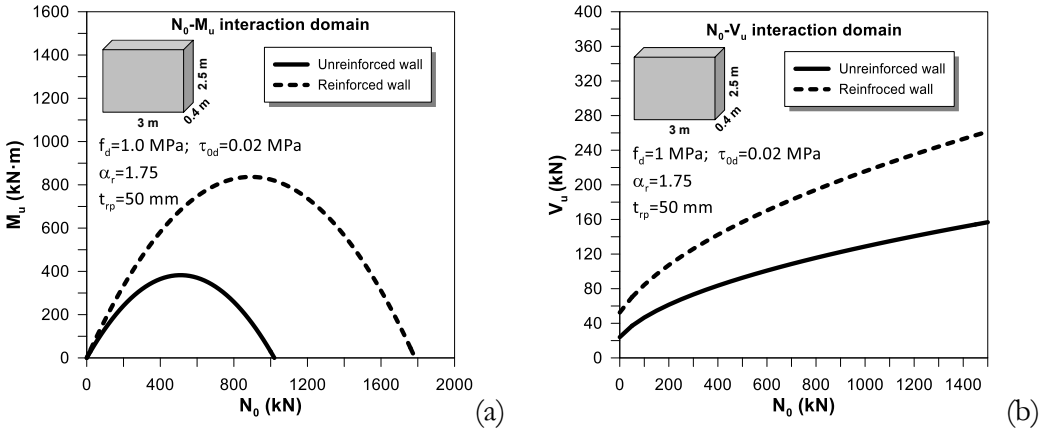

Figure 5.3 - Unreinforced and reinforced flexure and shear interaction diagrams for a sample masonry wall: (a) $N_0 - M_u$; (b) $N_0 - V_u$.

5.2 Optimization framework

5.2.1 Working principles

The optimization procedure herein proposed is based on the genetic algorithm metaheuristic technique. This class of soft-computing algorithms analyzes the research space through the handling of a set of variables that are gathered in a so-called design vector. Each tentative solution represents a possible retrofitting configuration. The procedure followed in the framework is schematically represented in Figure 5.4. The decision variables, namely the

parameters to optimize, are defined at the beginning, once one (or more) strengthening techniques are chosen. This will include the position of the reinforcement and its sizing (if needed). The algorithm starts generating a random initial population of design vectors (tentative solutions) and evaluates the objective function for each individual. For the current application, the objective function will compute the material and manpower cost to implement the reinforcement at the global level, namely the reinforcement of masonry piers. The fittest individuals are then selected, and through the application of the genetic operators, a new generation of tentative solutions is created. Reinforcements for local failure mechanisms are not included in the design optimization process as their design is independent and typically does not need optimization.

As can be observed from Figure 5.4, the optimization algorithm is the core of the framework, but two fundamental engineering decision phases are left to the designer. The first one is the initial selection of the design variables, which allows the possible definition of a restricted design space (e.g. limiting the optimization to a portion of the building or reducing the number of parameters to be optimized). This operation significantly influences the potential reduction of the computational cost. In the last phase, a restricted number of optimized solutions with similar fitness are compared. The most suitable is then selected by the designer considering the technical feasibility. The main features of the proposed framework are described in detail in the following sections.

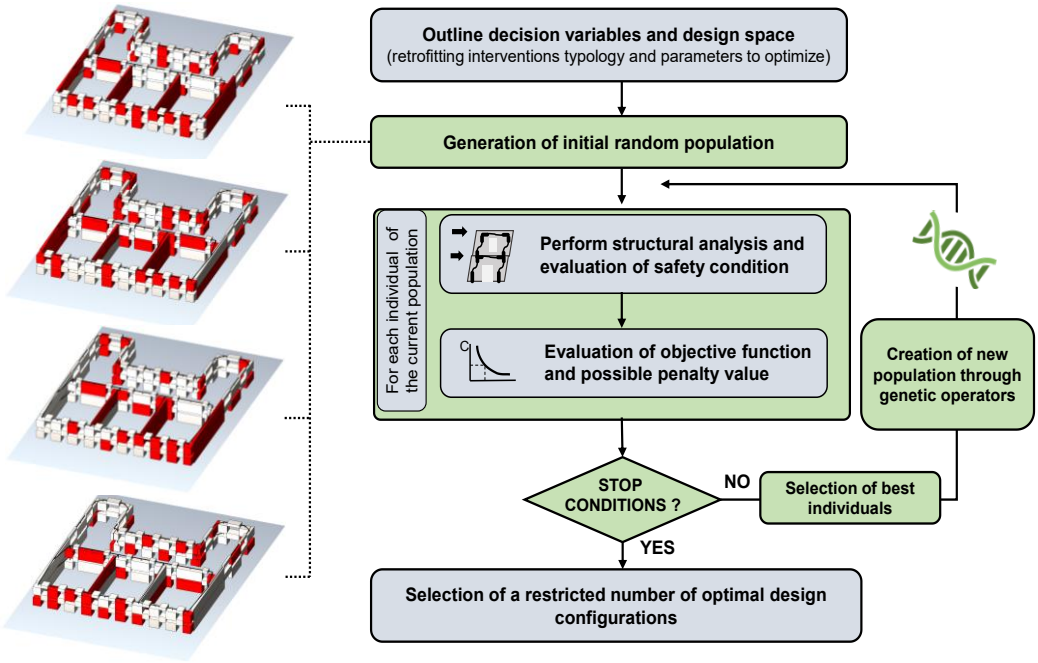

Figure 5.4 - Schematic flowchart of the optimization framework.

5.2.2 Design vector encoding

The optimization algorithm aims to pinpoint the topology of the walls to be reinforced so that the retrofitting cost is minimized. The topology optimization is performed by using binary variables to encode the presence or not of the reinforcement on each wall. All the decision variables are gathered in the design vector **b** so defined:

$$\mathbf{b} = \begin{bmatrix} \dots & b_{ij} & \dots \end{bmatrix}^T \tag{5.6}$$

where b_{ij} is a Boolean variable assuming the value 1 if the wall is retrofitted and 0 if not, namely:

$$b_{ij} \in B = (0 \;\; 1) \tag{5.7}$$

where B is the binary set. The subscripts i and j denote the position of the wall in plan and the story, respectively. It is noteworthy observing that walls included in the design vector can have different material properties, and so structures arranged with different typologies of masonry can be also handled by the optimization framework. In order to reduce the dimension of the research space, and so the computational burden required for the analysis, each Boolean variable can also represent a cluster of adjoining walls. Clustering is quite helpful to implement some architectural restraints, to which the seismic intervention must comply.

The choice of the optimization algorithm procedure is felt on genetic algorithms since the approach is particularly efficient in handling a research space defined by Booleans. The implementation or not of the reinforcement intervention as encoded in the design vector is fulfilled by modifying the geometrical and mechanical properties of the walls as provided by Equations (5.1)-(5.3).

5.2.3 Definition of the objective function

The objective function (OF) to be minimized, also called fitness function, evaluates the costs associated with the implementation of the reinforced plaster strengthening intervention. Since the cost is strictly related to the surface of retrofitted walls, the objective function simply appraises the total surface of reinforced plasters that is encoded by the design vector of each individual. To consider the feasibility of each solution (namely if all the safety checks are passed for an individual), the fitness function involves a penalty function, that is used

to fictitiously increase the fitness value of unfeasible individuals. The objective function ($OF(\mathbf{b})$) is, therefore defined as:

$$OF(\mathbf{b}) = C(\mathbf{b}) + \Pi(\mathbf{b}) \tag{5.8}$$

where C is the cost function and $\Pi(\mathbf{b})$ the penalty function. As can be noted, the objective function and the cost function depend on the design vector ($\mathbf{b}$) representing each individual.

Assuming that the cost per unit surface of reinforced plasters is a constant, the cost function here used will consider only the surface of reinforced plasters, so that:

$$C = \sum_{i=1}^{n_{rw}} A_{rp,i} \tag{5.9}$$

where $A_{rp,i}$ is the surface of reinforcement applied to the i^{th} reinforced wall, and n_{rw} is the number of reinforced walls. It is noteworthy observing that, since reinforced plasters are applied at both sides, the surface $A_{rp,i}$ corresponds to twice the area of the reinforced wall panel ($A_{rw,i}$), so that:

$$A_{rp,i} = 2 \cdot A_{rw,i} \tag{5.10}$$

The penalty function is instead defined as:

$$\Pi = p \cdot \sum_{i=1}^{n_a} \left(\sum_{j=1}^{n_{wf}} A_{wf,j} + \sum_{k=1}^{n_{ws}} A_{ws,k} \right)_i \tag{5.11}$$

where $A_{wf,j}$ and $A_{ws,k}$ are the areas of the n_{wf} and n_{ws} walls having a strength capacity/demand ratio lower than 1, with respect to flexure and shear safety checks respectively. The i index of the external sum counts the n_a seismic analyses performed, namely each different direction and sign considered for the seismic forces. Finally, p is a penalty coefficient fictitiously magnifying the weight of the sums Equation (5.11). The magnification of the penalty function allows the algorithm to be aware of the unfeasible individual's genomes when generating the new population. Obviously, for a feasible individual one obtains $\Pi = 0$.

5.2.4 Genetic operator subroutine

Genetic algorithms are a population-based class of metaheuristic algorithms inspired by the natural selections of species (Goldberg 1989 [79], Holland 1992 [77]). The main engine of optimal seeking is based upon the concept of survival of the fittest individuals. The algorithm starts generating a random population of tentative solutions (namely candidate retrofitting configuration) and evaluates the fitness associated with them. The pursuit of the research space minima is achieved by selecting the best tentative solutions and creating new individuals starting from their design vectors (namely the genome) through the parent selection, crossover, and mutation genetic operators. The first of these operators selects the parent tentative solutions, the second mixes the genomes of tentative solutions, and the third introduces some randomness in the genome of child individuals to prevent the algorithm stuck into local minima and enhance the genetic diversity of the population. A scheme describing the application of the genetic operators in creating a new individual is illustrated in Figure 5.5. The parent selection operator makes use of tournament selection (Kora and Yadlapalli 2017 [170]). Within the current population, k individuals are randomly chosen, and their fitness is evaluated. Among these individuals, the best two (in terms of fitness) are employed as parents. The parameter k is commonly called tournament size. The balancing of this parameter allows controlling of the selective pressure, namely a reduction of k will allow individuals with slightly poorer fitness to generate offspring. On the other hand, an increase of k will permit only the fittest individuals to pass the generation, with a consequent reduction in the diversity of the genetic pool.

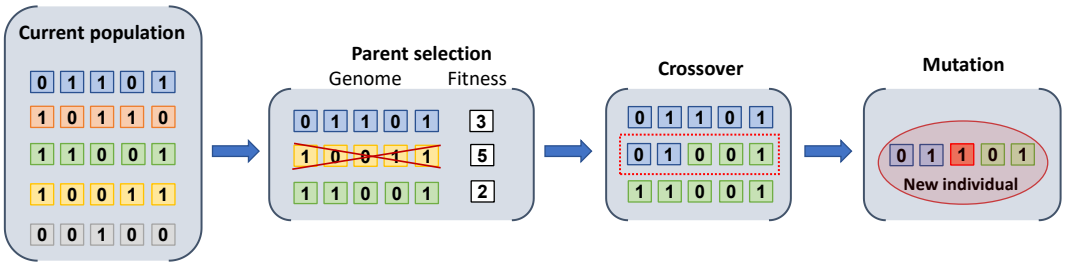

Figure 5.5 - Schematic representation of the application of the genetic operators in creating a new individual.

A *single-point crossover* is used to mix the parents' genome. It selects a random *crossover point* along the design vector and generates the offspring by taking the first part of the genome from the beginning to the crossover point from the first parent, and the remaining part from the crossover point to the end of the genome from the second parent (Figure 5.6(a)). In this way, the new individual has inherited a portion of the genome from both parents but keeps intact the

characteristics of locality. This means that if a portion of the genome is good in terms of its effect on overall fitness, this can be passed on to the offspring intact.

Finally, the mutation operator introduces slight changes in the structure of the offspring genome. This prevents the algorithm from being stuck in local minima and promotes the diversity of populations (Squillero and Tonda 2016 [171]). The mutation is also useful to recover good genetic material that may be lost during selection and crossover operations.

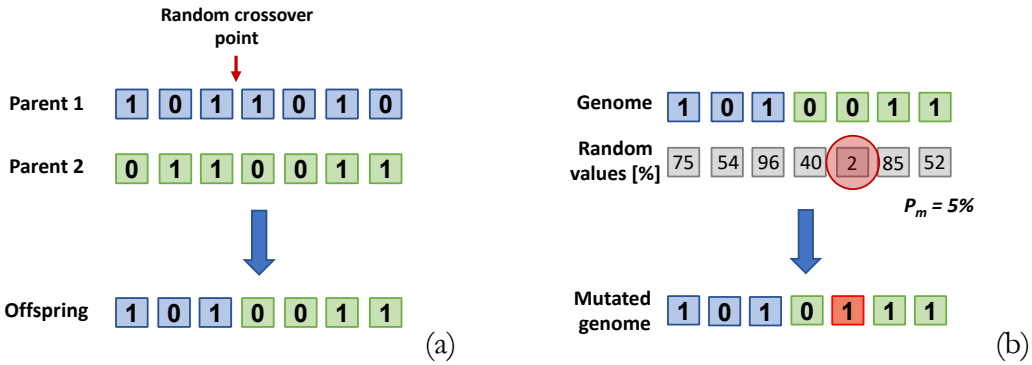

Figure 5.6 - Working principle of the genetic operators: (a) single-point crossover; (b) mutation.

This subroutine operates by setting first a mutation percentage probability (p_m). Then a random integer percentage number between 0% and 100% is drawn for each decision variable (Figure 5.6(b)). If the percentage number associated with a decision variable is smaller than the mutation probability, the value of the variable, which is a Boolean variable, is switched. The value of the mutation probability should be chosen properly since low values can reduce the effectiveness of the operator with which the exploitation phase is mainly entrusted. On the other hand, high mutation probability can lead to a radical modification of the genome, making useless the previous selection and crossover operation. Typical values of mutation probability, for this kind of problem, are commonly fixed around 1-5%.

The framework automatically interfaces MATLAB® with OpenSees. For each candidate solution, a set of MATLAB® subroutines modify the OpenSees model according to the genome collected in the design vector. The model of each individual is then moved to OpenSees for structural analysis. Results are post-processed in MATLAB® for safety checks, fitness evaluation, and application of the genetic operators. In the last stage, the survival selection operator is applied. The latter selects the new population to be analyzed based on a fitness ranking of the individuals, in which only the better ones are used as the new population. The optimization routine is stopped when no further cost reductions are obtained over a certain number of generations. A comprehensive flowchart of the GA framework is illustrated in Figure 5.7.

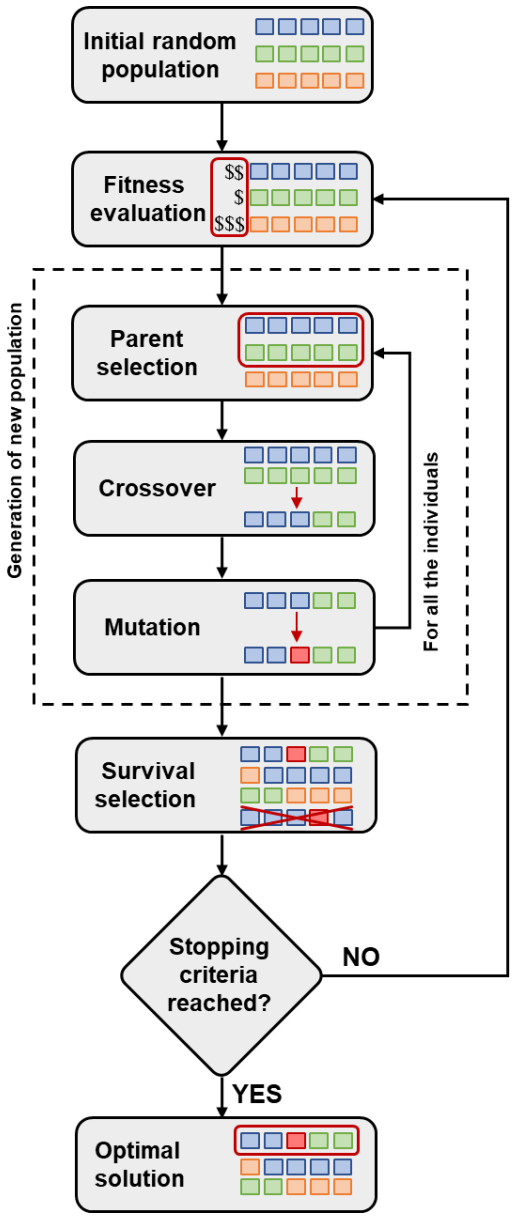

Figure 5.7 – Schematic flowchart of the genetic algorithm framework

5.3 Structural modelling and seismic analysis

5.3.1 Reference model for the masonry building structure

The optimization algorithm is interfaced with an FE solver to perform the structural analysis and the assessment of each tentative solution. For the current study, the optimization algorithm is interconnected with the OpenSees software platform. The masonry structure is defined as an elastic 3D-frame model by employing the Equivalent Frame Method (EFM), which has proven to be reliable for regular masonry building structures (Cattari et al. 2022 [172], Camata et al. 2022 [173]). According to the EFM, the structure is subdivided into masonry panels and spandrels, which are connected through rigid links. The

actual deformable length of the walls is evaluated as a function of the opening shape, according to the method by Braga and Dolce 1982 [174]. The remaining unreformable parts are considered as rigid links. In the current study, the elastic portion of masonry walls and spandrels are modelled as Timoshenko beams, using the *ElasticTimoshenkoBeam* elements implemented in OpenSees. The connection between the orthogonal walls is modelled through rigid trusses using the *rigidLink bar* element. A rigid diaphragm constraint is applied to the floors. In the FE model, reinforced plasters are modeled according to Equations (5.1) - (5.2), that is by modifying the elastic Young's and shear moduli, and the thickness of the element. The modification of the wall thickness is not only reflected as an increase of the stiffness of the element but also the structural weight and the corresponding masses are updated. A scheme of the reference modeling approach is provided in Figure 5.8. It is noteworthy to observe that the choice of a linear EFM model, although introducing several simplifications and generally being conservative, allows a noticeable reduction of the computational effort, which is a fundamental aspect to the feasibility of the framework.

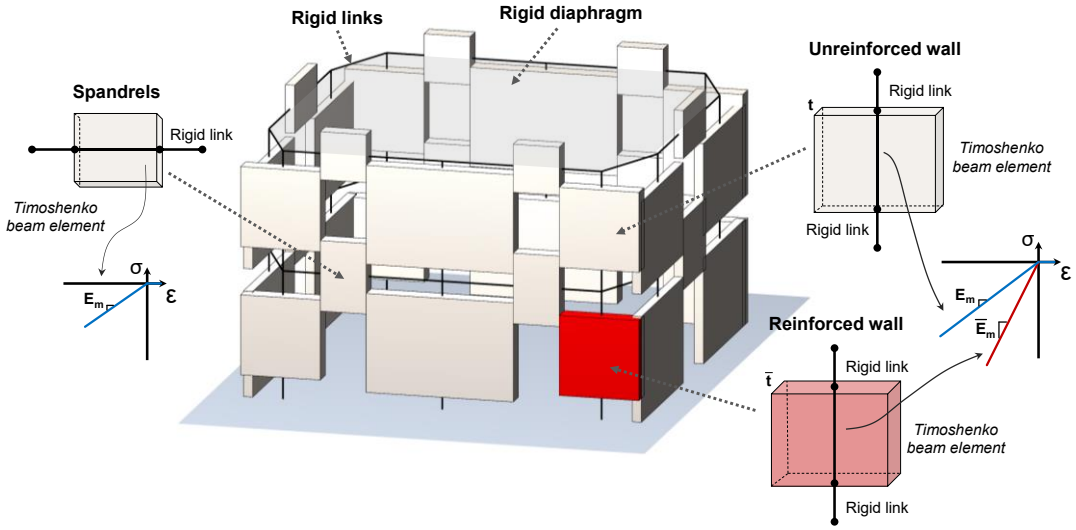

Figure 5.8 – Reference OpenSees FE model of the masonry structure.

5.3.2 Seismic analysis

The current optimization framework is conceived to be combined with linear seismic analysis (linear equivalent static analysis or response spectrum analysis), to determine the seismic demand in terms of internal forces on the frame elements. The choice of adopting linear seismic analyses differs from some recent studies which results are presented in the previous chapter of this Ph.D. thesis (and the related papers Di Trapani et al. 2020 [142], 2021 [175], 2022 [163]) where nonlinear static analysis is used. However, in the framework of the algorithm's efficiency, the adoption of a linear analysis allows a huge

reduction of the computational time needed to get the optimal solution. This kind of approach must be interpreted as a fast optimization of the reinforcement. The inelastic performance of the optimal retrofitting solution can anytime be assessed by a nonlinear analysis.

For structures with a regular distribution of masses and stiffness over the height Eurocode 8 part 1 [156], and Italian Technical Code [158], allow performing the very simple equivalent static seismic analysis. The latter is briefly recalled as it was used to analyze the case studies presented in the following sections. According to the equivalent static seismic analysis, the total horizontal seismic load is evaluated as:

$$F_h = S_d(T_1) \cdot (W / g) \cdot \lambda \tag{5.12}$$

Where $S_d(T_1)$ is the design spectral acceleration in correspondence with the vibration period T_1, W is the total weight of the structure according to the seismic combination of loads, g is the gravitational acceleration, and λ is a corrective factor that is *0.85* if $T_1 \leq 2 \cdot T_c$ (T_c being the corner period of the elastic spectrum) and the structure has more than two stories, or 1 otherwise. The fundamental period of vibration of structure (T_1) can be estimated in a simplified way as $T_1 = c_1 \cdot H^{3/4}$, where H is the total height of the building in meters and c_1 is 0.05 for masonry structures. The total seismic load (F_h) is linearly distributed over the height of the building proportionally to the product of the stories' height and weight. For each candidate solution, the combination of the seismic forces simultaneously acting in the two horizontal orthogonal directions (X and Z) is considered. Specifically, eight analyses are performed by applying 100% of the seismic load in the main direction (X or Z) and 30% in the perpendicular one. Positive and negative verses of actions are considered so that the following combinations are obtained for each analyzed individual:

$$\begin{cases} +1.0 \cdot E_X \pm 0.3 \cdot E_Z \\ -1.0 \cdot E_X \pm 0.3 \cdot E_Z \\ +0.3 \cdot E_X \pm 1.0 \cdot E_Z \\ -0.3 \cdot E_X \pm 1.0 \cdot E_Z \end{cases} \tag{5.13}$$

Seismic forces are applied at the center of mass of each floor. The accidental eccentricity of the center of mass is here neglected for the sake of simplicity.

5.3.3 Safety checks

Safety checks of masonry walls are carried out for the maximum in-plane flexural capacity (M_u) and shear capacity (V_u) of masonry walls. Flexural and

shear demands (M_d) and (V_d) on the walls are obtained from the seismic analysis of each candidate solution. For each analysis and wall, safety checks will simultaneously verify that:

$$\frac{M_u}{M_d} \geq 1 \;\; \& \;\; \frac{V_u}{V_d} \geq 1 \tag{5.14}$$

where M_u and V_u are respectively the ultimate flexural capacity and the shear capacity of the masonry wall evaluated according to Equations (5.4) and (5.5). Local out-of-plane mechanisms are not accounted by Equation (5.14), however, they can be added as an additional condition without losing the validity of the framework.

An effective representation of the current flexural and shear safety checks can be performed by defining the dimensionless domains. For the flexural domain, this can be done by normalizing Equation (5.4) by $f_d \cdot \ell^2 \cdot t$, that is:

$$m_u = \frac{M_u}{f_d \cdot \ell^2 \cdot t} = 0.5 \frac{\sigma_0}{f_d} \cdot \left(1 - \frac{\sigma_0}{0.85 \cdot f_d} \right) \tag{5.15}$$

By defining the normalized axial load as $n_0 = \sigma_0 \; / \; f_d$, from Equation (5.15) one obtains:

$$m_u = 0.5 \, n_0 \cdot \left(1 - \frac{n_0}{0.85} \right) \tag{5.16}$$

Similarly, the dimensionless shear domain can be defined by normalizing Equation (5.5) by $b / 1.5 \cdot \tau_{0d} \cdot \ell \cdot t$, so that:

$$v_u = \frac{V_u \cdot b}{1.5 \cdot \tau_{0d} \cdot \ell \cdot t} = \sqrt{1 + \frac{\sigma_0}{1.5 \cdot \tau_{0d}}} = \sqrt{1 + n_v} \tag{5.17}$$

where n_v is the ratio between the average normal stress and the diagonal tensile strength ($1.5 \cdot \tau_{0d}$) of the wall, that is:

$$n_v = \frac{\sigma_0}{1.5 \cdot \tau_{0d}} \tag{5.18}$$

In Equations (5.15) and (5.17), the geometrical and mechanical properties of the masonry f_d, τ_{0d}, and t are respectively changed in $\overline{f}_d$, $\overline{\tau}_{0d}$, and $\overline{t}$ if the wall is reinforced.

Dimensionless domains are defined by Equations (5.16) and (5.17) by varying n_0 and n_v. They allow to define unique interaction domains to graphically represent flexural and shear capacities of all the masonry walls of a structure, regardless of their geometrical dimensions and resistances

Figure 5.9).

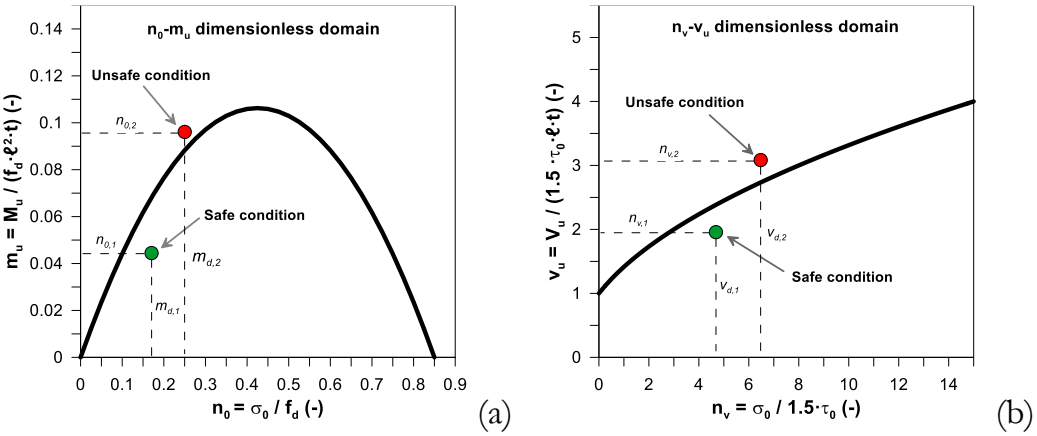

Figure 5.9 – Dimensionless interaction domains and safety checks: (a) flexure (n_0-m_u); b) shear (n_0 - v_u).

The demand points are expressed by the pairs n_0, m_d for flexure and n_v, v_d for shear, where m_d and v_d are defined as:

$$m_d = \frac{M_d}{f_d \cdot \ell^2 \cdot t} \qquad v_d = \frac{V_d}{\ell \cdot t \cdot 1.5 \cdot \tau_{0d}} b \tag{5.19}$$

Each demand point on the dimensionless diagram represents the condition of a wall with respect to the safety limits for a specific load combination. If one (or more) safety checks are not passed the entire candidate solution is defined as unfeasible and is treated according to the penalty approach defined in Equation (5.11). The use of dimensionless diagrams is particularly suitable to gather in a sole diagram of the safety checks for each wall and load combination.

5.4 Case study tests

5.4.1 Details of the case study structure

The proposed optimization framework is tested with the case study of a 3D masonry structure consisting of a C-shape two-story building having planar dimensions of 27.80 x 12.5 m and with a total height of 8 m (Figure 5.10).

The structure has a symmetrical axis along the Z direction. The optimization framework is tested on the building by making two different assumptions for the masonry constituting the wall. In the first case, the structure is supposed to be made of squared stone block masonry (SSM), and in the second case of coursed tender stone masonry (TSM).

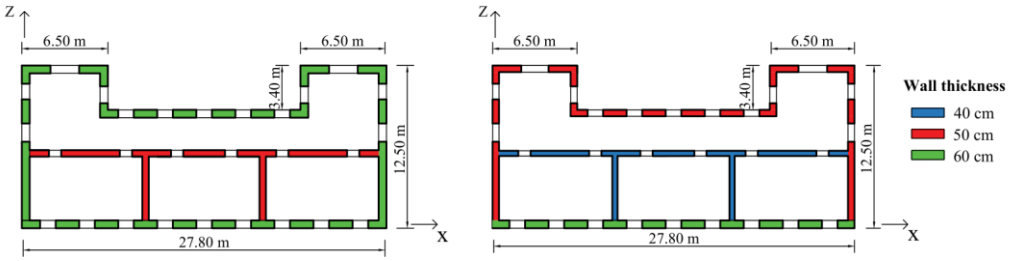

(a) (b)

Figure 5.10 – Geometrical dimensions of the case study structure: a) Ground floor; b) First floor.

The average values of the mechanical properties of the two types of masonries are reported in Table 5.2. The design values of the compressive strength (f_d) and shear strength (τ_{0d}) are obtained by Equation (5.3) assuming a knowledge level 2, so that $CF = 1.2$. The partial safety factor is $\gamma_m = 2$.

Table 5.2 – As-built mechanical properties of masonry for the case-study structures.

Masonry typology	f_m (MPa)	τ_{0m} (MPa)	E_m (MPa)	G_m (MPa)	w (kN/m³)
Squared stone blocks (SSM)	3.2	0.065	1750	575	21
Coursed tender stone (TSM)	2.6	0.060	1410	450	15

For both SSM and TSM the application of reinforced plasters implies an increment coefficient $\alpha_R = 1.5$ according to the Italian Technical Code 2018 [158] (Table 5.1). The mechanical properties of the reinforced masonries are reported in Table 5.3.

Table 5.3 – Mechanical properties of masonry strengthened by reinforced plaster for the case-study structures.

Masonry typology	$\overline{f}_m$ (MPa)	$\overline{\tau}_{0m}$ (MPa)	$\overline{E}_m$ (MPa)	$\overline{G}_m$ (MPa)	w (kN/m^3)
Squared stone blocks (SSM)	5.4	0.11	2975	977	21
Coursed tender stone (TSM)	3.9	0.09	2115	675	15

The building is supposed to be located in Cosenza (Italy) with a soil type C. The reference nominal life (V_N) is set 100 years. The resulting return period is $T_R = 975$ years. The fundamental vibration period evaluated for the structure is $T_1 = 0.23$ sec. Given the regularity of the building over the height, the behavior factor (q) is set equal to 3 according to NTC 2018 [158]. The reference elastic and design spectra are depicted in Figure 5.11

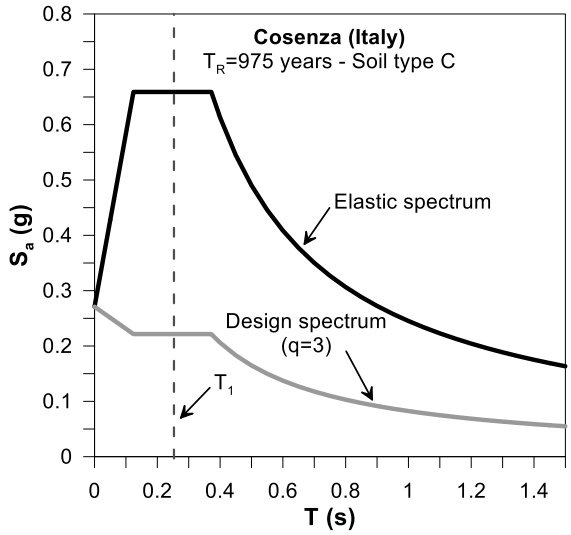

Figure 5.11 – Reference elastic and design spectra.

It is assumed that reinforced plasters are implemented with a thickness of $t_{rp} = 50$ mm for each side of retrofitted walls. Floors are supposed to be rigid in their plan so that a rigid diaphragm constraint is imposed at the floor nodes. A unit load of $q_{\text{floor}} = 5.6$ kN / m^2 and $q_{\text{roof}} = 5.0$ kN / m^2 is evaluated for the slab of the first floor and the roof respectively (seismic combination). The resulting total weight of the structure used for the seismic analysis is 9504 kN. In the equivalent frame model, vertical loads are modelled as point loads applied to the top node of each vertical element. Loads from the slabs are transferred to the nodes as a function of the respective tributary areas.

5.4.2 Preliminary assessment of as-built structures and non-optimized retrofitted structures

Seismic analyses and safety checks of the as-built structures have been carried out according to what was described in the previous section. This preliminary assessment allowed evaluating the walls that were not satisfying flexural and shear safety checks under the reference seismic demand. An overall graphical representation of the safety checks of the structure in the as-built configuration is depicted in Figure 5.12, where different colors are used to denote flexure, shear, and flexure/shear failures of SSM and TSM structures.

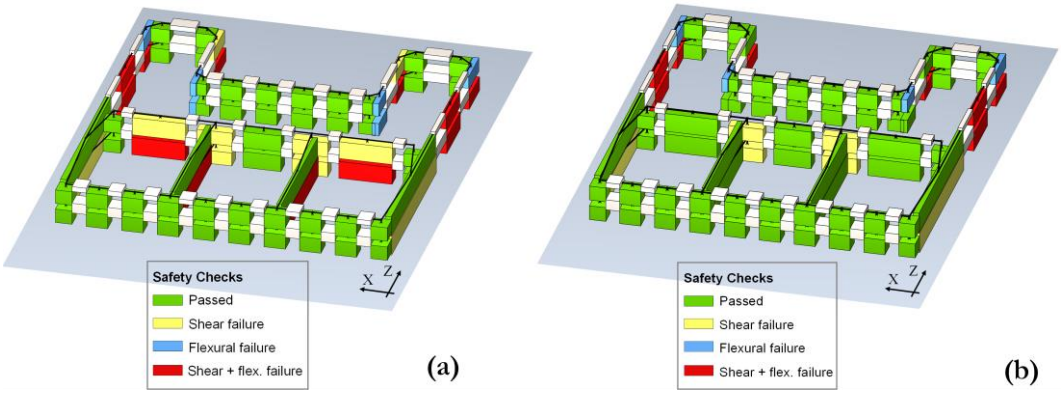

Figure 5.12 – Assessment of the structure in the as-built configuration: a) Squared stone masonry (SSM); b) Tender stone masonry (TSM).

For the SSM structure, 18 out of 78 walls (23%) did not satisfy shear and flexural verifications. For the TSM structure, the walls not passing safety checks were 28, which is 36% of the total. Details about the outcomes of the safety checks of the as-built structures are reported in Table 5.4.

Table 5.4 – Outcomes of safety checks for the as-built squared stone masonry (SSM) and tender stone masonry (TSM) structures.

Structural model	Walls failing in flexure (#)	Walls failing in shear (#)	Walls failing in flexure and shear (#)	Total number of walls (#)
SSM (As-built)	4	6	8	72
TSM (As-built)	6	10	12	72

Assessment of SSM and TSM structure was repeated by applying reinforced plasters to all the walls missing the safety checks. Considering both sides of the walls the surfaces subject to the application of reinforced plasters were 349.7 m^2

and 602 m² for the SSM and TSM structure respectively. In both cases this allowed the walls to pass safety checks, although the design of the reinforcement was carried out without any optimization criterion. Assuming an average retrofitting cost of 200 €/m², the total estimated cost for the retrofitting interventions was 69 940 € and 120 480 € for the SSM and TSM structure respectively (Table 5.5).

Table 5.5 – Reinforcement details and cost of non-optimized retrofitting interventions.

Structural model	Reinforced walls (#)	Walls failing in flexure and/or shear (#)	Total surface of reinforced plasters (m²)	Estimated retrofitting cost (€)
SSM (Non-optim.)	18	0	349.7	69 940
TSM (Non-optim)	28	0	602.4	120 480

Results of safety checks for every wall and load combination are graphically displayed in Figure 5.13 and Figure 5.14, where the outcomes of the unreinforced and reinforced structures are overlapped within the dimensionless domains.

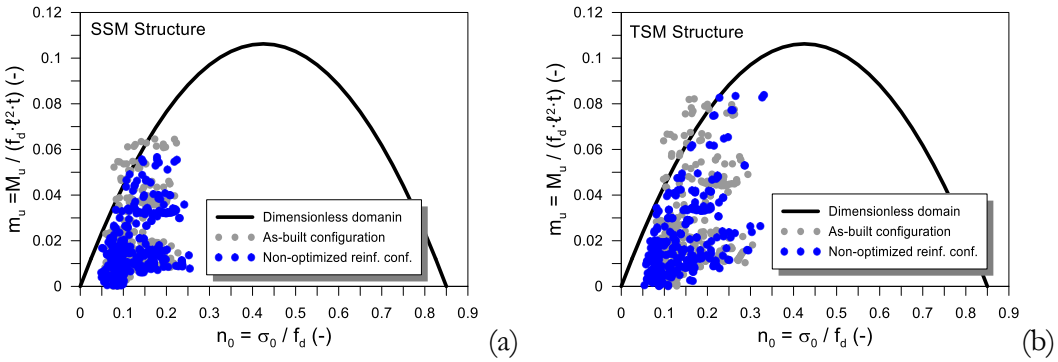

Figure 5.13 – Flexural safety checks for the as-built and non-optimized reinforced structures: (a) Squared stone masonry (SSM); (b) Tender stone masonry (TSM).

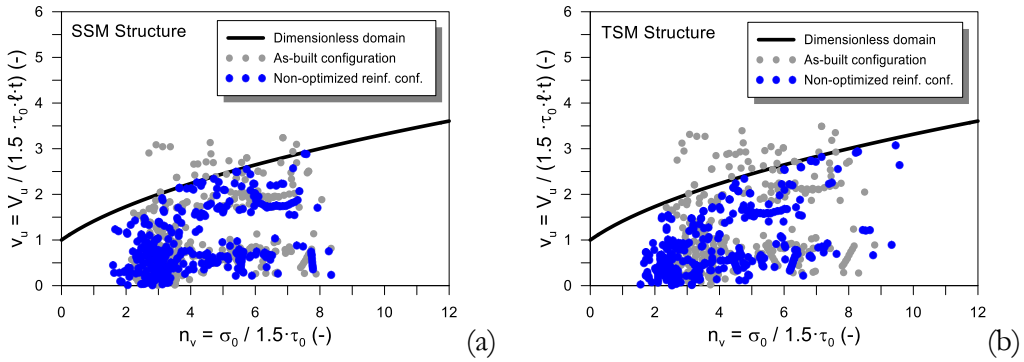

Figure 5.14 – Shear safety checks for the as-built and non-optimized reinforced structures: (a) Squared stone masonry (SSM); (b) Tender stone masonry (TSM).

5.4.3 Results of the application of the optimization framework

The proposed optimization framework has been tested with the case study structures above described. Some preliminary assumptions have been made to reduce the dimension of research space and to avoid unpractical retrofitting configurations. In particular, the adjoining walls were grouped into clusters (Figure 5.15), so that a cluster of walls became the unit element of the design vector. Besides the reduction of the computational effort, this assumption avoids considering solutions providing scattered reinforcement of the facades. Therefore, the 78 masonry walls were converted into 42 clusters. This allowed reducing the research space to 42 Booleans ($dim(\mathbf{b}) = 42$), instead of 78, which encodes the topology of the reinforcements for the structure. The dimension of the design space is reduced to $2^{42} \approx 4.4 \times 10^{12}$ different tentative solutions instead initial dimension of $2^{78} \approx 3.02 \times 10^{23}$.

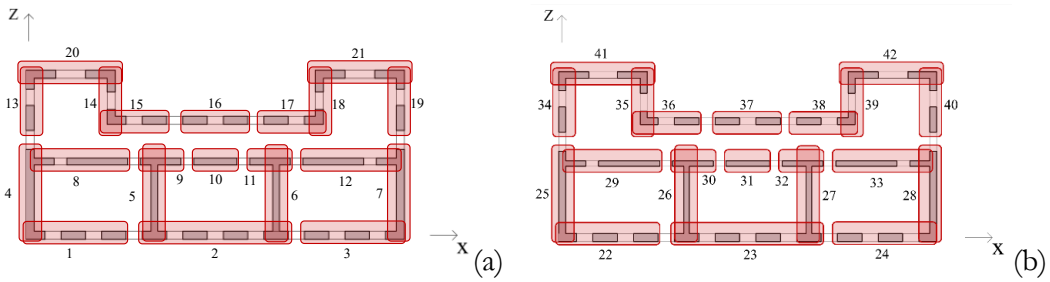

Figure 5.15 – Subdivision of the walls within the clusters: (a) ground storey; (b) first story.

The GA routine was run with an initial population ($\mathbf{P}$) of 200 tentative random solutions. The algorithm proceeded by generating 200 new children per generation through parent selection, crossover, and mutation operators. A tournament size $k = 3$ was used for the parent selection. The mutation probability (p_m) was set as 5%. The penalty coefficient (p) to be used in

Equation (5.11), was calibrated with a few trial analyses, which gave better results by setting $p = 5$. Stopping criteria have been set to a maximum of 25 generations (G_{max}) and a stall of *10* generations (S_{max}), representing the maximum number of generations in which the algorithm does not improve the optimal solution. GA parameters set-up is summarized in

Table 5.6 – GA setup parameters

Dimension of the design vector $dim(\mathbf{b})$	Population size P	Number of offspring O	Tournament size k	Mutation probability p_m	Max generations G_{max}	Max stall S_{max}
42	200	200	3	5%	30	10

The convergence history of the optimization carried out with the proposed GA routine for the SSM and TSM structures is shown in Figure 5.16 and Figure 5.17 in terms of the objective function values (surface of walls subject to retrofit) and the number of retrofitted clusters per individual.

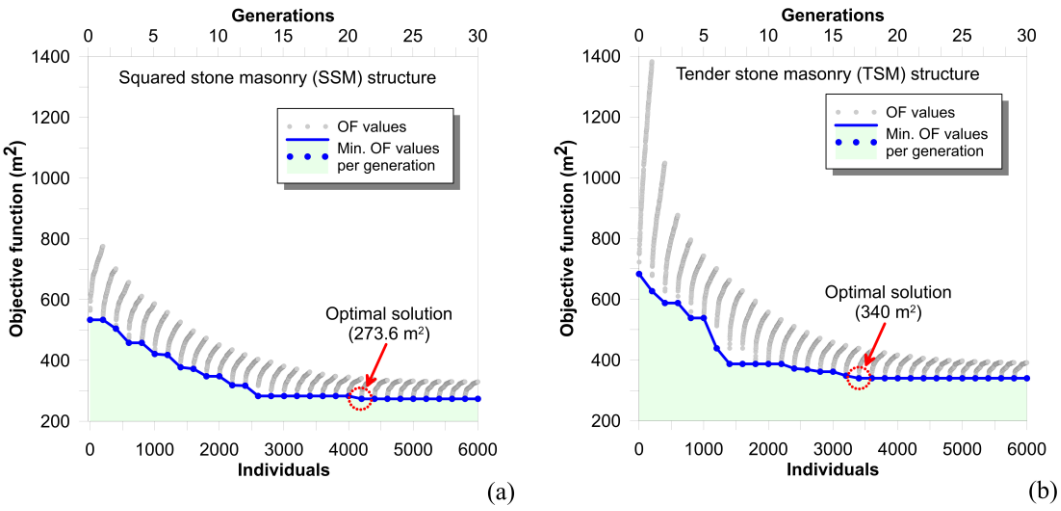

Figure 5.16 – GA optimization convergence history: (a) Squared stone masonry (SSM); (b) Tender stone masonry (TSM).

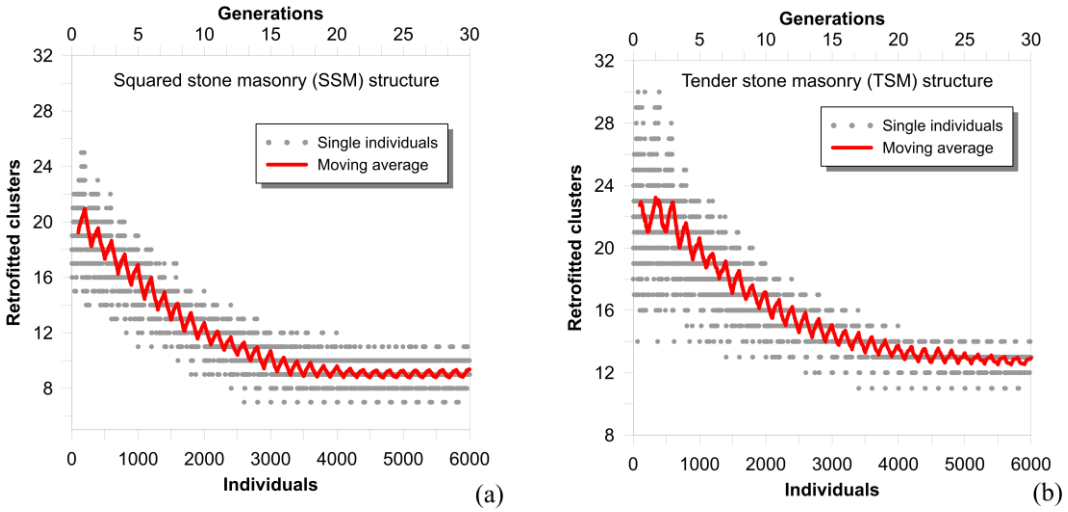

Figure 5.17 – Number of retrofitted clusters during the optimization history: (a) Squared stone masonry (SSM); (b) Tender stone masonry (TSM).

As can be observed from Figure 5.16(a) and Figure 5.16(b), the optimal solutions were found in the 23rd and 18th generations for the SSM and TSM structure respectively. In both cases, the exploration phase, in which the algorithm investigates roughly the research space seeking the general characteristics of the fittest individuals, was rather steep. It is noteworthy observing that the tender stone masonry case, despite starting from higher fitness values, converged five generations earlier. Further considerations can be made by observing the exploitation phase, where it can be noted that the algorithm maintains a certain diversity over the generations. This allows the algorithms to have the possibility to improve the optimal solution without getting stuck into local minima. The computational time was approximately 1.6 hours to complete the optimization routine using a standard computer, meaning approximately 1 second to analyze and assess each candidate solution.

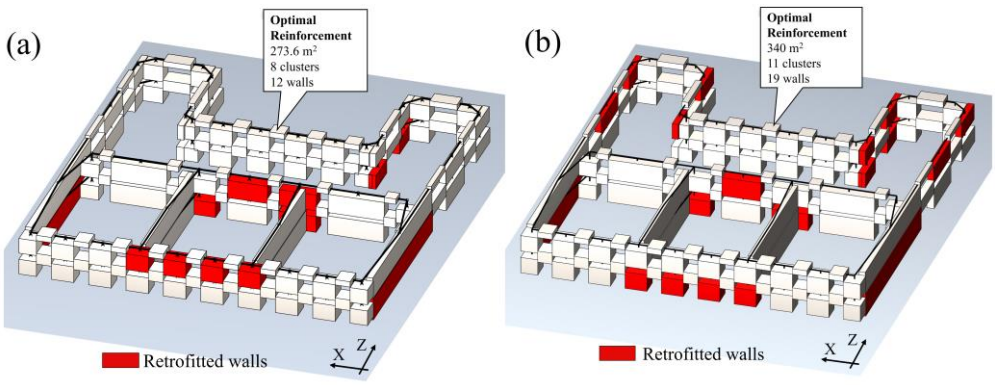

Figure 5.18 – Optimal reinforcement layouts for the case studies: (a) Squared stone masonry (SSM); (b) Tender stone masonry (TSM).

The optimal retrofit configurations found for the two case studies are depicted in Figure 5.18. For the squared stone masonry structure case the total optimized surface of reinforced plasters was 273.6 m^2. Reinforced clusters were 8, out of 42, with a total of 12 walls out of 78. As regards the tender stone masonry structure case, characterized by poorer strengths the total optimized surface of reinforced plasters was 340 m^2 for 11 clusters, out of 42 and 19 walls out of 78. From Figure 5.18 it can be also observed that, for both cases, the optimal retrofitting solutions found through the GA are also satisfactory from an engineering point of view. In fact, the proposed retrofitting configurations do not provide scattered reinforcement of the walls, but these tend to be concentrated in some specific areas. Also, the two-reinforcement layouts approximately reflect the symmetry of the structures along Z direction, confirming that a correct application of the framework can lead to reasonable engineering solutions. The slightly asymmetric layout of the reinforcement is justified by the fact that the optimization algorithm addresses the minimum cost configuration while changing the strength, and particularly the stiffness of some walls. This introduces some plan irregularity and so the optimal solution from the economic point of view may not result in a symmetrical reinforcement layout.

A further consideration about the optimization algorithm's effectiveness can be done by observing the trend of reduction of the average wall surface of reinforced walls. Figure 5.19 shows the ratio between the moving average of the overall surface of reinforced walls over the generations and the maximum average surface of reinforced walls.

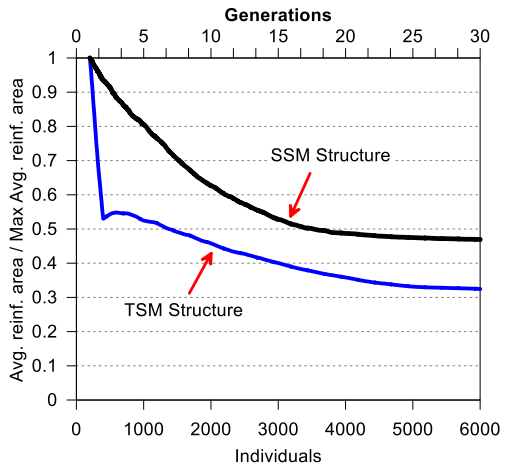

Figure 5.19 – Trend of the ratio between the moving average of the overall surface of reinforced walls and maximum average surface of reinforced walls during the retrofitting optimization of the two case studies.

It can be observed that for the SSM structure the average area of reinforcement was reduced by 53% with respect to the average of the initial population, while for the TSM structure, the same reduction was 68%. This result denoted the major effectiveness of the algorithm in optimizing the reinforcement of the TSM structure despite the average reinforcement demand for this structure being higher. Safety checks for the structures with the optimized reinforcements are represented with the dimensionless diagrams in Figure 5.20 and Figure 5.21. The latter overlaps with those of the non-optimized reinforced structures and the as-built structures.

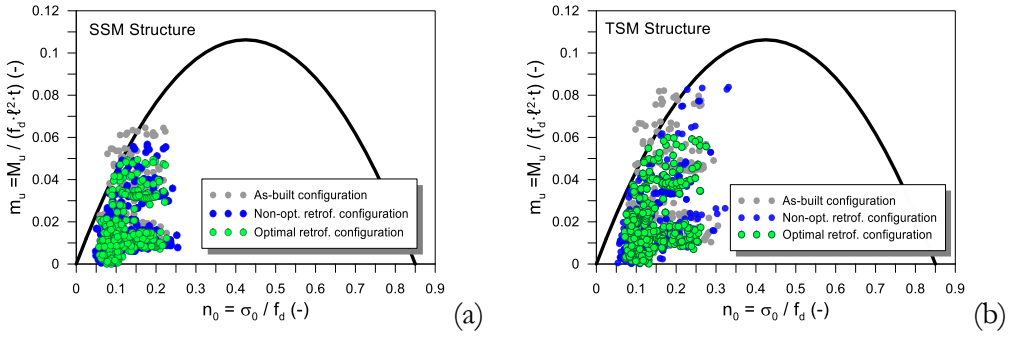

Figure 5.20 – Flexural safety checks comparisons of the as-built structure and non-optimized and optimized reinforced structures: (a) Squared stone masonry (SSM); (b) Tender stone masonry (TSM).

By comparing the optimal retrofitting solutions of SSM and TSM structures with the non-optimized retrofitted ones (consisting of the reinforcement of all the walls that were not passing safety checks), a significant reduction of the surfaces subject to reinforcement was found.

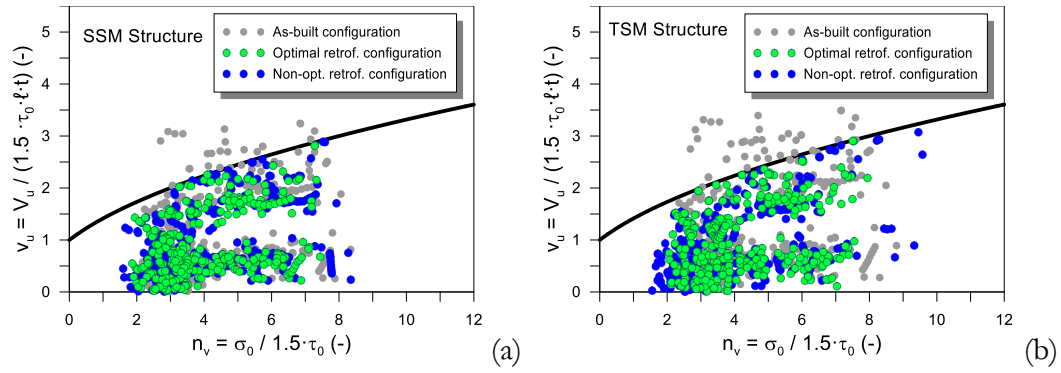

Figure 5.21 – Shear safety checks comparisons of the as-built structure and non-optimized and optimized reinforced structures: (a) Squared stone masonry (SSM); (b) Tender stone masonry (TSM).

In detail, the area of reinforced plaster for the SSM structure passed from 349.7 m² to 273.6 m² for the non-optimized and optimized retrofitted cases respectively, with a reduction of -21.8%. As regards the TSM structures, a major gain was obtained by the application of the proposed optimization framework. In fact, the structure passed from 602.4 m² of reinforced plasters needed for the non-optimized case to 340 m² for the optimal configuration. In this case, the reduction was -43.6%. Still assuming a unitary retrofitting cost of 200 €/m² the optimal solution found for the SSM structure had a total cost of 54 720 € instead of 69 940 € needed for the reinforcement in the non-optimized case. Considering the TSM structure, the retrofitting cost of the optimal solution was 68 000 € instead of 120 480 € resulting in the non-optimized case.

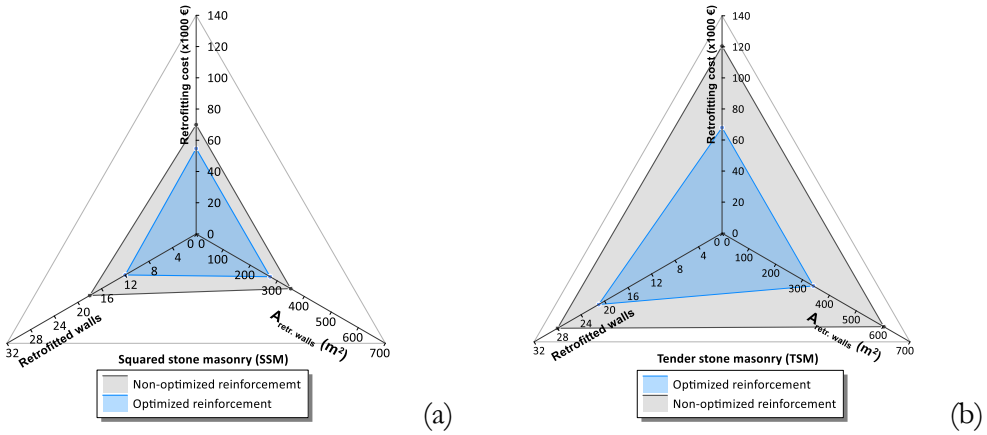

Figure 5.22 - Shear safety checks for the as-built and non-optimized reinforced structures: (a) Squared stone masonry (SSM); (b) Tender stone masonry (TSM).

It is noteworthy observing that, in both cases, the proposed framework was able to pinpoint more effective retrofitting solutions, in terms of costs and the surface of reinforced walls (Figure 5.22 and Table 5.7).

Table 5.7 – Results of the optimization procedure compared with the not-optimized configuration.

Case study	Retrofit design	Total surface of reinforced plasters (m²)	Retrofit cost (m²)	Cost percentage reduction (%)
SSM	Non-opt. Optimal	349.7 273.6	349.7 273.6	-21.8%
TSM	Non-opt. Optimal	602.4 340.0	349.7 273.6	-43.6%

This reduction was much more significant for the tender stone masonry case study structure, which was much more vulnerable to earthquake loads because of the poorer strengths. A general consideration can be drawn from this result.

What has been observed is that the application of such a kind of computational intelligence tool is much more helpful in more complex cases, namely where the difference between a non-optimized configuration retrofitting configuration and an optimized one can be relevant. Namely, if safety checks are not passed for a limited percentage number of walls, the adoption of an optimization algorithm could not bring an evident gain. On the contrary, the adoption of genetic algorithms optimization frameworks, like the one illustrated in this chapter, could make the difference in terms of intervention cost and invasiveness reduction, and therefore on the quality of the retrofitting design.

5.5 Conclusions

In this chapter, a novel computational intelligence-based optimization framework has been proposed, focusing on the topology optimization of reinforced plaster interventions in existing masonry structures subjected to seismic loads. The optimization routine combined a genetic algorithm developed in MATLAB® with a finite element model developed in OpenSees. The algorithm was tested on a case-study structure, considering two sub-cases of masonry quality: average quality masonry (squared stone unit masonry) and poor-quality masonry (coursed tender stone masonry). Results were compared with those from a non-optimized design of reinforcements, which involved retrofitting all walls that did not satisfy safety checks.

The proposed optimization framework effectively provides topology optimization of reinforcements in existing masonry structures while minimizing seismic retrofitting costs. The algorithm successfully addressed the optimization problem using the proposed penalty approach, despite handling the results of multiple seismic structural analyses and safety checks for each tentative solution. Both the SSM and TSM case studies demonstrated significant reductions in the number of reinforced walls needed to meet safety checks. Notably, a major gain was observed for the structure with poorer masonry, with a 43.6% reduction in reinforcements. This outcome demonstrates the robustness of the algorithm in accommodating varying demands for reinforcements based on the intrinsic vulnerability of the structure.

The use of linear elastic analysis allowed for a reduction in the computational effort of the optimization procedure. Designers can verify the outcomes with more refined structural analysis methods, such as nonlinear static analysis. The computational burden was manageable for the investigated case study, taking approximately a couple of hours with a standard laptop (4 cores). However, this duration largely depends on the size of the design vector and the potential use of parallel computing.

The outcomes of this optimization algorithm should be seen as a preliminary design tool to assist practitioners in identifying cost-effective configurations for retrofit interventions, even in complex structures.

This framework represents the first of its kind for the design of retrofitting in existing masonry structures on a structural scale. In the current scientific literature, no other methods address this specific problem for this type of structure.

Further improvements and generalizations of the proposed approach could include more design variables and local out-of-plane safety checks of masonry piers. Additionally, a comparative study between linear and nonlinear static-based optimization of seismic reinforcements would be desirable to balance computational effort and cost savings.

Chapter 6

Risk-targeted seismic retrofitting design procedure for non-ductile reinforced concrete frame structures

Earthquake engineering has long sought to enhance the resilience of structures against seismic events. Performance-Based Earthquake Engineering (PBEE) emerges as a pivotal framework, enabling engineers to predict and mitigate the impacts of earthquakes on buildings and infrastructure. Despite its advancements, the integration of risk-targeted approaches within PBEE remains less explored, particularly in the topic of seismic analysis. This chapter delves into the significance of incorporating risk assessments in PBEE, aiming to bridge this gap in earthquake engineering research. Retrofitting existing structures poses unique challenges that require detailed risk assessments and tailored engineering solutions. PBEE provides a systematic approach to assess these risks and implement retrofit strategies that significantly enhance the safety and performance of older buildings under seismic loads. By focusing on both the probability of seismic events and the consequent structural responses, PBEE enables a more comprehensive evaluation and implementation of retrofit measures, thereby ensuring that these structures meet current safety standards and perform adequately during earthquakes.

The necessity of a risk-targeted PBEE assessment is underscored by the potential for catastrophic losses in the event of major earthquakes. Traditional methods often rely on deterministic criteria that may not fully account for the complex interplay of seismic hazards, structural vulnerabilities, and the probabilistic nature of earthquake occurrences. By focusing on risk, engineers can prioritize resources and interventions more effectively, ensuring that mitigation efforts are both cost-efficient and impactful.

This study positions itself at the intersection of risk management and earthquake engineering, offering a novel contribution to the field. By presenting a comprehensive risk-targeted PBEE assessment framework, this chapter addresses the identified research gaps, providing insights into methodologies for seismic hazard assessment, ground motion selection, and the modeling of

structural responses and vulnerabilities. Through a detailed case study, the practical applications and benefits of the proposed framework are demonstrated, highlighting its potential to inform more resilient seismic design and retrofitting strategies.

6.1 Summary of state-of-the-art of risk-targeted PBEE assessment framework

Incorporating cutting-edge enhancements from recent research, this study integrates novel advancements within the PEER PBEE assessment methodology as proposed by Deb et al. 2021 [176].

In this section the main phases are outlined, underlining the most recent innovations introduced in this framework.

6.1.1 Seismic hazard, response spectra, and ground motion selections

The approach proposed by Deb et al. 2021 [177] redefines the selection of Intensity Measures (IMs) by adopting a spectral acceleration geometrically averaged across multiple periods $\left(S_{a,\text{avg.}}\right)$ (Baker and Cornell 2004 [178]; Kohrangi et al. 2016 [179]) which can be defined mathematically as:

$$S_{a,\text{avg}}(T_1,\ldots,T_n)=\left[\prod_{p=1}^{n} S_a\left(T_p\right)\right]^{1/n} \tag{6.1}$$

This offers a more nuanced understanding of seismic impacts. This methodology accounts for uncertainties in the predominant vibration modes of structures, adjustments in natural periods due to damage, and the increased relevance of longer-period spectral accelerations in assessing seismic response. It is particularly challenging to accurately estimate the fundamental vibration mode of a structure due to inherent model uncertainties. Furthermore, the nonlinear behaviors exhibited during strong earthquakes often result in significant period elongation, complicating the prediction and analysis of seismic response. These complexities make it essential to incorporate advanced modeling techniques in seismic retrofit design to adequately address and mitigate these critical factors.

The selection of ground motion records bridges Probabilistic Seismic Hazard Analysis (PSHA) and the ensuing probabilistic seismic response evaluation, necessitating that the earthquake ground motion records employed for ensemble nonlinear response history analyses of the target structure

maintain hazard or risk consistency. The ground motion selection algorithm proposed by Jayaram et al. 2011 [180] is implemented for the selection of site-specific risk-consistent ensembles of ground motion records representative of an appropriate number of seismic hazard levels considered. Furthermore, the PSHA can be customized to reflect site-specific characteristics, enhancing the accuracy and relevance of seismic hazard assessments and ensuring that the selected ground motions are truly representative of the local conditions.

This method first establishes the probability of spectral accelerations at different periods based on the seismic hazard level and Intensity measure (IM) value. It then selects earthquake records from the NGA-west database using a greedy optimization and subsequently matches Monte Carlo realizations of the target conditional spectrum. This allows for non-linear time history analysis (NLTHA) across a broad range of seismic intensities, supported by a sufficient volume of ground motion data to enable a thorough statistical assessment of the outcomes.

In Figure 6.1 an integrated view of the Probabilistic Seismic Hazard Analysis (PSHA) and Ground Motion (GM) selection process is presented. Figure 1a illustrates the seismic hazard curve, represented in terms of spectral acceleration with varying intensities, while Figure 6.1(b) showcases the Conditional Mean Spectrum alongside the spectra of selected records for a specific IM across a range of periods. This visualization underscores the process of seismic hazard analysis and ground motion record selection, highlighting the adherence to risk-consistency in the compilation of ground motion record ensembles for seismic response evaluations.

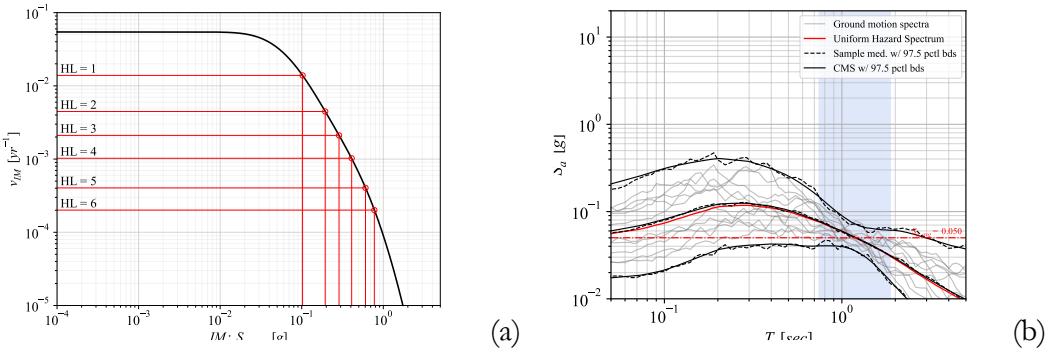

Figure 6.1 – Probabilistic seismic hazard analysis and GM selection: (a) seismic hazard curve in terms of $S_{a,\text{avg}}$, (b) Uniform Hazard Spectrum, Conditional Mean Spectrum range of natural variability, and alongside spectra from the selected ground motion records ensemble.

6.1.2 Conditional demand model

The Conditional Demand Model (CDM) serves as an integral component within the Performance-Based Earthquake Engineering (PBEE) framework, establishing a direct linkage between seismic hazard analysis and the anticipated structural responses to seismic events. This model enhances our understanding of potential damage by predicting how buildings and infrastructure are likely to react under various earthquake scenarios, thus acting as an essential tool for damage assessment. Moreover, accurate nonlinear modeling is particularly crucial in the seismic retrofit of existing structures, where understanding the behavior under seismic loads is more complex due to pre-existing conditions and limitations not present in the design of new structures.

The creation of the CDM is rooted in the analysis of the way structural models respond to an array of ground motions, particularly through nonlinear time-history analysis (NLTHA), as facilitated by the selection of ground motion records discussed in the previous section. This analysis yields a comprehensive dataset of engineering demand parameters (EDPs), capturing the range of structural responses.

Subsequent to data collection, the CDM is constructed by statistically fitting a probability distribution to the EDP data, with each set of data corresponding to different levels of seismic hazard. This modeling effort enables the precise estimation of EDP distributions conditioned on specific Intensity Measure (IM) levels, effectively mapping out the probability of various structural damage states being reached or exceeded.

Further analysis of the structural response ensembles across considered hazard levels leads to the development of seismic demand hazard curves. These curves are essential for understanding the probabilistic distribution of EDPs, conditioned upon a given level of IM. By utilizing fragility functions that define discrete damage states based on EDP values, we can probabilistically characterize the seismic demand imposed on structures. The process aims to elucidate the Mean Annual Rate (MARs) at which specific EDP values, denoted as δ, are likely to occur. This is accomplished through a convolution that integrates the conditional probability of exceeding EDP given an IM with the site-specific seismic hazard curve (SHC), represented as:

$$\nu_{\mathrm{EDP}}(\delta) = \int_{IM} P\left[\mathrm{EDP} > \delta \mid \mathrm{IM} = im\right] \cdot \left| d\nu_{IM}(im) \right| \tag{6.2}$$

where $\left| d\nu_{\mathrm{IM}}(im) \right|$ is the absolute value of the derivative of the seismic hazard curve which represents the rate at which specific IM values are exceeded annually. Identifying a set of EDPs for this analysis helps in characterizing the seismic demand on structures comprehensively, with a focus on limit states (LSs) relevant to the seismic evaluation of structures.

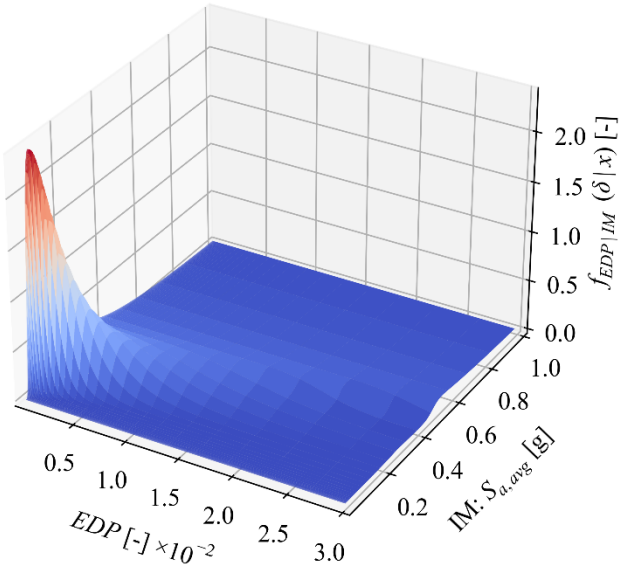

Figure 6.2 – Conditional demand model: representative of the interpolation of the model in EDP/IM space

6.1.3 Probabilistic Seismic Damage Hazard analysis and Uncertainty in capacity model

The Probabilistic Seismic Damage Hazard Analysis (PSDamHA) is designed to provide probabilistic forecasts of structural limit state (LS) exceedances, quantifying these predictions through Mean Annual Rates (MARs) or Mean Return Periods (MRPs) associated with such events. Unlike continuous damage measures, damage states are often categorized into a discrete set, each representing a distinct level of structural performance damage.

At the core of PSDamHA is the definition of limit states (LSs) through a performance or limit state function, mathematically formulated as:

$$Z_k = C_k - \mathrm{EDP}_k \tag{6.3}$$

where C_k denotes the capacity of the element and EDP_k represents the engineering demand parameter associated with the k^{th} limit state, both treated as random variables. This formulation underscores the probabilistic nature of structural capacity and demand in seismic assessments.

The MAR of exceedance for a specific LS is determined by integrating the conditional probability of LS exceedance given the EDP, with the EDP's Demand Hazard Curve, expressed as:

$$\nu_{\mathrm{LS}} = \int_{\mathrm{EDP}} P\left[Z < 0 \mid \mathrm{EDP} = \delta\right] \cdot \left| d\nu_{\mathrm{EDP}}(\delta) \right| \tag{6.4}$$

This integration process effectively convolves the likelihood of exceeding a limit state, conditional on a certain level of seismic demand, with the broader spectrum of seismic hazards represented through the EDP.

A key aspect of PSDamHA is the focus on the uncertainty inherent in Z_k, primarily arising from the variability in structural capacity (C_k) for the k^{th} LS. Accurately quantifying this uncertainty is critical and typically involves employing a predictive capacity model specific to each LS. This model aims to estimate the probability of LS exceedance given a certain demand level, leveraging experimental and numerical data to validate the model's predictions and ensure reliability.

Through the systematic analysis of LS functions and the quantification of uncertainties in structural capacities, PSDamHA offers a comprehensive framework for evaluating the seismic vulnerability of structures. It not only facilitates a deeper understanding of the probabilistic nature of seismic damage but also aids in the development of more informed and effective seismic retrofit strategies.

6.2 Contribution of collapse cases in the updated PEER PBEE assessment framework

In earthquake engineering, "collapse" can be intended as the inability of a structural system or component to support gravity loads after seismic events. This definition underscores the critical nature of assessing structural integrity and resilience under seismic conditions, particularly for ensuring the safety and stability of buildings and infrastructure during and after an earthquake.

Such an evaluation is crucial, particularly for existing structures, which often lack adequate seismic detailing or inherently possess low resistance to lateral forces, rendering them more vulnerable to collapse even under moderate seismic intensities. Many of these buildings were constructed under older regulations that did not account for current seismic knowledge, and they lack critical seismic details, leading to a significantly low capacity to withstand horizontal actions. This deficiency underscores the vital importance of collapse analysis for existing structures, as opposed to the design of new buildings. New constructions can incorporate advanced seismic designs from the outset, using contemporary engineering insights and materials that meet modern safety standards. In contrast, existing buildings must rely on retrofitting strategies to achieve similar levels of safety, making detailed collapse analysis essential to identify and reinforce potential weaknesses. Such proactive evaluations are key

to extending the life of older buildings and ensuring they can endure seismic events without catastrophic failure.

This susceptibility is also evident since in non-ductile structures collapses occur in the "EDP sensitive region" (Ibarra 2004 [181]) the range of Intensity Measures (IMs) closely associated with significant Engineering Demand Parameters of interest for the evaluation of the damage condition of the structures.

The calculated statistics from collapse capacity evaluations enable the derivation of closed-form solutions for estimating the mean annual frequency of collapse. These estimations are integral to the Probabilistic Seismic Demand Hazard Analysis (PSDemHA), providing a quantitative measure of the collapse risk that can be incorporated into comprehensive seismic risk assessments.

Collapse capacity assessment is conducted during the Demand Hazard Analysis phase. It involves detailed analysis under specific ground motions, employing adaptive strategies among various integration algorithms (e.g., Newton, Newton line-search, modified-Newton with initial tangent stiffness, Newton–Krylov, etc.), and leveraging different types of convergence tests and tolerance criteria to ensure model convergence. The failure of a model to converge, despite adjustments to algorithms and tolerance criteria, is indicative of a structural collapse which typically is associated with significant displacement values. This methodological approach highlights the complexities of accurately predicting collapse scenarios and underscores the importance of adopting robust and flexible analytical techniques to assess structural responses to seismic events accurately. While the analytical framework for collapse detection and assessment provides valuable insights into structural behavior under seismic loading, it is not without limitations. The accuracy of collapse predictions is contingent upon the fidelity of the structural models, the representativeness of the ground motion records, and the precision of the analytical methods employed.

In the following subsections, the details of how the conditional distribution of collapse is evaluated and how it is taken into account in the assessment framework are presented.

6.2.1 Conditional distribution of collapse

The collapse fragility function is defined as the conditional probability of exceeding the limit state capacity for a given level of ground motion intensity. For all the HL used in the evaluation of the conditional demand model, the collapse capacity values are estimated and fitted with an appropriate distribution function to the data providing a collapse fragility curve for the specific structure that accounts explicitly for the record-to-record variability according to the approach proposed by Ibarra et al. [181].

This information is used to generate the cumulative distribution function which describes the probability of collapse given the value of IM. Let C denotes the collapse event and $P[C \mid IM = im]$ the conditional probability of occurrence of the collapse given IM. This last ·probability is evaluated through the NLTHAs similarly to the conditional probability of EDP given IM as presented above.

The conditional probability curve can be employed directly to evaluate the probability of collapse at specific hazard levels (IM values) or to evaluate the mean annual probability of collapse by integrating the fragility curve over the hazard curve.

Once the conditional distribution of collapse is computed and hazard information for the site is available, the mean annual frequency of collapse.

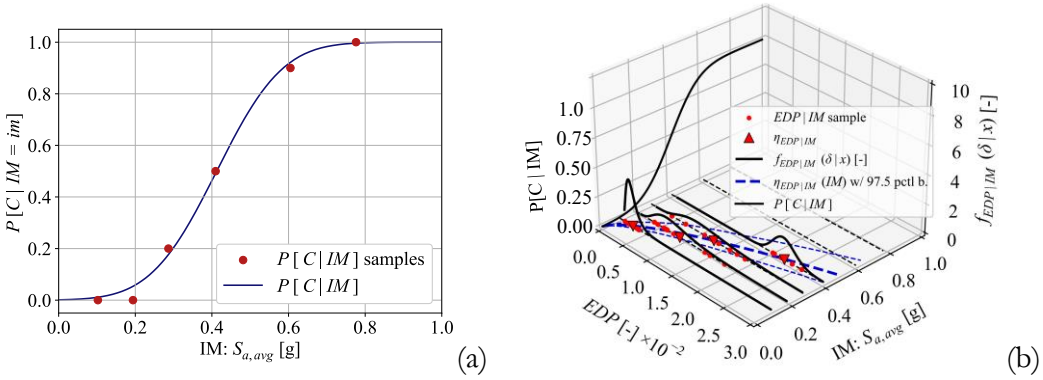

Figure 6.3 – Collapses cases: (a) conditional distribution of collapses w/r to IM, (b) Conditional distribution of EDP with respect to IM and the conditional distribution of collapses

6.2.2 Probabilistic Demand and Damage Hazard Analysis in case of collapse occurrences

In order to incorporate the possibility of collapse the probability of EDP occurrence conditional to the total probability theorem (TPT) can be expressed as:

$$P[\mathrm{EDP} > \delta \mid \mathrm{IM} = im] = P[C \mid \mathrm{IM} = im] \cdot P[\mathrm{EDP} > \delta \mid \mathrm{IM} = im, C] + P[C^c \mid \mathrm{IM} = im] \cdot P[\mathrm{EDP} > \delta \mid \mathrm{IM} = im, C^c] \quad (6.5)$$

where $P\left[C \mid \mathrm{IM}=im\right]$ and $P\left[C^{C} \mid \mathrm{IM}=im\right]$ are respectively the conditional probability of collapses and no collapse given IM. Based on this, the mean annual rate of occurrence of events $\{\mathrm{EDP}>\delta\}$ can be expressed as:

$$\nu_{\mathrm{EDP}}(\delta)=\left\{\int_{\mathrm{IM}} \mathrm{P}\left[\mathrm{C} \mid \mathrm{IM}=im\right]\left|d\nu_{\mathrm{IM}}(im)\right|\right\}\Big|_{EDP\to\infty} + \\ +\left\{\int_{\mathrm{IM}} \mathrm{P}\left[\mathrm{EDP}>\delta \mid \mathrm{IM}=im, C^{c}\right] \cdot P\left[C^{c} \mid \mathrm{IM}=im\right]\left|d\nu_{\mathrm{IM}}(im)\right|\right\} \tag{6.6}$$

this is stated under the hypothesis that in case of collapse the probability that $\mathrm{EDP}>\delta$ is certain regardless of the value of δ. This condition can be expressed mathematically as:

$$\mathrm{P}\left[\mathrm{EDP}>\delta \mid \mathrm{IM}=im, C^{c}\right]=1 \qquad \forall \delta>0 \tag{6.7}$$

In Figure 5a the demand hazard curve is depicted, it shows a horizontal asymptotical trend due to the collapse term, considering the collapses it becomes a mixed random variable in the real range of EDP and a concentrated term when the EDP tends to infinity.

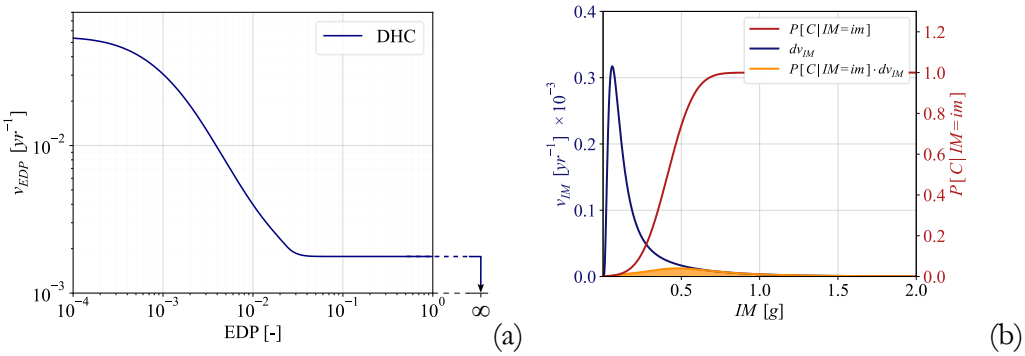

Figure 6.4 – (a) Demand Hazard Curve with collapse case; (b) graphical representation of the collapse contribution to the demand hazard analysis

Under the hypothesis that in case of a collapse occurred, EDPs become very sensitive when the system is close to collapse, and small perturbations in the input produce large variations in the response (Ibarra and Krawinkler [7]). For

this reason, it is assumed that the value of EDPs tends to infinity and the probability associated with its exceedance is unitary, which is mathematically expressed as:

$$P\left[\mathrm{EDP} > \delta \mid C\right] = 1 \qquad \forall \delta > 0 \tag{6.8}$$

Starting from this condition the PSDamHA can be assumed that the probability of exceedance of a limit state is unitary when the collapses occur, regardless of the LS under analysis. So, the MAR of exceedance of the LS can be rewritten as:

$$\nu_{\mathrm{LS}} = \int_{\mathrm{EDP}} P\left[Z < 0 \mid \mathrm{EDP} = \delta\right] \cdot \left| d\nu_{\mathrm{EDP}}(\delta) \right| + \int_{\mathrm{IM}} \mathrm{P}\left[\mathrm{C} \mid \mathrm{IM} = im\right] \left| d\nu_{\mathrm{IM}}(im) \right| \tag{6.9}$$

6.3 Risk-targeted performance-based seismic retrofitting design framework

The proposed framework is based on a parametric analysis of the search space to optimize the seismic retrofitting design process. This process begins with the user defining the decision variables (DVs), also known as design parameters. These variables represent key factors that influence the retrofitting design and include characteristics such as material properties, geometric dimensions, and structural configurations. For instance, geometric dimensions could involve the thickness and length of retrofitting elements, and structural configurations might encompass the layout and the position of retrofitting components within the existing structure. The choice of these parameters is critical as they directly impact the performance and effectiveness but also the cost and impact of the retrofitting solution in use.

The initial phase of selecting these parameters and their boundaries is of paramount importance. It is essential to choose realistic values that reflect the practical constraints and requirements of the retrofitting project. Additionally, the parameter range should be sufficiently narrow to ensure the analysis is efficient and does not lead to excessive computational demands.

Once the parameters and their boundaries are established, the search space is discretized to create a set of parameter combinations that define the retrofitting system. Each point in this discretized space represents a specific tentative solution, which will be subjected to the framework's analysis methodology.

Each point in the discretized search space, representing a specific tentative solution, is then analyzed using the framework's methodology. The detailed procedures and theoretical underpinnings of these stages have been elaborated in earlier sections of this thesis. The analysis, based on the method proposed by Deb et al. (2022) [177] includes five key stages: probabilistic seismic hazard analysis (PSHA), ground motion selection (GMS), ensemble nonlinear time-history analyses (NLTHA), probabilistic seismic demand hazard analysis (PSDemHA), and probabilistic seismic damage hazard analysis (PSDamHA).

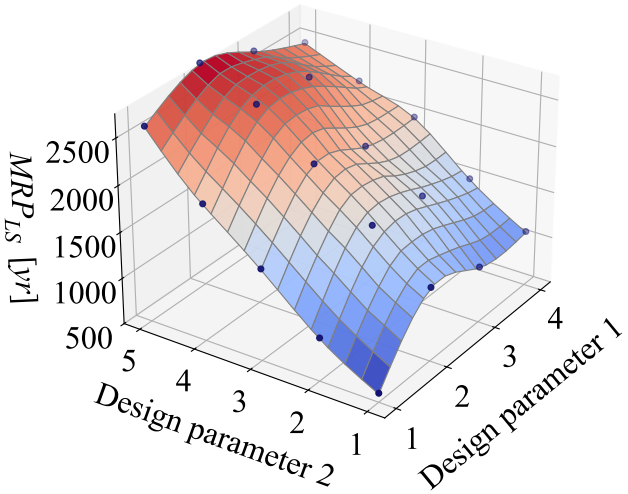

Figure 6.5 - Schematic representation of the MRP surface

The primary output of the seismic assessment framework is the MRP of exceeding a specific limit state (MRP_{LS}) as described in Section 6.2.2. By collecting MRP values for all combinations of retrofitting system parameters, a piecewise linear spatial interpolation is performed to construct the MRP surface. This surface represents the MRP of exceeding the analyzed limit state for each combination of decision variable values (Figure 6.6).

With the MRP surface constructed, it becomes straightforward to establish MRP threshold values (MRP_{target}) and derive retrofitting configuration curves for fixed risk levels. An additional step involves comparing the cost of each retrofitting configuration. This comparison provides a set of risk-fixed reinforcement configurations from which the engineer can make economic and technical considerations, ultimately selecting the most appropriate retrofitting strategy.

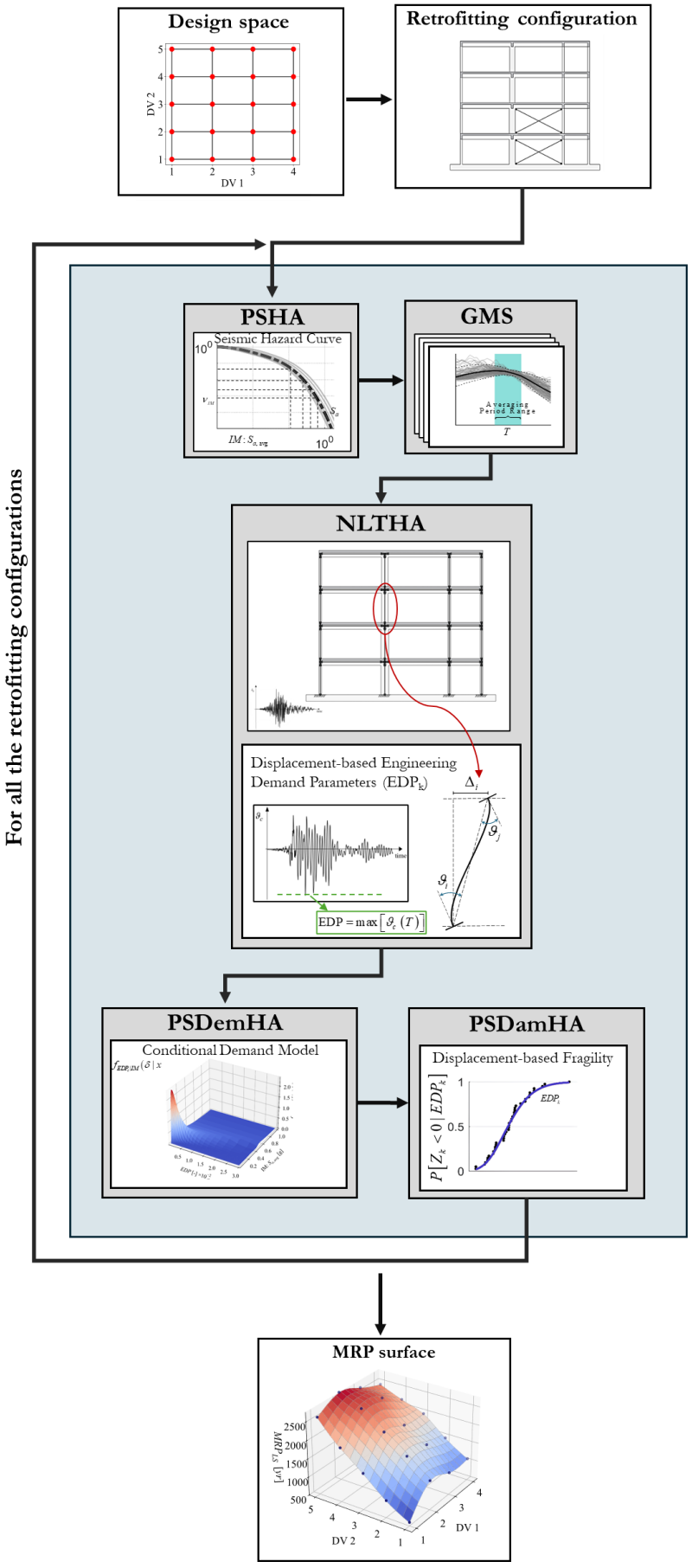

Figure 6.6 – Schematic flowchart of the workflow of the proposed design framework

6.4 Case Study Structure and Computational Model

The methodology outlined was applied to a four-story reinforced concrete (RC) plane frame. The case study structure for this model underwent pseudo-dynamic tests as part of the ICONS research program (Carvalho et al. 2001 [182], Pinto et al. 2002 [183]). The specimen was designed to reproduce in full scale a planar frame of an existing building in the 1970s, constructed according to the practices of that era in southern Europe and the Mediterranean area. In this study, the frame under investigation was considered to have undergone a seismic retrofitting intervention, employing a global strengthening intervention using concentric X-diagonal steel braces. The following section will detail the structure's characteristics and the modeling assumptions employed.

6.4.1 Details of the case study structure

The structure was designed solely for vertical load resistance, lacking specific seismic details, inelastic dissipation mechanisms, or particular provisions for ductility and strength (Varum [184]). The in-plan configuration of the structure is represented in Figure 6.7(a), and the dimensions of the beams and transversal slab are represented in Figure 6.7(b). The beams are 0.25 meters in width and 0.50 meters in depth, while the slabs of 0.15 meters thick. Details of the column reinforcement for the first and second stories are shown in Figure 6.7. In the upper two stories, the reinforcement in columns B and C is reduced. The effective widths of the slabs are 75 cm for short beams and 125 cm for long beams, as indicated in Pinto et al. 2002 [183] . The average unconfined concrete strength is $f_c = 16$ MPa, and the average yield strength of the steel is $f_y = 343.4$ MPa.

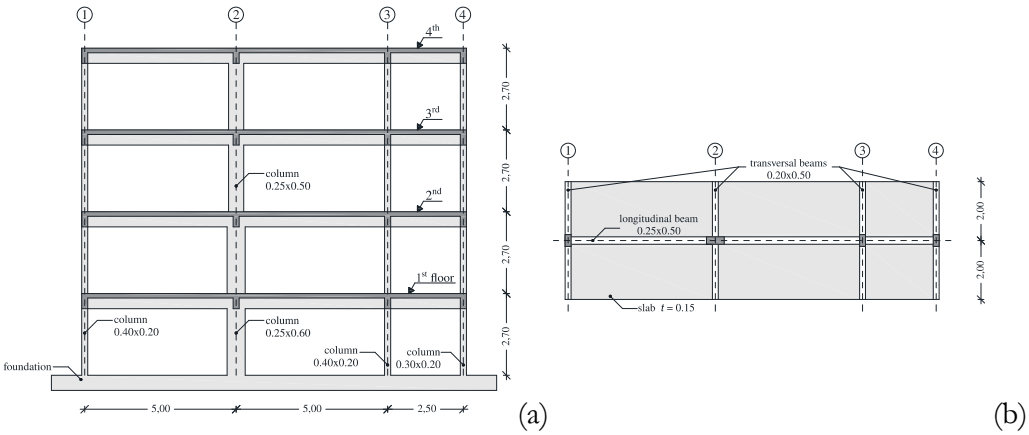

Figure 6.7 – Case study concrete frame: (a), elevation view and geometrical dimensions (b) in-plane view of the slabs

The proposed framework can interface with any finite element (FE) software capable of non-linear dynamic analyses, utilizing the OpenSees software platform [141] for this study. The model has been created using force-based beam elements with distributed plasticity with five Gauss-Lobatto points (Figure 6.8). Concrete elements employ the *Concrete02* uniaxial material model, and the confinement effect exerted by the transversal stirrups has been modeled according to the approach proposed by Razvi and Saatchioglu 1992 [150]. Additionally, the *MinMax* material model, combined with *Concrete02* material, excludes fiber contributions beyond specific strain thresholds aiding in the modeling of concrete crushing phenomena. This approach allows the assessment of the collapse and the evaluation of the collapse fragility of the dynamic response of deteriorating systems through the modeling of the material's deteriorating structural properties as proposed by Krawinkler and Lignos 2009 [185]. Steel rebars are modeled using the Steel02 Giuffrè-Menegotto-Pinto model, elastoplastic behavior with linear strain hardening, supposed to be $\eta = 0.01$ according to Campione et al. 2016 [149].

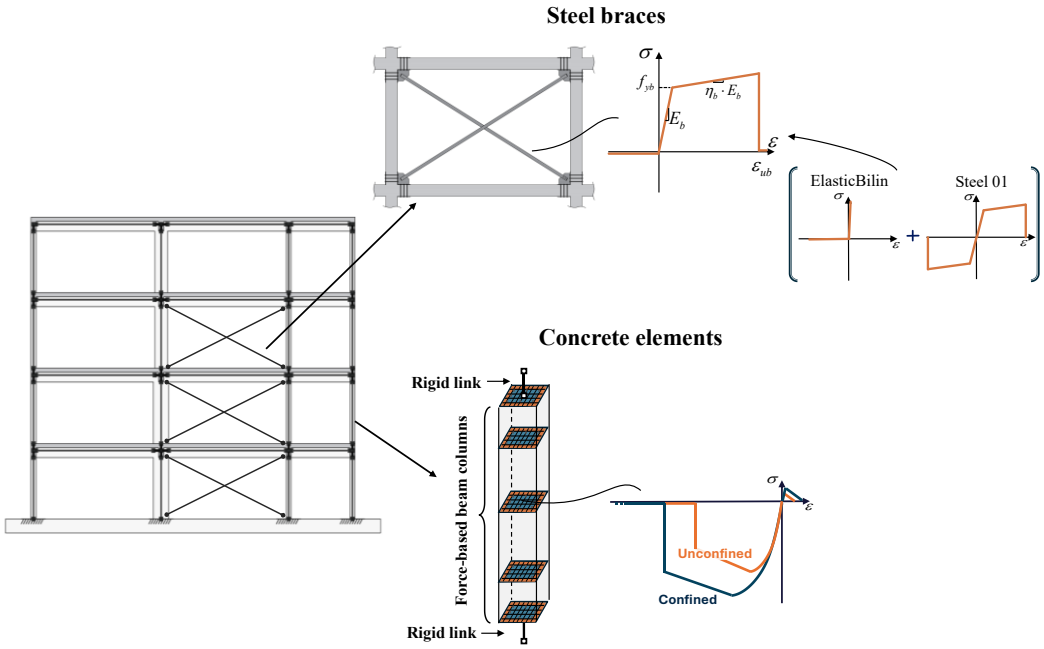

Figure 6.8 – Definition of the fiber-section and truss elements in OpenSees

Corotational geometric transformation has been employed to have the most precise evaluation of the structural response particularly when significant non-linearities of material are attained, even if Adam and Krawinkler 2003 [186] proved that large displacement formulation produces about the same responses as conventional (small displacements) formulations, even in cases where collapse is close.

6.4.2 Modeling of steel braces

In the scope of this case study analysis, steel braces have been chosen as the retrofitting method. This global retrofitting technique is aimed at enhancing lateral strength, stiffness, and ductility. The connections are designed to function as a "nominally pinned joint" (as defined in Eurocode 3 part 1 [156]), which means it can transmit axial forces without significant moment development. Furthermore, local strengthening of weak RC members and column-beam joints will be considered as needed to enhance the effectiveness of the intervention and to prevent local collapses, which are outside the scope of the current study. The braces are supposed to be made of S275 structural steel having nominal yielding stress $f_{yb} = 275\ \text{MPa}$, elastic modulus $E_b = 210\ \text{GPa}$, strain hardening ratio of $\eta_b = 0.01$, and ultimate strength $f_{ub} = 430\ \text{MPa}$.

To simulate the differential mechanical responses of steel braces under tension and compression, the constitutive law for these elements combines *Steel01* with an *ElasticBilinear* uniaxial material defined in series (Figure 6.8Figure 6.9). The former models the fundamental mechanical properties of steel, while the latter, defined with fictitiously high stiffness in tension and almost negligible stiffness in compression, is used to model the instability of the braces when compressed. This modeling assumption is considered valid because the extreme slenderness of these structural elements leads to a buckling compression value that is supposed to be negligible. This assumption, while simplifying the model, ensures that instability occurs within the elastic range, preserving the integrity of the structural response under typical load conditions.

6.4.3 Design variables and general assumptions.

To manage the computational demands of the analysis and to facilitate the representation of results in a three-dimensional space, to represent the results in an accessible manner, a two-dimensional design space of design variables was selected. This approach allows for a streamlined yet comprehensive examination of the key factors that influence the retrofit outcomes while ensuring the analysis remains computationally feasible.

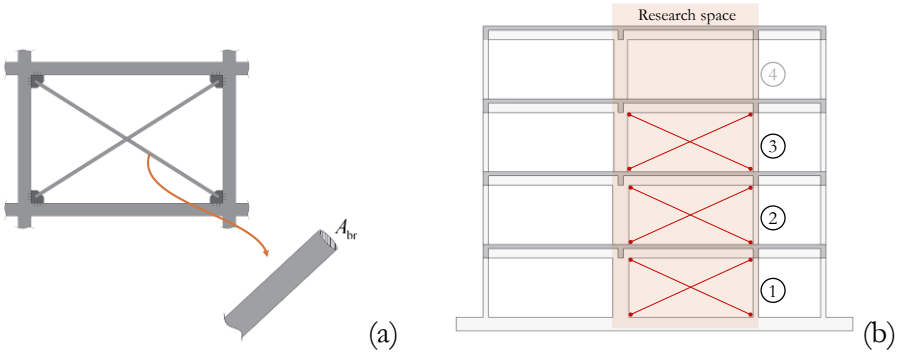

Figure 6.9 – Restricted design space representation for the case study structure

These two parameters of the problem can be encapsulated in a design vector as follows:

$$\mathbf{b} = \left(n_{br} \quad A_{br} \right)^T \tag{6.10}$$

where n_{br} is the number of floors where the braces are implemented starting from the first, and A_{br} is the cross-section area of the braces.

In particular for the case study structure under analysis, to reduce the dimension of the problem but especially to allow a graphical representation of the results, the following restrictive hypotheses are also made:

i. The bracing cross-section area is comprised in the range of between 1.12 cm^2 and 2.78 cm^2 with 5 intermediate values (Table 6.1 – Overview of the various cross-section configurations adopted for the braces).

$$A_{br} = \{1.12, \quad 1.45, \quad 1.74, \quad 2.24, \quad 2.78\} \tag{6.11}$$

ii. The frame fields where bracings can be designed are those associated with the inner spans of the frame (Figure 6.9)

$$n_{br} = [1, 4] \tag{6.12}$$

The resulting size of the design space is then of 20 different combinations of braces diameters and positions inside the structure.

Table 6.1 – Overview of the various cross-section configurations adopted for the braces

Configuration	Brace Arrang. L-shape profiles (UNI 5783-66 [187])	Cross-section area (cm^2)
1	1×20×3	1.12
2	1×20×4	1.45
3	1×30×3	1.74
4	2×20×3	2.24
5	2×30×3	2.78

In the PSHA phase, the intensity measure $S_{a,\text{avg.}}$ is evaluated across ten periods uniformly spaced in the log-space $\left[T_1,\ 2.5\,T_1\right]$ where T_1 represents the fundamental period of the structure. This approach addresses the uncertainties and variability of the fundamental period, as discussed in Section 6.1.1. These adjustments account for the reduction in stiffness due to damage accumulation and the associated uncertainties in estimating this value related to the model uncertainties.

6.4.4 Engineering Demand Parameter and associated damage LSs

In the case under study, the Engineering Demand Parameter (EDP) is assumed to be the chord rotation of the structural concrete elements. This parameter is crucial as it allows for a comprehensive and exhaustive analysis of the structural response and damage during time-history analyses (Pérez-Irizarry et al. 2016 [188], Cai et al. 2014 [189]). By focusing on chord rotation, the study effectively captures the rotational deformations that should be indicative of potential structural failures, providing a detailed assessment of seismic reliability. As for the limit state, this study considers the near-collapse state as the critical threshold. This limit state is significant as it represents a condition where the structure, while severely damaged, still retains some residual load-carrying capacity.

The predictive capacity model for the ultimate rotation capacity of concrete members under cyclic loading is evaluated according to the equation adopted in Eurocode 8 part 3 [8] and proposed by Panagiotakos and Fardi (2001) [190] which, upon being exceeded, deterministically predicts the exceedance of the Limit State of near collapse (NC).

$$\vartheta_u^{\,pred.} = 0.016 \cdot 0.33^{\nu} \cdot \left(\frac{\max\left(0.001, \omega'\right)}{\max\left(0.01, \omega\right)} \cdot f_c \right)^{0.225} \cdot \left(\frac{L_V}{h} \right)^{0.35} \cdot 25^{\left(\alpha \cdot \rho_{sx} \cdot \frac{f_{ywe}}{f_c} \right)} \tag{6.13}$$

where ν is the normalized axial force, f_c and f_{yw} are respectively the compressive strength of the concrete and stirrups yielding stress (MPa), L_v is the shear span, ω and ω' are respectively the mechanical ratio of tension and compression reinforcement steel, ρ_{sx} is the volumetric transverse reinforcement ratio, and α is the confinement effectiveness coefficient evaluated according to Sheikh and Uzumeri 1982 [191], adopted also in the CEB/FIP Model Code 90 [192]:

$$\alpha = \left(1 - \frac{s_h}{2 \cdot b_c}\right) \cdot \left(1 - \frac{s_h}{2 \cdot h_c}\right) \cdot \left(1 - \frac{\sum b_i^2}{6 \cdot b_c \cdot h_c}\right) \tag{6.14}$$

The predictive capacity model does not incorporate uncertainties related to the capacity of the columns, such as material and geometric properties, or variations in geometry. To quantify these uncertainties, the fragility function is employed. It is obtained by comparing the deterministic capacity models and comparing their prediction of LS exceedances with experimental data from tests conducted in laboratories, thereby assessing the accuracy of limit state (LS) exceedance predictions.

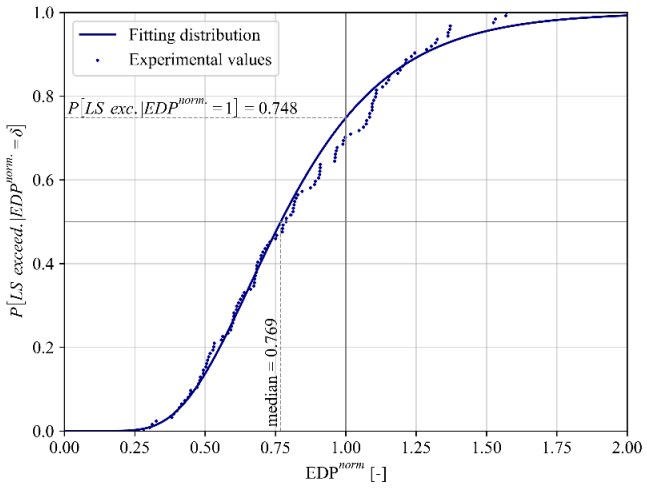

Figure 6.10 – Normalized fragility curve for the Near Collapse chord rotation of reinforced concrete structural elements

For this study, the PEER Structural Performance Database (SPD) (Berry et al. 2004 [193]) has been employed, which aggregates results from cyclic, lateral-load tests conducted on reinforced concrete columns. The database provides raw results from these experimental tests along with comprehensive geometric and mechanical information about the columns tested. The dataset utilized in this analysis comprised columns meeting specific criteria to ensure consistency and relevance to the study's objectives. The columns selected had rectangular cross-sections with square stirrups, they reached flexural collapse during the

test, utilized no high concrete with a strength less than 50 MPa, and were classified as slender (with a length-to-height ratio greater than 2). Additionally, these columns were under low compressive force ($\nu \leq 0.6$). A total of 125 results were analyzed under these conditions. The criterion for reaching the limit state was set as a 15% reduction in resistance, following the approach established by Panagiotakos and Fardis (2001) [190]. The data was then processed to evaluate the normalized fragility curve according to the approach proposed by Deb et al. 2022 [194]. For the definition of the fragility function, a log-normal distribution was employed (Ibarra and Krawinkler 2005 [195]), as depicted in Figure 6.10.

6.4.5 Damage hazard analysis

In the final phase of the PBEE assessment procedure, the objective is to determine the mean annual rate of exceedance for a specified limit state. This phase employs the fragility function determined in the previous section, particularly for the collapse limit state.

Using the fragility function illustrated in Figure 6.10 in conjunction with the demand analysis results from Equation (6.4), the mean frequency of limit state exceedance for each column can be determined. Figure 6.11 depicts the demand curves (grey curves) and the denormalized fragility curves for the columns (red curves) in the case study structure.

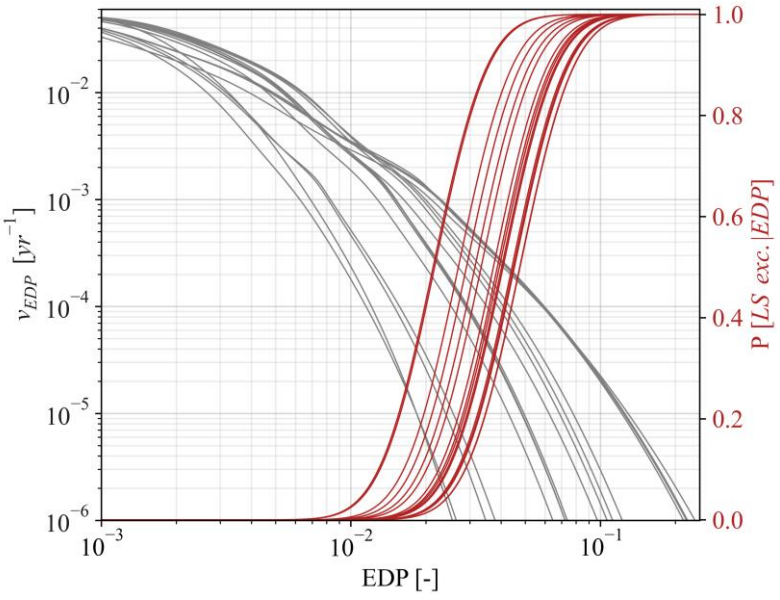

Figure 6.11 - Demand curves (in grey) and denormalized fragility curves (in red) for the case study columns.

Following this analysis, it is possible to ascertain the mean frequency of exceedance, which in this framework is assumed to be the minimum value obtained for each column. This is represented as:

$$\nu_{\mathrm{LS}}^{\mathrm{struct.}} = \min_{\mathrm{columns}} \left\{ \nu_{\mathrm{LS}}^{\mathrm{col}=1}, \nu_{\mathrm{LS}}^{\mathrm{col}=2}, \ldots, \nu_{\mathrm{LS}}^{\mathrm{col}=i} \right\} \tag{6.15}$$

This assumption is justified for collapse limit state analyses because the attainment of the limit state by any structural element results in a condition where the remaining capacity and plasticity reserves are so diminished that it is reasonable to consider the overall structure to be near collapse.

Hence, the Mean Annual Rate of exceedance for the limit state can be determined, which is simply the inverse of the mean annual frequency of exceedance of the limit state:

$$\mathrm{MRP}_{\mathrm{LS}}^{\mathrm{struct.}} = \frac{1}{\nu_{\mathrm{LS}}^{\mathrm{struct.}}} \tag{6.16}$$

This parameter serves as a key output of the seismic reliability analysis. This process is conducted for each retrofitting condition to provide a comprehensive evaluation of the structure's seismic performance across the various configurations.

6.4.6 Estimation of retrofitting costs

For each configuration, the second input analyzed, in addition to the mean return period of limit state exceedance, is the cost of implementing the retrofitting intervention. Specifically, considering that the case study presented in this chapter involves the use of steel braces, the cost can be estimated as:

$$C(\mathbf{b}) = C_{\mathrm{br}}(\mathbf{b}) \; + \; C_{M}(\mathbf{b}) \tag{6.17}$$

where $C_{br}(\mathbf{b})$ represents the cost of the steel braces, calculated as:

$$C_{\mathrm{br}}(\mathbf{b}) = \sum_{i=1}^{n_{\mathrm{br}}} \left(W_{\mathrm{br},i} \cdot c_{\mathrm{br}} \right) = \sum_{i=1}^{n_{\mathrm{br}}} \left(2 \cdot L_{\mathrm{br,i}} \cdot A_{\mathrm{br,i}} \cdot \gamma_s \cdot c_{br} \right) \tag{6.18}$$

Where $W_{br,i}$ is the weight of the i^{th} brace estimated starting from the self-weight of the steel ($\gamma_s = 7850 \mathrm{kg/m^3}$), the length of the brace ($L_{br,i}$), the cross-section area of the brace ($A_{br,i}$ defined as Equation (6.12)), and c_{br} that is the

manpower and material cost per unit weight of steel (estimated in $c_{br} = 12 \ \text{€} / \text{kg}$),

In the above Equation (6.17), the term $C_M(\mathbf{b})$ accounts for the cost of demolition and reconstruction of plasters and infill walls where the braces will be installed, estimated as:

$$C_{\mathrm{M}}(\mathbf{b}) = n_{\mathrm{br}} \cdot c_{\mathrm{br,m}} \tag{6.19}$$

where n_{br} is the number of braces (as defined in Equation (6.11)) and $c_{br,m}$ is the cost for the demolition of one infill panel, assumed to be $c_{br,m} = 1000 \ \text{€} / \text{each}$

The values of the prices are referenced to the period during which this thesis was written, and they do not affect the validity of the proposed method outlined in this chapter.

6.5 Results of the application of the PBEE framework for retrofitted existing structures

Following the procedure presented in this chapter, the case study structure's analysis yielded an MRP surface, as depicted in Figure 10. This MRP surface allows for the establishment of various target MRP levels, facilitating a risk-informed design procedure. In Figure 10, target MRPs of 2500 years, 2000 years, and 1500 years are illustrated, demonstrating the application of the framework for different risk thresholds.

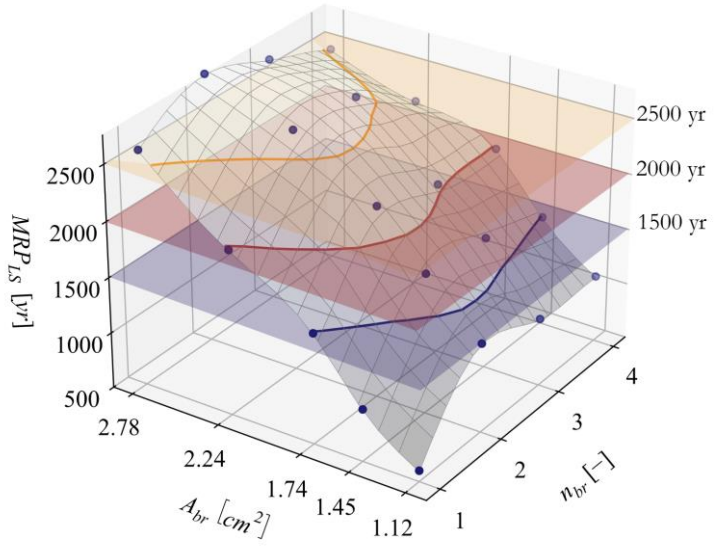

Figure 6.12 – MRP surface for the case study structure with target levels of 2500, 2000, and 1500 years.

It is noteworthy to observe from the MRP surface the trend at a fixed brace area, retrofitting only the first-floor results in the lowest MRP value However, retrofitting more than two floors leads to a reduction in the MRP value for limit state exceedance. This trend can be attributed to the dual effect of the braces. On one hand, they increase the structure's capacity and dissipate energy through yielding, reducing displacement demand. On the other hand, they also increase the initial stiffness of the structure, which raises the seismic demand.

As the diameter of the braces increases, there is a corresponding increase in the MRP value. Initially, this increase is more pronounced but becomes more gradual as the diameter continues to grow. This behavior reflects the complex interplay between increased structural capacity and seismic demand.

Figure 6.13 – Figure 6.13, Figure 6.14, and Figure 6.15 present the results of the analysis, respectively for MRP target of 2500 years, 2000 years, and 1500 years, specifically illustrating the different reinforcement configurations for the three target MRPs of limit state exceedance. The properties of these configurations are summarized in Table 6.2, which provides a comprehensive overview of the optimal retrofitting strategies identified through the analysis.

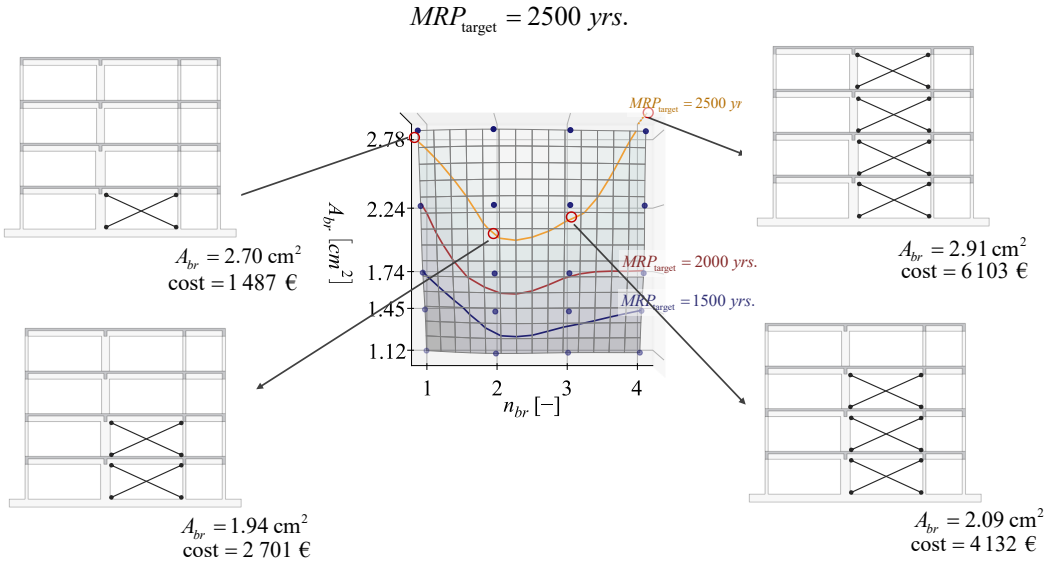

Figure 6.13 – Optimal reinforcement configuration for the target MRP level of 2500 years

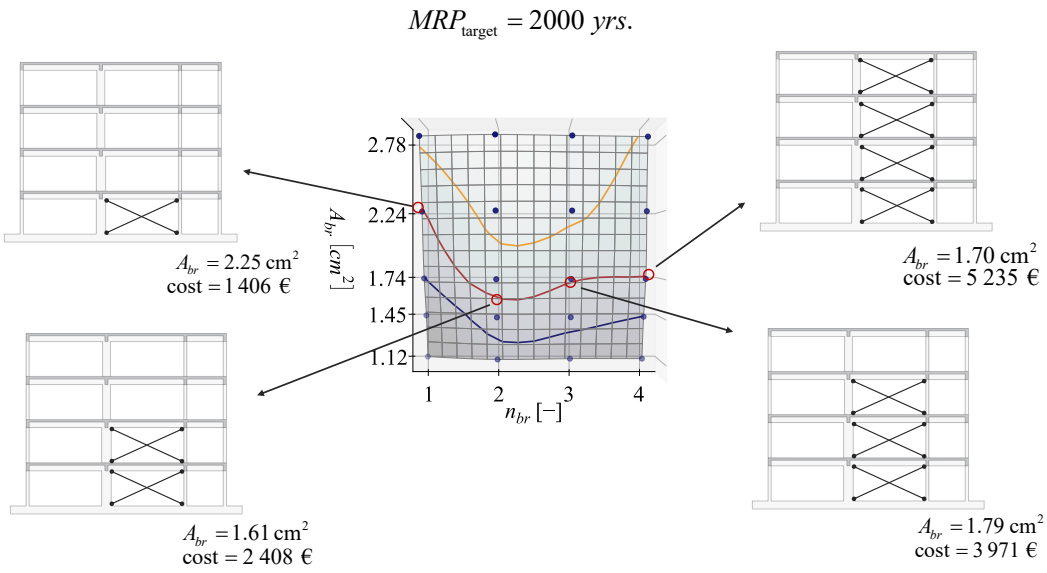

Figure 6.14 – Optimal reinforcement configuration for the target MRP level of 2000 years

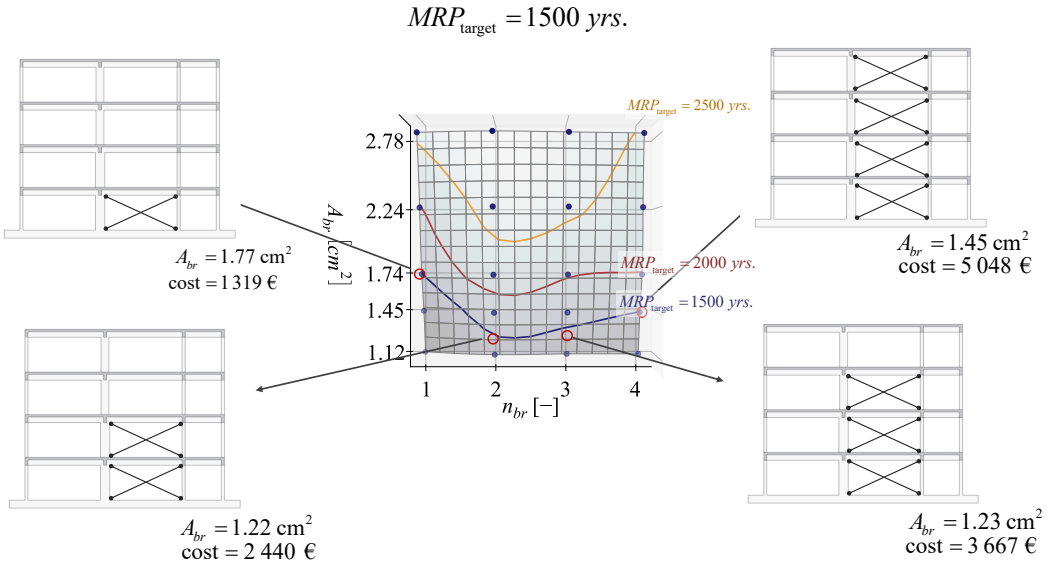

Figure 6.15 – Optimal reinforcement configuration for the target MRP level of 1500 years

Among these configurations, the designer must select the appropriate one based on the allocated project budget. This approach ensures that the designer makes a well-informed decision, grounded in scientific methodology, and allows for precise control over the desired level of risk. By providing a clear, quantified basis for decision-making, the framework supports the development of retrofitting strategies that are both cost-effective and effective in enhancing structural resilience.

Table 6.2 – Summary of optimal retrofitting configurations for the case study structure

MRP_{target} [years]	Numb. of braces n_{br}	Cross-section area of braces A_{br} [cm²]	Cost [€]
2500	1	2.70	1 487
	2	1.94	2 701
	3	2.91	4 132
	4	2.09	6 103
2000	1	2.25	1 406
	2	1.61	2 408
	3	1.79	3 971
	4	1.70	5 235
1500	1	1.77	1 319
	2	1.22	2 440
	3	1.23	3 667
	4	1.45	5 048

As shown in Figure 6.16 , which represents the relationship between the number of braces (n_{br}) and the associated costs for different target MRP levels, the cost increases linearly with the number of floors retrofitted. Higher target MRPs require more robust retrofitting, reflected in the increased costs. The orange curve, representing the highest target MRP of 2500 years, shows the steepest increase, indicating that achieving higher seismic resilience entails significantly higher costs. The curves for 2000 years and 1500 years show a more moderate cost increase, highlighting the trade-off between cost and seismic performance.

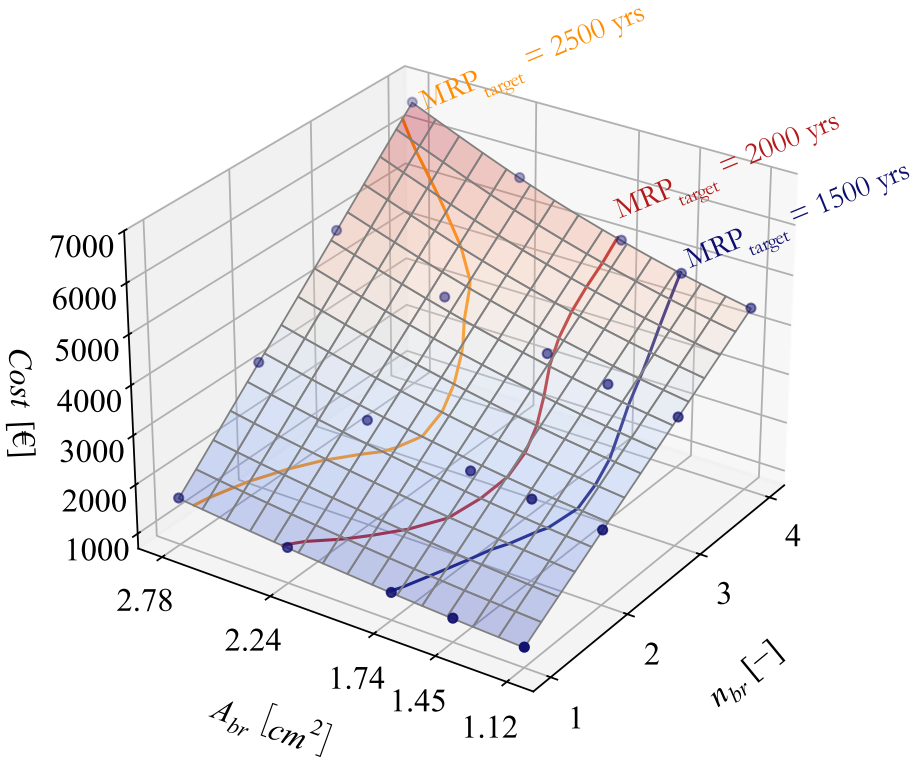

Figure 6.16 – Relationship between the design parameters and associated costs for different target MRPs

Additionally, the difference in costs for different target MRPs, once the number of floors to be retrofitted is chosen, is not substantial. This suggests that, after deciding the extent of the retrofit, opting for a higher target MRP does not dramatically increase the overall cost, providing an economically feasible pathway to enhanced seismic resilience.

By fixing these target MRP levels, proposed framework users can perform a comprehensive risk-informed design, ensuring that the retrofitting strategies meet the desired safety and performance criteria.

Figure 6.16 illustrates the relationship between the number of braces ($x\, n_{br}$) and the associated costs for different target Mean Return Periods (MRPs). The graph clearly demonstrates that as the number of floors retrofitted with braces increases, the total cost also rises. This linear cost increase is observed across all target MRP levels, reflecting the direct correlation between the extent of retrofitting and the financial investment required.

The steepest cost increase is observed for the highest target MRP of 2500 years (orange curve), indicating that achieving higher seismic resilience entails significantly higher costs. In contrast, the cost increases for the 2000 years (blue curve) and 1500 years (green curve) target MRPs are more moderate, highlighting the trade-off between cost and seismic performance.

Notably, the difference in costs for different target MRPs, once the number of floors to be retrofitted is chosen, is not substantial. This suggests that after deciding the extent of the retrofit, opting for a higher target MRP does not dramatically increase the overall cost. This finding implies an economically feasible pathway to enhanced seismic resilience, where slight increases in budget can yield significant improvements in structural performance.

Figure 6.16 underscores the importance of considering both economic and performance factors in the design of seismic retrofitting strategies. By visualizing the cost implications of different retrofitting extents and target MRPs, engineers and decision-makers can make informed choices that balance safety and financial constraints, ultimately contributing to more resilient and sustainable infrastructure.

This approach allows for a more tailored and effective design process, accounting for different acceptable levels of risk and providing a clear pathway for optimizing structural safety and resilience.

6.5.1 Future extension and scalability of the framework

The proposed framework in this chapter has demonstrated its effectiveness in designing retrofitting strategies for existing concrete structures. However, there are several promising avenues for further enhancement and scalability of this methodology. Specifically, the authors suggest three distinct directions for future research and development:

- Optimization Methods Development: Developing advanced optimization methods to identify the optimal solution for retrofitting can significantly reduce the need for exhaustive analysis across the entire search space, thereby lessening the computational burden. By implementing these methods, it will be possible to analyze more complex structures and expand the range of optimization parameters, overcoming the limitations of the reduced search space used in the case study presented.
  Key challenges in this direction include identifying optimization algorithms that can efficiently navigate a non-homogeneous, potentially discrete, and multi-dimensional search space. The goal is to ensure that these algorithms are capable of performing an efficient and effective search, balancing precision and computational resources.

- Enhanced Model Uncertainties and Parameters: To improve the robustness of the framework, it is crucial to incorporate a broader

range of uncertainties in the model. Currently, the framework accounts for record-to-record variability and capacity model uncertainties.

Future work should include additional sources of uncertainties such as the mechanical properties of materials, which can exhibit significant variability in existing structures, and model form uncertainties. By addressing these additional uncertainties, the framework will provide more reliable and comprehensive results. Moreover, extending the framework to include the estimation of losses can facilitate a thorough comparison between the initial costs associated with materials and retrofitting implementation and the long-term reduction in costs over the structure's service life. This holistic approach will enable better cost-benefit analyses and more informed decision-making.

- Simplified Practical Design Approaches: Making the framework more accessible and less computationally intensive is another critical direction for future development. This can be achieved by integrating surrogate models to handle the most computationally demanding aspects of the framework, such as demand estimation. In time-history analyses, implementing reduced-order models that utilize nonlinear hinges, or employing surrogate models such as artificial neural networks and various stochastic emulators, can significantly streamline the process. These surrogate models can approximate complex simulations with high accuracy, thus reducing the computational effort required while maintaining the reliability of the results. This approach will make the framework more practical for widespread use in engineering practice, particularly in scenarios where computational resources are limited.

By pursuing these research directions, the proposed framework can be further refined and scaled to address a broader range of structural retrofitting challenges. The integration of optimization methods, enhanced uncertainty modeling, and practical design approaches will collectively contribute to the development of a more versatile, efficient, and robust framework for the performance-based design of retrofitting strategies for existing concrete structures. This ongoing research will not only advance the current state of the art but also provide valuable tools for engineers and practitioners involved in the preservation and enhancement of structural safety and resilience.

6.6 Conclusions

In this chapter, a comprehensive performance-based earthquake engineering (PBEE) framework for the seismic retrofitting of existing non-ductile reinforced concrete structures was developed and applied. This methodology effectively balances seismic performance, measured by the Mean Return Period (MRP) of limit state exceedances, against retrofitting costs, identifying optimal retrofit strategies that meet or exceed target MRPs at minimal costs.

The analysis of the case study structure resulted in the generation of an MRP surface, facilitating a risk-informed design procedure. This surface enables the establishment of various target MRP levels (2500 years, 2000 years, and 1500 years), providing clear guidelines for retrofitting decisions based on different risk thresholds. This approach ensures that retrofitting strategies can be tailored to meet specific safety and performance objectives, making it a valuable tool for engineering practice.

The proposed method has demonstrated its validity through the implementation in a straightforward case study. The successful application in this case study highlights the practicality and effectiveness of the framework in real-world scenarios. Utilizing such procedures can significantly aid the design phase of retrofitting interventions, offering a scientifically rigorous and formal tool for determining the necessary reinforcement configuration for a risk-based design. This approach not only improves the accuracy of retrofitting designs but also enhances their efficiency by optimizing the allocation of resources.

The proposed methodology ensures informed decision-making based on specific risk targets and budget constraints. By integrating a systematic evaluation of seismic performance and associated costs, the framework provides a comprehensive basis for developing retrofitting strategies that are both cost-effective and resilient. This balance between cost and performance is crucial for the sustainable management of infrastructure, particularly in regions prone to seismic activity. Additionally, the ability to adapt the framework to different risk levels allows for greater flexibility and customization in retrofitting projects.

Furthermore, the framework's ability to generate detailed MRP surfaces for different configurations enables engineers to visualize and compare the potential impacts of various retrofitting strategies. This visualization aids in identifying the most effective approaches and supports transparent communication with stakeholders about the benefits and trade-offs of different options. By providing a clear, quantifiable basis for decision-making, the methodology enhances the reliability and effectiveness of retrofitting interventions, ultimately contributing to the improved safety and resilience of existing structures.

Future work should focus on refining the optimization methods to further enhance the efficiency and accuracy of the framework. Expanding the framework to incorporate a broader range of uncertainties and practical design considerations will increase its applicability and robustness. For instance, integrating more comprehensive models of material behavior, structural interactions, and environmental impacts will provide a more holistic assessment of retrofitting strategies. Additionally, the development of user-friendly software tools based on the framework can facilitate its adoption in engineering practice.

Continued development of this methodology is expected to provide valuable tools for engineers and practitioners involved in the preservation and enhancement of structural safety and resilience. By addressing the evolving challenges in seismic retrofitting, the framework will support the ongoing efforts to protect infrastructure and communities from the devastating effects of earthquakes. Ultimately, the adoption of such advanced methodologies will lead to safer, more resilient built environments and contribute to the sustainable development of earthquake-prone regions.

6.6.1 Acknowledgments

The author acknowledges the Texas Advanced Computing Center (TACC) at The University of Texas at Austin for providing HPC resources that have contributed to the research results reported within this chapter http://www.tacc.utexas.edu.

Conclusions

This thesis aimed to address the critical need for formal, standardized methods for the seismic retrofitting of existing structures. The research activities focused on developing a suite of four distinct design frameworks aimed at assisting engineers in designing seismic retrofitting for reinforced concrete frame structures and masonry buildings. These frameworks are designed to provide efficient and cost-effective retrofitting solutions.

The first three methods are based on the genetic algorithm (GA) approach. The initial framework targets the minimization of implementation costs for retrofitting existing RC frame structures. In particular, it has been focused on tackling the optimization problem in the case of analyses for structure with both ductility and brittle failure deficiencies. The second method broadens the scope of this first framework by incorporating expected annual losses, thus addressing both initial implementation costs and long-term financial effects. The third method, specifically designed for masonry structures, employs a topological optimization algorithm to determine the most effective reinforcement configurations especially in case of employing retrofitting techniques that modify masses and stiffness of structural elements.

The fourth method utilizes a performance-based earthquake engineering (PBEE) design procedure for the design of seismic retrofitting of non-ductile RC frame structures.

The major innovations presented in this thesis include the formalization of retrofitting optimization problems and the development of new genetic operators to address both ductility and brittle deficiencies. Additionally, a novel penalty-free technique was proposed for handling multiple boundaries that cannot be directly compared. The use of linear static elastic analyses was validated for assessing the safety of tentative reinforcement configurations, streamlining the optimization process. This work also pioneers the optimization of interventions on masonry structures and proposes a scientific-based method for uncertainty analysis during the design of reinforcement interventions for concrete structures.

An extensive application of tools like those proposed in this thesis can significantly facilitate the design phase of such interventions, optimizing resource utilization, enhancing the safety of the building heritage. The comprehensive and systematic approaches developed here ensure cost-effective and reliable retrofitting solutions while maintaining compliance with safety standards and extending the service life of structures.

The research activities presented in this thesis align with the United Nations' 2030 Agenda for Sustainable Development, particularly targeting Sustainable Development Goal (SDG) 11, which aims to make cities and human settlements inclusive, safe, resilient, and sustainable. By providing tools to determine the optimal design of retrofitting systems, these methodologies enhance the effectiveness of such interventions. This leads to widespread improvements in structural safety and more efficient management of allocated funds, ensuring that resources are used effectively to maximize safety and resilience benefits.

The methodologies proposed in this thesis are designed to not only improve structural performance during seismic events but also promote sustainable practices in the construction and retrofitting industry. By optimizing retrofitting solutions, the frameworks developed aim to minimize material use and waste, reduce the carbon footprint of construction activities, and enhance the overall sustainability of the built environment. These approaches encourage the adoption of innovative and efficient construction techniques that align with the principles of sustainable development.

The work presented in this thesis contributes to a relatively new and under-explored area within the scientific literature that has seen a significant surge of interest in recent years. The proposed frameworks have demonstrated considerable validity and robustness, offering substantial improvements in the seismic retrofitting of existing structures. However, there remain several open avenues for further development that can be addressed in the coming years to enhance and expand upon these initial findings. In particular, the following research directions are suggested:

- Environmental Impact Consideration: Developing optimization frameworks that include quantification of environmental impacts of materials used minimizing the carbon footprint of seismic retrofitting.
- Use of metamodels or reduced models: Implementing metamodels to expedite the structural assessment phase, which is the most computationally intensive part of the optimization algorithms. Metamodels can approximate complex models with adequate

accuracy, significantly reducing computational time and resources, thereby rendering the application of these algorithms more accessible and efficient in real-life applications.

- Optimization Algorithms for PBEE Framework: Enhancing the PBEE framework with optimization algorithms to streamline the analysis process, avoiding the need for extensive full-fledged parametric analyses. This improvement would make the framework more accessible and practical for widespread use, reducing the computation burden required.

- Comparative Analysis of Linear and Nonlinear Assessments: Conducting detailed comparisons between linear (static or dynamic) and nonlinear static assessment results. By quantifying the errors associated with using linear analysis methods, which are significantly faster, this approaches will lead to a considerable speed-up in the execution of structural assessments, making the overall process more efficient.

- Development and Validation of Advanced Optimization Algorithms: Future work should focus on developing and validating more advanced optimization algorithms, such as those based on Bayesian optimization. These algorithms can be compared to the GA to evaluate their efficiency and effectiveness, ensuring that the most suitable algorithm is tailored for solving these complex problems.

- Economic and Environmental Loss Analysis: Extending reliability analysis to include a comprehensive comparison between rigorously estimated economic losses and retrofitting implementation costs. Additionally, developing methods to estimate environmental impacts with an approach similar to economic loss analysis would provide a more complete picture of the benefits and trade-offs of retrofitting interventions.

By addressing these future research directions, the field of seismic retrofitting can continue to evolve, providing engineers with advanced tools and methodologies to safeguard structures, ensure safety, and promote sustainability in the face of seismic retrofitting of existing structures. The continued innovation in this domain is essential for mitigating the risks associated with aging structures and enhancing the resilience of the building heritage

References

[1] A. Hermelink, N. Deshmukh, S. Kerasioti, T. Venetis, and V. Sarlis, "Building Stock Observatory (BSO)," Mar. 2024.

[2] V. Palermo, G. Tsionis, and M. Sousa, "Building stock inventory to assess seismic vulnerability across Europe," 2018. doi: 10.2760/530683.

[3] H. Crowley *et al.*, "ETH Library European Seismic Risk Model (ESRM20)," 2021, doi: 10.3929/ethz-b-000590388.

[4] V. Silva *et al.*, "Global Earthquake Model (GEM) Exposure Map (version 2018.1)," 2018.

[5] Research center of the Italian National Chamber of Engineers, "I costi dei terremoti in Italia," 2014.

[6] Istat - Italian National Institute of Statistics, "Il sistema dei conti della sanità per l'Italia," 2017.

[7] FIEC - European Construction Industry Federation, "Statistical Report N°63 (Edition 2020)," 2020.

[8] European Committee for Standardization, *Eurocode 8: Design of structures for earthquake resistance—Part 3: Assessment and retrofitting of buildings*. 2010.

[9] C. D. Poland, J. Hill, R. L. Sharpe, and J. Soulages, "Vision 2000: Performance Based Seismic Engineering of Buildings," 1995.

[10] Federal Emergency Management Agency, "FEMA 273 - FEMA 274 - NEHRP Guidelines for the seismic rehabilitation of buildings."

[11] Federal Emergency Management Agency, "FEMA 274 - NEHRP Commentary on the guidelines for the seismic rehabilitation of buildings," 1997.

[12] Federal Emergency Management Agency, "FEMA 356 - Prestandard and commentary for the seismic rehabilitation of buildings," Nov. 2000.

[13] Structural Engineering Institute, Structural Engineering Institute. Seismic Retrofit of Existing Buildings Standards Committee, American Society of Civil Engineers, and Structural Engineering Institute., *Seismic evaluation and retrofit of existing buildings : ASCE/SEI, 41-17*.

[14] A. K. Chopra, "Dynamics of structures," 2002, *Pearson Prentice Hall*.

[15] P. Fajfar, T. Vidic, and M. Fischinger, "Consistent inelastic design spectra: Hysteretic and input energy," *Earthq Eng Struct Dyn*, vol. 23, no. 5, pp. 523–537, 1994, doi: 10.1002/eqe.4290230505.

[16] S. Sugano, "State-of-the-art in techniques for rehabilitation of buildings," 1996.

[17] Georgios. Tsionis, Roberta. Apostolska, Fabio. Tauver, and European Commission. Joint Research Centre. Institute for the Protection and the Security of the Citizen., "Seismic strengthening of RC buildings. Report EUR 26945 EN," Publications Office, 2014.

[18] P. D. Gkournelos, T. C. Triantafillou, and D. A. Bournas, "Seismic upgrading of existing reinforced concrete buildings: A state-of-the-art review," Aug. 01, 2021, *Elsevier Ltd.* doi: 10.1016/j.engstruct.2021.112273.

[19] M. R. Maheri, R. Kousari, and M. Razazan, "Pushover tests on steel X-braced and knee-braced RC frames," *Eng Struct*, vol. 25, no. 13, pp. 1697–1705, 2003, doi: 10.1016/S0141-0296(03)00150-0.

[20] G. E. Thermou and A. S. Elnashai, "Seismic retrofit schemes for RC structures and local-global consequences," 2006, *John Wiley and Sons Ltd.* doi: 10.1002/pse.208.

[21] I. Vanzi, "When should seismic retrofitting of existing structures be implemented in order to minimize expected losses," *Journal of Earthquake Engineering*, vol. 13, no. 1, pp. 53–73, 2001.

[22] C. Nuti and I. Vanzi, "To retrofit or not to retrofit?," *Eng Struct*, vol. 25, no. 6, pp. 701–711, 2003.

[23] G. M. Calvi, "Choices and criteria for seismic strengthening," *Journal of Earthquake Engineering*, vol. 17, no. 6, pp. 769–802, 2013, doi: 10.1080/13632469.2013.781556.

[24] A. Formisano, C. Castaldo, and G. Chiumiento, "Optimal seismic upgrading of a reinforced concrete school building with metal-based devices using an efficient multi-criteria decision-making method," *Structure and Infrastructure Engineering*, vol. 13, no. 11, pp. 1373–1389, Nov. 2017, doi: 10.1080/15732479.2016.1268174.

[25] E. Cosenza *et al.*, *The Italian guidelines for seismic risk classification of constructions: technical principles and validation*, vol. 16, no. 12. Springer Netherlands, 2018. doi: 10.1007/s10518-018-0431-8.

[26] H. Nazmfar, A. Saredeh, A. Eshgi, and B. Feizizadeh, "Vulnerability evaluation of urban buildings to various earthquake intensities: a case study of the municipal zone 9 of Tehran," *Human and Ecological Risk Assessment*, vol. 25, no. 1–2, pp. 455–474, Feb. 2019, doi: 10.1080/10807039.2018.1556086.

[27] N. Caterino, I. Iervolino, G. Manfredi, and E. Cosenza, "Multi-criteria decision making for seismic retrofitting of RC structures," *Journal of Earthquake Engineering*, vol. 12, no. 4, pp. 555–583, May 2008, doi: 10.1080/13632460701572872.

[28] T. L. Santy, "The analytical hierarchy process: Planning, priority setting, resource allocation," *Decision Making Series, McGraw Hill, New York, USA*, 1980.

[29] C.-L. Hwang, K. Yoon, C.-L. Hwang, and K. Yoon, "Methods for multiple attribute decision making," *Multiple attribute decision making: methods and applications a state-of-the-art survey*, pp. 58–191, 1981.

[30] R. R. Yager, "On ordered weighted averaging aggregation operators in multicriteria decisionmaking," *IEEE Trans Syst Man Cybern*, vol. 18, no. 1, pp. 183–190, 1988.

[31] A. Bradshaw, P. Rajeev, and S. Tesfamariam, "Multi criteria decision making tool for the selection of seismic retrofitting techniques," *Significance*, vol. 50, p. 3, 2011.

[32] M. Zerbin and A. Aprile, "Sustainable retrofit design of RC frames evaluated for different seismic demand," *Earthq. Struct*, vol. 9, no. 6, pp. 1337–1353, 2015.

[33] M. Zerbin and A. Aprile, "Sustainable retrofit design of RC frames evaluated for different seismic demand," *Earthquake and Structures*, vol. 9, no. 6, pp. 1337–1353, 2015, doi: 10.12989/eas.2015.9.6.1337.

[34] A. Anelli, M. Vona, S. Santa-Cruz, M. Laterza, and N. Tarque, "MCDM methods for the identification of intervention strategies for seismic retrofitting of school buildings," in *Proceedings of the World Engineering Conference on Disaster Risk Reduction–WECDRR 2016*, 2016.

[35] S. Opricovic, "Multicriteria optimization of civil engineering systems," *Faculty of civil engineering, Belgrade*, vol. 2, no. 1, pp. 5–21, 1998.

[36] S. Santa-Cruz, X. Brioso, and C. Córdova-Arias, "Selection of seismic retrofitting techniques through a multi-criteria methodology and BIM tools to improve transparency," in *Proceedings of the 11th National Conference in Earthquake Engineering*, 2018.

[37] N. Caterino and E. Cosenza, "A multi-criteria approach for selecting the seismic retrofit intervention for an existing structure accounting for expected losses and tax incentives in Italy," *Eng Struct*, vol. 174, pp. 840–850, Nov. 2018, doi: 10.1016/j.engstruct.2018.07.090.

[38] C. Passoni, A. Marini, A. Belleri, and C. Menna, "A multi-step design framework based on life cycle thinking for the holistic renovation of the existing buildings stock," in *IOP Conference Series: Earth and Environmental Science*, IOP Publishing, 2019, p. 012134.

[39] G. Gabbianelli, W. Carofilis, and R. Monteiro, "Evaluation of different retrofit strategies for RC school buildings using integrated multi-criteria procedures," in *Proceedings of the 17th World conference on Earthquake Engineering*, 2020, pp. 1–12.

[40] S. Labò, C. Passoni, A. Marini, A. Belleri, J. Zanni, and P. Riva, "A framework for the sustainable renovation of existing structures:

application to a reference building," in *Proceedings of the 17th World Conference on Earthquake Engineering (17WCEE)*, 17th World Conference on Earthquake Engineering, 2021, pp. 1–12.

[41] R. Gentile and C. Galasso, "Simplified seismic loss assessment for optimal structural retrofit of RC buildings," *Earthquake Spectra*, vol. 37, no. 1, pp. 346–365, Feb. 2021, doi: 10.1177/8755293020952441.

[*42*] M. J. N. Priestley and G. M. Calvi, "Towards a capacity-design assessment procedure for reinforced concrete frames," *Earthquake Spectra*, vol. 7, no. 3, pp. 413–437, 1991.

[43] W. W. C. Gallo, G. Gabbianelli, and R. Monteiro, "Assessment of Multi-Criteria Evaluation Procedures for Identification of Optimal Seismic Retrofitting Strategies for Existing RC Buildings," 2022, *Taylor and Francis Ltd.* doi: 10.1080/13632469.2021.1878074.

[44] M. S. Es-haghi, M. S. Barkhordari, Z. Huang, and J. Ye, "Multicriteria Decision-Making Methods in Selecting Seismic Upgrading Strategy of High-Rise RC Wall Buildings," *Journal of Structural Engineering*, vol. 148, no. 4, Apr. 2022, doi: 10.1061/(asce)st.1943-541x.0003304.

[45] N. Clemett, W. W. Carofilis Gallo, G. J. O'Reilly, G. Gabbianelli, and R. Monteiro, "Optimal seismic retrofitting of existing buildings considering environmental impact," *Eng Struct*, vol. 250, Jan. 2022, doi: 10.1016/j.engstruct.2021.113391.

[46] R. Couto, G. Mucedero, R. Bento, and R. Monteiro, "Understanding the Impact of Seismic Hazard and Climate Conditions on Multi Criteria–Based Retrofitting of Existing Buildings," *Sustainability*, vol. 16, no. 10, p. 4318, 2024.

[47] F. Nigro, G. Della Corte, and E. Martinelli, "Assessment of alternative design approaches for seismic upgrading of RC frame structures with steel exoskeletons," *Eng Struct*, vol. 305, Apr. 2024, doi: 10.1016/j.engstruct.2024.117623.

[48] A. Formisano and F. M. Mazzolani, "On the selection by MCDM methods of the optimal system for seismic retrofitting and vertical addition of existing buildings," *Comput Struct*, vol. 159, pp. 1–13, Jul. 2015, doi: 10.1016/j.compstruc.2015.06.016.

[49] S. S. Zuluaga, S. Kallioras, and A. Tsiavos, "Optimization of Synergetic Seismic and Energy Retrofitting Based on Timber Beams and Bio-Based Infill Panels: Application to an Existing Masonry Building in Switzerland," *Buildings*, vol. 12, no. 8, Aug. 2022, doi: 10.3390/buildings12081126.

[50] W. W. Carofilis Gallo, N. Clemett, G. Gabbianelli, G. O'reilly, and R. Monteiro, "Seismic Resilience Assessment in Optimally Integrated Retrofitting of Existing School Buildings in Italy," *Buildings*, vol. 12, no. 6, Jun. 2022, doi: 10.3390/buildings12060845.

[51] M. Caruso, R. Pinho, F. Bianchi, F. Cavalieri, and M. T. Lemmo, "Multi-criteria decision-making approach for optimal seismic/energy retrofitting of existing buildings," *Earthquake Spectra*, vol. 39, no. 1, pp. 191–217, Feb. 2023, doi: 10.1177/87552930221141917.

[52] E. Ching and J. V. Carstensen, "Truss topology optimization of timber–steel structures for reduced embodied carbon design," *Eng Struct*, vol. 252, no. February 2021, p. 113540, 2022, doi: 10.1016/j.engstruct.2021.113540.

[53] E. Ramm, "Conceptual design by structural optimization.," in *Conference Proceedings of EURO-C 1998*, 1998, pp. 879–896.

[54] J. Kato, *Material optimization of fiber reinforced composites applying a damage formulation*. 2010.

[55] S. Nikbakt, S. Kamarian, and M. Shakeri, "A review on optimization of composite structures Part I: Laminated composites," *Compos Struct*, vol. 195, pp. 158–185, 2018.

[56] Z. Gürdal, R. T. Haftka, and P. Hajela, *Design and optimization of laminated composite materials*. John Wiley & Sons, 1999.

[57] O. Sigmund, "Systematic design of metamaterials by topology optimization," in *IUTAM Symposium on Modelling Nanomaterials and Nanosystems: Proceedings of the IUTAM Symposium held in Aalborg, Denmark, 19–22 May 2008*, Springer, 2009, pp. 151–159.

[58] H. T. Kollmann, D. W. Abueidda, S. Koric, E. Guleryuz, and N. A. Sobh, "Deep learning for topology optimization of 2D metamaterials," *Mater Des*, vol. 196, p. 109098, 2020.

[59] Y. Wang, Z. Wang, Z. Xia, and L. H. Poh, "Structural design optimization using isogeometric analysis: A comprehensive review," 2018, *Tech Science Press*. doi: 10.31614/cmes.2018.04603.

[60] H. A. Eschenauer and N. Olhoff, "Topology optimization of continuum structures: a review," *Appl. Mech. Rev.*, vol. 54, no. 4, pp. 331–390, 2001.

[61] M. P. Bendsoe and O. Sigmund, *Topology optimization: theory, methods, and applications*. Springer Science & Business Media, 2013.

[62] F. Y. Cheng and K. Z. Truman, *Structural optimization: Dynamic and seismic applications*. CRC Press, 2017.

[63] A. Kaveh, *Applications of metaheuristic optimization algorithms in civil engineering*. Springer, 2017.

[64] S. S. Rao, *Engineering optimization: theory and practice*. John Wiley & Sons, 2019.

[65] P. W. Christensen and A. Klarbring, *An introduction to structural optimization*, vol. 153. Springer Science & Business Media, 2008.

[66] W. Prager, *Introduction to structural optimization*, no. 212. Springer, 1974.

[67] I. Giagkiozis and P. J. Fleming, "Methods for multi-objective optimization: An analysis," *Inf Sci (N Y)*, vol. 293, pp. 338–350, 2015.

[68] R. Falcone, C. Lima, and E. Martinelli, "Soft computing techniques in structural and earthquake engineering: a literature review," *Eng Struct*, vol. 207, no. January, p. 110269, 2020, doi: 10.1016/j.engstruct.2020.110269.
[69] A. Das, H. S. Das, and H. S. Das, "Impact of cuckoo algorithm in speech processing," *Applications of Cuckoo search algorithm and its variants*, pp. 207–228, 2021.
[70] J. L. Ribeiro Filho, P. C. Treleaven, and C. Alippi, "Genetic-algorithm programming environments," *Computer (Long Beach Calif)*, vol. 27, no. 6, pp. 28–43, 1994.
[71] J. O. Royset and R. J.-B. Wets, *An optimization primer*. Springer, 2022.
[72] G. B. Dantzig, "Linear programming," *Oper Res*, vol. 50, no. 1, pp. 42–47, 2002.
[73] M. Frank and P. Wolfe, "An algorithm for quadratic programming," *Naval research logistics quarterly*, vol. 3, no. 1–2, pp. 95–110, 1956.
[74] P. T. Boggs and J. W. Tolle, "Sequential quadratic programming," *Acta numerica*, vol. 4, pp. 1–51, 1995.
[75] N. A. Barricelli, "Esempi numerici di processi di evoluzione," *Methodos*, vol. 6, no. 21–22, pp. 45–68, 1954.
[76] I. Rechenberg, "Cybernetic solution path of an experimental problem," *Roy. Aircr. Establ., Libr. transl.*, vol. 1122, 1965.
[77] J. H. Holland, *Adaptation in natural and artificial systems: an introductory analysis with applications to biology, control, and artificial intelligence*. MIT press, 1992.
[78] P. J. M. Van Laarhoven, E. H. L. Aarts, P. J. M. van Laarhoven, and E. H. L. Aarts, *Simulated annealing*. Springer, 1987.
[79] D. E. Goldberg, "Evolutionary algorithm in search, optimization and machine learning," *Reading, Addison Wesley*, vol. 8, 1989.
[80] J. Kennedy and R. Eberhart, "Particle swarm optimization," in *Proceedings of ICNN'95-international conference on neural networks*, ieee, 1995, pp. 1942–1948.
[81] L. M. Gambardella and M. Dorigo, "Solving symmetric and asymmetric TSPs by ant colonies," in *Proceedings of IEEE international conference on evolutionary computation*, IEEE, 1996, pp. 622–627.
[82] R. Storn and K. Price, "Differential Evolution-A simple and efficient adaptive scheme for global optimization over continuous spaces," 1995.
[83] K. Deb, A. Pratap, S. Agarwal, and T. Meyarivan, "A Fast and Elitist Multiobjective Genetic Algorithm: NSGA-II," 2002.
[84] R. Falcone, A. Ciaramella, and F. Carrabs, "Artificial Neural Network for Technical Feasibility Prediction of Seismic Retrofitting Intervention," *Structures*, vol. 41, no. April, pp. 1220–1234, 2022, doi: 10.1016/j.istruc.2022.05.008.

[85] S.-R. Yi and A. Taflanidis, "Stochastic Emulation with Enhanced Partial Replication Strategy for Seismic Response Estimation," in *14th International Conference on Applications of Statistics and Probability*, 2023.

[86] G. Quaranta, W. Lacarbonara, and S. F. Masri, *A review on computational intelligence for identification of nonlinear dynamical systems*, vol. 99, no. 2. Springer Netherlands, 2020. doi: 10.1007/s11071-019-05430-7.

[87] N. D. Lagaros, V. Plevris, and N. Ath, *The Mosaic of Metaheuristic Algorithms in Structural Optimization*, no. 0123456789. Springer Netherlands, 2022. doi: 10.1007/s11831-022-09773-0.

[88] N. D. Lagaros, M. Papadrakakis, and G. Kokossalakis, "Structural optimization using evolutionary algorithms," *Comput Struct*, vol. 80, no. 7–8, pp. 571–589, 2002.

[89] V. Govindaraj and J. V Ramasamy, "Optimum detailed design of reinforced concrete continuous beams using genetic algorithms," *Comput Struct*, vol. 84, no. 1–2, pp. 34–48, 2005.

[90] V. Govindaraj and J. V Ramasamy, "Optimum detailed design of reinforced concrete frames using genetic algorithms," *Engineering Optimization*, vol. 39, no. 4, pp. 471–494, 2007.

[91] C. C. Mitropoulou, N. D. Lagaros, and M. Papadrakakis, "Life-cycle cost assessment of optimally designed reinforced concrete buildings under seismic actions," *Reliab Eng Syst Saf*, vol. 96, no. 10, pp. 1311–1331, 2011.

[92] G. S. Papavasileiou and D. C. Charmpis, "Seismic design optimization of multi–storey steel–concrete composite buildings," *Comput Struct*, vol. 170, pp. 49–61, 2016.

[93] M. Babaei and M. Mollayi, "Multi-objective optimization of reinforced concrete frames using NSGA-II algorithm," *Engineering Structures and Technologies*, vol. 8, no. 4, pp. 157–164, 2016.

[94] T. D. Pham and W.-K. Hong, "Genetic algorithm using probabilistic-based natural selections and dynamic mutation ranges in optimizing precast beams," *Comput Struct*, vol. 258, p. 106681, 2022.

[95] A. Kanyilmaz, P. R. N. Tichell, and D. Loiacono, "A genetic algorithm tool for conceptual structural design with cost and embodied carbon optimization," *Eng Appl Artif Intell*, vol. 112, no. March, p. 104711, 2022, doi: 10.1016/j.engappai.2022.104711.

[96] Q. Wang, H. Fang, and X. K. Zou, "Application of Micro-GA for optimal cost base isolation design of bridges subject to transient earthquake loads," *Structural and Multidisciplinary Optimization*, vol. 41, no. 5, pp. 765–777, May 2010, doi: 10.1007/s00158-009-0470-5.

[97] X. K. Zou, J. G. Teng, L. De Lorenzis, and S. H. Xia, "Optimal performance-based design of FRP jackets for seismic retrofit of reinforced concrete frames," *Compos B Eng*, vol. 38, no. 5–6, pp. 584–597, Jul. 2007, doi: 10.1016/j.compositesb.2006.07.016.

[98] O. Lavan and G. F. Dargush, "Multi-objective evolutionary seismic design with passive energy dissipation systems," *Journal of Earthquake Engineering*, vol. 13, no. 6, pp. 758–790, Jul. 2009, doi: 10.1080/13632460802598545.

[99] G. F. Dargush and R. S. Sant, "Evolutionary aseismic design and retrofit of structures with passive energy dissipation," *Earthq Eng Struct Dyn*, vol. 34, no. 13, pp. 1601–1626, Nov. 2005, doi: 10.1002/eqe.497.

[100] N. Pollini, O. Lavan, and O. Amir, "Minimum-cost optimization of nonlinear fluid viscous dampers and their supporting members for seismic retrofitting," *Earthq Eng Struct Dyn*, vol. 46, no. 12, pp. 1941–1961, Oct. 2017, doi: 10.1002/eqe.2888.

[101] H. Seo, J. Kim, and M. Kwon, "Optimal seismic retrofitted RC column distribution for an existing school building," *Eng Struct*, vol. 168, pp. 399–404, Aug. 2018, doi: 10.1016/j.engstruct.2018.04.098.

[102] G. Mahdavi, K. Nasrollahzadeh, and M. A. Hariri-Ardebili, "Optimal FRP jacket placement in RC frame structures towards a resilient seismic design," *Sustainability (Switzerland)*, vol. 11, no. 24, pp. 1–22, 2019, doi: 10.3390/su11246985.

[103] G. Minafò and G. Camarda, "An open-source GA framework for optimizing the seismic upgrading design of RC frames through BRBs," *Eng Struct*, vol. 251, no. PA, p. 113508, 2022, doi: 10.1016/j.engstruct.2021.113508.

[104] R. Laguardia and P. Franchin, "Risk-Based Optimization of Bracing Systems for Seismic Retrofitting of RC Buildings," 2022, doi: 10.1061/(ASCE)ST.1943.

[105] R. Falcone, F. Carrabs, R. Cerulli, C. Lima, and E. Martinelli, "Seismic retrofitting of existing RC buildings: a rational selection procedure based on Genetic Algorithms," *Structures*, vol. 22, pp. 310–326, Dec. 2019, doi: 10.1016/j.istruc.2019.08.006.

[106] C. Chisari and C. Bedon, "Multi-objective optimization of FRP jackets for improving the seismic response of reinforced concrete frames," *American Journal of Engineering and Applied Sciences*, vol. 9, no. 3, pp. 669–679, Sep. 2016, doi: 10.3844/ajeassp.2016.669.679.

[107] F. Braga, R. Gigliotti, and R. Laguardia, "Intervention cost optimization of bracing systems with multiperformance criteria," *Eng Struct*, vol. 182, pp. 185–197, Mar. 2019, doi: 10.1016/j.engstruct.2018.12.034.

[108] S. Dempe and A. B. Zemkoho, "On the Karush–Kuhn–Tucker reformulation of the bilevel optimization problem," *Nonlinear Anal Theory Methods Appl*, vol. 75, no. 3, pp. 1202–1218, 2012.

[109] J. Shin and S. Park, "Optimum retrofit strategy of FRP column jacketing system for non-ductile RC building frames using artificial neural network

and genetic algorithm hybrid approach," *Journal of Building Engineering*, vol. 57, Oct. 2022, doi: 10.1016/j.jobe.2022.104919.

[110] M. M. Gharagoz, M. Noureldin, and J. Kim, "Machine learning-based design of a seismic retrofit frame with spring-rotational friction dampers," *Eng Struct*, vol. 292, Oct. 2023, doi: 10.1016/j.engstruct.2023.116053.

[111] G. S. Papavasileiou and D. C. Charmpis, "Seismic design optimization of multi-storey steel-concrete composite buildings," *Comput Struct*, vol. 170, pp. 49–61, 2016, doi: 10.1016/j.compstruc.2016.03.010.

[112] G. S. Papavasileiou, D. C. Charmpis, and N. D. Lagaros, "Optimized seismic retrofit of steel-concrete composite buildings," *Eng Struct*, vol. 213, Jun. 2020, doi: 10.1016/j.engstruct.2020.110573.

[113] L. P. Chaves and J. Cunha, "Design of carbon fiber reinforcement of concrete slabs using topology optimization," *Constr Build Mater*, vol. 73, pp. 688–698, Oct. 2014, doi: 10.1016/j.conbuildmat.2014.10.011.

[114] M. Bruggi, G. Milani, and A. Taliercio, "Design of the optimal fiber-reinforcement for masonry structures via topology optimization," *Int J Solids Struct*, vol. 50, no. 13, pp. 2087–2106, Jun. 2013, doi: 10.1016/j.ijsolstr.2013.03.007.

[115] M. Bruggi, G. Milani, and A. Taliercio, "Simple topology optimization strategy for the FRP reinforcement of masonry walls in two-way bending," *Comput Struct*, vol. 138, pp. 86–101, 2014.

[116] M. Bruggi, G. Milani, and A. Taliercio, "Optimal FRP reinforcement of masonry walls under in- and out-of-plane loads," in *Key Engineering Materials*, Trans Tech Publications Ltd, 2015, pp. 429–436. doi: 10.4028/www.scientific.net/KEM.624.429.

[117] M. Beheshti and P. Asadi, "Optimal seismic retrofit of fractional viscoelastic dampers for minimum life-cycle cost of retrofitted steel frames," *Structural and Multidisciplinary Optimization*, vol. 61, no. 5, pp. 2021–2035, 2020.

[118] C.-K. Chiu and W.-Y. Jean, "Evaluating Procedure of Optimal Seismic Retrofit Level for a Low-Rise Reinforced Concrete Building," *Journal of Advanced Concrete Technology*, vol. 9, no. 3, pp. 287–299, 2011.

[119] Y. Daniel and O. Lavan, "Gradient based optimal seismic retrofitting of 3D irregular buildings using multiple tuned mass dampers," *Comput Struct*, vol. 139, pp. 84–97, Jul. 2014, doi: 10.1016/j.compstruc.2014.03.002.

[120] I. Gidaris and A. A. Taflanidis, "Performance assessment and optimization of fluid viscous dampers through life-cycle cost criteria and comparison to alternative design approaches," *Bulletin of Earthquake Engineering*, vol. 13, no. 4, pp. 1003–1028, Apr. 2015, doi: 10.1007/s10518-014-9646-5.

[121] D. C. Charmpis, M. C. Phocas, and P. Komodromos, "Optimized retrofit of multi-storey buildings using seismic isolation at various elevations: assessment for several earthquake excitations," *Bulletin of Earthquake Engineering*, vol. 13, no. 9, pp. 2745–2768, Sep. 2015, doi: 10.1007/s10518-015-9737-y.

[122] X. Zou, Q. Wang, and J. Wu, "Reliability-based performance design optimization for seismic retrofit of reinforced concrete buildings with fiber-reinforced polymer composites," *Advances in Structural Engineering*, vol. 21, no. 6, pp. 838–851, Apr. 2018, doi: 10.1177/1369433217733760.

[123] A. M. Puthanpurayil, O. Lavan, and R. P. Dhakal, "Multi-objective loss-based optimization of viscous dampers for seismic retrofitting of irregular structures," *Soil Dynamics and Earthquake Engineering*, vol. 129, p. 105765, 2020.

[124] A. Reggio, R. Greco, G. C. Marano, and G. A. Ferro, "Stochastic Multi-objective Optimisation of Exoskeleton Structures," *J Optim Theory Appl*, vol. 187, no. 3, pp. 822–841, 2020, doi: 10.1007/s10957-020-01778-8.

[125] D. De Domenico and I. Hajirasouliha, "Multi-level performance-based design optimisation of steel frames with nonlinear viscous dampers," *Bulletin of Earthquake Engineering*, vol. 19, no. 12, pp. 5015–5049, Sep. 2021, doi: 10.1007/s10518-021-01152-7.

[126] L. Velasco, A. Hospitaler, and H. Guerrero, "Optimal design of the seismic retrofitting of reinforced concrete framed structures using BRBs," *Bulletin of Earthquake Engineering*, vol. 20, no. 10, pp. 5135–5160, Aug. 2022, doi: 10.1007/s10518-022-01394-z.

[127] P. Omidian and N. Khaji, "A multi-objective optimization framework for seismic resilience enhancement of typical existing RC buildings," *Journal of Building Engineering*, vol. 52, Jul. 2022, doi: 10.1016/j.jobe.2022.104361.

[128] A. J. Dereje and J. Kim, "Robust seismic retrofit design framework for asymmetric soft-first story structures considering uncertainties," *Structural Engineering and Mechanics*, vol. 86, no. 2, pp. 249–260, Apr. 2023, doi: 10.12989/sem.2023.86.2.249.

[129] M. Adane, S. Chun, and J. Kim, "Optimum distribution of steel frame assembly for seismic retrofit of framed structures," *Steel and Composite Structures*, vol. 50, no. 3, pp. 337–345, Feb. 2024, doi: 10.12989/scs.2024.50.3.337.

[130] Z. Yi and H. Burton, "Methodology for effective and efficient regional seismic retrofit using machine learning and stochastic optimization," *Structure and Infrastructure Engineering*, vol. 20, no. 2, pp. 286–300, 2024, doi: 10.1080/15732479.2022.2088811.

[131] S. Park and J. W. van de Lindt, "Genetic Optimization for Seismic Retrofit of Soft-Story Woodframe Buildings Using FEMA P-807

Methodology," *Journal of Performance of Constructed Facilities*, vol. 29, no. 6, Dec. 2015, doi: 10.1061/(asce)cf.1943-5509.0000637.

[132] M. Mrozek and D. Mrozek, "Analysis of location of composites reinforcement of masonry structures with use topological optimization," *Applications in Engineering Science*, vol. 3, Sep. 2020, doi: 10.1016/j.apples.2020.100015.

[133] M. Tonekaboni, "Probabilistic based economic assessment of seismic retrofit methods for structures," *ARPN Journal of Engineering and Applied Sciences*, vol. 9, no. 11, 2014.

[134] K. Aljawhari, R. Gentile, and C. Galasso, "A fragility-oriented approach for seismic retrofit design," *Earthquake Spectra*, vol. 38, no. 3, pp. 1813–1843, Aug. 2022, doi: 10.1177/87552930221078324.

[135] R. Gentile, S. Pampanin, and C. Galasso, "A computational framework for selecting the optimal combination of seismic retrofit and insurance coverage," *Computer-Aided Civil and Infrastructure Engineering*, vol. 37, no. 8, pp. 956–975, 2022.

[136] C. Lima, F. Nigro, and E. Martinelli, "Conceptual design formulation and comparative assessment of a seismic retrofit procedure for existing RC structures based on combining member- and structure-level techniques," *Structures*, vol. 55, pp. 1096–1108, Sep. 2023, doi: 10.1016/j.istruc.2023.06.062.

[137] E. Bruschi, V. Quaglini, and P. M. Calvi, "A simplified design procedure for seismic upgrade of frame structures equipped with hysteretic dampers," *Eng Struct*, vol. 251, p. 113504, 2022, doi: 10.1016/j.engstruct.2021.113504.

[138] R. Falcone, A. Ciaramella, F. Carrabs, N. Strisciuglio, and E. Martinelli, "Artificial neural network for technical feasibility prediction of seismic retrofitting in existing RC structures," *Structures*, vol. 41, pp. 1220–1234, Jul. 2022, doi: 10.1016/j.istruc.2022.05.008.

[139] Y. F. Wu, T. Liu, and D. J. Oehlers, "Fundamental principles that govern retrofitting of reinforced concrete columns by steel and FRP jacketing," *Advances in Structural Engineering*, vol. 9, no. 4, pp. 507–532, 2006, doi: 10.1260/136943306778812769.

[140] P. Fajfar, "A Nonlinear Analysis Method for Performance-Based Seismic Design," *Earthquake Spectra*, vol. 16, no. 3, pp. 573–592, 2000, doi: 10.1193/1.1586128.

[141] F. McKenna *et al.*, "OpenSees," *University of California, Berkeley: nd*, 2010.

[142] F. Di Trapani, M. Malavisi, G. C. Marano, A. P. Sberna, and R. Greco, "Optimal seismic retrofitting of reinforced concrete buildings by steel-jacketing using a genetic algorithm-based framework," *Eng Struct*, vol. 219, 2020, doi: 10.1016/j.engstruct.2020.110864.

[143] F. Di Trapani, A. P. Sberna, and G. C. Marano, "A new genetic algorithm-based framework for optimized design of steel-jacketing retrofitting in shear-critical and ductility-critical RC frame structures," *Eng Struct*, vol. 243, no. January, p. 112684, 2021, doi: 10.1016/j.engstruct.2021.112684.

[144] C. A. Coello Coello, "Theoretical and numerical constraint-handling techniques used with evolutionary algorithms: A survey of the state of the art," *Comput Methods Appl Mech Eng*, vol. 191, no. 11–12, pp. 1245–1287, 2002, doi: 10.1016/S0045-7825(01)00323-1.

[145] N. D. Lagaros, M. Kournoutos, N. A. Kallioras, and A. N. Nordas, "Constraint handling techniques for metaheuristics: a state-of-the-art review and new variants," *Optimization and Engineering*, 2023, doi: 10.1007/s11081-022-09782-9.

[146] A. E. Eiben and J. E. Smith, *Introduction to evolutionary computing*. Springer, 2015.

[147] U. A.J. and S. P.D., "Crossover Operators in Genetic Algorithms: a Review," *ICTACT Journal on Soft Computing*, vol. 06, no. 01, pp. 1083–1092, 2015, doi: 10.21917/ijsc.2015.0150.

[148] G. Syswerda, "Uniform Crossover in Genetic Algorithms," in *3rd International Conference on Genetic Algorithms*, 1989.

[149] G. Campione, L. Cavaleri, F. Di Trapani, G. Macaluso, and G. Scaduto, "Biaxial deformation and ductility domains for engineered rectangular RC cross-sections: A parametric study highlighting the positive roles of axial load, geometry and materials," *Eng Struct*, vol. 107, pp. 116–134, 2016.

[150] M. Saatcioglu and S. R. Razvi, "Strength and ductility of confined concrete," *Journal of Structural engineering*, vol. 118, no. 6, pp. 1590–1607, 1992.

[151] M. Menegotto, "Method of analysis for cyclically loaded RC plane frames including changes in geometry and non-elastic behavior of elements under combined normal force and bending," in *Proc. of IABSE Symposium on Resistance and Ultimate Deformability of Structures Acted on by Well Defined Repeated Loads, 1973*, 1973.

[152] G. Campione, L. Cavaleri, F. Di Trapani, and M. F. Ferrotto, "Frictional Effects in Structural Behavior of No-End-Connected Steel-Jacketed RC Columns: Experimental Results and New Approaches to Model Numerical and Analytical Response," *Journal of Structural Engineering*, vol. 143, no. 8, p. 04017070, 2017, doi: 10.1061/(asce)st.1943-541x.0001796.

[153] R. Montuori and V. Piluso, "Reinforced concrete columns strengthened with angles and battens subjected to eccentric load," *Eng Struct*, vol. 31, no. 2, pp. 539–550, 2009, doi: 10.1016/j.engstruct.2008.10.005.

[154] J. B. Mander, M. J. N. Priestley, and R. Park, "Theoretical stress-strain model for confined concrete," *J. Struct. Eng*, vol. 114, no. 8, pp. 1804–1826, 1989.

[155] F. Di Trapani, G. Bertagnoli, M. F. Ferrotto, and D. Gino, "Empirical equations for the direct definition of stress–strain laws for fiber-section-based macromodeling of infilled frames," *J Eng Mech*, vol. 144, no. 11, p. 04018101, 2018.

[156] European Committee for Standardization, *Eurocode 8: Design of structures for earthquake resistance-part 1: general rules, seismic actions and rules for buildings*. 2005.

[157] D. E. Biskinis, G. K. Roupakias, and M. N. Fardis, "Degradation of shear strength of reinforced concrete members with inelastic cyclic displacements," *ACI Struct J*, vol. 101, no. 6, pp. 773–783, 2004, doi: 10.14359/13452.

[158] Italian Ministry of Infrastructure and Transport, "Ministerial Order n.8 January 17th, 2018. Norme tecniche per le costruzioni. (In Italian)," 2018.

[159] F. Di Trapani and M. Malavisi, "Seismic fragility assessment of infilled frames subject to mainshock/aftershock sequences using a double incremental dynamic analysis approach," *Bulletin of Earthquake Engineering*, vol. 17, no. 1, pp. 211–235, 2019, doi: 10.1007/s10518-018-0445-2.

[160] L. Cavaleri, F. Di Trapani, M. F. Ferrotto, and L. Davì, "Stress-strain models for normal and high strength confined concrete: Test and comparison of literature models reliability in reproducing experimental results," *Ingegneria Sismica*, 2017.

[161] G. De Martino, M. Di Ludovico, A. Prota, C. Moroni, G. Manfredi, and M. Dolce, "Estimation of repair costs for RC and masonry residential buildings based on damage data collected by post-earthquake visual inspection," *Bulletin of Earthquake Engineering*, vol. 15, no. 4, pp. 1681–1706, 2017, doi: 10.1007/s10518-016-0039-9.

[162] C. Del Vecchio, M. Di Ludovico, S. Pampanin, and A. Prota, "Repair costs of existing rc buildings damaged by the l'aquila earthquake and comparison with FEMA P-58 predictions," *Earthquake Spectra*, vol. 34, no. 1, pp. 237–263, 2018, doi: 10.1193/122916EQS257M.

[163] F. Di Trapani, A. P. Sberna, and G. C. Marano, "A genetic algorithm-based framework for seismic retrofitting cost and expected annual loss optimization of non-conforming reinforced concrete frame structures," *Comput Struct*, vol. 271, p. 106855, 2022, doi: 10.1016/j.compstruc.2022.106855.

[164] Italian National Research Council (CNR), "Instructions for design, execution and control of strengthening interventions through fiber-reinforced composites," *CNR-DT 200*, vol. 4, 2005.

[165] A. P. Sberna, C. Demartino, I. Vanzi, G. C. Marano, and F. Di Trapani, "Cost-effective topology optimization of masonry structure reinforcements by a linear static analysis-based GA framework," *Bulletin of Earthquake Engineering*, 2024, doi: 10.1007/s10518-024-01900-5.

[166] M. J. N. Priestley and F. Seible, "Design of seismic retrofit measures for concrete and masonry structures," *Constr Build Mater*, vol. 9, no. 6, pp. 365–377, 1995, doi: 10.1016/0950-0618(95)00049-6.

[167] N. Gattesco, C. Amadio, and C. Bedon, "Experimental and numerical study on the shear behavior of stone masonry walls strengthened with GFRP reinforced mortar coating and steel-cord reinforced repointing," *Eng Struct*, vol. 90, pp. 143–157, 2015.

[168] N. Gattesco and I. Boem, "Experimental and analytical study to evaluate the effectiveness of an in-plane reinforcement for masonry walls using GFRP meshes," *Constr Build Mater*, vol. 88, pp. 94–104, 2015.

[169] V. Turnšek and F. Čačovič, "Some experimental results on the strength of brick masonry walls," *Proceedings of the 2nd International Brick Masonry Conference*, pp. 149–156, 1971, [Online]. Available: http://www.hms.civil.uminho.pt/ibmac/1970/149.pdf

[170] P. Kora and P. Yadlapalli, "Crossover operators in genetic algorithms: A review," *Int J Comput Appl*, vol. 162, no. 10, 2017.

[171] G. Squillero and A. Tonda, "Divergence of character and premature convergence: A survey of methodologies for promoting diversity in evolutionary optimization," *Inf Sci (N Y)*, vol. 329, pp. 782–799, 2016.

[172] S. Cattari, A. M. D'Altri, D. Camilletti, and S. Lagomarsino, "Equivalent frame idealization of walls with irregular openings in masonry buildings," *Eng Struct*, vol. 256, p. 114055, 2022.

[173] G. Camata *et al.*, "Validation of non-linear equivalent-frame models for irregular masonry walls," *Eng Struct*, vol. 253, p. 113755, 2022.

[174] F. Braga and M. Dolce, "Un metodo per l'analisi di edifici multipiano in muratura antisismici," *Proc. Of the 6th IB Ma. C., Roma*, 1982.

[175] F. Di Trapani, A. P. Sberna, and G. C. Marano, "A new genetic algorithm-based framework for optimized design of steel-jacketing retrofitting in shear-critical and ductility-critical RC frame structures," *Eng Struct*, vol. 243, no. January, p. 112684, 2021, doi: 10.1016/j.engstruct.2021.112684.

[176] A. Deb, A. L. Zha, Z. A. Caamaño-Withall, J. P. Conte, and J. I. Restrepo, "Updated probabilistic seismic performance assessment framework for ordinary standard bridges in California," *Earthq Eng Struct Dyn*, vol. 50, no. 9, pp. 2551–2570, 2021, doi: 10.1002/eqe.3459.

[177] A. Deb, J. P. Conte, and J. I. Restrepo, "Comprehensive treatment of uncertainties in risk-targeted performance-based seismic design and assessment of bridges," *Earthq Eng Struct Dyn*, vol. 51, no. 14, pp. 3272–3295, 2022, doi: 10.1002/eqe.3722.

[178] J. W. Baker and C. A. Cornell, *Uncertainty specification and propagation for loss estimation using FOSM method*. Pacific Earthquake Engineering Research Center, 2004.

[179] M. Kohrangi, P. Bazzurro, and D. Vamvatsikos, "Vector and Scalar IMs in Structural Response Estimation, Part II: Building Demand Assessment," *https://doi.org/10.1193/053115EQS081M*, vol. 32, no. 3, pp. 1525–1543, Aug. 2016, doi: 10.1193/053115EQS081M.

[180] N. Jayaram, T. Lin, and J. W. Baker, "A computationally efficient ground-motion selection algorithm for matching a target response spectrum mean and variance," *Earthquake spectra*, vol. 27, no. 3, pp. 797–815, 2011.

[181] L. F. Ibarra, *Global collapse of frame structures under seismic excitations*. Stanford University, 2004.

[182] E. C. Carvalho and E. Coelho, "Seismic assessment, strengthening and repair of structures," *Ecoest2-Icons Report*, no. 2, 2001.

[183] A. V Pinto, G. Verzeletti, J. Molina, H. Varum, R. J. Silva Moura Pinho, and E. Coelho, "Pseudo-dynamic tests on non-seismic resisting RC frames (bare and selective retrofit frames)," 2002.

[184] H. Varum, "Seismic assessment, strengthening and repair of existing buildings," Universidade de Aveiro, 2003.

[185] H. Krawinkler and D. G. Lignos, "How to predict the probability of collapse of non-ductile building structures," in *Seismic Risk Assessment and Retrofitting: With Special Emphasis on Existing Low Rise Structures*, Springer, 2009, pp. 343–365.

[186] C. Adam and H. Krawinkler, *Large displacements of elastic-plastic frames exposed to pulse-type ground motion*. na, 2003.

[187] UNI - Italian National Unification, "Angular Beams with Equal Sides Round Edges," Milan.

[188] Angel L Perez-Irizarry and Gustavo J Parra-Montesinos, "Evaluation of Seismic Behavior of Coupling Beams with Various Types of Steel Fiber Reinforced Concrete," *Crc*, no. December, 2016.

[189] J. Cai, G. Bu, C. Yang, Q. Chen, and Z. Zuo, "Calculation methods for inter-story drifts of building structures," *Advances in Structural Engineering*, vol. 17, no. 5, pp. 735–745, 2014.

[190] T. B. Panagiotakos and M. N. Fardis, "Deformations of reinforced concrete members at yielding and ultimate," *ACI Struct J*, vol. 98, no. 2, pp. 135–148, 2001, doi: 10.14359/10181.

[191] S. Sheikh and S. M. Uzumeri, "Analytical Model for Concrete Confinement in Tied Columns.," *Journal of the Structural Division*, vol. 108, no. ST12, pp. 2703–2722, 1982, doi: 10.1061/jsdeag.0006100.

[192] C.-F. M. Code, "CEB-FIP model code for concrete structures, euro-international committe for concrete," *Bulletin*, no. 213/214, 1990.

[193] M. Berry, M. Parrish, and M. Eberhard, "PEER structural performance database user's manual (version 1.0)," *University of California, Berkeley*, 2004.

[194] A. Deb, J. P. Conte, and J. I. Restrepo, "Comprehensive treatment of uncertainties in risk-targeted performance-based seismic design and

assessment of bridges," *Earthq Eng Struct Dyn*, vol. 51, no. 14, pp. 3272–3295, 2022, doi: 10.1002/eqe.3722.

[195] L. F. Ibarra and H. Krawinkler, "Global Collapse of Frame Structures under Seismic Excitations," Sep. 2005.